University of

Strathclyde

Mechanical

Engineering

# DESIGN STUDY OF A REGENERATIVE PUMP USING NUMERICAL AND EXPERIMENTAL TECHNIQUES

Francis Joseph Quail

# UNIVERSITY OF STRATHCLYDE GLASGOW

## DEPARTMENT OF MECHANICAL ENGINEERING

## **TITLE:** DESIGN STUDY OF A REGENERATIVE PUMP USING NUMERICAL AND EXPERIMENTAL TECHNIQUES

This thesis is submitted in accordance with the regulations for the award of Doctor of Philosophy in Mechanical Engineering at the University Of Strathclyde Glasgow Scotland

Signed

Eur Ing Francis Joseph Quail
**Chartered Engineer**
CEng, BEng (Hons), FIMechE, FIEI, FIES, IAENG

Date

*"If you can not measure it, you can not improve it."* ***Lord Kelvin*** *(1824 – 1907)*

*"Energy and persistence conquer all things."* ***Benjamin Franklin*** *(1706 - 1790)*

# Acknowledgments

I would like to express sincere appreciation to Dr Tom Scanlon and Dr Matt Stickland for their assistance and guidance during this project. I would also like to express gratitude to Mr. Drew Irvine, Mr. Tom Farmer, Mr. Duncan Lindsay and Mr. Dave Cunningham for their help in the manufacturing processes.

I would like to thank my wife, children and parents for their support, encouragement and understanding during this work. This work is dedicated to them with all my love and thanks.

**"Frater, ave atque vale" - (Catullus c. 84 - 54 BC)**

# Abstract

Pumps are the single largest user of electricity in industry in the European Union and energy savings of 3% would result in a 1.1TWH p.a. reduction in consumption or a saving of 0.54 Mton of $CO_2$ production. This thesis considers a numerical and experimental analysis of a regenerative pump, not only to resolve the flowfield and match unit performance, but also to assess potential performance improvement. There is limited published data to allow a more intuitive approach to selection of this pump type. Regenerative pumps are the subject of increased interest in industry, as they are low cost, low specific speed, compact and able to deliver high heads with stable performance characteristics and other benefits. The hydraulic efficiency of regenerative pumps, however, is low, usually less than 50%. The complex flow-field within the pump represents a significant challenge to detailed mathematical modelling.

This thesis presents the use of a commercial CFD code in conjunction with new experimental testing to simulate the flow within the regenerative pump. The CFD results demonstrate that it is possible to represent the helical flowfield for the pump only witnessed in experimental flow visualisation until now. The CFD performance results also demonstrate reasonable agreement with the experimental data which, to date, has only been successfully modelled using mathematical models with correction factors. The research contained in this thesis also considers a design process in conjunction with a novel method of rapid manufacture used in the development of modified regenerative pump impellers. A novel method is presented to manufacture the complex blade profiles that are robust enough for testing, in a rapid and cost effective manner.

# Table of Contents

# List of Figures

Number Page

# List of Tables

Number Page

# Nomenclature

| | | |
|---|---|---|
| A | Cross sectional area | ($m^2$) |
| TWh | Terawatt Hour | |
| MTon | Metric Ton | |
| C | Clearance | (m) |
| $CO_2$ | Carbon Dioxide | |
| D | Diameter | (m) |
| $\eta$ | Efficiency | (%) |
| rpm | Revolutions per minute | |
| R | Radius | (m) |
| U | Peripheral velocity | (m/s) |
| W | Tangential velocity | (m/s) |
| V | Absolute velocity | (m/s) |
| Z | Number of Blades | |
| b | Width | (m) |
| $\beta^1$ | Flow angle | (°) |
| $\beta$ | Blade angle | (°) |
| $\omega$ | Angular speed | (rad/s) |
| g | gravitational const. | ($m/s^2$) |
| H | Head | (m) |
| m | Mass transfer rate | (kg/s) |
| N | Rotational Speed | (rpm) |
| NPSH | Net positive suction head | (m) |
| p | Pressure | (Pa) |
| P | Power | (W) |
| T | Torque | (Nm) |
| L | Characteristic length | (m) |
| Q | Flowrate | ($m^3/s$) |
| Re | Reynolds Number | |
| $\rho$ | Density | ($kg/m^3$) |
| $\mu$ | Dynamic viscosity | (kg/ms) |
| $\upsilon$ | Kinematic viscosity | ($m^2/s$) |

| | | |
|---|---|---|
| $\xi$ | Uncertainty | |
| $\sigma$ | Slip factor | |
| $\alpha$ | Shock factor | |
| $\psi$ | Head Coefficient | |
| $\phi$ | Flow Coefficient | |
| IP | Power Coefficient | |
| $T_i$ | Turbulence Intensity | |
| $\varepsilon$ | Turbulence dissipation rate | $m^3/s^3$ |
| k | Turbulent kinetic energy term | $m^2/s^2$ |
| y+ | Boundary layer wall function | |
| **Subscripts** | | |
| 1 | position of inlet flow to the impeller blade | |
| 2 | position of outlet flow from the impeller | |
| c | channel | |
| g | centroid | |
| h | hub | |
| m | meridional (circulatory component) | |
| i | impeller | |
| t | tip | |
| u | tangential component | |
| s | solid body rotation | |
| $\theta$ | peripheral angle | |
| **Acronyms** | | |
| 1D | One-dimensional | |
| 2D | Two-dimensional | |
| 3D | Three-dimensional | |
| AI | Analogue input | |
| AO | Analogue output | |
| ABS | Acrylonitrile butadiene styrene | |
| AVF | Absolute velocity formulation | |
| CNC | Computer numerically controlled | |
| CAD | Computer aided design | |

| | | |
|---|---|---|
| CFD | Computational Fluid Dynamic | |
| DRU | Data retrieval unit | |
| DAC | Data acquisition card | |
| FS | Full scale | |
| FDM | Fused deposition modelling | |
| Hex | Hexahedral | |
| BSL | Best straight line | |
| MRF | Multiple Reference Frame | |
| mV | millivolts | |
| NI | National Instruments | |
| PGA | Programmable gain amplifier | |
| RANS | Reynolds Averaged Navier Stokes | |
| RNG | ReNormalization Group | |
| RSM | Reynolds Stress Model | |
| RM | Rapid manufacturing | |
| RP | Rapid prototyping | |
| RT | Rapid tooling | |
| RTV | Room temperature vulcanizing | |
| SE | Sudden expansion | |
| SC | Sudden contraction | |
| SRP | Subtractive rapid prototyping | |
| Tet | Tetrahedral | |
| EU | European Union | |
| HPC | High Performance Computer | |
| CFD | Computational Fluid Dynamics | |
| RMS | Root mean square | |
| SWF | Standard Wall Function | |
| NWF | Near Wall Function | |
| BEP | Best Efficiency Point | |

# Introduction

Although regenerative turbomachines have found a fairly wide range of applications, they are applied in limited numbers and they have been very much neglected so far as attempts to improve their design and performance are concerned. The interest today in the use of such pumps in industrial applications is increasing. The supporting analytical work and publications are quite limited ETSU (2001). The nature of the flow has been proposed by a number of authors who have developed theoretical models to predict the performance of the machines, Badami (1997). The majority of these methods suffer from two basic defects which severely limit their use as a design tool. The first of these is that they contain empirically derived loss coefficients which are not directly related to design parameters. They therefore give no indication of how the design might be modified to reduce the losses, and cannot be used to evaluate designs which differ significantly from those on which the models were based. The second defect is that they are derived from an essentially one-dimensional analysis, Andrew (1990). Most of the theories presented relied on assumptions not based on detailed measurements or precise CFD modelling, Meakhail et al. (2005).

Given this dearth of information, it is hardly surprising that most designs of regenerative turbomachines retain a fairly basic geometrical configuration, with simple vanes, either machined or cast into the impeller.

This thesis develops a method of not only emulating the pump flowfield using the commercial CFD code, FLUENT version 6.3.26. (2006), but also matches the modelling to corresponding experimental data.

Most authors agree that, not only improved efficiency but also additional substantial pressure increase could be achieved, if the flow mechanism, and hence losses, were better understood Song et al. (2003). In this work, the results of the CFD modelling are compared to experimental data obtained by the author. The use of a commercial CFD code, FLUENT 6.3.26 (2006), to match the flow pattern in a regenerative pump to empirical test data, is a robust method of analysing the complex flow regime within the regenerative pump. Unstructured grid CFD flow solvers have been developed and used in industry for many years to deal with pump applications Fluent (2006). This thesis set out to not only match CFD predictions with experimental results, but also to resolve the flowfield within this type of pump. A more intuitive approach could be adopted to the pump design with a better understanding of the flow regime within the pump.

To allow such geometric changes to be tested a novel method of rapid manufacturing is presented in this thesis to allow experiments to be conducted. This study also considers potential future opportunities to modify the pump design.

# Chapter 1

## The Regenerative Pump

### 1.1 Overview

The regenerative pump uses an impeller with turbine-type blades mounted on the periphery running in an annular channel surrounding the periphery of the wheel, (fig. 1). In the design, the impeller has radial teeth machined into the impeller and the fluid passes through an open annular channel and circulates repeatedly through the impeller vanes. The helical motion of the fluid within the pump is considered in Chapter 2 of this thesis (fig. 1). The regenerative pump is also sometimes referred to as a peripheral pump, turbulence pump, friction pump, turbine pump, drag pump, side channel pump, traction pump or vortex pump, Engeda (2003).

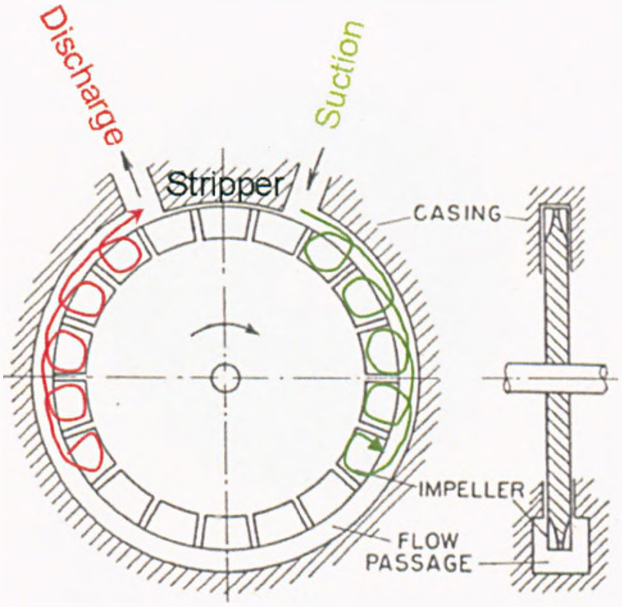

**fig. 1** Regenerative Pump

The regenerative pump is characterised by a unique impeller design. The impeller disc has a large number of blades machined into its periphery, (fig. 2). Generally, a blade row exists on each side of the disc to minimise axial thrust. In a traditional centrifugal pump, fluid enters the impeller adjacent to the shaft centreline and then is accelerated outward, exiting the impeller at it's outside diameter, Buse (1977). The regenerative pump in this study differs from centrifugal pumps, in that the fluid enters near the impeller outer diameter, is accelerated through approximately 320 degrees of rotation and exits the pump discharge at, or near, the same radial location as the inlet. A sector or "stripper" of about 40 degrees, separates the inlet from the outlet. In the stripper, the casing walls are parallel to the impeller shroud and are positioned in very close proximity to the rotating impeller to minimise leakage between the high pressure exit and the lower pressure inlet.

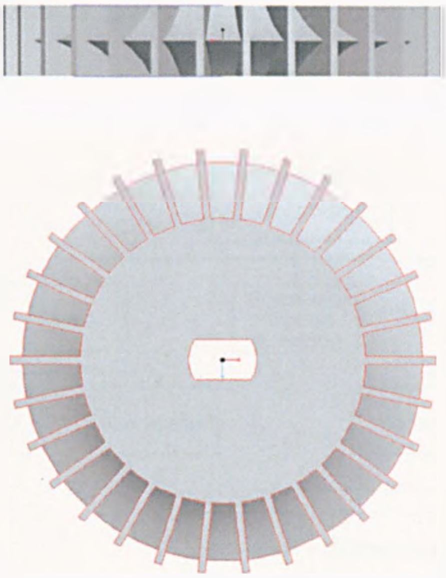

**fig. 2** Regenerative pump impeller

The regenerative pump can achieve more head for a given impeller diameter and speed than typical centrifugal pump types, Muller (2004) and Hollenberg et al. (1979). There is disagreement regarding the strict detail of the fluid mechanics involved, Grabow (1966). Most authors agree that the pump's head generation capability is related to the regenerative aspect of the pump whereby fluid entering an impeller blade is accelerated not only tangentially in the direction of rotation, but also radially outward into the casing channel by centrifugal force. As the fluid impinges on the casing wall, it is redirected back onto an adjacent blade, where additional energy is imparted. This process repeats itself many times during a single rotation of the impeller. In spite of having operating characteristics that mimic a positive displacement pump, (power directly proportional to head, with maximum power required at shutoff, and a steep head-capacity curve), the regenerative pump is a kinetic pump, Volk (2005). That is, kinetic energy is imparted to the fluid by the series of impulses given to the fluid by the rotating impeller blades, (fig. 3).

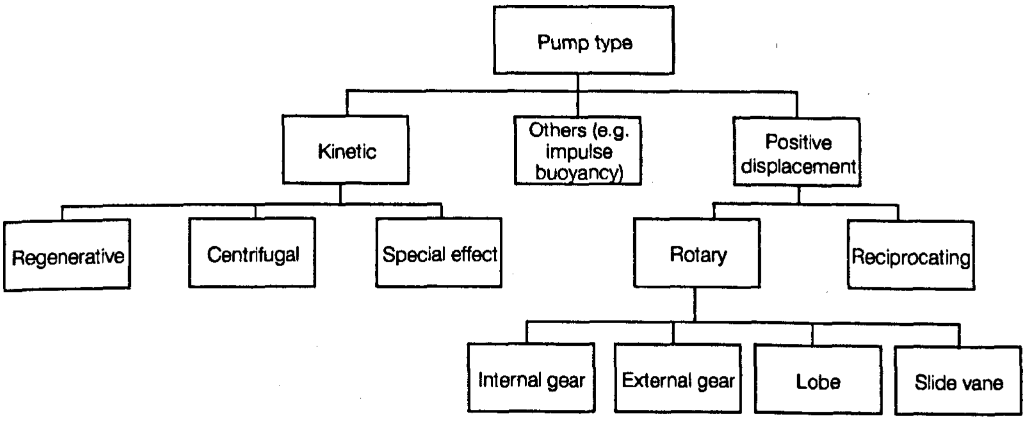

**fig. 3** Pump classification

At inlet, the pumped fluid is split between both sides of the impeller and continuously circulated between the blades and the annular channel, (fig. 1). This produces a helical or corkscrew like flow path, as the impeller imparts energy to the fluid as it is transported around the pump. These repeated increases in fluid velocity are referred to as regeneration. This results in progressively higher pressure as the pumped fluid approaches the discharge port. The fluid flow velocity in the casing channel is lower than the fluid flow velocity in the impeller. Thus a force exists between the fluid in the channel and the fluid in the impeller which develops a rotating or circular motion when the flows unite.

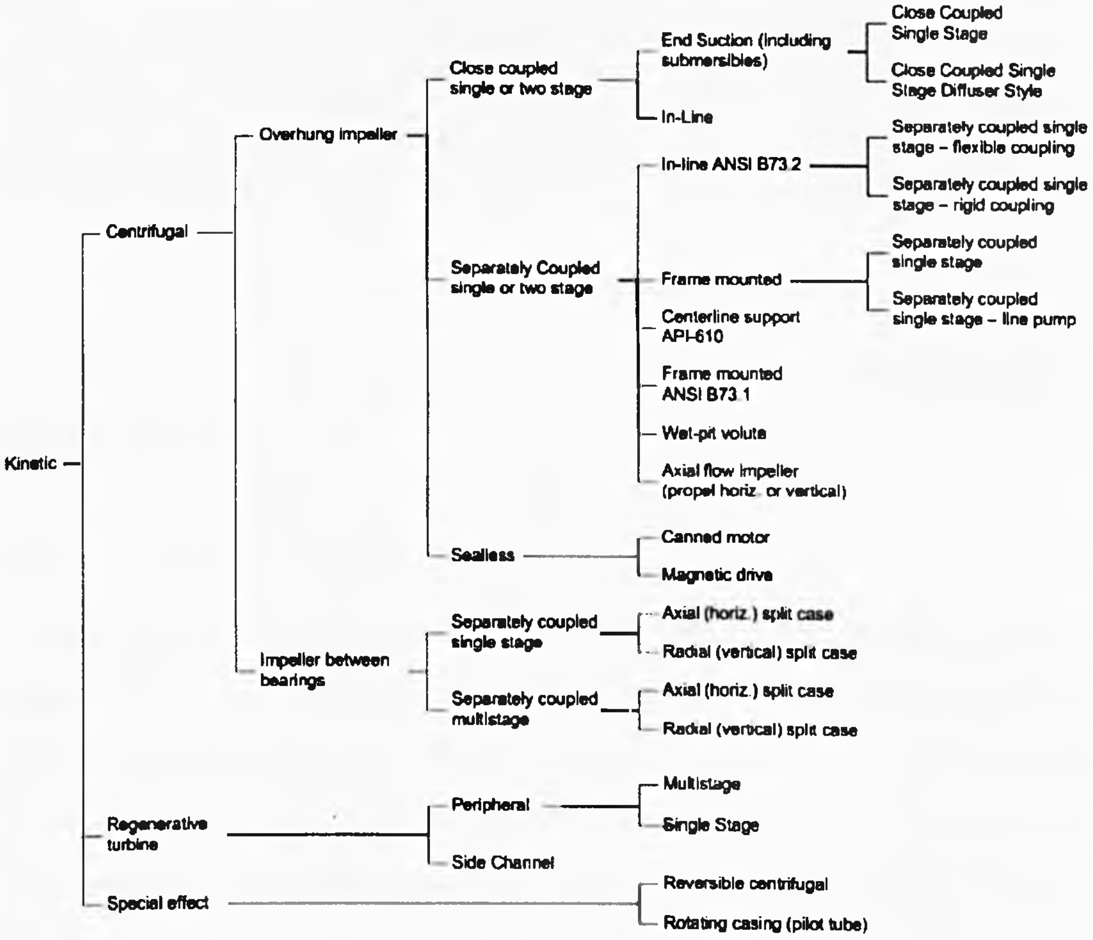

**fig. 4** Kinetic pump classification
(source: Hydraulic Institute www.pumps.org)

Generally the pump can be sub-classified according to the number of channels used (fig. 4). Pumping action is provided by the series of impulses given to the fluid by the rotating blades. Normally a regenerative pump has a double sided channel in which the fluid circulates. The repeated fluid circulation during the flow process, or 'multistaging', principally allows regenerative pumps to generate high heads at relatively low specific speeds, although shaft speeds may be greater than 6000 RPM Iverson (1955). Some applications where these pumps are found are, for example, in boiler houses, chemical plants, canneries, dairies, greenhouses, cement plants, distilleries, breweries, boats/ships and factories (Table 1).

| | | |
|---|---|---|
| Boiler feed | Booster service | Car washers |
| Condensate return | Refrigeration | Petroleum pumping |
| Bio-medical pumping | Hot/volatile liquids | Caustic fluids |
| Sump service (clear water) | Marine (potable water) | Viscous fluids |
| Brine circulation | Water treatment | Chemicals |
| Coolant pumping | Refineries | Aero/Auto Fuel pumps |

**Table 1** - Typical regenerative pump applications

The low specific speeds make it attractive for lubrication control, filtering and booster applications.

## 1.2 Purpose of study

Pumps are the single largest user of electricity in industry in the European Union and energy savings of 3% would result in a 1.1TWH p.a. reduction in consumption or a saving of 0.54 Mton of $CO_2$ production as outlined by the IMechE Fluid machinery group symposium (2007). Reducing environmental impact and making savings is a considerable challenge for the pump industry. This thesis considers a numerical and experimental analysis of a regenerative pump to simulate the flowfield and unit performance ETSU (2001), with a view to improving its efficiency. There is limited published data and insufficient design guiding criteria to allow more intuitive industrial selection of this pump type, particularly to meet more stringent European pump selection criteria detailed in EU Directive 2005/32/EC (2005).

The hydraulic efficiency of regenerative pumps is low, usually less than 50%, and existing numerical models are limited in matching the flow characteristics across a running range, Raheel et al. (2005). The complex flow-field within the pump represents a significant challenge to detailed mathematical modelling, as there is considerable flow separation in the impeller blading, Hollenberg et al. (1979). To date, the most fruitful research work has come from test data on specific units and corresponding flow visualisation studies conducted, (Chap. 2.5).

This thesis presents the use of a commercially available finite volume based Navier-Stokes solver; FLUENT version 6.3.26, in conjunction with new experimental testing to not only assess the flow within the regenerative pump, but also to identify the geometric features of the pump that reduce the pump's efficiency. The University of Strathclyde Departmental experience in parallel-architecture computation was used to run the CFD model of the regenerative pump with a High Performance Computer facility (HPC). The HPC system consists of 100 Opteron processors accessing a total available memory of 236 GB RAM.

## 1.3 Project scope

Most of the previous work relating to regenerative pumps was largely dependent upon assumptions not based on detailed measurements or CFD predictions ,Meakhail et al. (2005). Generally, in designing conventional turbomachines, the input variables are: design flowrate, design head rise and rotational speed, Salsbury (1982). For axial and radial turbomachines, the impeller diameter is usually selected by the relation of specific speed and specific diameter, (Appendix A1). Currently, however, in regenerative machines there is no sufficient guiding data and, usually, the impeller diameter is determined from the given design conditions, Raheel et al. (2005). Most prior analysis contains empirically derived loss coefficients which are not directly related to design parameters. Therefore, they give no indication of how the design might be modified to increase efficiency, and cannot be used to evaluate designs which differ significantly from those on which the models were based. Furthermore, the previous models are derived from an essentially one-dimensional analysis. Most of the theories presented relied on assumptions not based on detailed measurements or precise CFD modelling, Song et al. (2003).

The challenge of the author's research was to develop a CFD model to represent the complex fluid motion, within a regenerative pump. From this point it would be feasible not only to improve the pumps efficiency but also to obtain additional substantial pressure if the flow mechanisms, and hence losses, were better understood, Badami (1997).

Although powerful computational facilities and more robust CFD codes have been developed in recent-years there is still a need to validate and verify the predictions. Although these codes are widely used in the turbomachinery industry for assessing and predicting pump performance, it is still essential to check the veracity of such models against experimental test.

In this study a new pump and test arrangement is developed and the experimental set-up and procedure is detailed in chapter 3. Rapid manufacturing methods are used to produce robust and dimensionally accurate test components as part of the experimental process. Corresponding new CFD models are developed to compare to the experimental test results. It is not only in matching pump performance predictions with experimental data, there is also an opportunity to compare flow visualisation models with previous published flow visualisation studies conducted in the 1940's and 1950's. Until now it has been accepted in many publications that the best knowledge of the flow field of the regenerative pump has come from these conducted flow visualisation experiments. Finally this study is extended to consider performance improvement by testing and analysis of modified impeller blade profiles.

# Chapter 2

# Regenerative Pump Theory

## 2.1 Overview

Authors have suggested simplified theoretical models for the regenerative pump and its geometry, Badami (1997) and Wilson et al. (1955). Several theories have appeared in the literature concerning the operational principle of the regenerative pump. However, the number of publications and literature are small in comparison to that available for other turbomachines, e.g. axial or centrifugal pumps, Raheel et al. (2005). The flow in a regenerative pump has the fluid repeatedly passing through the impeller in contrast to the fluid passing the impeller once as with most continuous flow machines. This multistaging (or repetitive action of the impeller blading on the fluid), makes regenerative pumps capable of developing very high pressure ratios in a single impeller. It is from this internal 'multistaging', or regenerative flow pattern, that the pump derives it's name. Most of the theories presented rely on assumptions not based on detailed measurements or precise CFD modelling, Burton (1962). An overview of the two main theoretical principles is detailed below with references and comments on the general validity.

## 2.2 Literature search and theorems of operation

Fig. 5, illustrates an impeller rotating within an annular chamber. The fluid enters the pump casing and flows to both sides of the impeller through a suction port in the casing. This arrangement makes the unit a double suction unit and balances the axial hydraulic thrust on both sides of the impeller.

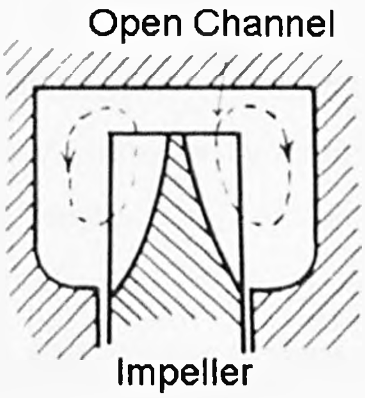

**fig. 5** Impeller /Channel arrangement

The theory of operation can be divided into two main categories. In the turbulence and mixing theory, Senoo (1954), the impeller momentum is transferred by turbulent shear stresses. The fluid mass transfer, between the impeller and the side channel, is effected by a mixing process in side channel. When explaining the working process of the regenerative flow pump, Weinig (1955), propose that the energy transfer from the fluid in the impeller to the fluid in the side channel is caused by the shear stresses.

Comparing this to the circulation or liquid filament theory, the impeller momentum is transferred by the action of centrifugal forces on the fluid moving on helical (fig. 6) flow paths, Kuprjasin (1957).

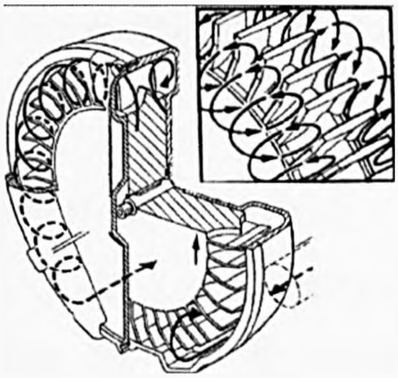

**fig. 6** Pump fluid flow path

A transfer of momentum takes place between the impeller and the delivered flow in the side channel, Pfaff (1959), Kuprjasin (1957).

Once the fluid enters the pump, it is directed into the vanes, which push the fluid forward and imparts a centrifugal force outward to the impeller periphery. An orderly circulatory flow is therefore imposed by the impeller vane, which increases fluid velocity. Fluid velocity (kinetic energy) is then available for conversion to pressure, in the casing channel.

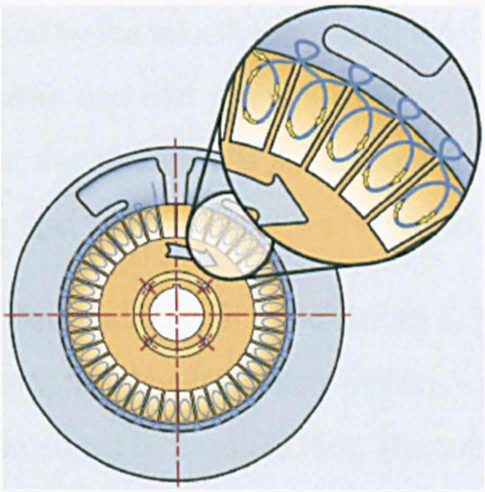

**fig. 7** Helical flow path

As the circulatory flow reaches the fluid channel periphery, it is then redirected by the casing fluid channels, around the side of the impeller, and back into the inner diameter of the impeller blades, where the process begins again, fig. 7. This cycle is repeated many times as the fluid passes through the pump. Each pass through the vanes generates more fluid velocity, which can then be converted into more pressure in the casing channel.

## 2.3 Turbulence and Mixing Theory

Senoo (1956), for example, considers that a shearing action takes place between the edges of the rotor vanes and the fluid in the channel; Pfleiderer (1961) regard the channel as one having three stationary relatively smooth sides, and a very rough surface moving across its fourth side and dragging the fluid along.

This theory proceeds from the assumption that the mass of fluid in the channel is entrained due to shear stresses originating in the fluid flow between the impeller and the fluid being delivered. The shearing action takes place between the edges of the impeller vanes and the fluid in the channel.

Shear stresses acting on the boundary between the impeller and the channel of the pump are only caused by the velocity gradient of the fluid elements contained within the moving impeller and that of the fluid flowing in the side channel at reduced velocity. Under these conditions the secondary flows resulting from the centrifugal force on the fluid in the impeller are neglected.

Although experimental flow visualisation work, Bartels (1947), has demonstrated that the flow field has in fact helical circulatory motion, a comparative analysis of the two theories was carried out by Senoo (1956). The author expressed the belief that, whilst the two theories are compatible, each had limits in validity. Crewdson (1956), defines a flow correlation for the channel flows based on Iverson (1955), which neglects the circulation effects detailed in Burton (1962).

## 2.4 Circulation or Liquid Filament Theory

Bajbakov (1960) and others, consider that the flow between the rotor and the channel is mainly a helical or toroidal motion as the fluid travels along the channel. In fluid mechanics, helicity is the extent to which corkscrew like motion occurs. The fluid in the channel passes into the impeller vanes and out again several times as it crosses the channel. Each time the fluid leaves the impeller it has been accelerated to an effective velocity at least up to that of the impeller and it then mixes with the slower moving fluid in the channel, driving the latter forward. The helical motion is maintained by centrifugal force, which is greater in the moving impeller than in the slower moving fluid in the channel.

The impeller momentum is transferred to the channel flow by a mixing of the flow in the side channel. The helical flow, develops from the flow velocity of the fluid in the side channel being lower than the circumferential velocity of the impeller (fig. 8). The flow in the impeller and the flow in the casing unite and the force differential induces a helical flow in the circumferential direction. The fluid enters into the impeller passages several times thus adding angular velocity, Wilson et al. (1955). The fluid is then projected into the side channel, where a mixing process reduces its velocity with a consequential increase in pressure along the side channel Badami (1997). Fluid motion can be described by means of two components, the tangential component that determines the effective flowrate of the pump (channel flow) and the circulation component that determines the circulatory flow in the pump. Simplified modelling by Wilson et al. (1955) developed the basis of the theoretical analysis of the fluid motion inside the pump and is broadly accepted today. Several assumptions were made and an arbitrary control volume was applied to the pump with the application of fluid dynamics equations.

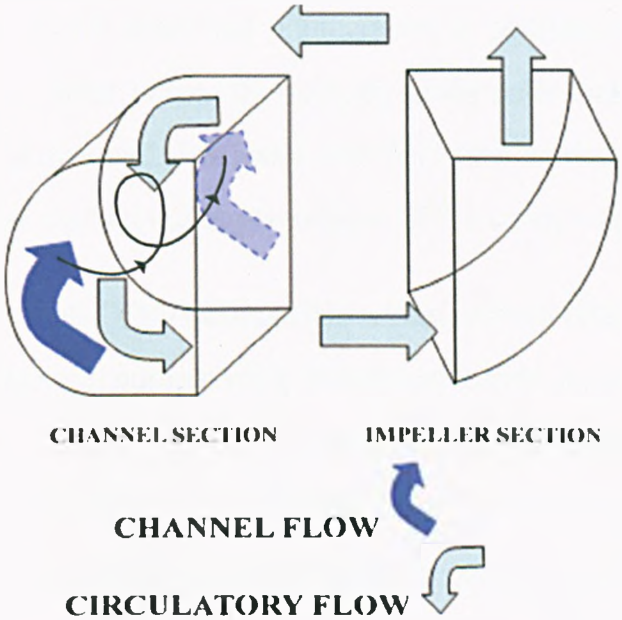

**fig. 8** Control volume- channel /circulatory flow

The energy transfer from the impeller to the fluid of the passage flow in the side channel is not affected directly, but through the mixing process between the circulation and the passage flow which has losses Grabow (1966). The proposers of the circulation theorm suggest impeller momentum can be calculated from the difference between the angular momentum entering and leaving the side channel, excluding the losses. These losses are mainly empirically derived and relate to the experiment on which they were conducted

## 2.5 Conducted Helical Flow Visualisation Experiments.

Although the turbulence mixing theory can have some interesting applications, experimental testing on regenerative pumps have observed the fluid flow in its helical circulatory motion induced by the centrifugal field. Experiments conducted by Lazo et al. (1953) & Lutz (1953), used a small thread probe at different points in the annular flow passage of the pump, to determine the direction of the flow velocity. They were able to corroborate the helical streamlines when plotting the results. Bartels (1947) examined photographs of peripheral pumps operated in Germany in 1947 which constantly pumped sandy water that were returned to the manufacturer for overhaul. The water channel in the pump had clear evidence of helical scratches marked out by the erosion of the sandy water.

Consequently Bartels (1947) established an experiment where a wax coating was applied to a peripheral pump casing. Ground glass and pulverised coal was added to the water and pumped through the system, and a photographic technique was used to capture the pattern of erosion to the pump. A helix angle was measured for the pump that demonstrated the helical flow paths. Whilst Wilson et al. (1955) has argued against the Turbulence and mixing theory having “seen” the existence of the helical patterns in Lazo et al. (1953) & Lutz (1953) there are no recent publications of successful attempts to capture the flow visualisation.

## 2.6 Theoretical Assumptions and Losses

In order to propose theoretical models Raheel et al. (2005), have assumed the following:

(i) Steady flow without leakages is assumed. Leakages are considered separately to avoid complexity in the basic model.

(ii) Fluid is incompressible

(iii) All processes are adiabatic

(iv) There are no end effects due to suction and discharge

(v) The pump flow is characterised by the tangential and circulatory velocity

(vi) Tangential pressure gradient is independent of radius

(vii) Tangential pressure gradient is constant throughout the Linear region

The circulation theory, first proposed by Wilson et al. (1955), and most universally accepted today, supports the helical or corkscrew flow motion within the pump. This motion has been clearly demonstrated in several flow visualisation experiments Bartels (1947) and Lutz (1953).

Whilst the flow visualisation experimental results give accurate data to support the flow pattern that has been replicated by other researchers, there are limitations with the proposed circulation theory mathematical models.

The loss coefficients that are presented in the models are empirically derived Raheel et al. (2005). In this sense they are more related to the geometric design of the experiment on which they were conducted rather than the design parameters related to the regenerative pump. Badami (1997) for example needed extensive experimental support to determine these coefficients in order to predict performance with his model. The limitations in such an approach are, that they give limited indication on how the design might be modified to reduce such losses, and become less representative when designs are evaluated which significantly vary from the geometry of those where the loss coefficients were first derived.

The circulation models also take no account of spanwise variation in the geometry, Andrew (1990). This essentially reduces the assessment to a 1-D analysis, when only the mean streamline is accounted for. With this lack of precise information, most designs of regenerative pumps are of standard radial blades either machined or cast into the impeller.

With the continued presence of large unexplained losses the regenerative pump, despite other interesting performance characteristics, has poor hydraulic efficiency of the order of 35-50%. Indeed the highest ever reported efficiency for this pump type was 50% by Crewdson (1956).

The consensus of publications to date is that mathematical models in the literature do not fully explain the behaviour of regenerative pumps and predict the performance accurately. In the past, theories were presented to explain the behaviour of regenerative pumps and to calculate their performance. Most of these models required extensive experimental support or performance prediction, Meakhail et al. (2005). All the previous theories rely on assumptions not based on detailed measurements or precise CFD calculations which would lead to a better understanding of the complex flow inside the regenerative pump.

The main losses associated with the circulation theory, proposed by Wilson et al. (1955), include hydraulic losses in the circulation process, shock and slip losses on the impeller blades, tangential head losses in the side channel, port losses in the pump and leakage losses (Table 2).

| Loss | Detail | Figure 9 |
|---|---|---|
| Channel turning losses | Due to the 180° turning of the fluid through the channel. | A-B |
| Blade turning losses | Due to the turning of the fluid through the blades 90°. | C-D |
| Channel and blade mixing losses | Due to mixing fluid leaving impeller tip and incoming channel through flow. | D-E |
| Sudden Expansion losses | Due to the sudden increase in flow area when the fluid flows from the blades to the channel. | E-A |

**Table 2** Main losses associated with circulation theory

As detailed in Table 2 and depicted in fig. 9, circulatory or hydraulic losses have two main contributors. The head loss of circulatory velocity through the impeller region and the head loss of circulatory velocity through the channel region. The sum of these two losses is the total circulatory loss.

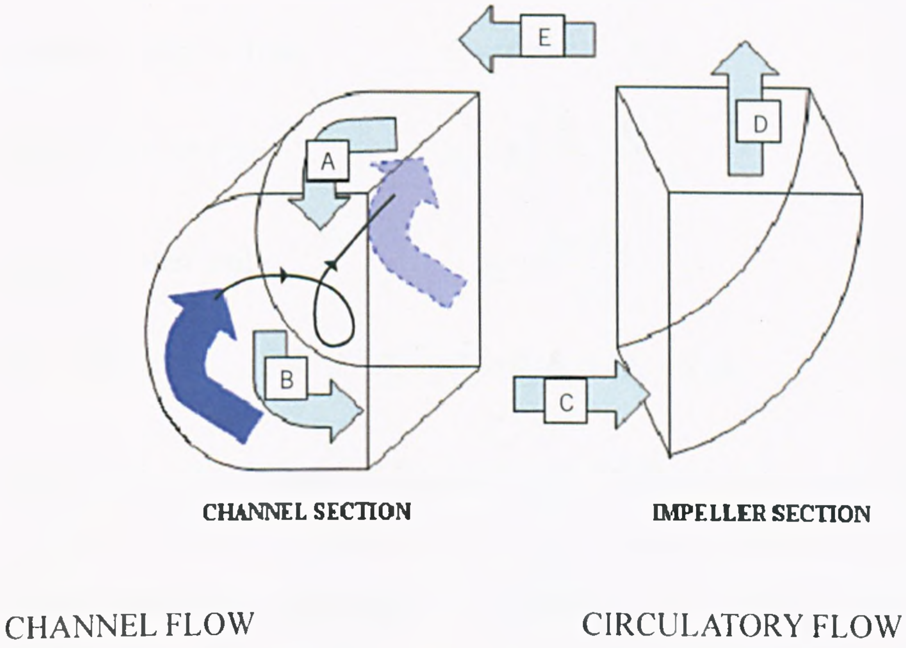

**fig. 9** Control volume hydraulic losses

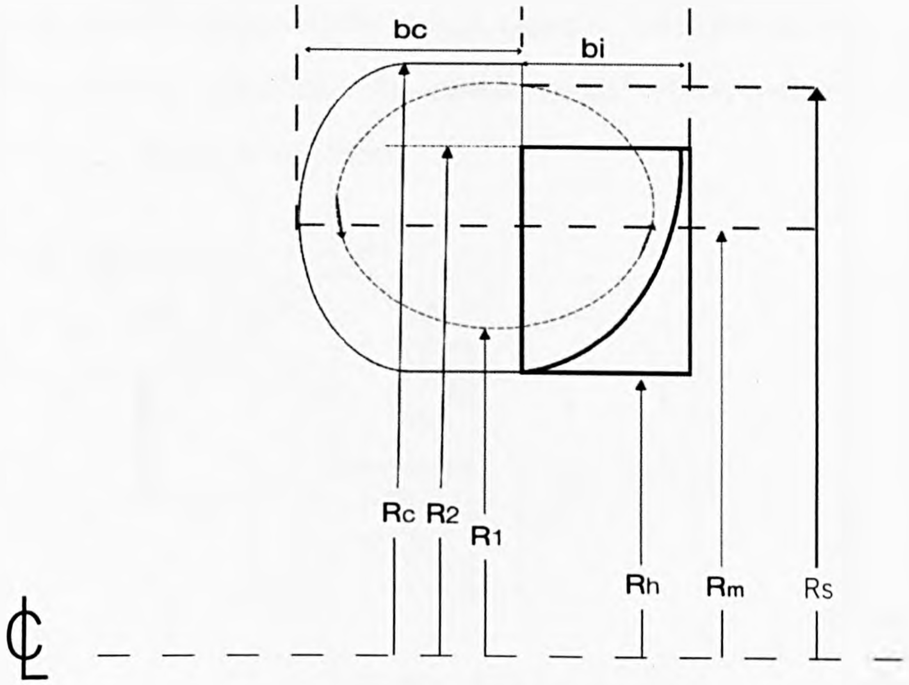

**fig. 10** Impeller and channel schematic

Meridional radius - $$R_m = \sqrt{[0.5(R_2^2 + R_h^2)]} \qquad (1)$$

Impeller entry radius - $$R_1 = 0.5(R_m + R_h) \qquad (2)$$

Channel entry radius - $$R_s = 0.5(R_c + R_m) \qquad (3)$$

Area impeller entry - $$A_1 = \pi\left(\frac{R_m^2 - R_h^2}{Z}\right) \qquad (4)$$

Area impeller exit - $$A_2 = \frac{2\pi R_2 b_i}{Z} \qquad (5)$$

Channel area - $$A_c = (R_c - R_h)b_c + (R_c - R_2)b_i \qquad (6)$$

The dimensional features of the pump are detailed in fig 10. The pressure difference between any two adjacent blades of an impeller, causes a tendency for the fluid leaving the impeller to deviate from the path prescribed by the blade surface backward with respect to the positive direction of impeller rotation. The result is that the fluids' tangential velocity at exit is less than that which would be expected from the velocity triangle based on the outlet blade angle (fig. 11). To allow for this reduction in the ideal tangential velocity a slip factor is usually introduced Wilson et al. (1955).

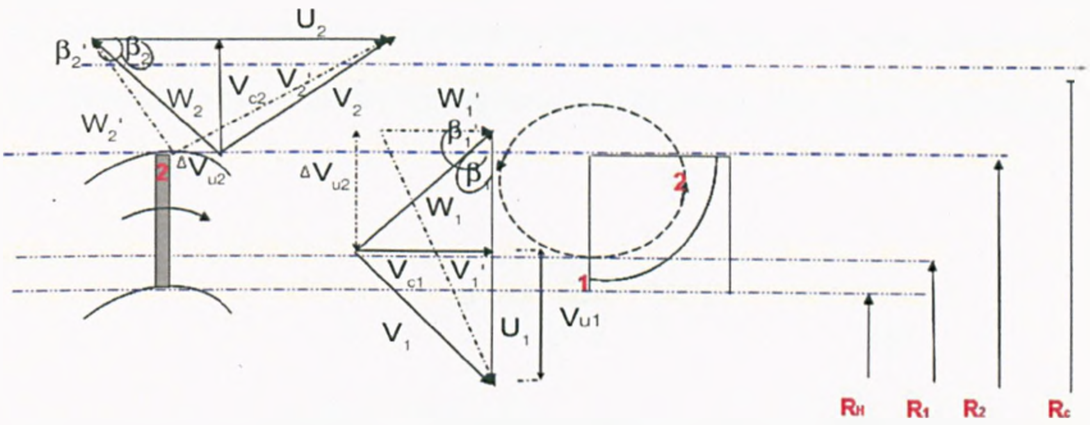

**fig.11** Velocity triangles

The energy of circulation of the fluid depends on the slip expressed as a ratio of the real tangential fluid velocity $W_2'$ at the impeller outlet to the ideal tangential fluid velocity at the tips of the blades $W_2$.

$$\sigma \quad \frac{W_2'}{W_2} \qquad (7)$$

The idea of a slip factor relates to the degree of guidance provided by the vanes and in particular an indication of how effective the fluid receives the energy transfer from the impeller arrangement. There is substantial literature on slip factors for centrifugal pumps Brennen (1994). Some of this focuses on the calculation of slip factors for inviscid flow in radial cascades with blades that are more complex than the infinitely thin, logarithmic spiral blades used by Busemann (1928). Useful reviews of some of this work can be found, for example, in the work of Ferguson (1963), Stanitz (1952) and Wislicenus (1947). Other researchers attempt to find slip factors that provide the best fit to experimental data. In doing so, they also attempt to account for viscous effects in addition to the inviscid effect for which the slip factor was originally devised. As an example of this approach, Wiesner (1967) reviews the existing empirical slip factors, and suggests one that seems to yield the best comparison with the experimental measurements. Other published works have approached applying a correction in this manner.

Busemann (1928) determined the value of the coefficient σ for a two dimensional flow between impeller blades. Busemann (1928) proved that σ is a function of the ratio

$$\sigma = f\left(\frac{r_1}{r_2}\right) \qquad (8)$$

and the number of blades Z. The excess energy of the fluid circulating between the impeller and the channel in the casing depends on the difference between the tangential component of the mean fluid velocity $u_t$ and the velocity of the flow in the channel.

In the published work to date **sudden expansion losses** are given in the form of:

$$K_{SE} = K_{car}\left(1 - \frac{A_i}{A_c}\right)^2 \qquad (9)$$

$A_i$ – Impeller Area

$A_c$ – Channel area

**Sudden contraction loss** – due to the sudden decrease in flow area when the fluid flows from the channel to the blades B - C (*)

$$K_{SC} = K_{car} \cdot 0.5\left(1 - \frac{A_i}{A_c}\right)^{0.75} \qquad (10)$$

$A_i$ – Impeller Area

$A_c$ – Channel area

(*) Note this loss is not adequately considered in the published works to date, it is carried in the shock loss terms.

**Shock or incidence losses** are caused by the difference between blade angle and flow angle when the fluid enters the impeller and are estimated as the difference in tangential velocity.

Head losses caused by channel friction are referred to as **tangential head losses** and are calculated as a function of the average tangential velocity in the side channel Vc, usually by applying the classic pipe loss formula.

It is important to define the slip losses and shock losses for the regenerative pump as they have a significant bearing on the performance characteristics of the pump obtained in the results, Chapter 5. As with other kinetic type pumps the regenerative pump generates pressure from the circumferential velocity imparted to the fluid by the impeller. It will be shown that both the shock and slip losses have a significant effect on the performance of the pump particularly at the higher and lower flowrates in the performance characteristics.

## 2.7 Governing Equations

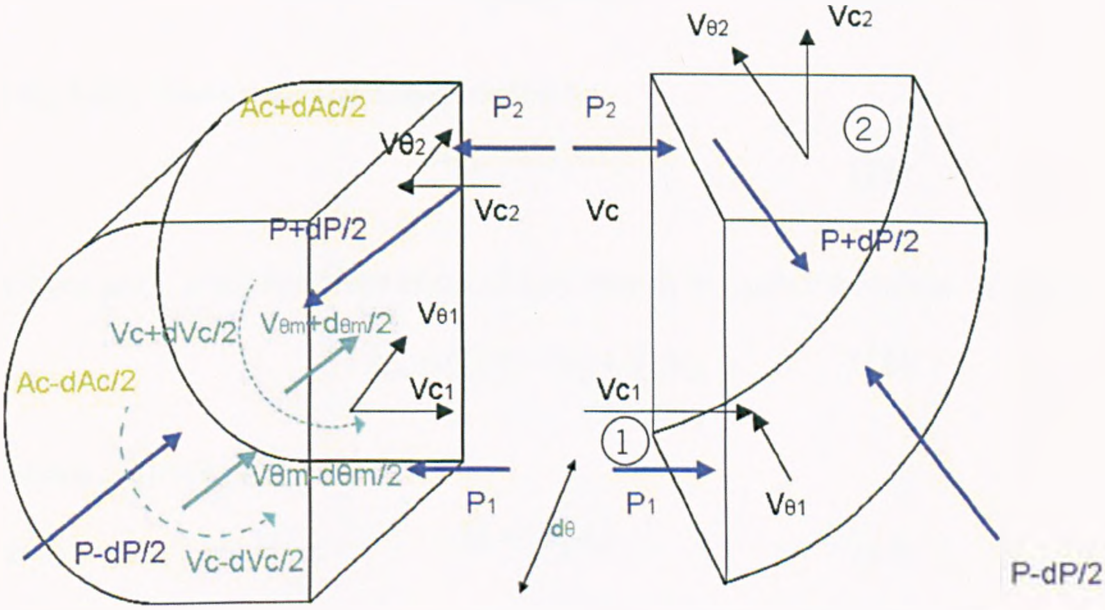

CHANNEL SECTION IMPELLER SECTION

**fig. 12** Control volume - open channel and impeller

$$v_{\theta 1} = \alpha U_1 \qquad (11)$$

$$v_{\theta 2} = \sigma U_2 \qquad (12)$$

Where

W = Tangential Velocity

U = Impeller velocity

V = absolute velocity of the fluid

$\sigma$ = Slip factor

$\alpha$ = shock factor

$\omega$ = angular speed in radians per unit time

$Q_s$ = Flow due to solid body rotation = $\omega r_g A_c$ (13)

In figure 12 the circulatory velocity at point 1 and 2 is assumed equal thus

$$V_{C1}=V_{C2}=V_C \qquad (14)$$

Circulatory flowrate can be approximated by:

$$dQ_c = C_r V_c dX_g \qquad (15)$$

Where $gH_{cb}$ is the head loss of circulatory velocity through the impeller region.

$$V_{\theta m} = Q / A_c = (V_{\theta 1} + V_{\theta 2})/_2 \qquad (16)$$

Where $r_g=0.5(R_{tip}+R_{hub})$

Where $$Q_s = \omega r_g A_c \qquad (17)$$

Where $gH_{cc}$ is the head loss associated with circulatory velocity through the channel region

Wilson et al. (1955) and others showed that:

$$\frac{Q}{dQ_C} v_c dV_c = \left(1 - \frac{Q}{Q_s}\right)(U_2 V_{\theta 2} - U_1 V_{\theta 1}) - gH_c \qquad (18)$$

Where $gH_{cc} + gH_{cb} = gH_c$ is the sum of the head losses related to the circulatory velocity **and are corelated to experimental data with correction factors.**

Clearly the models presented are limited due to their reliance on empirically based loss correlation, and also the one dimensional approach to solving the governing equations. Critically it will be shown that, due to the effect of these losses (shock and slip) in the overall performance results, particularly at the "off-design" conditions i.e. high and low flowrates as an alternative approach to predicting the flow is presented in this study. At this stage it is worth considering typical performance characteristics for regenerative pumps.

## 2.8 Performance Characteristics

The ability of the regenerative flow pump to produce higher pressure ratios than that of centrifugal or axial flow machines for a given impeller tip speed is detailed by Hollenberg et al. (1979).

There are three main characteristics in the performance of regenerative pumps.

1. They have relatively low efficiencies, Song et al. (2003)
2. They develop high power consumption at off-design conditions, Volk (2005)
3. They develop high head at low specific speeds, Wilson et al. (1955).

Comparison with centrifugal pumps, Salisbury (1982) or Ferguson (1963), is useful because both machines can operate in the low range of the specific speed band. From published data, e.g. Buse (1977), it is stated that the regenerative pump can generate a head from 2.5 to 10 times the head generated by a typical centrifugal pump with comparable diameter and rotational speed. Both regenerative pumps and centrifugal pumps are “kinetic” type pumps (fig. 3).

Both pump types generate pressure and flow from the tangential and circumferential velocities imparted to the fluid by the speed and shape of the impeller. In both pumps, pressure and flow can be modulated by throttling a discharge valve. Table 3 makes a generic comparison between regenerative and centrifugal pumps for indicative purposes.

| Single Stage | Range of (Ns) | Range of ($\phi$) | Range of ($\psi$) |
|---|---|---|---|
| Pump | $N\sqrt{\frac{Q}{H^{\frac{3}{4}}}}$ | $\frac{Q}{\omega D^3}$ | $\frac{gH}{\omega^2 D^2}$ |
| Centrifugal Pump | 10-100 | 0.01-0.02 | 0.2-1 |
| Regenerative Pump | 1-10 | 0.05-0.01 | 1-6 |

**Table 3** - General comparison of pump types

Due to their low specific speeds, regenerative pumps can replace multi-stage centrifugal pumps in some applications, e.g. aircraft engine fuel pumps and in fire appliances mobile high pressure water pumps. Regenerative pumps typically have straight line H-Q characteristic with a fairly steep gradient (fig. 13). The head capacity curve of a regenerative pump has a different shape (fig. 13). It is nearly linear and slopes downward. At low to moderate heads, the flow is typically much smaller than that of a centrifugal pump. However, the slope never approaches a horizontal plane. Therefore, throttling a valve for a regenerative pump will permit more precise changes in flow, without major overshooting or undershooting of the duty point.

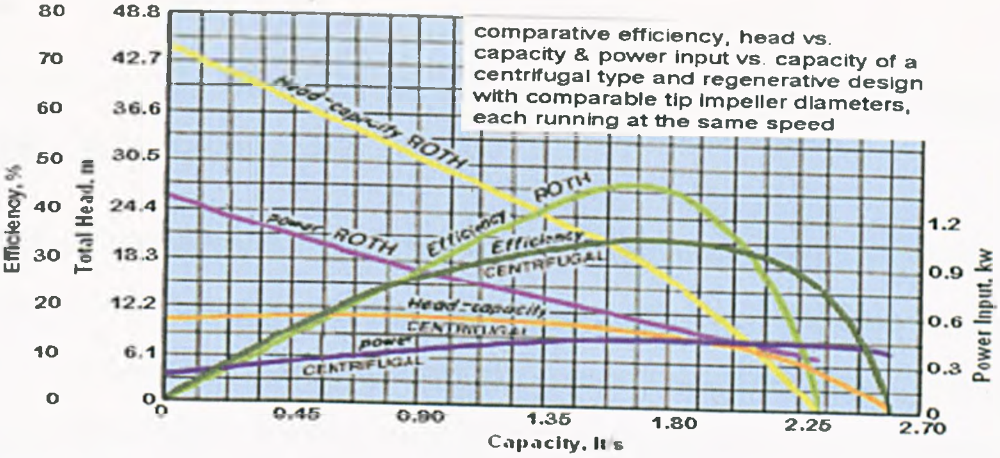

**fig. 13** Generalised pump characteristics (Roth Pumps (2006))

When compared to other pumps, e.g. axial flow, mixed flow and centrifugal pumps the regenerative pump can cover many duties (Table 1). When compared with reciprocating pumps the regenerative pump offers the following advantages. (table 4).

| |
|---|
| Continuous delivery free from pressure fluctuations, Badami (1997). |
| Will operate against a closed valve without exceeding a predetermined pressure, Bajbakov (1960). |
| They develop high head at low flowrates and relatively low shaft speeds i.e. they are applied for low specific speed operation, Wilson - (1955). |
| Can be designed to meet several duties with a defined characteristic, Raheel et al. (2005). |
| Absence of high vibration, simple construction, compact size and weight, Muller et al. (2004). |
| If the fluid supply source runs dry the regenerative pump cavity remains filled with liquid, unlike other pumps. This allows the pump to operate under dry suction conditions in this event, Song et al. (2003). |
| The regenerative pump can handle fluids with 20% entrained gasses. Under the same conditions other pumps would experience vortexing or cavitation, Volk (2005). |
| The regenerative pump is capable of reversible impeller rotation, with an accompanying reversal of the suction and discharge porting, Pfaff (1959). |

**Table 4** - Regenerative pump main advantages

## 2.9 Summary

The complex flow-field within the pump represents a significant challenge to detailed mathematical modelling.

The circulation theory is most universally accepted, and supports the helical or corkscrew flow motion observed within the pump. Although the turbulence mixing theory can have some interesting applications, experimental testing on regenerative pumps have observed the fluid flow in its helical circulatory motion induced by the centrifugal field.

Published mathematical models are limited due to their reliance on empirically based loss correlation, and the one dimensional approach to solving the governing equations. Indeed some terms, for example contraction losses, are not adequately considered and are grouped with the shock loss term. Slip correlations are based on centrifugal devices where there is no tangential energy gradient and thus cannot apply to regenerative pumps which are designed to develop tangential pressure gradient. The objective of the current study is to apply 3D numerical techniques to not only resolve the complex flow field, but to also compare the predicted results with new experimental testing. The numerical results are compared to not corrected with experimental testing.

# Chapter 3

## Experimental work

### 3.1 Introduction

As outlined in Chap. 2, previous mathematical modelling for the regenerative pump have limitations for accurate performance prediction. These models required extensive experimental correction, particularly at off-design conditions Song et al. (2003). In this thesis the CFD results were not corrected by, but only compared with, experimental data to evaluate how representative of the pump flowfield they were. A range of performance data was obtained to allow, not only the modelling domain to be defined, but also to evaluate the accuracy of the CFD model predictions at those performance points. If a CFD model could be made representative enough to accurately predict performance, particularly across a range of points, then this would not only be a critical advancement in the knowledge of the flowfield within the pump but would also be useful as a tool to optimise regenerative pump design to increase the performance (Chap. 6). This Chapter sets out the experimental procedure used for obtaining the required test data, and describes a novel manufacturing technique used in the production of the optimised blade impellers.

### 3.2 General Arrangement

The experimental rig, (fig. 14), was a closed loop arrangement, where a reservoir tank stores and ultimately receives the working fluid, in this case water. The fluid was drawn to the pump from the tank through an inlet flow valve. The fluid flowrate was measured using a hall effect turbine flowmeter situated downstream of the inlet flow valve and upstream of the pump.

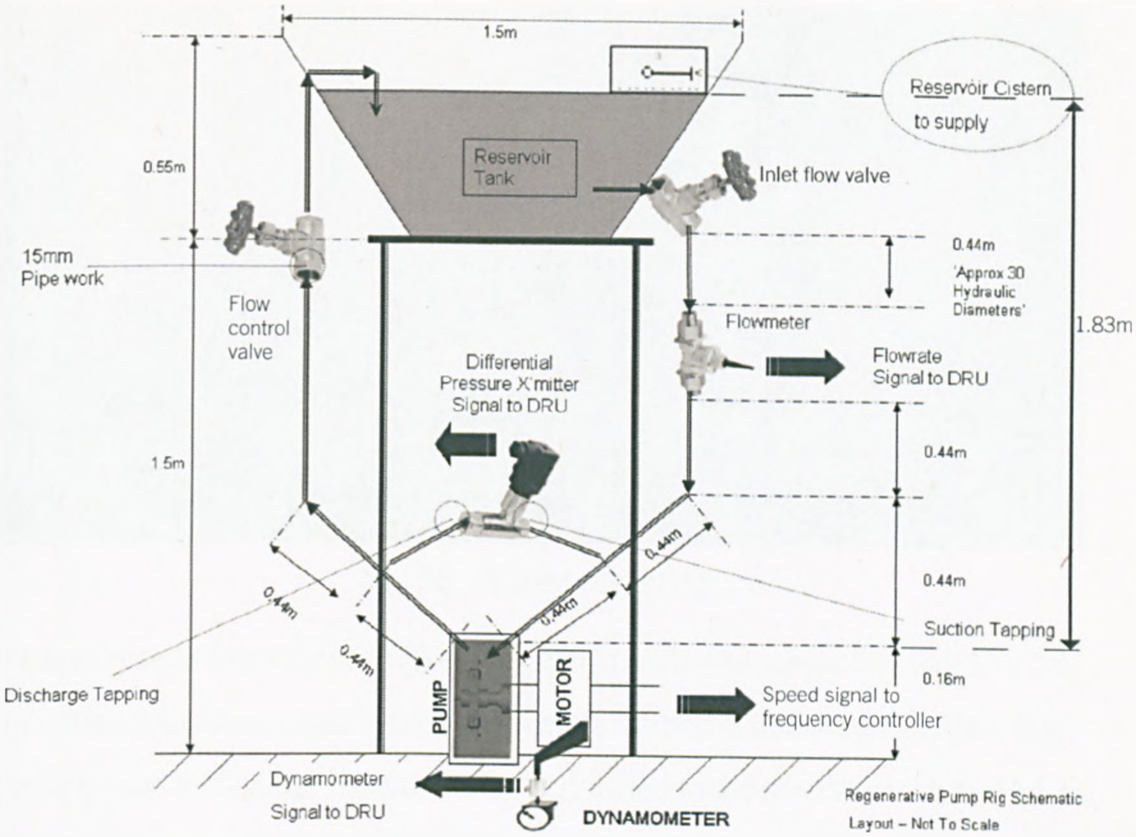

**fig. 14** Experimental test rig schematic

The pump itself was driven by a 3kW induction motor operating at a constant speed of 3000rpm. The motor housing was coupled to a dynamometer containing a load cell to measure strain and hence deduce input torque to be used for pump efficiency calculations. The loadcell strain measurement was calibrated against force and was converted to a reaction torque. The fluid flowrate was adjusted via the flow control valve metering the flow to allow a range of measurements to be taken to develop a performance operating characteristic. For the range of flows the corresponding pump inlet / outlet pressures and input torque values were measured.

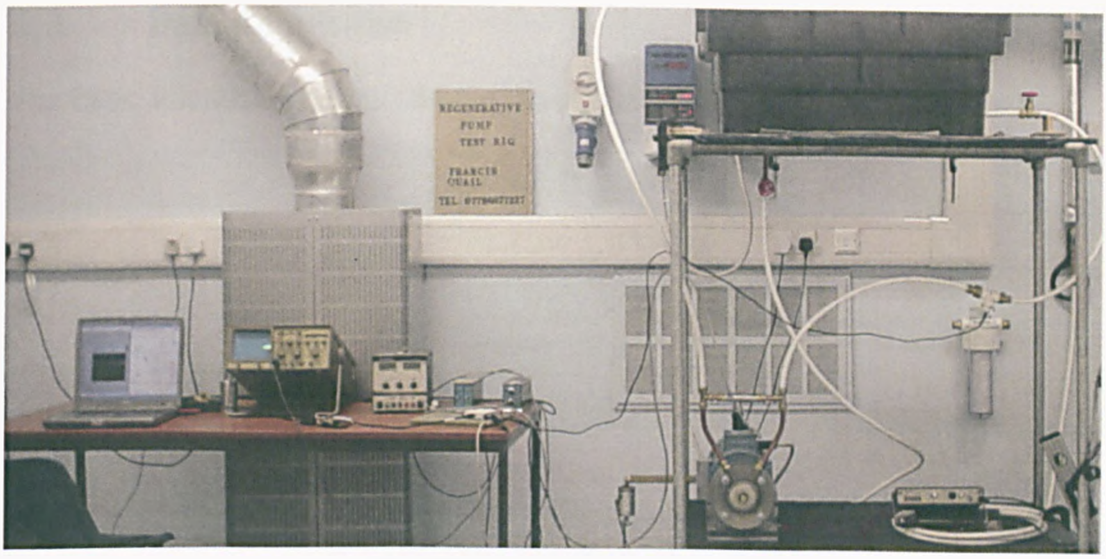

**fig. 15** Experimental rig

The supply tank was located 1.83 m above the pump inlet centre line (fig. 15). The downstream valve was used to provide a simple method of obtaining a variable head characteristic for testing. The pump was connected to the reservoir tank by 15mm supply and discharge lines. The outlet from the inlet flow valve ran to the inlet of the flowmeter which then ran into the pump inlet port. The back pressure on the discharge line was obtained by closing and opening the flow control downstream of the valve nearest to the pump discharge. Back pressure and flowrate was varied by closure of the valve in the discharge line. A range of measurements were taken to establish the head – flowrate characteristics at the constant running speed of the pump.

In the rig arrangement, (fig. 15), measures where taken to minimise effects which could reduce the inlet pressure to the pump. Selection of optimal inlet line length and bore were considered, as well as pump elevation and the effect of upstream discontinuities, (bends, contractions etc), that can reduce pump inlet pressure. Regenerative pumps, typically, require lower net positive suction heads, (NPSH) than other kinetic pumps, Muller (2004). Indeed as detailed later in Chapter 3.7 the lowest NPSH requirement for the pump was estimated to be 0.25m, Appendix A.

## 3.3 Data Acquisition

The basic quantities measured from the instrumentation are listed in table 5:

| |
|---|
| Suction Pressure |
| Differential Pressure |
| Rotational Speed |
| Power Input |
| Flowrate |

**Table 5** - Data acquired

The National Instruments USB - 6008 Data Acquisition Card (DAC) was used in the testing. The NI USB-6008 provides connection to eight analogue input (AI) channels, to analogue output (AO) channels and a 32bit counter when using a full speed USB interface. The USB 6008 has 1 analogue to digital convertor (ADC). The multiplexer roots 1 (AI) channel at a time to a programmable gain amplifier (PGA), that provides the input gains. The PGA gains are automatically calculated based on the voltage range measured. A lap top computer Windows XP operating system was used in the tests with National Instrumentation LABVIEW 8.5 (2007) to develop a programme that works with the NI DAC and stores data onto the computer hard disc.

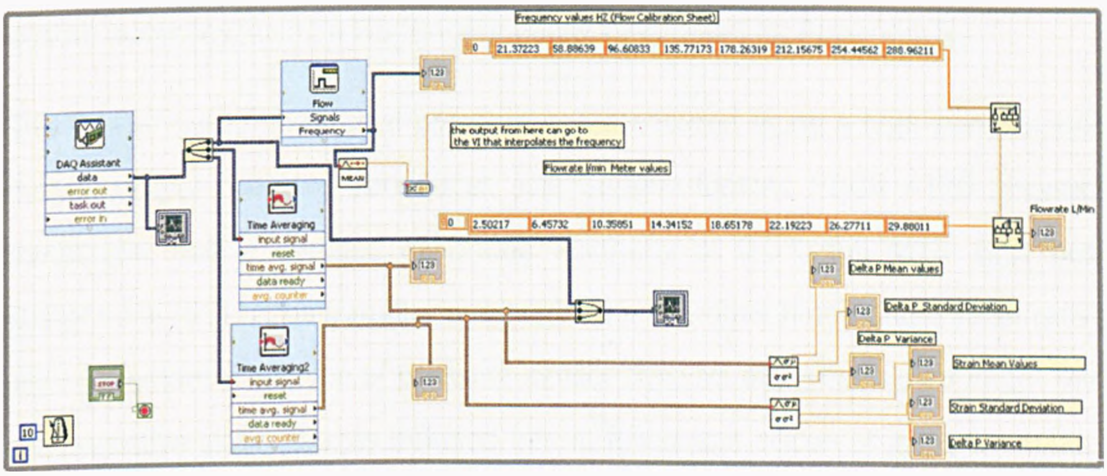

the output from here can go to
the VI that interpolates the frequency

**fig. 16** Schematic of data acquisition arrangement

Figure 16 shows the LABVIEW programme block diagram. In the test, the USB 6008 is connected to the lap top via a lap top USB port. The system records the data simultaneously from the input sensors. The sample mode on the timing function was set to continuous samples which specified the task acquired samples until stopped. The sampling rate of 1K (Hz) was set and the sampled data was averaged and stored to the hard disc. The signals from all sensors was monitored simultaneously and the recorded data was imported to a spreadsheet for analysis. The pressure, strain and flowrate sensors were calibrated by the manufacturers. Most measurement devices are designed for measuring or reading voltage. Estimation of the uncertainty of these measurements are detailed in Appendix A.

The pump suction pressure was measured using a combination pressure / vacuum gauge fitted on the inlet side above the pump centre line. The Bourdon gauge used essentially a coiled tube which, as it expands due to pressure increase, causes a rotation of an arm connected to the tube. Aneroid gauges of this type are based on metallic pressure sensing elements which flex elastically under the effect of a pressure difference across the element. The deflection of the pressure sensing element was related by a linkage connected to a needle and calibrated to a dial to indicate gauge pressure. It was necessary to determine the pump inlet pressure and so assess the cavitation margin. The gauge was calibrated prior to testing to ensure accuracy, using a Budenberg gauge calibration rig Appendix B.

The overall pump differential pressure was measured using a high performance milivolt output pressure transducer. The General Electric PDCR 4170 pressure transducer had a certified calibrated accuracy of 0.6% full scale (FS) best straight line (BSL). The transducer contained a micromachined pressure sensitive silicon element. This type of pressure sensor consists of a silicon diaphragm with piezoresistive strain gauges diffused into it, fused to a silicon or glass backplate. The resistors are connected as a wheatstone bridge, the output of which is directly proportional to the pressure.

A Calibration test was conducted prior to testing and an estimation of ± 0.6% was calculated appendix A.

The ABB MT100L28-2 MK 110011-5 model 3 phase Induction motor was connected to a IMO Jaguar CDII550 frequency controller. Certificate of calibration results indicated at 50hz the motor ran at 2890 rpm and at 60hz the motor ran at 3470 rpm. The speed controller was set at 51.9 hz to maintain a constant 3000 rpm running speed. To ensure this during a loading cycle, separate calibration tests were conducted where a hand held tachometer was connected to the impeller shaft during testing. As the pump was run through a performance curve, readings were taken to ensure a constant speed of 3000 rpm was maintained throughout the tests. The tachometer was separately calibrated by techniques with an accuracy estimation of ± 0.05% (fig 17).

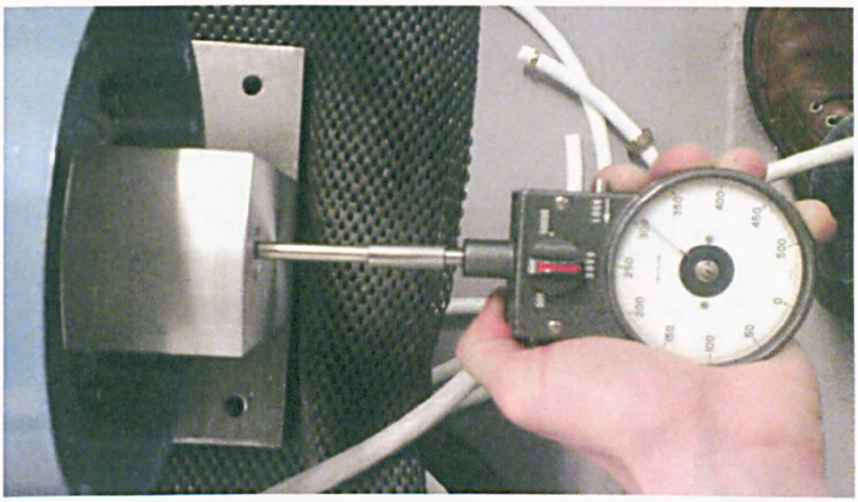

**fig. 17** Tachometer speed check of running pump.

The motor housing was coupled to a dynamometer containing a load cell to measure strain and hence indicate the input torque to the pump for use in pump efficiency calculations. The loadcell strain measurement was calibrated using weights and, knowing the torque arm, was converted to a reaction torque to indicate the Power input to the pump (fig. 18), Appendix A.

The canister loadcell ETHER type UF2 was calibrated prior to testing by hanging known weights from the bottom dead centre anchor point (fig 18). After hanging the weight the deflection (strain) mV signal is recorded from the strain channel (AIO) in mV. A range of recordings were taken from 0g applied load to 400g applied load. The torque arm for the load cell was determined from the centre line, the measurement from the bottom dead centre anchor point to the impeller shaft centre. In this way the running characteristic strain measurement mV could be converted to an equivalent applied load and, hence, the force action through the measurement torque arm could be assessed as a torque, and hence power input to the impeller. A sample calculation is contained within Appendix A. The calculated uncertainty after repeatability tests were conducted was determined to be ± 4.3%

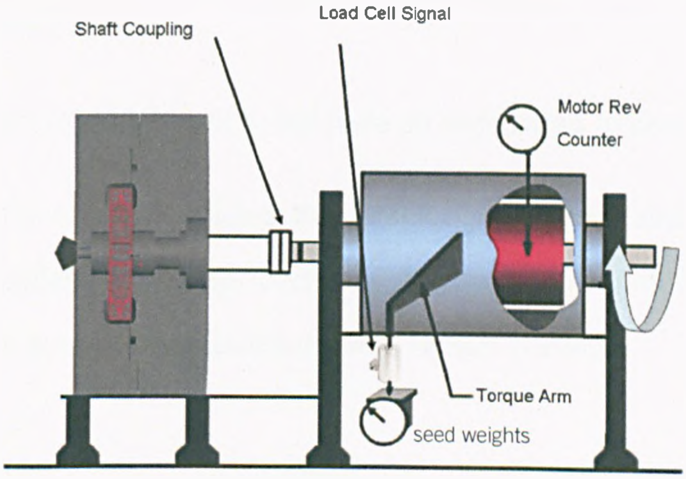

**fig. 18** Loadcell arrangement

Flow was measured using an RS Components V10981 Hall Effect flowmeter, in which the fluid flow is directed to an axial turbine wheel in a measuring chamber. The rotation of the rotor is detected with a Hall Effect sensor. A Hall Effect sensor is a transducer that varies its output voltage in response to changes in magnetic field. Hall sensors are used for proximity switching, positioning, speed detection and current sensing applications. The output frequency of these pulses is directly proportional to the flowrate and the total number of pulses the total volume passed. All turbine flowmeters require a fully formed up-stream flow profile. Care was taken to locate the flowmeter in a straight length of pipe some distance from any component that could introduce an asymmetric or swirling velocity profile. The manufacturer recommended a length of 30 pipe diameters.

The manufacturer quoted accuracy (non-linearity, repeatability, hysterosis) at ±5% FS. A calibration test was conducted prior to testing and an estimation of ±5% was calculated Appendix A.

## 3.4 Sources of error in test results:

The measurements were collected using a data acquisition unit and pump characteristic (flow, head, power and efficiency coefficients) were calculated as detailed in Appendix A.

Every independent measurement $X_i$ will have an associated uncertainty $\xi x_i$.

When measurements are combined the "stack-up" of uncertainties determines the final experimental uncertainty. To estimate the overall experimental uncertainty $\xi_R$, the root of the sum of the squares is used, Kirkup (1994)

$$\xi_R = \pm\sqrt{\Sigma(\delta_i \xi_{x_i})^2} \tag{19}$$

Where R is the dependent variable of interest, i, is the index representing the measured variable and $\delta_i$, the sensitive coefficient of R with respect to $X_i$ given as:

$$\delta_i = \frac{\delta R}{\delta X_i} \tag{20}$$

*For pump efficiency, input power and head we have:*

$$\xi_\eta = \pm \rho g \left[ \left( \xi_Q \frac{H}{P} \right)^2 + \left( \xi_H \frac{Q}{P} \right)^2 + \left( \xi_P \frac{QH}{P^2} \right)^2 \right]^{1/2} \qquad (21)$$

A calculation procedure for estimation of the uncertainty in the instrumentation is detailed in Appendix A. For a standard radial blade case of the regenerative pump, a 5% error was determined for the flowrate, a 0.6% error for the head and 4.3% error in the power calculation. Applying equation (21) this equates to a pump efficiency error of 6.6% (Appendix A). Whilst the random scatter was evaluated from repeatability tests and sensitivity analyses, the systematic inaccuracy due to aggregate systematic errors in transducers and changes in performance due to build-to-build differences are difficult to evaluate, Woollatt et al. (2005). To achieve this, it is essential that the data acquisition system incorporates procedures which evaluate the quality of the data as it is acquired, and that on-line analysis tools are in place, to allow comparison of the actual data with expected, and, if necessary, analysis of the raw measurements to verify accuracy. As indicated in figure 16 the National Instruments software was used to build a virtual instrument that filtered the raw data to assess it's quality. Time averaging and mean/standard deviation and variance calculation capability was included in the programme.

### 3.4.1 Measurement Uncertainty Comparison

The uncertainty results of the analysis are dependent upon the accuracy of the instrumentation that is used to make the efficiency measurement.

In this study the pressure and flow sensor manufacturer calibrations are assumed. A calibration test was conducted for the loadcell during the current study to verify the load/strain relationship as part of the operation for the dynanometer.

It is common for differential pressure transducer to have an accuracy of within ±0.6% Wulff (2006). The accuracy was estimated to be 0.6% Appendix A. The

ETHER UF2 loadcell calibrated by the direct application of weights (dead weight calibration), Appendix A.

Casada (1999) pointed out that flowrate is usually the most difficult parameter to measure when assessing pump operation. Flow meters are usually capable of measuring volumetric flow rates with an accuracy range of ±5% of full-scale readings. Lindsay, et al. (1994). A repeatability test was conducted on the flowmetre and the accuracy of the RS VI0981 flowmeter estimated to be ±5% Appendix A.

Having conducted a loadcell calibration of the Ether UF2 loadcell, Appendix A, it was estimated the uncertainty in the device was in the order of 4.3%. Dynamometers are typically within ±5% of full-scale readings; (as detailed by), Martyr et.al (2007)

Shaft speed for the motor was controlled directly by the IMO controller. The accuracy of this was determined in a calibration test using a hand held tachometer. The tachometer had itself been calibrated to ±0.06%. According to Doebelin et al. (1990), typical shaft speed accuracy can be of the order of ± 0.06% of full-scale readings which is essentially a negligible error. In this study, we will follow Doebelin's reported accuracy and consider the error negligable

Similarly considering the uncertainty in the dimensionless expression detailed in Chapter 5 and applying the root of the sum of the squares, kirkup (1994) the following can be determined:

Dimensionless coefficient of flow $\phi = \frac{Q}{\omega D^3} \quad - \quad \xi_\phi = \pm 5\%$

Dimensionless head coefficient $\psi = \frac{gH}{\omega^2 D^2} \quad - \quad \xi_\psi = \pm 0.6\%$

Dimensionless coefficient of flow $IP = \frac{P}{\rho \omega^3 D^5} \quad - \quad \xi_{IP} = \pm 4.3\%$

## 3.5 Test Procedure

The pump casing was attached to the rig support frame and the impeller shaft was coupled to the motor drive shaft. Ensuring that the pump components were clean and assembled to close tolerances, the pump was then checked for freedom of movement (Figs. 19, 20).

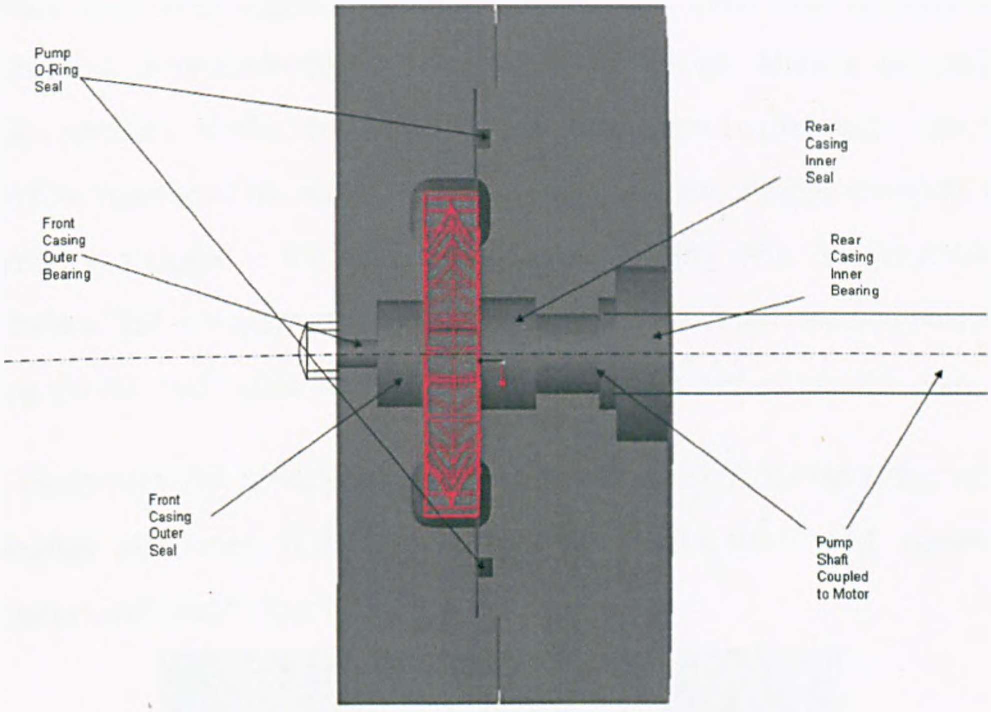

**fig. 19** Pump assembly

It was important to avoid running the motor dry with the close tolerances (particularly across the stripper region (fig 25) as the impeller could make contact with the casing leading to wear damage and performance loss. The level in the water tank was maintained at 1.83m (6ft) above the pump inlet. This suction head was constant throughout the pump tests. In order to ensure this value, the reservoir contained a cistern arrangement fig. 14, which maintained a constant tank level. The system tank level of 1.83m relates to the distance from pump inlet to the reservoir tank fluid surface level. A clearly visible witness line feature in the tank interior was used to indicate this point . The main water feed to the tank was turned on if required to bring the tank to this level prior to each test. The inlet flow valve to the reservoir was then opened to allow water to flood the pump. The flow control valve on the pump discharge line was fully opened so that the full flowrate would be passed through the pump. The motor was then started and run up to test speed of 3000 rpm (51.9hz). The pump flow control valve was then gradually closed and the corresponding readings recorded. The National instrumentation software recordings logged for strain, flowrate and differential pressure were continuously recorded throughout the test via the NI DAC. Manual recordings of suction pressure, shaft speed and tank level were taken as previously described. From fully open until the appropriate shut valve position, a range of results were obtained and logged in the data acquisition system (fig. 16). One advantage of this form of test arrangement was that the level of fluid in the reservoir never falls during the test and hence the pump is operating to a constant suction head.

The measurements collected from the data acquisition unit and the manual recordings were used to develop pump characteristic flow, head, power and efficiency coefficients Appendix A.

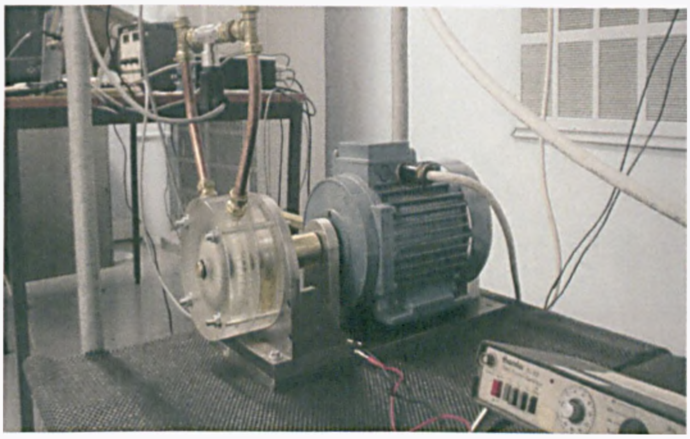

**fig. 20** Pump coupled to motor

Before any testing was conducted, great care was taken to ensure that the system was assembled properly. All the clearances were checked to ensure the assembled unit was sealed and allowed free frictionless movement. To improve the design of the regenerative pump, a number of changes were taken, including:

## The Motor

Initially a single phase 220V induction type was considered. Difficulties were encountered in aligning the pump and motor shafts with consequent problems in pump casing sealing. To eliminate possible overloading, the design was changed to pump motor system as a coupled integral unit. The size of the motor was increased to a three phase, 440V induction type (fig. 20).

## The Impeller

The standard test radial impeller for the regenerative pump had 30 blades of diameter 74.5mm. The pump was a double suction shape designed with alignment of the blades to balance axial thrust. In this design the impeller has radial teeth or vanes machined into each side at its periphery (fig. 21).

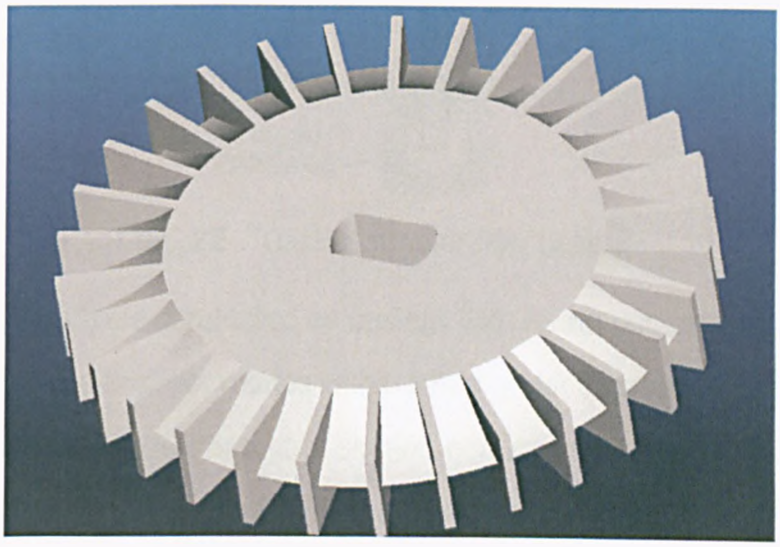

**fig. 21** Radial impeller

The tests were carried out on impellers of 12mm width. The impeller blade thickness was 1.3mm. As described earlier the test procedure was to measure flowrate, input power, suction pressure and differential pressure for a variety of mass flowrates.

Initially an impeller design was to be threaded directly to the motor shaft. With concerns about strength of the thread during testing, under loading a central insert of reinforced brass, was consequently selected. Detailed drawings are included in Appendix C.

## The Casings

Typically regenerative pumps have standard square cut design of rectangular cross-section (fig. 22), for the annular casing passage.

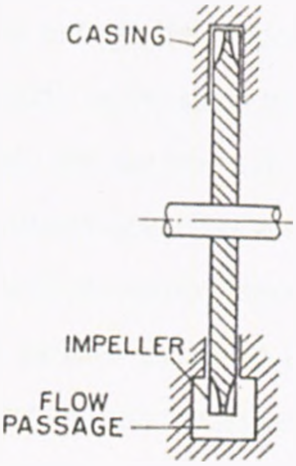

**fig. 22** Casing annular flow passage

In the study tests were conducted on casings with round cut passage profile (figs. 23, 24), where the impeller rotates within this annular passage. The fluid entered both sides of the impeller through a suction port and this design, in effect, made the unit a double suction unit. Detailed drawings are included in Appendix C.

**fig. 23** Front casing

**fig. 24** Rear casing

### Suction / Discharge Ports

The fluid entered the suction port and into the casing and flowed to both sides of the impeller. The casing had a barrier wall or "stripper" through which the impeller passes with close clearance (fig. 25). The suction and discharge flows were separated via the stripper. In this region, the open channel had a clearance of 3 mm from the sides and tip of the impeller, and allowed only fluid within the impeller (and small leakage flow) to pass through to the suction side. When the stripper is small, more work is done on the fluid due to the increased pumping region, but the leakage flow through the stripper gap from the outlet to inlet is increased, Wilson et al. (1955). In the study the stripper angle is 48° to ensure adequate separation between the low pressure inlet port and the high pressure outlet port to maintain a hydraulic seal. This prevented large scale leakage from the discharge to suction side of the pump. Although this will reduce performance head rise in the pump, as detailed by Senoo (1948), there can be significant benefits to optimising the inlet and stripper region design. Indeed Senoo indicated optimisation of the inlet port design can have as much as a 10% effect on pump efficiency.

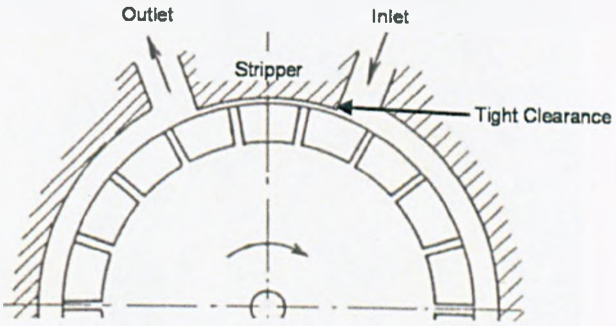

**fig. 25** Stripper detail

## 3.6 Manufacture

After production of a standard radial impeller, fig. 21, using conventional milling techniques, fig. 26, subsequent modification of the blade profiles presented a considerable challenge even for the most skilled machine operators.

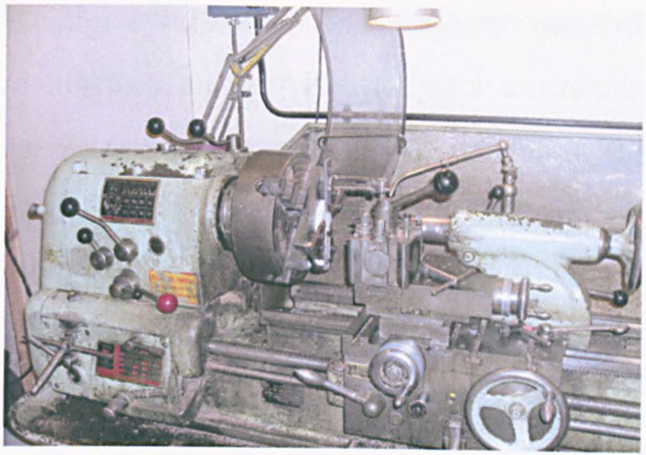

**fig. 26** Conventional radial blade machining

The complexity of the modified blade profiles, for example as shown in fig. 27, would normally have necessitated the use of expensive CNC machines with 5-axis capability. This thesis presents an accurate alternative manufacturing technique to create suitable impeller prototypes rapidly, and cost effectively, for use in experiments in conjunction with the CFD modelling. The challenge of developing a robust manufacturing process to produce the complex blade profiles was crucial to allow testing to proceed.

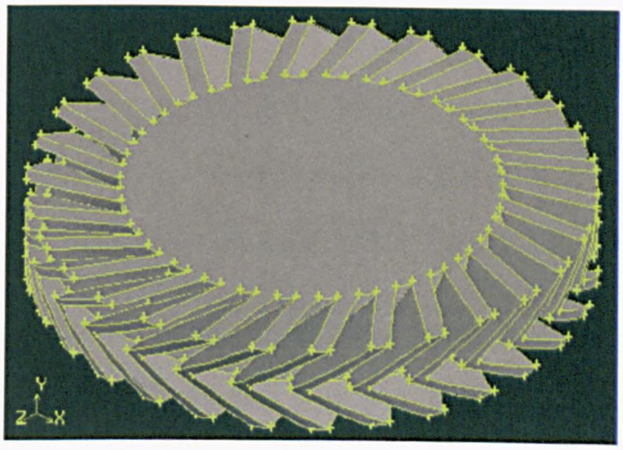

**fig. 27** Chevron blade detail

The need for manufacturing methods that can produce dimensionally accurate, small and complex parts is a challenging one. Industrial findings have indicated as much as a 3% efficiency variation can occur in manufactured pumps, IMechE fluid machinery group symposium (2007). Having determined that the baseline radial impeller (fig. 21), with parallel blade surfaces, was the limit of operator controlled milling techniques, an alternative approach was required to facilitate the production of increased complexity variants of this standard. There was a need to produce prototypes that could be manufactured quickly and cheaply, using rapid manufacturing techniques. The key technologies of rapid manufacturing (RM) are rapid prototyping (RP) and rapid tooling (RT). RP is a technology for quick fabrication of physical models or functional prototypes directly from computer aided design (CAD) data. RT involves the production of moulds and tooling inserts using RP.

Previous means of producing new impellers typically took many man-hours, large amounts of tooling, and skilled labour. For example, drawings were sent to skilled craftsmen where the two dimensional design on paper was followed and a three-dimensional prototype was produced in wood. This typically was not a speedy process with high skilled labour costs. The complexity of the blade profiles, need for strength, accuracy/surface finish and quality whilst considering the relative size, presented problems with such an approach.

In this thesis, RP systems are considered to build prototypes for the regenerative pump impeller using 4 axis milling machine, 3D printing, Fused Deposition Modelling (FDM) and FDM in conjunction with RTV process (vacuum forming).

Subtractive Rapid Prototyping (SRP), is used to describe traditional computer numerically controlled (CNC) cutting where material is removed from a solid block with a rotating cutter. In the strictest sense RP applies to both additive and subtractive processes since both create prototypes in a relatively rapid fashion. In recent years, RP has generally referred to the innovative additive processes which build up a model, one layer at a time. This additive process allows the creation of extremely complex parts that cannot be produced by traditional SRP machines. RP parts are generally created as conceptual models for designers and manufacturers to evaluate at the product development stage. RM parts are usually made for inclusion in a finished product.

The first method considered for producing the optimised blades was with 4 axis CNC Milling. CNC machines can exist in virtually any of the forms of manual machinery, like horizontal mills. A 4th axis allows rotation of machine parts. The part can be machined and then rotated, or continuously spun as it is machined. The most advanced CNC milling-machines, the 5-axis machines, add two more axes in addition to the three normal axes (XYZ). The fifth axis (B axis) controls the tilt of the tool itself. In the case of the regenerative pump impeller the set-up and fixture difficulties particularly for the nine, optimised blade configurations had to be considered. A toolpath simulation is indicated in fig 28.

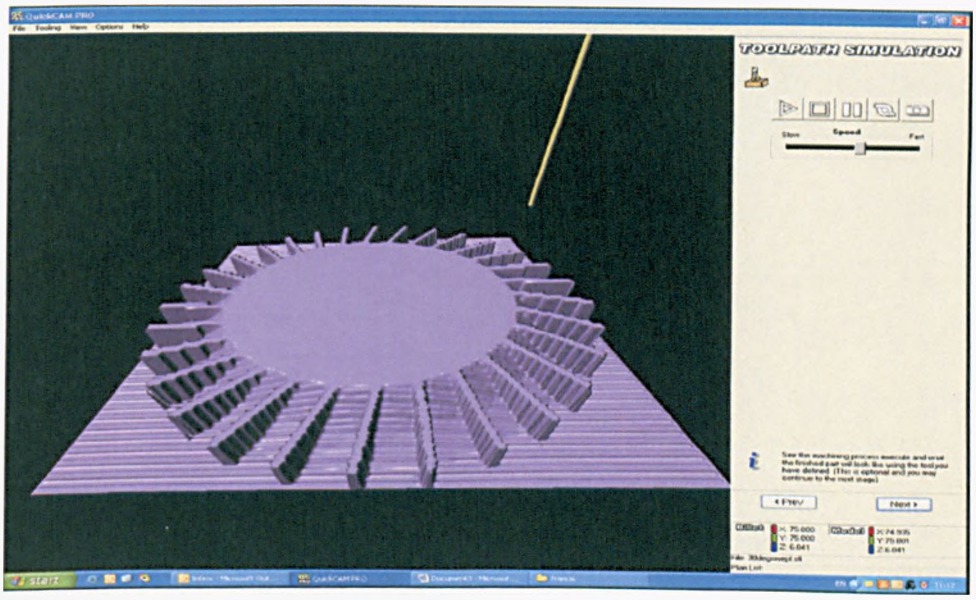

**fig. 28** CAM toolpath plot of the impeller

The Impeller would have had to be turned and refixed to allow symmetric machining. The geometry of the optimised impellers that were to be assessed contained difficult overhangs and interior volumes (between blades), that proved problematic for the four axis machines. The need to machine one side of the components (fig. 29), then turn the component across a split line and continue machining, would introduce repeatability and alignment issues for the operator. This would increase manufacturing time and would have been a source of possible error and was hence discounted as a production method.

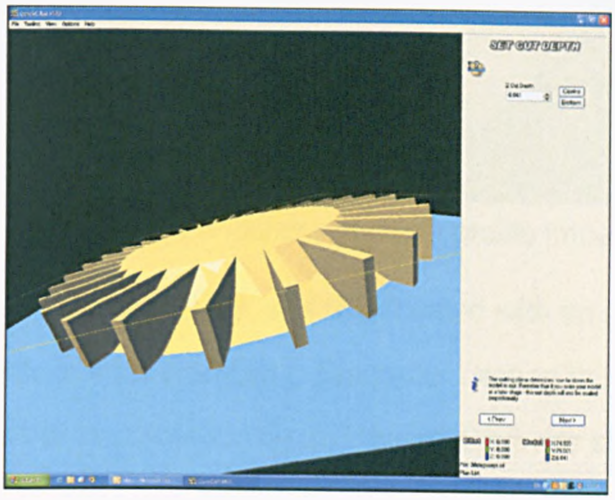

**fig. 29** CAM tool splitline plot of Impeller

The next method to be considered was 3D printing rapid prototyping technology, using a Z Corporation Z402 3D printer. A three dimensional object was created by layering and connecting successive cross sections of material. 3D printers are generally faster, more affordable and easier to use than other additive fabrication technologies. Layers of a fine powder (plaster, corn starch, or resins) are selectively bonded by "printing" an adhesive from the inkjet printhead in the shape of each cross-section as determined by a CAD file (figs. 30, 31).

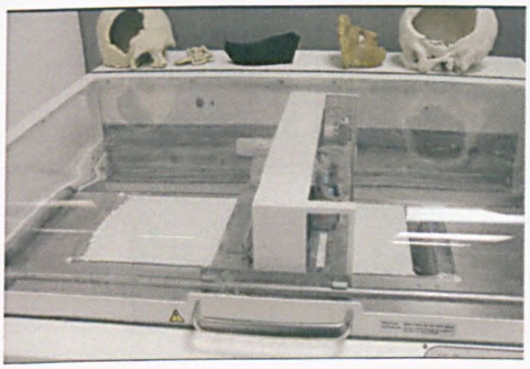

**fig. 30** 3D- printer

**fig. 31** Bonded shape impeller laydown

**fig. 32** Printed impeller - chevron profile impeller

The finished printed impeller fig. 32, was then coated with an infiltration material to prevent the structure from crumbling. Even after coating the specimen proved too fragile to test in the experimental rig and this method was also discounted.

The next process to be considered was Fused Deposition Modelling (FDM) using a Stratasys SST machine. FDM systems consist of two movable heads (one for building the part and one for the supports) which deposit threads of molten material onto a substrate (fig. 33). The material was heated just above its melting point so that it solidifies immediately after extrusion and cold-welds to the previous layers. When the first layer is complete, the platform lowers by one layer thickness and the process begins again, (0.1mm).

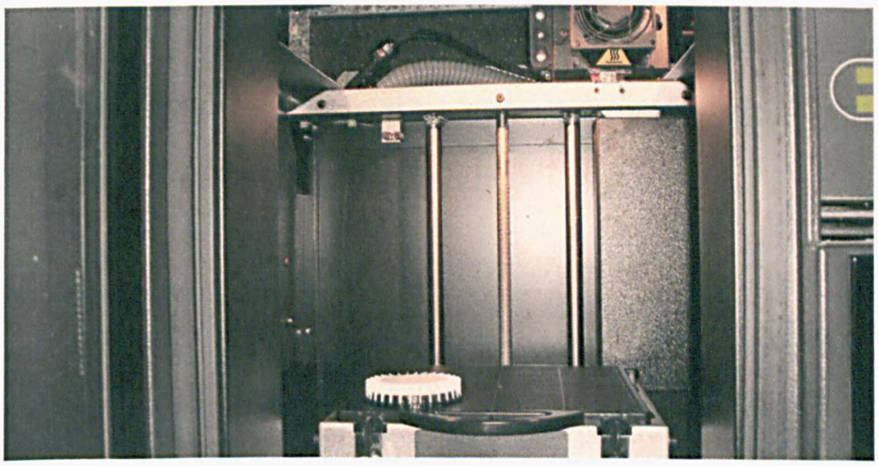

**fig. 33** FDM impeller production

The part was removed from the platform, the supports were removed and the specimen was ready. (fig. 34)

**fig. 34** FDM impeller

The technology was developed by S. Scott Crump in the late 1980s and was commercialised in 1990. The FDM technology is marketed commercially by Stratasys (2001), which also holds a trademark on the term.

Several materials were considered with various strength and temperature characteristics. As well as acrylonitrile butadiene styrene (ABS) polymer, the FDM technology can also be used with polycarbonates, polycaprolactone, polyphenylsulfones and waxes. A “water-soluble” material was used for making temporary supports while manufacturing was in progress (brown support material indicated in fig. 34). Marketed under the name “WaterWorks” by Stratasys (2001) this soluble support material was dissolved in a heated sodium hydroxide solution with the assistance of ultrasonic agitation.

ABS, ($C_8H_8 \cdot C_4H_6 \cdot C_3H_3N$) n, is a common thermoplastic used to make light, rigid, molded products such as golf club heads (due to its good shock absorbance). It is a copolymer made by polymerizing styrene and acrylonitrile in the presence of polybutadiene. The proportions can vary from 15 to 35% acrylonitrile, 5 to 30% butadiene and 40 to 60% styrene. The advantage of ABS is that this material combines the strength and rigidity of the acrylonitrile and styrene polymers with the toughness of the polybutadiene rubber. The most important mechanical properties of ABS are resistance and toughness. A variety of modifications can be made to improve impact resistance, toughness, and heat resistance. The impact resistance can be amplified by increasing the proportions of polybutadiene in relation to styrene and also acrylonitrile, although this causes changes in other properties.

The FDM part was produced using ABS and run on test. However the impeller blades broke apart (fig. 35) and, after close inspection, it was observed that the extruded material had small voids across the blade thickness. This was due to insufficient material lay down as a result of the relative blade size and not material weekness. This method was discounted as a direct solution to production of the blades.

**fig. 35** Failed FDM impeller

Of the processes described, only the FDM process was able to produce a specimen for test, although it consequently failed. To produce a mechanically stronger impeller, FDM in conjunction with vacuum forming was next considered. RT, as previously mentioned, involves the production of moulds and tooling inserts using RP. Room temperature vulcanizing (RTV) is a relatively inexpensive and fast way to fabricate prototype or pre-production tools. RTV tools are also known as silicone rubber moulds. The most widely used form of RTV moulding is vacuum casting (fig. 36). The range of materials with improved strength characteristics and the ability of better filling of the impeller profile to prevent voids made RTV attractive. A porous or vented silicon rubber mould was used and was placed on a table or container where vacuum was applied. The liquid to be cast was driven into the mould by atmospheric pressure, while the vacuum also removes trapped air that would otherwise impede the free flow of the liquid casting material, and hence create voids.

**fig. 36** RTV mould containing impeller

Vacuum Casting was widely used for producing accurate silicone tools for casting parts with fine details and very thin walls. Vacuum castings are precise replicas of the patterns, dimensionally accurate with all profiles with surfaces faithfully reproduced.

The main difficulty until this point had been producing impellers with such small dimensions that could be produced mechanically strong enough to survive the fluid loading within the running pump.

The vacuum casting process includes the following main steps:

The first step was to produce a pattern using the RP process (FDM in this case) (fig. 33)

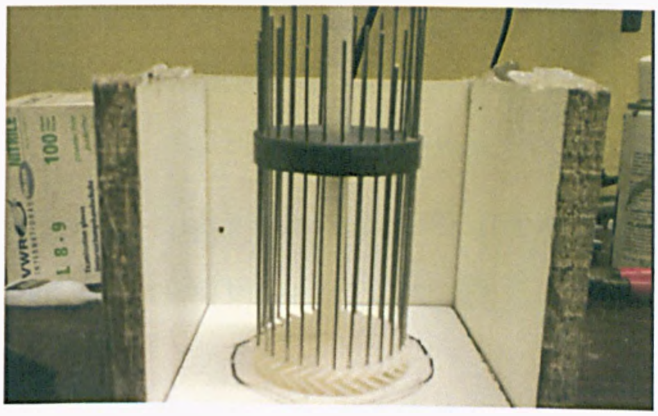

**fig. 37** Gated vented FDM blade

The impeller blade with a chevron profile shown here was prepared by adding venting and gating to the pattern; this was needed, as the vacuum is imposed during casting, to allow air to escape (fig. 37).

**fig. 38** Suspension and parting of master pattern

The pattern was fitted with a casting gate and set up on the parting line, and then suspended in a mould casting frame. The pattern needed to have adequate mould material on all sides and still have the parting line identifiable to facilitate removal (fig. 38).

**fig. 39** Mould pouring

Once the two-part silicone-rubber was de-aerated and mixed, it was poured into the mould casting frame around the pattern. (fig. 39)

**fig. 40** Pattern removal

After curing the mould inside a heating chamber, the next stage was the removal of the pattern from the silicone mould by cutting along the parting line and then closing and sealing the mould; (fig. 40)

The computer-controlled equipment mixes and pours the resin inside the vacuum chamber. As this takes place in a vacuum, the mould was filled completely without leaving any air pockets or voids. The MCP vacuum casting system requires initial investment in a vacuum chamber with two sections.

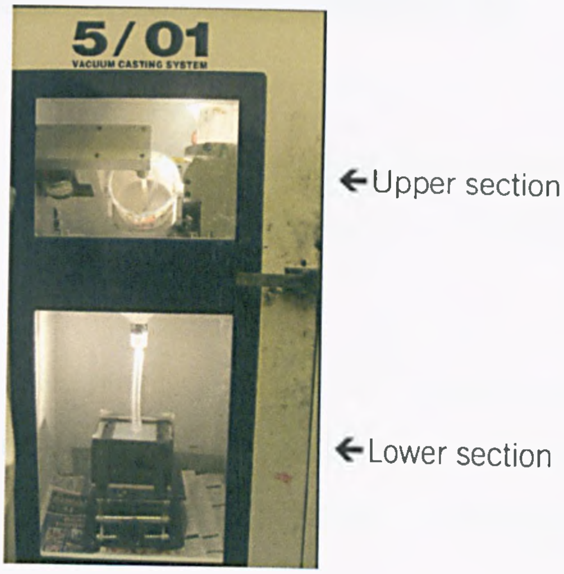

**fig. 41** Vacuum casting impeller

The upper section was for mixing the resin and the lower was for casting the resin into the mould. (fig. 41)

**fig. 42** Impeller mould

After casting the resin, the mould is moved to the heating chamber for between two to four hours to cure the urethane part. (fig. 42).

**fig. 43** Removing gate risers

The gate and risers were removed from the casting to make an exact copy of the pattern. After hardening, the casting was removed from the silicone mould. (fig. 43)

The use of RT technology enabled prototype production impellers to be fabricated with significantly reduced time frames. The success of the methodology has lead to further, more complex, blade profiles being assessed in the experimental test procedure.

Rapid prototyping techniques are extremely useful in helping the pump designer to conduct preliminary testing on a low-cost prototype. Based on the results obtained, the ability to modify or improve the designs before resorting to more costly fabricating methods has proven extremely beneficial in this current research.

The results have shown that FDM/RTV was a viable and feasible method of producing prototypes for testing (fig. 44). Further refinements of the technique are currently being pursued so that, for example, surface finish is enhanced for the parts produced.

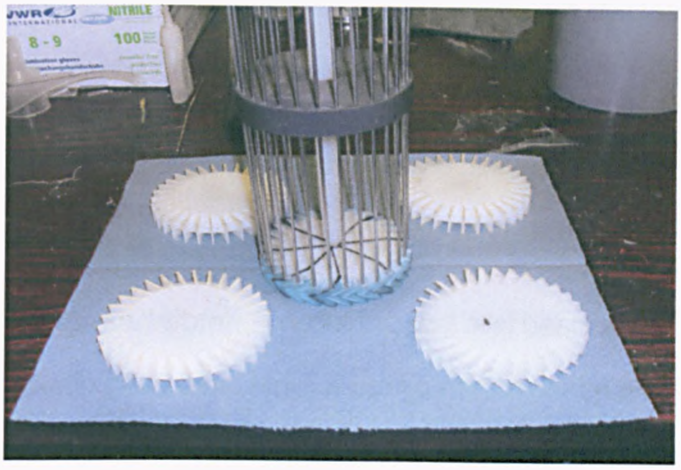

**fig. 44** RM complex blade profiles

## 3.7 Manufacturing Accuracy

The completed FDM patterns where checked for dimmensional accuracy and found to be within 0.1mm (0.005") of the drawing spec. This is equivalent to one layer of extruded material. This is in agreement with a published accuracy report, Grimm (2005), indicating expected accuracy to within ±0.2%.

Similarly for the RTV process the molded component was also tested for dimmensional accuracy and compared to drawing and was found to be within 0.1mm (0.005"). This also compares favourably with research conducted by Rahmati et al. (2007) for RTV accuracy which likewise found expected accuracy to within ±0.2%

## 3.8 Cavitation effects:

Cavitation or vaporisation is the formation of bubbles inside the pump. This may occur when the fluids local static pressure (which is dependant upon the local speed of the fluid) becomes lower than the fluids saturation pressure at the local temperature. Vaporisation itself doesn't cause any damage, however, when the velocity is decreased and pressure increased, the vapour will evaporate and collapse. During this collapse high velocity water jets impinge on surrounding surfaces. The force of this impingement often exceeds the mechanical strength of the impacted surface and can lead to:

Material loss/erosion of blade surfaces especially when pumping water based fluids.

Increase in noise and vibration reducing seal and bearing life. Partial chocking of impeller passages which reduce pump performance and can lead to total head loss in extreme cases.

In considering the regenerative pump rig (fig. 15) two situations could clearly reduce cavitation margin.

Having the pump located at a level close to the fluid reservoir tank.

Pumping the fluid through long pipe runs with small internal bores, multiple pipe losses, (elbows, bends, fittings) and pump inlet design features.

Net positive suction head (NPSH) indicates how much the pump suction pressure exceeds the fluid vapour pressure and is a characteristic of the system design. Typically, pump manufacturers measure NPSH in a test rig similar to that of figure 15. The system is run in a closed loop where flow, total head and power are measured. In order to provide low NPSH, a vacuum pump can often be used to lower the pressure in the reservoir tank which will provide a low pressure at pump inlet. The pressure in the reservoir tank is lowered until a drop of 3% of the total head is measured, when this occurs the NPSH is calculated and recorded as the NPSH for that operating point. Heating coils can also be used, which increase the water temperature thereby increasing the saturation pressure and lowering the NPSH as required. In the study the rig was arranged to try and minimise effects which would reduce the pump inlet pressure. The rig pipe work was increased to 15mm diameter lines and the length of the runs was reduced particularly on the feed side to the minimum lengths indicated in figure 15. This meant that the inlet line was kept below 2m, however, sufficient length between measuring devices and discontinuities was maintained as per manufacturer recommendations (fully developed flow) diameter lengths. Similarly, as detailed in figure 15, the tank surface level was not permitted to exceed a maximum of 1.83m (6ft).

Regenerative pumps typically require low NPSH. Under similar conditions other kinetic pumps would require an additional 6 to 8 times NPSH to operate adequately Muller (2004). Under similar conditions as was conducted for the current study a centrifugal pump would have experienced cavitation. The results for the current study indicated the lowest NPSH requirement for the pump was 0.25m fig. 45.

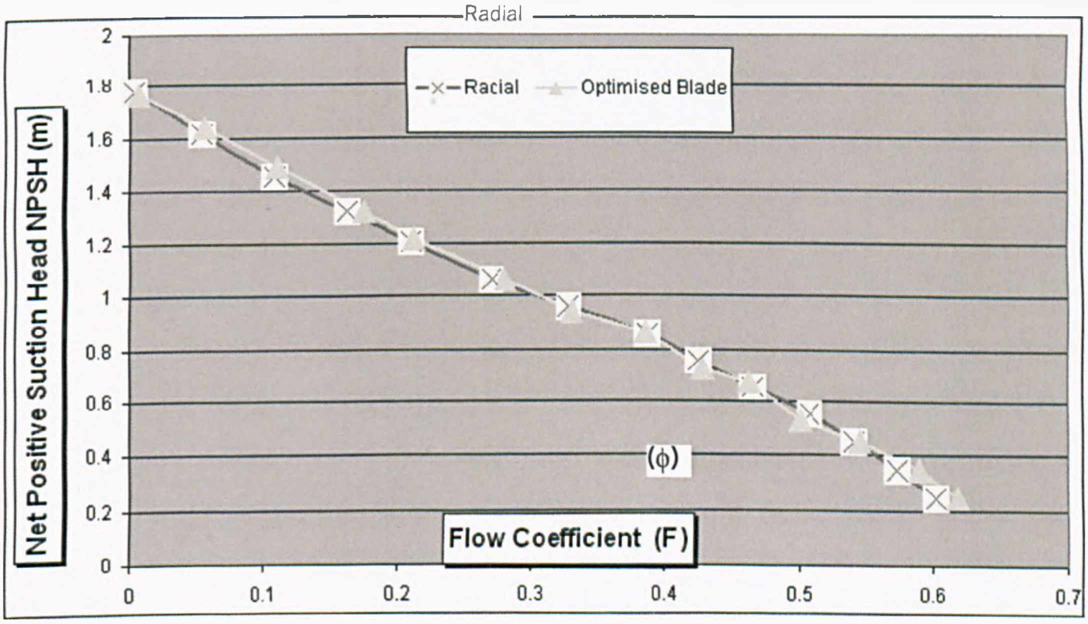

**fig. 45** NPSH v's flow coefficiency

## 3.9 Summary

An experimental rig was developed to not only permit performance testing of a standard baseline radial bladed regenerative pump, but to allow comparison with modified blade designs. A representative range of performance data was necessary to evaluate the accuracy of the CFD model predictions. The modified impeller blades were developed using a novel rapid manufacturing process that produced not only complex blade profiles but produced them in a robust enough form to facilitate experimental testing. The experimental rig was developed in a manner to limit cavitation effects and to allow measurement uncertainties associated with the conducted testing to be considered.

# Chapter 4

# CFD Modelling

## 4.1 Introduction

In determining the complexity of the regenerative pump CFD model, it was necessary to consider how much computational resources were available. During the research work, a High Performance Computing, (HPC), facility at Strathclyde University was used. The HPC system consisted of 100 Opteron processors, accessing a total available memory of 236 GB of RAM. Departmental experience in parallel-architecture computation with the HPC facility enhanced the CFD research on the regenerative pump.

The computing resources initially used for the calculations of the standard regenerative pump, (straight vane impeller, round cut flow passages), was a DELL precision PWS380 Intel pentium dual core workstation. Fluent 6.3.26 guidelines suggest 1 CPU can handle models up to and between 1 to 1.5 million cells. After initial matching to the conventional radial impeller, a series of optimised blade profiles were assessed using the HPC facility. The modified blade standards considered, for 10 performance boundary conditions, were run for 1000 iterations. Having the large computational resource, of the HPC enabled this to be done in a much more time effective manner. The analysis using the HPC facility was essentially 100 times faster than using the single workstation.

From the outset it was necessary to detail the main modelling assumptions. These assumptions are set out in table 6.

| |
|---|
| Steady incompressible flow |
| Neglect secondary physical effects (e.g. heat transfer) |
| Unsteady interactions are neglected (e.g. vortex shedding) |
| End effects neglected (suction, discharge) |

**Table 6** - Modelling Assumptions

## 4.2 Model Geometry

The basic regenerative pump geometry was created in Pro-Engineer Wildfire Version 1.0 (fig. 46)

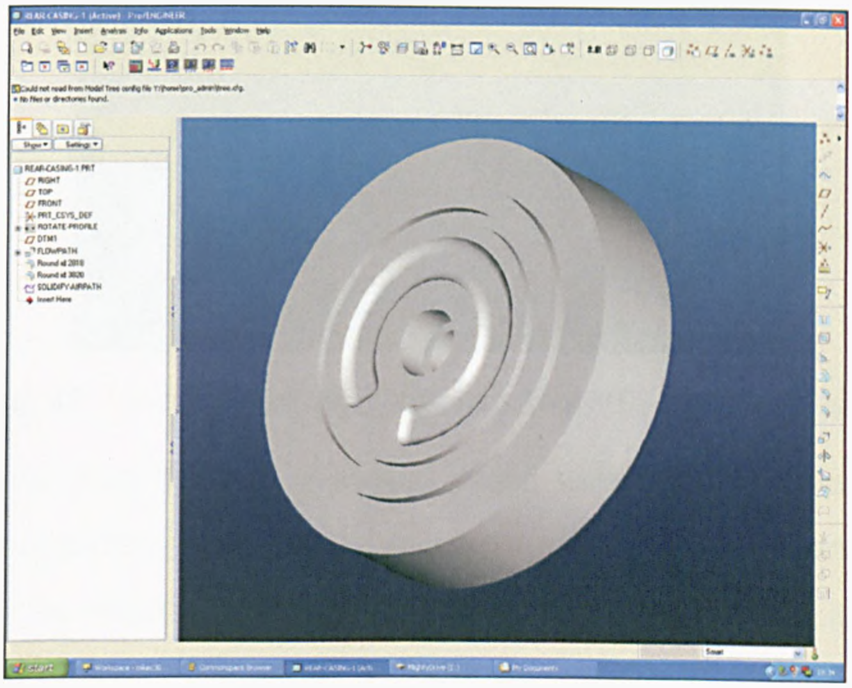

Could not read from Model Tree config file T:/home/pro_admin/tree.cfg.
• No files or directories found.

**fig. 46** CAD casing generation

In order to ensure a representative match to the experimental pump, it was essential to capture the geometry of the pump components. To ensure this, manufacturing drawings (Appendix C) were used for the computational model to include as many features as possible, such as the exact fillets, rounded edges, tip clearances, side wall round cut profiles etc. These were cross-checked with the inspected production parts to minimise deviation which have been detailed to cause as much as 3% variation in efficiency terms, IMechE Fluid machinery group symposium (2007). This ensured the closest and most complete representation of the pump geometry.

GAMBIT, (Geometry and Mesh Building Intelligent Toolkit) version 2.4.6, (FLUENT 2006) was the commercial pre-processing tool selected. This tool was used for importing the IGES (Initial Graphics Exchange Specification - CAD files) (fig. 47). It is a single, integrated pre-processor for CFD analysis.

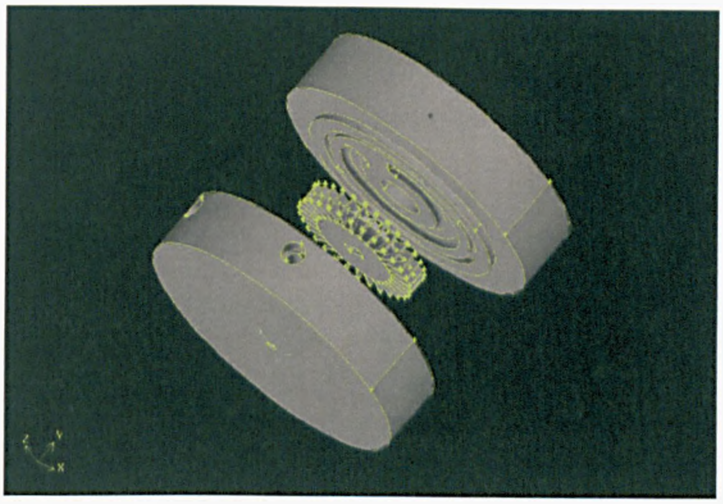

**fig. 47** Imported CAD geometry into GAMBIT – exploded view

The external pump features, (non fluid wetted surfaces), were deleted using the Gambit geometry tools. That is, only the fluid flow regimes relevant to the computational model were retained using 'Boolean' operations to e.g. unite, subtract, intersect, revolve, sweep and split volumes (fig. 48). Gambit also has facilities like automated 'clean-up' tools to rectify geometry quality problems. Gambit was also used for mesh quality examination; boundary zone assignment and mesh export to FLUENT.

Gambit uses CAD functionality (vertices, edges, faces and volumes), to draw the flow domain

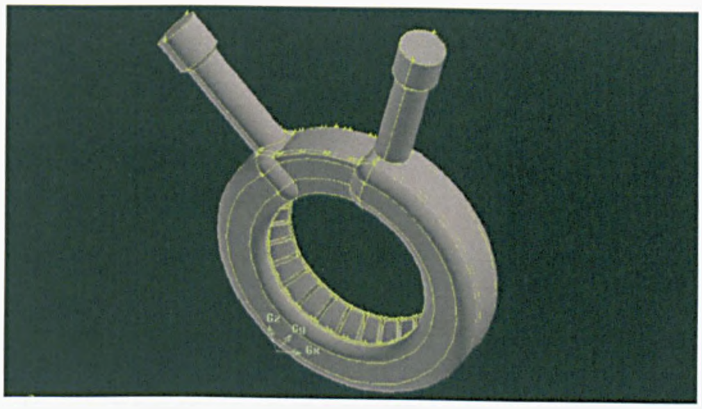
**fig. 48** Pump fluid flow regime

## 4.3 Computational domain

Prior to developing the computational domain for the study, it was important to consider some general points for the regenerative pump. These are outlined in table 7:

| Consideration | Comment |
|---|---|
| What resolution for the pump is required | Choose Multi-zone system model - MRF |
| The placement of the pump inlet and outlet boundaries | Place inlet and outlet boundaries away from the rotating components. At least 1chord distance or more |
| The location grid interfaces for multi-zone models | Choose interface locations which are "midway" between components. |
| Separate meshes where generated for rotating (impeller) and stationary (casing passage) zones | Multiple-reference-frame (MRF) model |

**Table 7** - Computational domain general considerations

Swirling and rotating flows create a unique set of flow physics for which special input requirements and techniques must be applied. The Multiple-Reference-Frame (MRF) model is appropriate for multiple component analyses where interaction effects are considered small. In the case of the regenerative pump the multiple components are the pump impeller + casing passage (fig. 49).

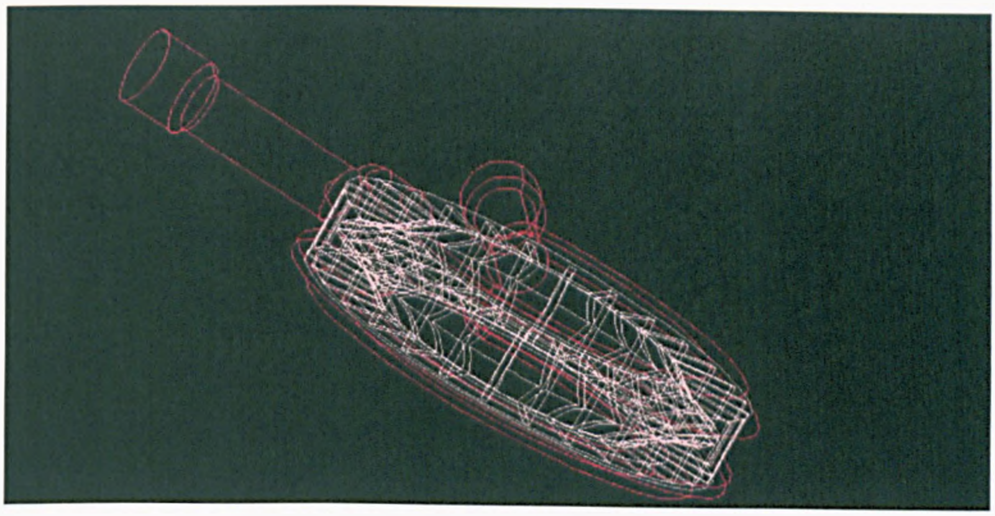

**fig. 49** Regenerative pump flow field assembly

The pump flow would then be solved in local rotating reference frames, where fluxes are locally transformed from one frame to another at the pump zone interfaces (Table 8). This technique is also known as the "Frozen Rotor" approach. Separate meshes are generated for the rotating, (impeller), and the stationary, (casing passages), fluid zones FLUENT (2006).

| | |
|---|---|
| Boundary Conditions | Selected MRF cell zone. Specified rotation axis origin, rotation-axis direction and rotational velocity origin. |
| Boundary Conditions | All walls are stationary relative to its adjacent cell zone in the moving zones by default. Pump stationary (non rotating) walls inside the MRF region (fluid in casing) were declared stationary in absolute reference frame. |

**Table 8** - MRF general considerations

For the regenerative pump domain considerations, three areas were considered;

1. The features of the pump geometry required to get a good flow field simulation.
2. If the geometry can be simplified.
3. What the flow environment is.

These points are addressed in table 9.

| | |
|---|---|
| Number of components | Impeller, blade passages, stripper, inlet/outlet etc |
| Component interaction | Weak interaction in steady-state conditions |
| Flow regime | Low speed with incompressible flow (Appendix A)<br>High Reynolds number with turbulent flow |
| Working fluid | Incompressible fluid (water). |
| Physical processes | Turbulence<br>Adiabatic<br>Multiphase physics (cavitation) |

**Table 9** - Computational domain flow environment

The MRF model is appropriate for incompressible flows where the flowfield is considered to respond instantly to changes in rotor position. A different approach would be required to consider compressibility of the fluid, for example in regenerative blowers, Hollenberg et al. (1979), Sixsmith et al (1977). For the current analysis where the fluid is treated as incompressible, the use of a MRF at multiple fixed rotor positions is a suitable and a recommended approach, FLUENT guidelines (2006), FLUENT application briefs (2001) and (2005).

The MRF approach is , whilst a recommended approach, subject to constraints. The computational domain is divided into stationary and rotating fluid zones. The flow equations are solved in each fluid zone and flow in each zone is assumed to be steady. This is clearly an approximation, particularly at the inlet and outlet interfaces. At the interfaces between the rotating and stationary zones appropriate transformations of the velocity vector and velocity gradients are performed to compute fluxes of mass, momentum, energy and other scalars. MRF will depend on the velocity formulation used. At boundaries between two sub domains the diffusion and other terms in the governing equations in one sub domain require values for velocities in the adjacent sub domain. Absolute velocity formulation was recommended for flow coming from a stationary inlet domain. MRF ignores the relative motions of the zones with respect to each other and does not account for the fluid dynamic interaction between stationary and rotating, components. Ideally the flow at the MRF interfaces should be relatively uniform or mixed out; which is true for the majority of the pump mesh domain. However, at the inlet and outlet regions of the pump this is clearly an approximation. There is, to an extent, swirling and significant relative motion (fig 60, 61) across the interface at these regions which in the MRF Solution will be ignored. This approximation in these regions will be addressed in the future research work when a transient analysis is conducted. The effect of the approximation in the inlet and outlet region will be accounted for and the unsteady interaction for example shock and wake interaction will be assessed.

Having considered the modelling issues and approach to planning the CFD analysis with respect to computational domain, the next step was to define the meshing requirements.

## 4.4 Domain mesh construction

There are many ways to generate a mesh for CFD, where different approaches can yield grids of equivalent overall resolution and quality, Woollatt et al. (2005). The main points considered for the regenerative pump mesh are outlined in table 10:

| |
|---|
| Maintain good cell quality |
| Provide appropriate grid resolution in high gradient regions (Chap. 4.7) |
| Ensure smoothness in regions where the grid transitions from fine to coarse resolutions |
| Minimise the total cell count (to keep CPU times reasonable) |

**Table 10** - Meshing guideline considerations

Turbomachinery CFD has traditionally employed structured quad/hex meshes. This was because, generally, blade row flow passages lend themselves to structured, mapped meshes. Furthermore CFD algorithms were developed using finite difference approaches which required a structured cell arrangement. With modern unstructured flow solvers such as Fluent 6.3.26, the option to choose between structured, unstructured and hybrid meshes is available. Unstructured Tet, (Tetrahedral), meshes have cells arranged in an arbitrary fashion, with no grid index and no constraints on cell layout (fig, 50). In considering the unstructured Tet mesh, FLUENT 6.3.26 CFD guidelines strive to use structured, hex elements whenever possible. The use of an unstructured Tet mesh for the regenerative pump was chosen to mesh regions which would be difficult to mesh using Hex Elements (Casings). The benefit of Tet meshes is that most volumes can be meshed without decomposition, regardless of the pump complexity. In considering the Unstructured Tet mesh approach for the regenerative pump model the points in Table 11 were considered.

| Advantages | Disadvantages |
|---|---|
| Can handle very complex geometries while maintaining good cell quality | Increased cell count versus equivalent hex mesh |
| Tri/Tet mesh generation algorithms are highly automated | Numerical error (false diffusion) can be higher than equivalent hex mesh |

**Table 11** - Tetrahedral mesh selection advantages and disadvantages

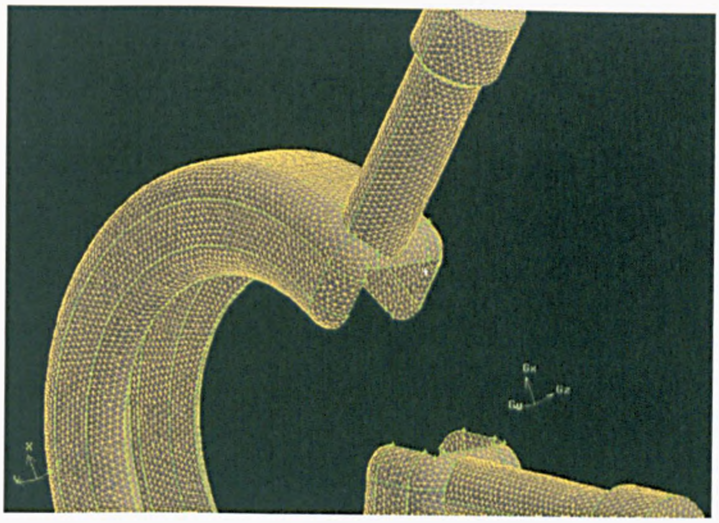

**fig 50** Regenerative pump meshed casing flow passages unstructured Tet mesh

Specifically, when considering the regenerative pump, there are a number of meshing considerations to take account of, and these are listed in Table 12.

| |
|---|
| Quality of the tetrahedral mesh is highly dependent on the quality of the triangular mesh on the boundaries (fig. 54). |
| Initialisation process may fail or highly skewed tetrahedral cells may result if there are highly skewed triangles on the boundaries |
| Large cell size variation between adjacent boundary triangles. |
| Small gaps that are not properly resolved with appropriately sized triangular mesh. |

**Table 12** - Regenerative pump Tetrahedral Mesh challenges

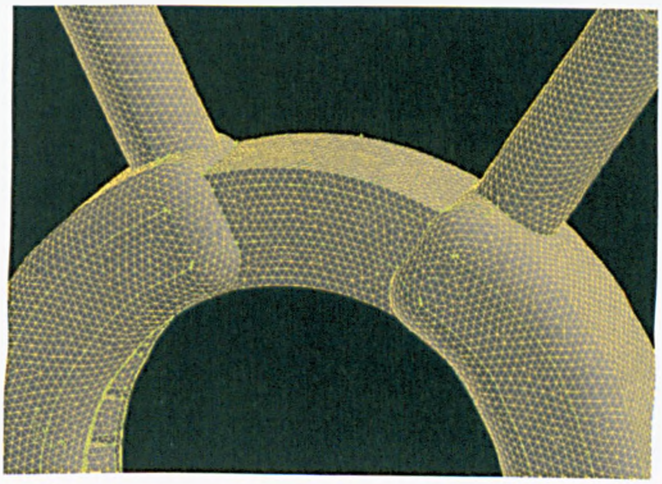

**fig. 51** Regenerative pump tetrahedral mesh

A tetrahedral volume mesh was used in the initial simulation which was less time consuming to build than a hexahedral mesh (fig. 51). Considering accuracy, and also with increased benefits in post processing, it was decided to develop a hybrid mesh, that was a decomposed Hex mesh for the impeller region of the pump and a Tet mesh for the more complex casing geometry. The impeller was meshed using hexahedral elements, due, in part, to the symmetrical nature of this part of the geometry and ability to be decomposed. Furthermore, this allowed increased post-processing functionality, particularly for contour plotting on the blade faces. The remainder of the domain was meshed using tetrahedral elements (fig. 52).

| Advantages | Disadvantages |
|---|---|
| Lower Cell Count (In general) than equivalent unstructured mesh | Cannot easily deal with complex geometry |
| Reduced numerical error (false diffusion) flow is aligned with the mesh | Cell quality suffers with increased geometry complexity |

**Table 13** - Hexahedral mesh selection advantages and disadvantages

The relative benefits and challenges with this approach are listed in table 13.

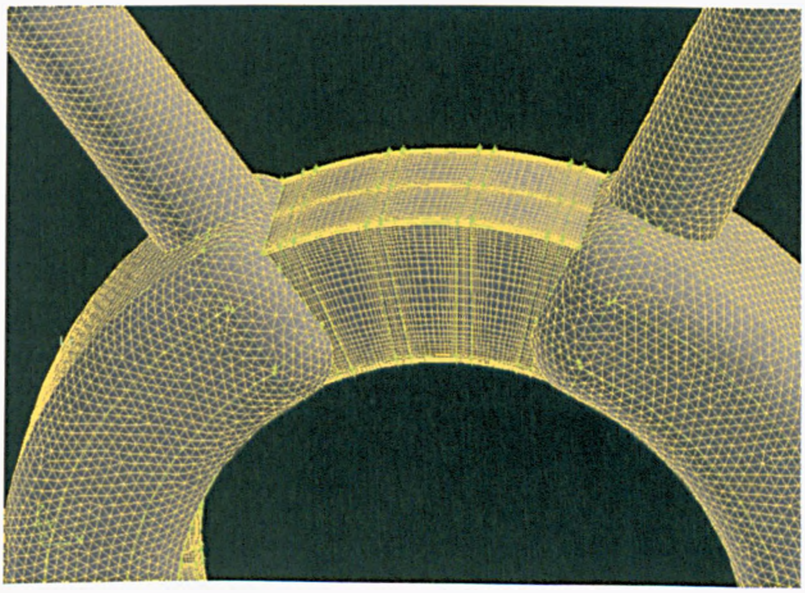

**fig. 52** Regenerative pump hybrid TET/HEX mesh

## 4.5 Solver set-up

Having decided on a modelling approach and mesh strategy for the regenerative pump, the mesh was generated and imported into Fluent 6.3.26 for application of the boundary conditions and subsequent analysis. Choices and options considered in the solver are as detailed in table 14.

| Solver choice |
|---|
| Velocity formulation |
| Gradient option |
| Turbulence model |
| Material properties |
| Boundary conditions |
| Interfaces (mixing planes, grid interfaces) |

**Table 14** - FLUENT solver options

For turbomachinery applications, pressure-based solvers are recommended for incompressible flows, FLUENT (2006). In this solver, the velocity field is obtained from the momentum equations and the pressure field is extracted by solving a pressure or pressure correction equation, which is obtained by manipulating continuity and momentum equations. Density-Based solvers are recommended for high speed compressible flows, and were not appropriate for this regenerative pump analysis. The velocity formulation selected was to use Absolute Velocity Formulation (AVF) as the fluid inflow comes from a stationary domain. In this case, absolute total pressures are used in the regenerative pump model. As the gradient option affects how gradient quantities are numerically calculated, node-based gradients were used for unstructured Tet meshes to improve accuracy. The Reynolds Averaged Navier Stokes (RANS) equations require turbulence models for closure. There are a wide range of different turbulence closure models, the turbulence models available in Fluent are listed in Table 15

| |
|---|
| – Spalart-Allmaras (1992) |
| – $k-\varepsilon$ (standard-LAUNDER et al. 1974, RNG YAKHOT et al. (1986), Realisable-SHIH et al (1995)) |
| – k-ω (Wilcox, SST) |
| – Reynolds stress model |
| – Other (V2F, Low Reynolds number k-e models) |

**Table 15** - Turbulence models

Realisable k – ε turbulence models were considered for the regenerative pump model as suitable for complex flows involving high curvature and swirl, Spalart (1992). Realisable k – ε is a variant of the standard k–ε model, Launder et al. (1974). It's 'realisability' stems from changes that allow certain mathematical constraints to be obeyed which ultimately improve the performance of this model. The selection of the Realisable k – ε turbulence model in conjunction with the regenerative pump is also widely used in other industrial pump applications of CFD, Wisler (1985). Although detailed analysis of the numerical code are not within the scope of this research, the turbulence models contained inside them are, by no means, universal. A considerable amount of research effort has been devoted to the validation of classical turbulence models in industrially relevant flows and to the development of the most general methods. Typically Fluent Turbomachinery best practices are considered and applied in the study, FLUENT (2006).

Typically the flow was deemed to be turbulent in pumps when $Re \geq 2,300$. For the particular case of the regenerative pump

$$\mathrm{Re}_L \equiv \frac{\rho U L}{\mu} \qquad (22)$$

Measured experimental pump mass flowrate $\dot{m} \approx 0.2862$ kg/s

Pump inlet area $A=\left(\frac{\pi}{4}\right)D^2$ =7.854*10e$^{-5}$ m$^2$

Free stream fluid velocity in the pump inlet, V = 3.65m/s from

$$V=\frac{\dot{m}}{\rho A} \tag{23}$$

Characteristic length (or pipe diameter), D= 10mm

Fluid density for water, $\rho$ = 998.2 kg/m$^3$

Fluid viscosity for water (dynamic), $\mu$ = 0.001003 Kg/m-s

Re = 3.63 x 10$^4$ Hence the flow in the regenerative pump inlet is fully turbulent.

The role of CFD analysis in rotating machinery design, particularly in pumps, is to simulate the flow field over a range of operating conditions. Design conditions are often less complicated to analyse as the flows are steady. Off-Design conditions are usually harder to analyse as the flows may be unsteady. This particular study considered steady state flow conditions for the regenerative pump. Transient conditions will be considered in the scope of the future work. Another consideration in relation to the model is 'near wall' modelling.

Accurate 'near wall' modelling is important. Successful prediction of frictional drag, pressure drop, separation, etc depends on the reliability of the local wall shear predictions. Most k – ε turbulence models are not valid in the 'near wall' region FLUENT (2006). Thus special 'near wall' treatment was required to provide proper boundary conditions. Those considered were Standard wall functions and Non-equilibrium wall functions.

Considering intial solver settings, first order discretisation was selected. When the flow is aligned with the grid, the first-order upwind discretisation may be acceptable. When the flow is not aligned with the grid, first-order discretisation increases the numerical discretisation error (numerical diffusion). For tetrahedral grids, (as initially selected for the regenerative pump), and since the flow is never aligned with the grid, more accurate results are obtained by using the second-order discretisation (second order upwind, PRESTO). Although first-order discretisation generally yields better convergence than the second-order scheme, it will generally yield less accurate results, especially on Tet grids. Typically turbomachinery cases choose the second-order scheme from the start of the calculation.

Pressure-based solvers (SIMPLE, SIMPLEC, PISO and COUPLED) are recomended for incompressible flows in turbomachinery FLUENT (2006), and SIMPLE was selected for the study.

The use of SWF or NWF is relevant for most high Re applications which, is the case of the regenerative pump. The choice of core turbulence model is more important. Best practice guidelines suggest avoiding placing the wall adjacent cells in the buffer region FLUENT (2006), ie in the region $5<y^+<30$.

For standard, or non-equilibrium wall functions, each wall-adjacent cell's centroid should be located within the log-law layer, $30 < y^+ < 300$. A $y^+$ value close to the lower bound ($y^+ \sim 30$) is most desirable.

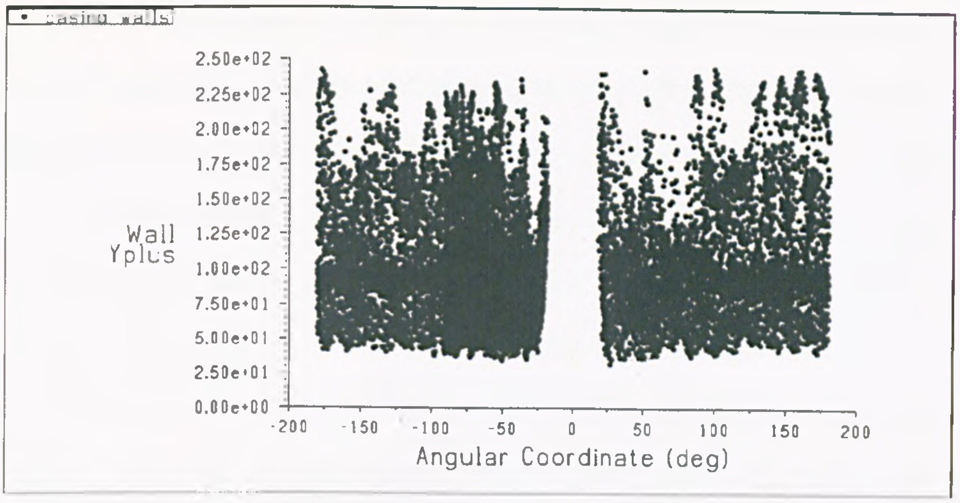

**fig 53** Regenerative pump $y^+$ variation with angular position

A plot of $y^+$ for the regenerative pump indicates the preferred range of variation in fig. 53.

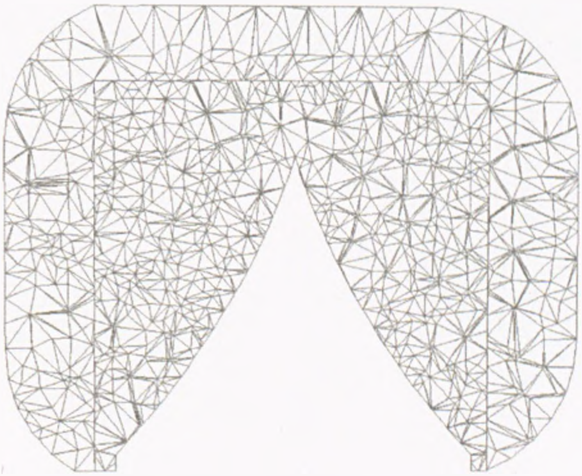

**fig 54** Tetrahedral cells in the fluid zone close to the wall boundary

Good initialisation of the solution is often the key to obtaining rapid and robust convergence of turbomachinery problems. Moving reference frame problems add complexity to the solution, because of large flow gradients resulting from the rotation of the fluid domain. It is essential to minimize cell skewness and aspect ratio. Skewness was kept below 0.9 with aspect ratios of greater than 5:1 to be avoided (fig. 54 and fig. 55). Initially the model was a complete Tet mesh (impeller and casing) which resulted in a 440,000 cell model; however the impeller was decomposed to prevent numerical error (false diffusion) across the flowfield and for greater post-processing control (impeller surfaces plots). The grids were adapted until there were only small differences in results (mass flow < 1%). Four adapted grid sizes where assessed, 400,000; 700,000; 1.4 million and 2.2 million cells. Grid independence was established at around 1.4 million cells, Table 16. When compared to other typical MRF pump models of similar complexity the results compared more favourably with the experimental test results. FLUENT (2001) and (2005). There was no significant change in the solution at around 1.4 million cells.

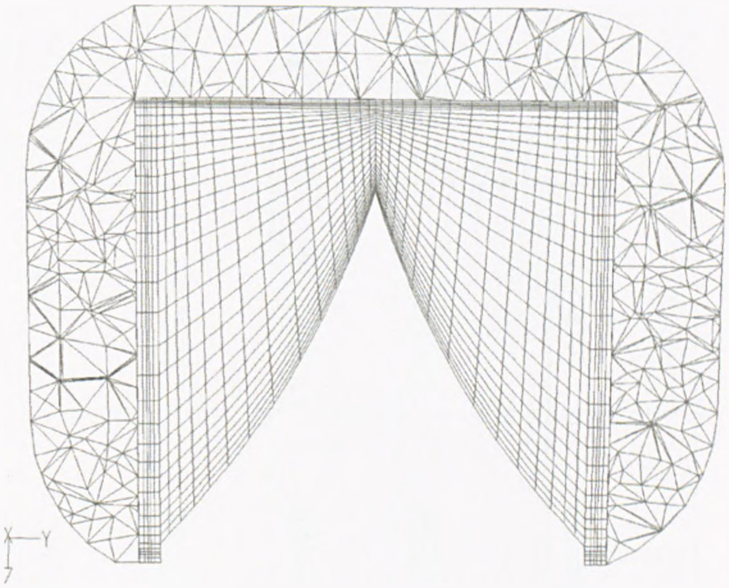

**fig 55** Tetrahedral/Hexahedral cells in the fluid zone close to the wall boundary

| Blade | 1st Cell Count | 2nd Cell Count | 3rd Cell Count | 4th Cell Count | Iteration Convergence Count | Grid Independence Established <1% Change) |
|---|---|---|---|---|---|---|
| Radial Tetrahedral | 437317 | 735498 | 1256784 | 2265788 | 358 | 1256784 |
| Radial Hexahedral | 465788 | 788552 | 1452265 | 2162255 |  | 1452265 |
| Swept 30 Deg Hexahedral | 425767 | 748556 | 1366258 | 2068852 | 485 | 1366258 |
| Swept 45 Deg Hexahedral | 439625 | 756828 | 1396725 | 2106547 | 407 | 1396725 |
| Chevron 60 Deg Hexahedral | 478556 | 798228 | 1468802 | 2232216 | 705 | 1468802 |
| Chevron 45 Deg Hexahedral | 445788 | 789922 | 1440089 | 2188952 | 748 | 1440089 |

**Table 16** - Cell count for impeller classification regenerative pump model

## 4.6 Calculating the CFD solution

The entire flow field is discretised and described by a set of incompressible Navier–Stokes equations. The commercial code, FLUENT 6.3.26, is a solver based on the finite volume method. The domain is discretised into a finite set of control volumes or cells. Partial differential equations are discretised into a system of algebraic equations. All algebraic equations are then solved numerically to render the solution field. Specifically, the solver in Fluent, with the correct inputs (material properties, boundary conditions, physical model – turbulence, moving zone etc), then solve the transport equations (mass, momentum and energy). The discretised conservation equations are solved iteratively. Convergence is reached when the changes in solution from one iteration to the next are negligible. Residuals provide a mechanism to help monitor this trend (fig. 56).

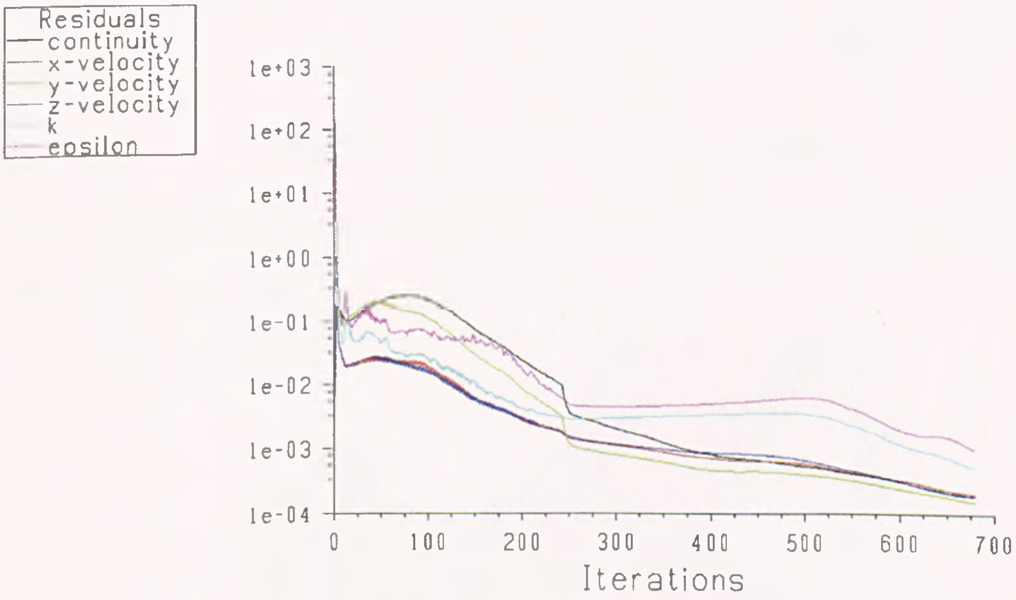

**fig. 56** Typical residuals plot regenerative pump

Solution convergence is an important issue in CFD due to the iterative nature of the solution. The non-linearity of the equations that govern the fluid flow require iteration to solve. For any equation, an approximate solution is obtained at each iteration that results in a small imbalance. This small imbalance is called a residual. Reduction in the residuals is not the only indicator of convergence. Reports of forces or mass balances, for example, are also used to judge convergence. Mass flowrates between the inlet to the pump and the outlet of the pump will add to zero for a converged solution. Numerical reports or plots can be generated during the calculation updates after each iteration fig. 57. These reports can be used to monitor the progression of the solution with respect to the quantities of interest.

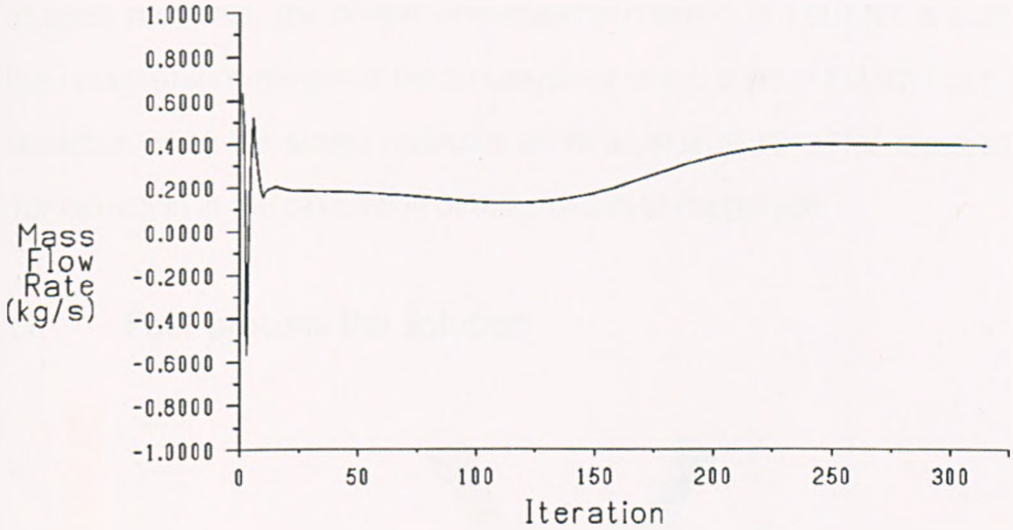

**fig. 57** Monitors for regenerative pump

It is possible to also create animations of the solution while the solver is performing calculations (fig. 58).

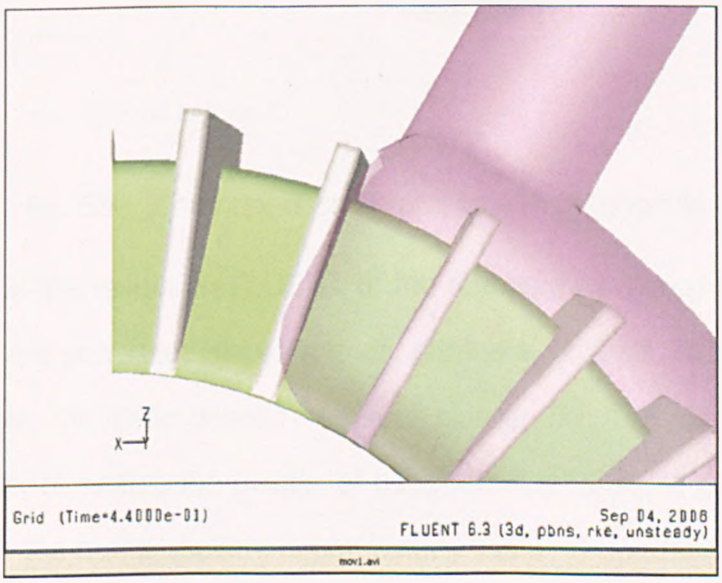

**fig. 58** Animation for regenerative pump

In considering the regenerative pump converged solution, it is important to state numerical controls and modelling modifications that were considered to enhance convergence and maintain stability. Convergence can be hindered by a number of factors, for example, large numbers of computational cells, very conservative under-relaxation factors and complex flow physics, are often the main causes. For most problems, the default convergence criterion in FLUENT is sufficient. When assessing convergence the convergence check is set in FLUENT to halt the calculation when the scaled residuals fall to a value of $10^{-3}$. This represents an error reduction in the calculation of three orders of magnitude.

## 4.7 Post-process the solution

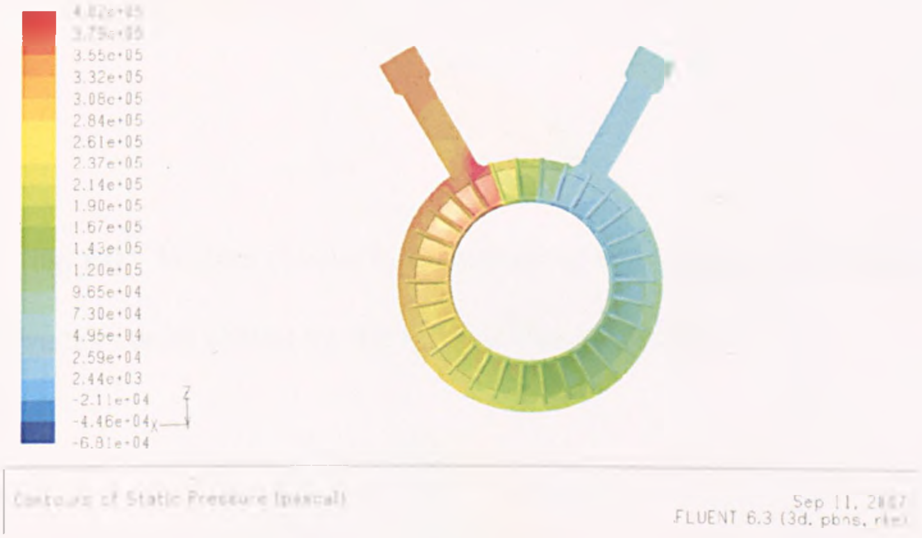

**fig. 59** Contours of static pressure in regenerative pump

To examine the results in FLUENT of the regenerative pump solution, graphical displays were generated showing grids, contours, profiles, vectors and pathlines, for example, the static pressure contour plot fig. 59. The ability of the graphics functionality to enable the display of parameters across grid components as well as through the pump section, is particularly useful in this study. Graphs can also be generated using data plotted directly from FLUENT (fig. 64).

FLUENT allows the plotting of contour lines or profiles superimposed on the physical domain. Contour lines are lines of constant magnitude for a selected variable (static pressure, velocity magnitudes etc.). A profile plot draws these contours projected onto the surface along a reference vector by an amount proportional to the value of the plotted variable at each point on the surface. The iso-surface creation option enabled views of the pump plane mid-section across the impeller (fig. 60, 61).

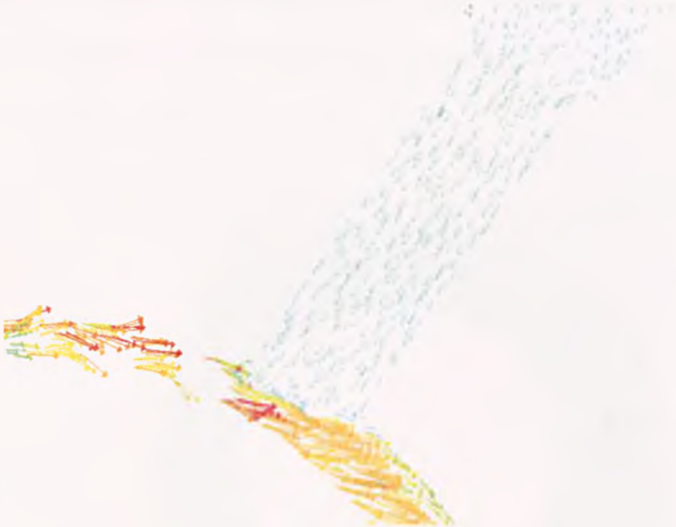

**fig. 60** Vectors of velocity magnitude at inlet to regenerative pump

Other vectors were plotted for the regenerative pump case.

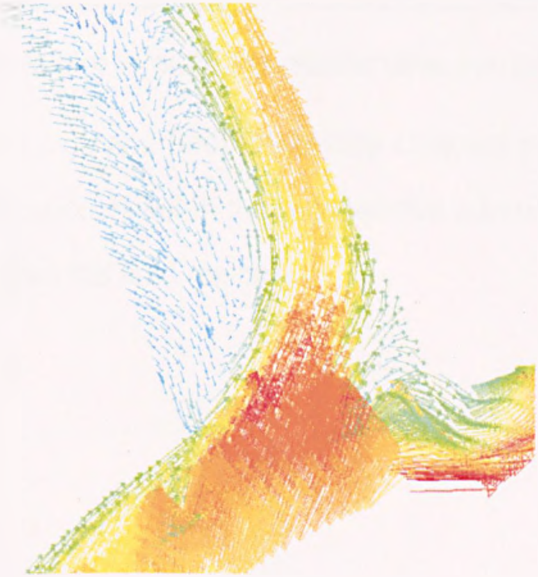

**fig. 61** Velocity vectors plot showing swirl at outlet of regenerative pump

Vectors can be drawn in the entire domain, or on selected surfaces. By default, one vector is drawn at the centre of each cell, with the length and colour of the arrows representing the velocity magnitude (fig. 61). This is a particularly useful tool when demonstrating, for example, the high degrees of swirl at outlet of regenerative pumps.

Pathlines are used to visualise the flow of massless particles in the problem domain. The particles are released from the regenerative pump casing walls using the tools in the surface menu (fig. 62).

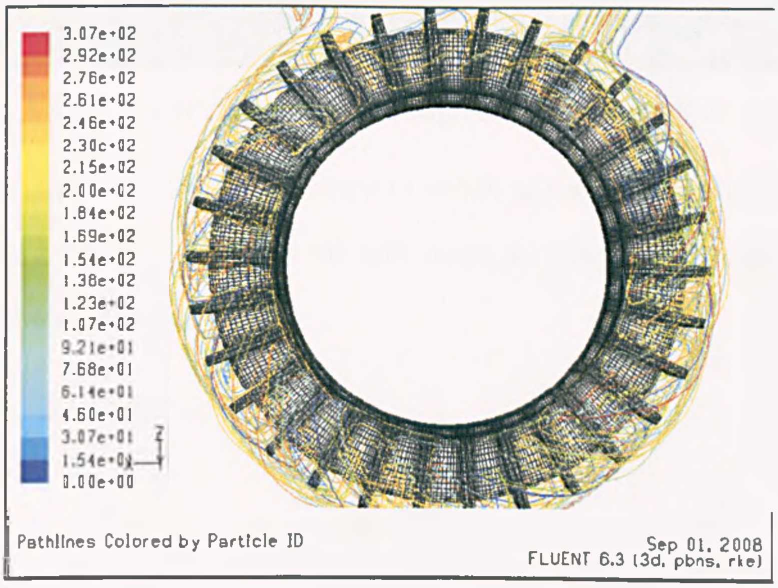

**fig. 62** Pathlines plot through the regenerative pump fluid regions

As seen in the pathlines plot, and from the helicity contours plot fig. 63, the clear helical or corkscrew like motion within the regenerative pump can be plotted with the angular position within the fluid regions.

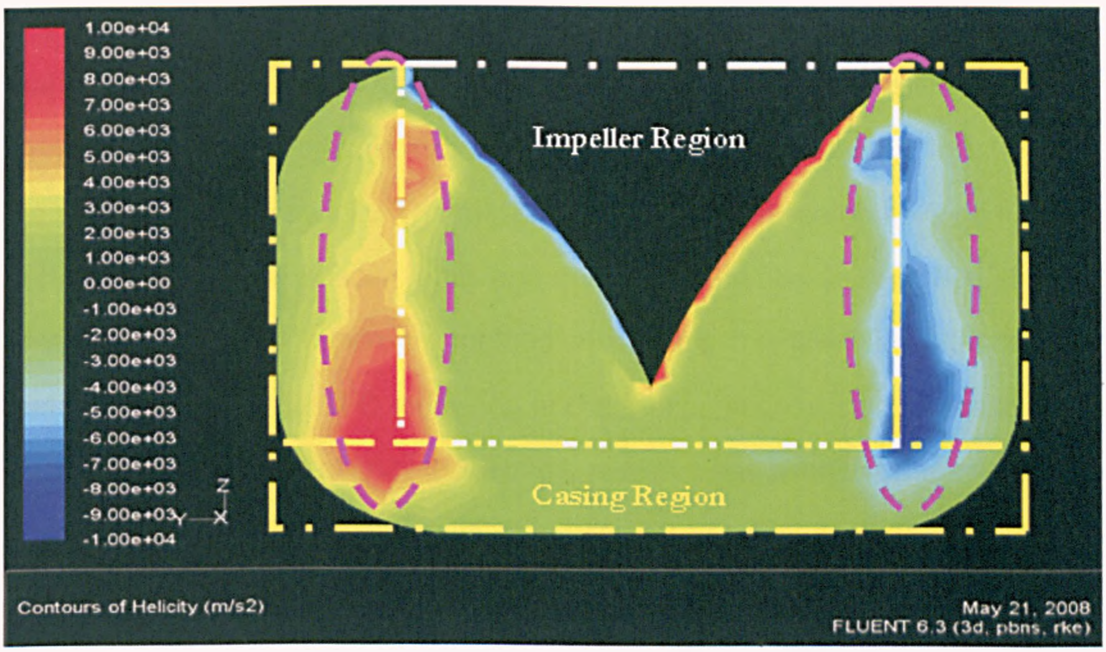

**fig. 63** Contours of helicity through section of impeller/casing

In fluid mechanics helicity is the extent to which corkscrew like motion occurs. If a fluid moves and also undergoes rotation about an axis parallel to the direction of motion there will be helical flow.

Formally, helicity is defined as:

$$H = \int u \cdot w dv \qquad (24)$$

where u = fluid velocity

where w = $\nabla \cdot u$

where we assume that the veolcity vector field u exists in cartesian space and is hence given by:

$$u = ui + vj + wk \qquad (25)$$

the vector operator $\nabla$, del is given by:

$$\nabla = i \frac{\partial}{\partial x} + j \frac{\partial}{\partial y} + k \frac{\partial}{\partial z} \qquad (26)$$

The complex flow regime within the regenerative pump does not lend itself easily to mathematical analysis. For regenerative pumps the helicity is established from the circulation flow that produces vortices and the tangential (peripheral) that stretches the vortices creating helicity. The most fruitful results in research have come from performance data on specific units and corresponding flow visualisation studies. This is, however, an expensive method of defining the flowfield. Although the matching between the CFD modelling and the experimental data, is reasonable, significant contribution of knowledge in the research has been the depiction of the flow patterns through the CFD modelling (figs. 60-64). Clearly in figs. 62, 63 and 64, the helical or corkscrew motion has been captured for the regenerative pump. This work, has defined the flow field in a way that has not been demonstrated in the published mathematical models to date.

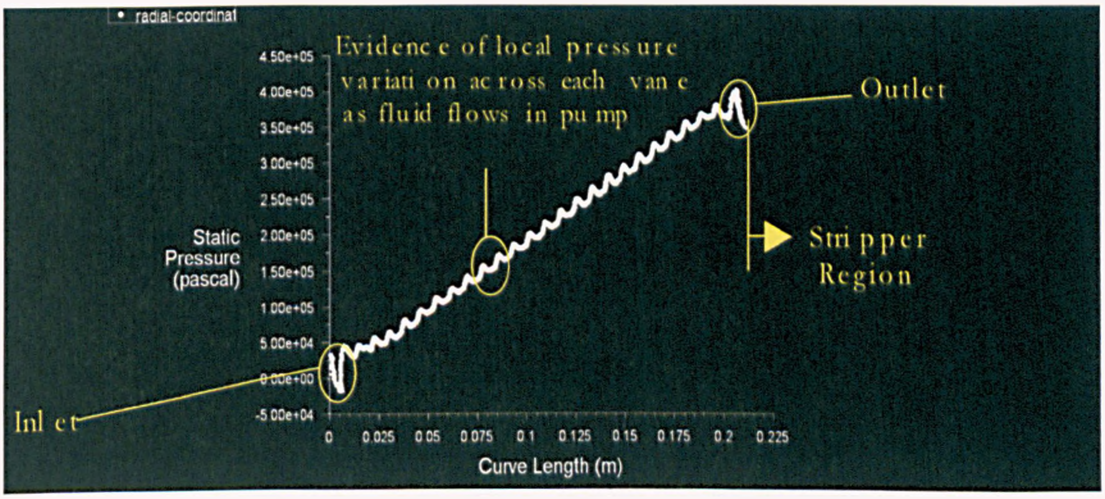

**fig. 64** Static Pressure rise variation with angular position

## 4.8 Modifications to the model and blade modification

The CFD predictions for the standard radial impeller profile were compared to the corresponding radial impeller experimental test results. From these findings, the flow-field was assessed using both performance results and flow visualisation plots, to consider how geometric features affect the pump performance. A simple analytical approach was considered to align the inlet flow with the impeller blades to minimise the shock losses (fig. 65). Impeller blade angle and profile was modified to profile align the blades as detailed in Appendix A for a design condition.

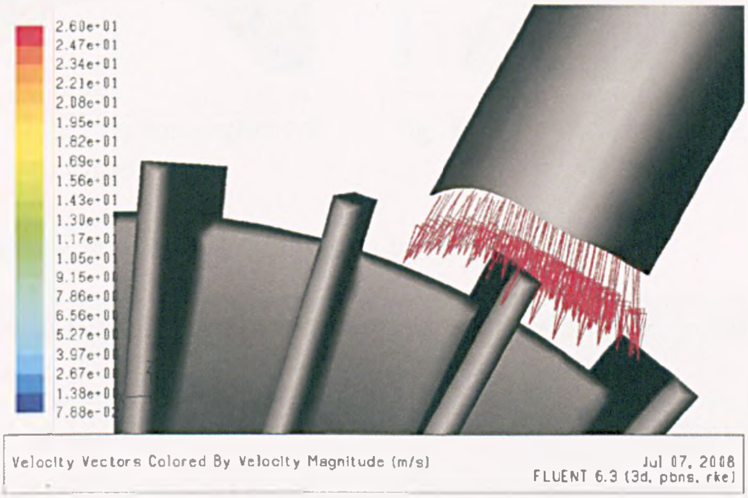

**fig. 65** Inlet vector alignment to impeller

The study was extended to consider nine modified impeller blade profiles. The initial baseline arrangement (radial impeller) was used to assess flow alignment, flow direction and performance distribution Appendix A. From the surface integrals of the area weighted average velocity values from FLUENT, components for velocity triangles were developed to describe the baseline flow field (Appendix A). From these values of velocity magnitude, an approach angle and an exit angle was calculated. Alternate blade configurations were then selected to better align the flow both at inlet and outlet from the pump (fig. 66, 67). Modified blade profiles (Appendix C) were then manufactured, for assessment based on aligning the flow and trying to reduce losses.

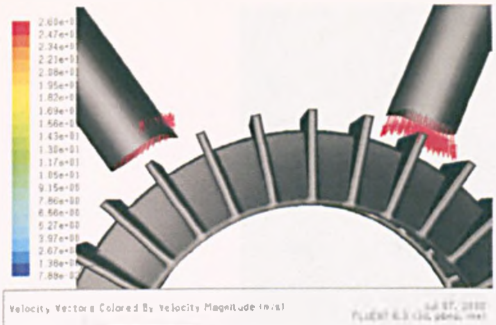

**fig. 66** Outlet vector alignment to impeller

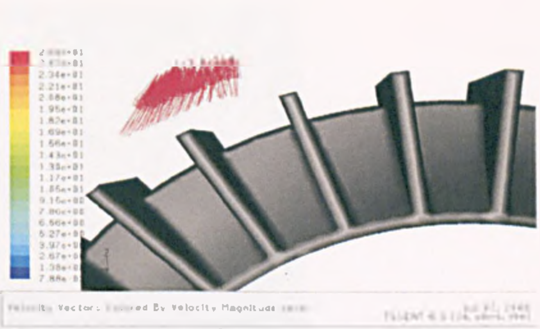

**fig. 67** Inlet/Outlet vector alignment to impeller

Some of the blade profiles are outlined in table 17.

| |
|---|
| Radial Impeller Blade – Tetrahedral Casing and Tetrahedral Impeller (fig. 66) |
| Radial Impeller Blade – Tetrahedral Casing and Hexahedral Impeller (fig. 67) |
| Swept Forward 30 Degree Impeller – Tetrahedral Casing and Hexahedral Impeller (fig. 68) |
| Swept Back 30 Degree Impeller – Tetrahedral Casing and Hexahedral Impeller |
| Swept Forward 45 Degree Impeller – Tetrahedral Casing and Hexahedral Impeller (fig. 69) |
| Swept Back 45 Degree Impeller – Tetrahedral Casing and Hexahedral Impeller |
| Chevron Profile 45 Degree Forward Impeller – Tetrahedral Casing and Hexahedral Impeller (fig. 70) |
| Chevron Profile 45 Degree Backward Impeller – Tetrahedral Casing and Hexahedral Impeller |
| Chevron Profile 60 Degree Forward Impeller – Tetrahedral Casing and Hexahedral Impeller (fig. 71) |
| Chevron Profile 60 Degree Backward Impeller – Tetrahedral Casing and Hexahedral Impeller |

**Table 17** - Impeller blade profiles considered in study

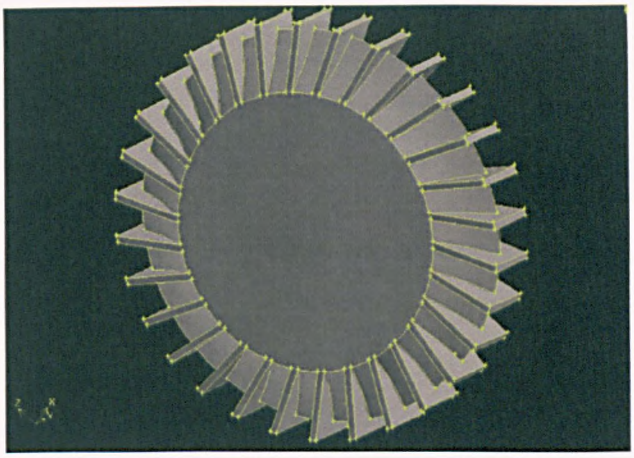

**fig. 68** Swept 30 Deg Impeller blade profile

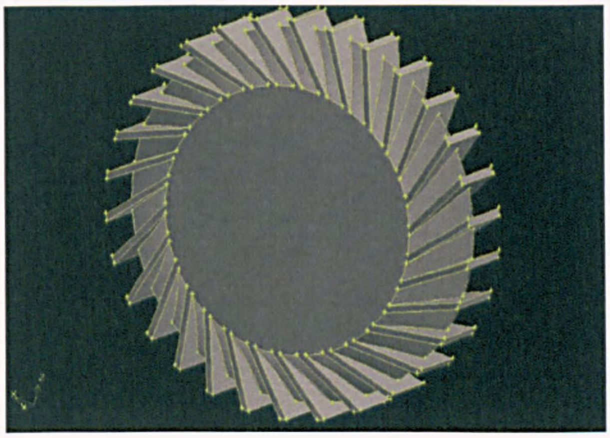

**fig. 69** Swept 45 Deg Impeller blade profile

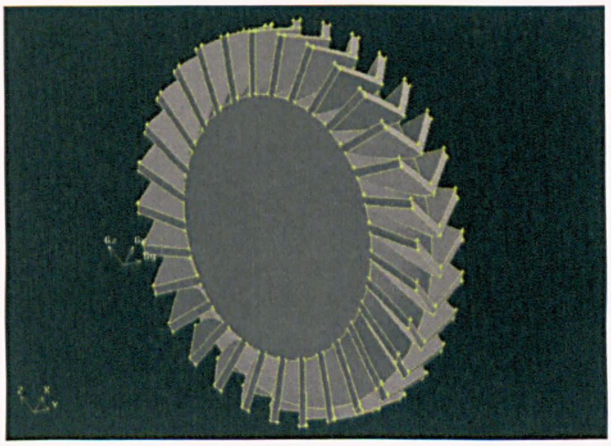

**fig. 70** Chevron 45 Deg Impeller blade profile

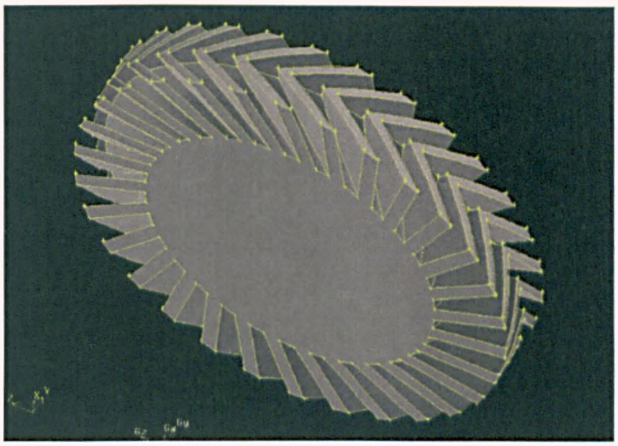

**fig. 71** Chevron 60 Deg Impeller blade profile

The modified blades (Table 17) were modelled in FLUENT as per Chap. 4.2 – 4.6, for a range of boundary conditions. The boundary conditions were those obtained from corresponding experimental testing of the respective blades. The results of this testing and numerical analysis are detailed in Chapter. 5. It was critical to identify losses in the regenerative pump CFD model such as flow separation, tip clearance effects, boundary layers, shocks, wakes etc. This allowed better comparison to the experimental results. The benefits of CFD analysis for the regenerative pump matching include improved performance, reduced testing, compressed design cycle and a better understanding of flow physics.

## 4.9 Summary

Availability of a High Performance Computing facilities and advances in CFD codes with particular reference to turbomachinery applications were used to develop a baseline radial blade standard CFD model. Results of this were used to consider an approach to improved flow alignment on modified blade standards. The CFD modelling performance results were not only to be compared to the experimental testing but also to the best flow visulisation experimental testing previously conducted in the 1940's and 1950's. The CFD models were produced in a manner that could not only demonstrate the overall performance characteristics of the pump but also to allow flowfield representation to be captured.

# Chapter 5

# Matching procedure and results

## 5.1 Introduction

Having outlined, in Chap. 4, the CFD modelling approach for the regenerative pump, the next step was to evaluate and compare the results to the experimental data. A 3D CFD simulation of a regenerative pump is extremely time consuming to create, as detailed in Chap. 4, but, comparing the development of a fully instrumented test rig to record performance and flow visualisation to an equivalent level, would be equally challenging and extremely costly. When assessing the approach to matching the regenerative pump, experimental results and CFD predictions, it is important to consider the strengths and weaknesses of CFD and experimental methods. Some limitations of CFD modelling and of experimental testing are outlined in Tables 18 and 19. From these considerations observations are made regarding the accuracy of each approach. The integration of the modelling and testing is considered and the results presented for the study.

## 5.2 Strengths and weaknesses of CFD

The strengths and weaknesses of CFD compared to experiment are considered in Table 18.

| Strengths | Weaknesses |
|---|---|
| Information across the full geometry available | Uncertanties are not easily quantified |
| Minimal set up costs relative to experiment | Less effective at predicting losses |
| Repeatability | Complex flowfields are often difficult to resolve |
| Quicker to set up and modify than experimental test | Unsteady effects are not captured in steady state analysis |

**Table 18** - Strengths & weaknesses of CFD compared to experimental testing

Some sources of uncertainty of the CFD modelling approach are not easy to quantify. Some examples of this are detailed in table 19.

| Uncertainty | Example |
|---|---|
| Definition Errors | Incorrect boundary conditions or geometry simplifications |
| Numerical Errors | Discretisation errors, convergence errors |
| Model Errors | Turbulence modelling, Physical model assumptions |
| User/code Errors | Input errors made by user/programmer |

**Table 19** - Principle sources of uncertainty in CFD

It is not often readily quantifiable as to how uncertainty in CFD modelling can be addressed. Numerical errors, for example, can be particularly difficult to quantify, insufficient iterations or numerical approximations in the differential equations are two examples listed in Table 19. Placing far field boundary conditions too close to areas of interest, for example, can have a significant impact on the accuracy of the solution (definition error). The choice of model or treatment of, for example, turbulence, may not be appropriate for a given application. One turbulence model does not suit all conditions. In the case of this study for a regenerative pump, a moving reference frame model was selected as appropriate for a steady state turbomachinery problem. The model is, however, limited as transient effects e.g. vortex shedding, are not captured. Typically for design point performance predictions, transient effects can, and are, normally neglected in the turbomachinery industry FLUENT turbomachinery guidelines (2006). However, at off design points, these effects may become significant. Halstead et al. (1997), for example, showed that errors as large as 35% can occur when unsteady transient effects are not properly assessed in turbomachinery applications. The simplification of the true geometry, or modelling features inaccurately, can also lead to large, unquantifiable errors. These errors may become significant, relative to accurate matching, with the experimental data.

The main benefits of CFD include enabling a number of different concepts to be assessed in the initial design stage, without the expense and effort of experimental testing, Jameson (1999). The advances in CFD mean that more complex concepts can be considered, with greater confidence in the results obtained. In this respect, it is still essential to verify the numerical model with experimental testing and, although there are also challenges with acquiring accurate test results, in some respects these uncertainties are often more quantifiable.

## 5.3 Strengths and weaknesses of experimental testing

The strengths and weaknesses of experimental testing are considered in Table 20.

| Strengths | Weaknesses |
|---|---|
| True flow performance results | Expensive |
| Performance & losses truly defined | Incomplete information, as it is limited to instrumentation locations. |
| Quantify uncertainties | Instrumentation limitations |
| Data can be obtained on unsteady effects | Instrumentation may affect performance or be unable to reach points of real interest (e.g. impeller blade tips) |
| Possible to obtain a large amount of data for various running conditions | Instrumentation failures may have a large impact |

**Table 20** - Strengths & weaknesses of experimental test relative to CFD

Clearly, as detailed in table 20, the major consideration for experimental testing is the instrumentation. This does not simply mean the accuracy or reliability of the instrumentation, but the location and method of data acquisition which can lead to major problems for accurate data retrieval and processing. The size of the Impeller in the regenerative pump tested meant that any intrusive measurement probes would be relatively large compared to the scale of the pump. This could lead to disturbances in the flow and even interaction effects with, for example, rotating components. Over instrumenting an experiment can not only prove costly but can also lead to the experiment becoming unrepresentative when compared back to the model. It will be shown later that a validated model can assist in this regard.

As with advances in CFD and computing capabilities, so too with improved data acquisition and instrumentation techniques, it is possible to spend large amounts of resource on advanced hardware. However this has to be balanced against how accurate measurements can be taken particularly in close proximity to areas of interest e.g. blade tips, casing walls. In advance of considering how the CFD modelling and experimental testing results matched, it is prudent to comment on the relative accuracy and repeatability of both.

## 5.4 Accuracy & Repeatability

It is clear that in considering experimental testing, accuracy and repeatability are both significant factors. Comparing this to CFD it is evident that accuracy will also be an important factor. In CFD however repeatability should, for the same boundary conditions be subject to less variation and uncertainty. As detailed in Chapter 4 the quality of for example the meshing has a large influence on the accuracy of the results. Aspect ratio and skewness are for example not only critical in the model to the accuracy of the results but also often determine the ability of the solution to converge.

Over the last 10 years even with advances in the computational code and the processing power of e.g. HPC systems, CFD accuracy still remains a challenging task. Many factors, for example turbulence modelling, mesh selection, geometry approximation, solver choice and boundary condition all can introduce uncertainty into the analysis, table 19.

It is therefore essential to ensure that where possible CFD solutions are validated with experimental test results.

Experimental test results themselves, as detailed in Appendix A6, are also subject to uncertainty. Furthermore when experimental results do not exist, for example when a new design is considered, it is difficult to quantify the uncertainty. Wollatt et al. (2005), demonstrated that even with a group of expert CFD users when tasked with modelling a new design they produced significant variations in the results. When experimental data was obtained and compared to the group this variation was of the order of 3% even in collaborated results. Despite this, CFD can be a powerful tool if consistent approaches are adopted in the modelling strategy (consistency in grids, boundary conditions, physical models etc.), and the model is at some point verified to experimental data. Whilst uncertainty is an issue for CFD, as previously detailed, repeatability should be easier to control for the same given conditions. Accuracy and repeatability are more easily managed in testing, although there is consideration to the absolute level of accuracy obtained. Random variation in testing can be evaluated from repeated testing. Systematic errors in instrumentation are usually quoted from calibration tests, and for the case of the regenerative pump, are used in the uncertainty analysis detailed in Appendix A6. Changes in performance as a result of build to build variation are more difficult to assess. Build clearances and consistent assembly procedures were implemented to try to minimise this effect, however, unlike CFD modelling, this repeatability is more difficult to control.

In 2007 the institution of Mechanical Engineers produced a report suggesting that in the pump manufacturing industry build to build variation was of the order of 3%. It is interesting that this is of the same order of magnitude as the reported uncertainty in CFD modelling reported by Wollatt et al. (2005)

## 5.5 Basic Integration of CFD & experiment.

As discussed, there was not only a need for a representative 3-dimensional model, there was also a need to have a representative test rig (minimise uncertainty). It was essential to ensure that the benefits arising from the test are maximised, with the correct balance of instrumented pump against cost. In order to obtain the maximum benefit, the test parameters needed to be clearly and accurately measured, through correct rig instrumentation design.

**fig. 72** Velocity vectors plot showing swirl at outlet of regenerative pump

Developing the instrumentation system to determine the overall performance characteristics for a pump include power imput, pressure rise and mass flow. The acquisition of accuarate pump performance data is essential. However, before the instrumentation arrangement for the test was defined, the CFD performance simulations associated with the geometries were carefully analysed. This identified geometric locations where it was particularly important e.g. highly swirling outlet flow (fig. 72). CFD modelling for subsequent regenerative pump tests determined the extent of instrumentation required, and defined the best positions to locate it. This is because it is always the case that the amount of instrumentation, e.g. such as the number of pressure tappings, is severely constrained by physical limitations, manufacturing costs, and the cost of the instrumentation itself. It is later shown in the results that a suitably validated CFD model can assist in this regard.

The quality of the comparison will be influenced by a number of positional inaccuracies unless precautions are taken. When data is taken from fixed instrumentation, (e.g. pressure tappings), the locations of the instrumentation positions need to be carefully considered and thought through. When measurement devices are positioned near, for example, rotating impellers, care needs to be taken to ensure that the flow field environment e.g. inlet/outlet ports or impeller tip region, do not affect the integrity of the measured parameters. Interaction effects, and other mechanical device effects, need to be considered.

Another issue when comparing CFD and experiment is the correct representation of the desired geometry which actually exists from manufacture and assembly. There are limits to the extent to which this may be achieved. If, for example, the ideal tip clearance was considered for the regenerative pump instead of the actual build clearance, significant variations in the magnitude of the leakage losses would result.

There is significant scope for the greater application of CFD in, for example, developing the specification and best positions for instrumentation. CFD may also be used to great effect in developing test methodologies and techniques, as it may be used to assess the degree of flow disturbance of instrumentation and to determine the limits within which a given probe or transducer may be used. The use of CFD to develop and validate experimental procedures is very beneficial, and is considered in the scope of the future work, to continue to maximise and improve the performance of the regenerative pump. Only after establishing reasonable concurrence between the CFD modelling and experimental data, can design modification proceed for the regenerative pump. This is considered in the following section.

## 5.6 Results of CFD modelling & experimental testing.

The following series of plots compare the experimental test results and the CFD modelling predictions obtained for the regenerative pump. Dimensionless plots are used to illustrate the regenerative pump performance characterisitcs as is typically done throughout the pump industry.

The actual performance characteristics of rotodynamic machines is determined by experimental testing. If every size and speed combination was tested even for pumps with the same geometry the number of performance characteristics obtained would become extremely large even for that particular group of pumps. Dimmensional analysis and the affinity laws are used by replacing the vaiables in these performance charachteristics with dimmensionless expressions. Thus these expressions can be used to compare machines of equivalent points on the performance characteristic. Thus the similarity laws can be used to express the relationships between such corresponding points in the following way:

In conventional dimensionless terms:

Flow coefficient $\phi = \frac{Q}{\omega D^3}$ = constant (27)

Head coefficient $\psi = \frac{gH}{\omega^2 D^2}$ = constant (28)

Power coefficient $IP = \frac{P}{\rho \omega^3 D^5}$ = constant (29)

Pump Efficiency $\eta = \frac{Q \Delta p}{P}$ = constant (30)

For this study, the geometric variations in the pump standard are in impeller design. All other geometric features are constant. The impeller variations are indicated in Table 21. The detailed drawings for the impeller profiles are presented in Appendix C.

| Blade | Code | Figure |
|---|---|---|
| Standard Radial profile | Radial | 84 & 85 |
| 30 Deg Swept Forward | 30SF | 86 & 87 |
| 30 Deg Swept Backward | 30SB | 88 & 89 |
| 45 Deg Swept Forward | 45SF | 90 & 91 |
| 45 Deg Swept Backward | 45SB | 92 & 93 |
| 45 Deg Chevron Forward | 45CF | 94 & 95 |
| 45 Deg Chevron Backward | 45CB | 96 & 97 |
| 60 Deg Chevron Forward | 60CF | 98 & 99 |
| 60 Deg Chevron Backward | 60CB | 100 & 101 |

**Table 21** – Impeller blade profile identification code

The actual test and CFD data is presented in tabular form in Appendix D and a sample test calculation is detailed in Appendix A. The following plots detail the performance characteristics for the radial standard regenerative pump and the optimised blade profiles listed in Table 21 both for the experimental results (figs. 73-79) and the CFD predictions (figs. 80-83). For indicative purposes, a select number of plots are included to demonstrate the CFD / Experimental match (figs. 84-97).

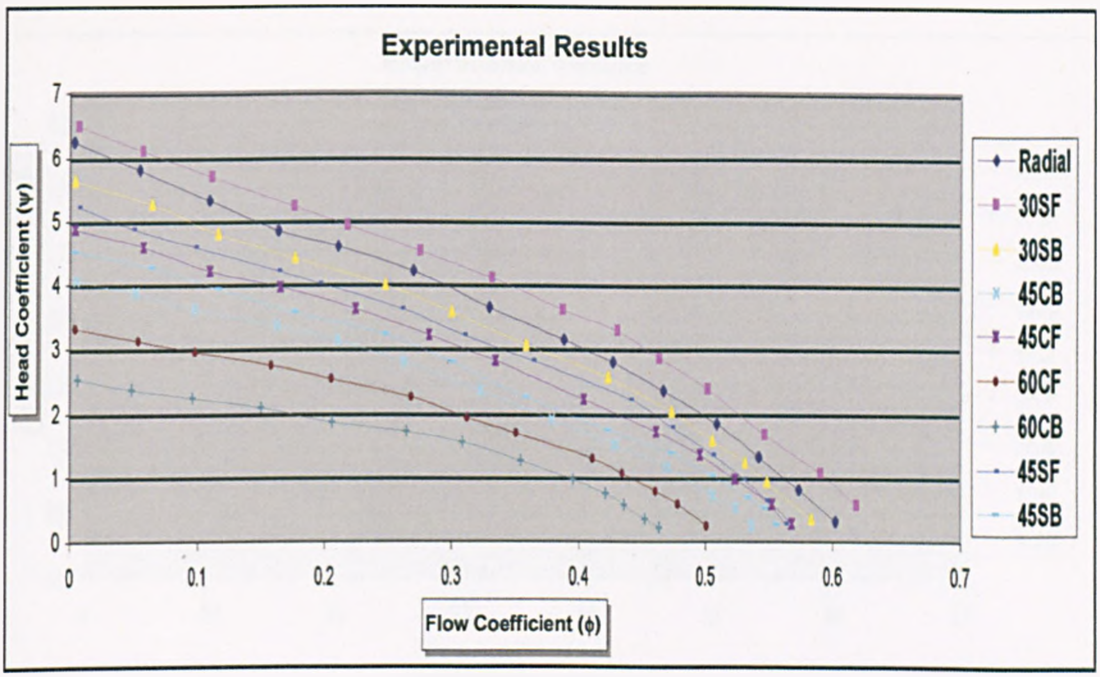

fig. 73 Head coefficient versus flow coefficient for experimental results

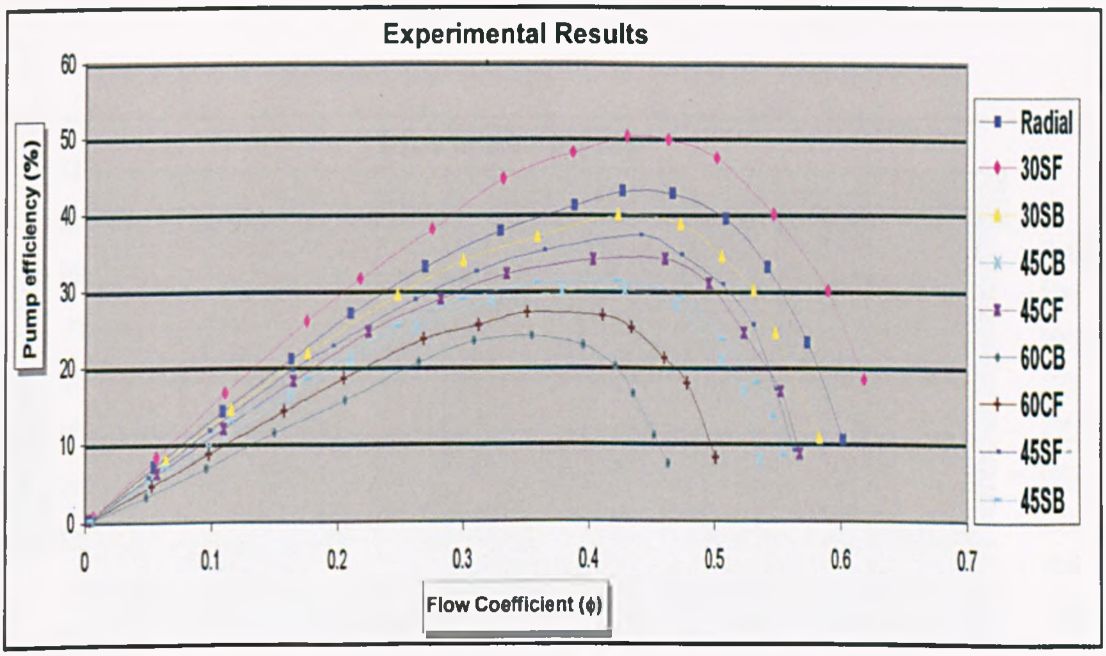

fig. 74 Efficiency versus flow coefficient for experimental results

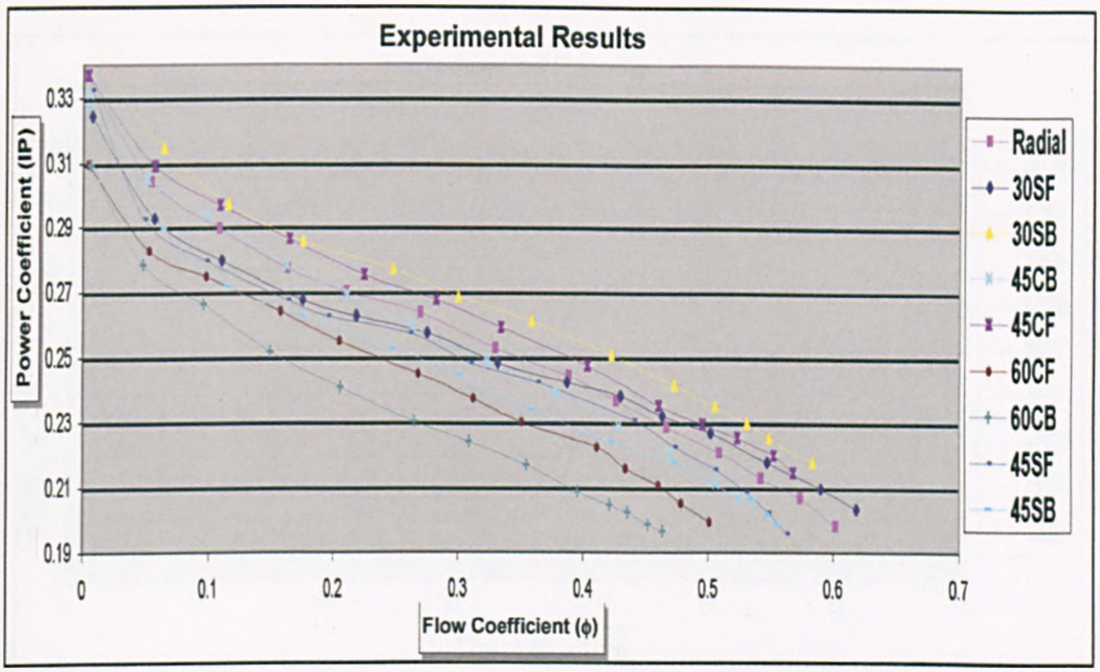

fig. 75 Power coefficient versus flow coefficient for experimental results

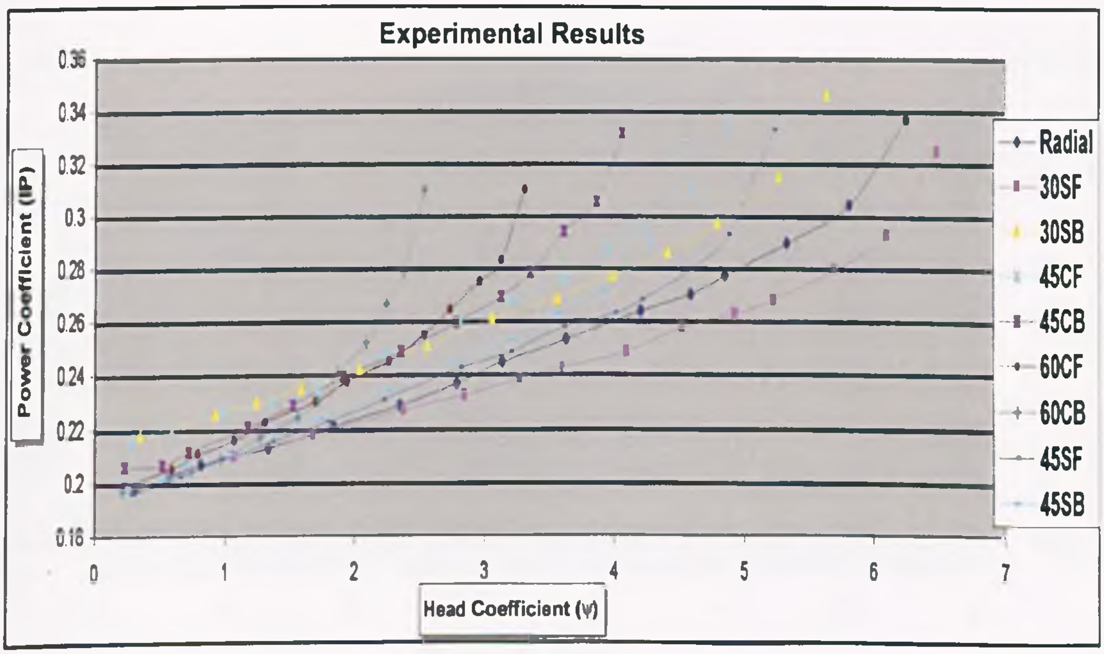

fig. 76 Power coefficient versus head coefficient for experimental results

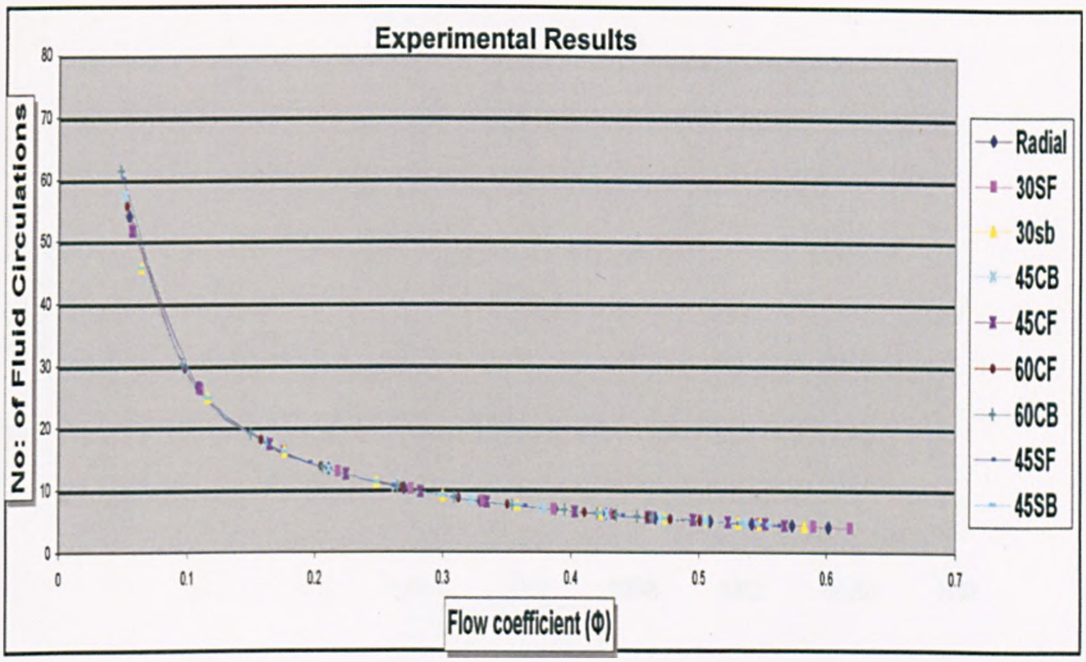

fig. 77 Number of circulations versus flow coefficient for experimental results

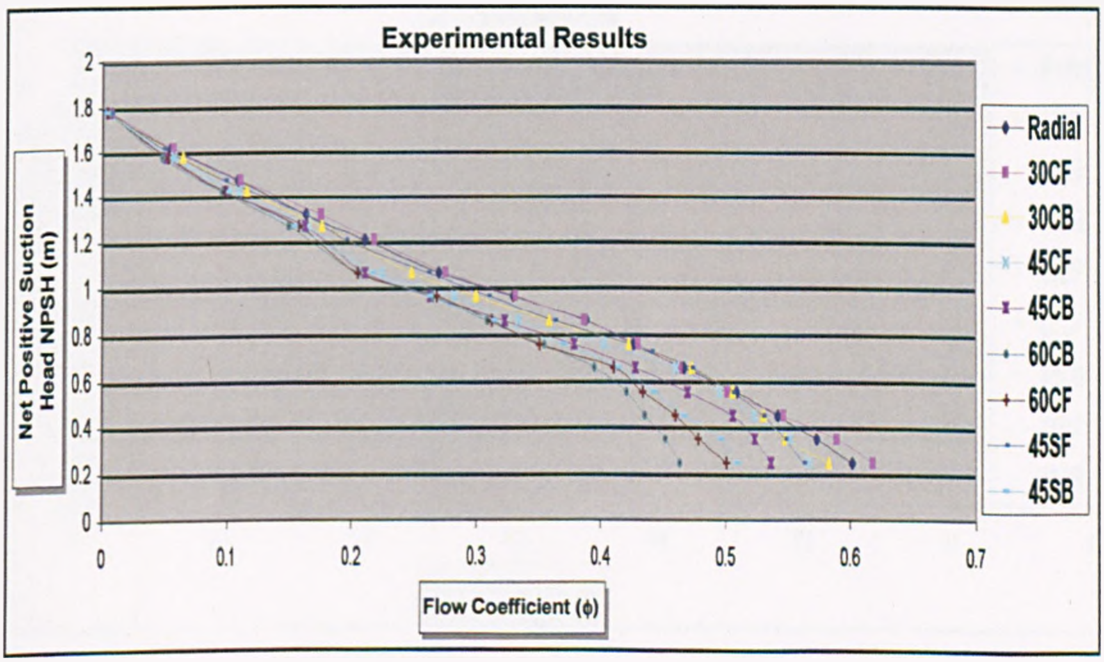

fig. 78 NPSH versus flow coefficient for experimental results

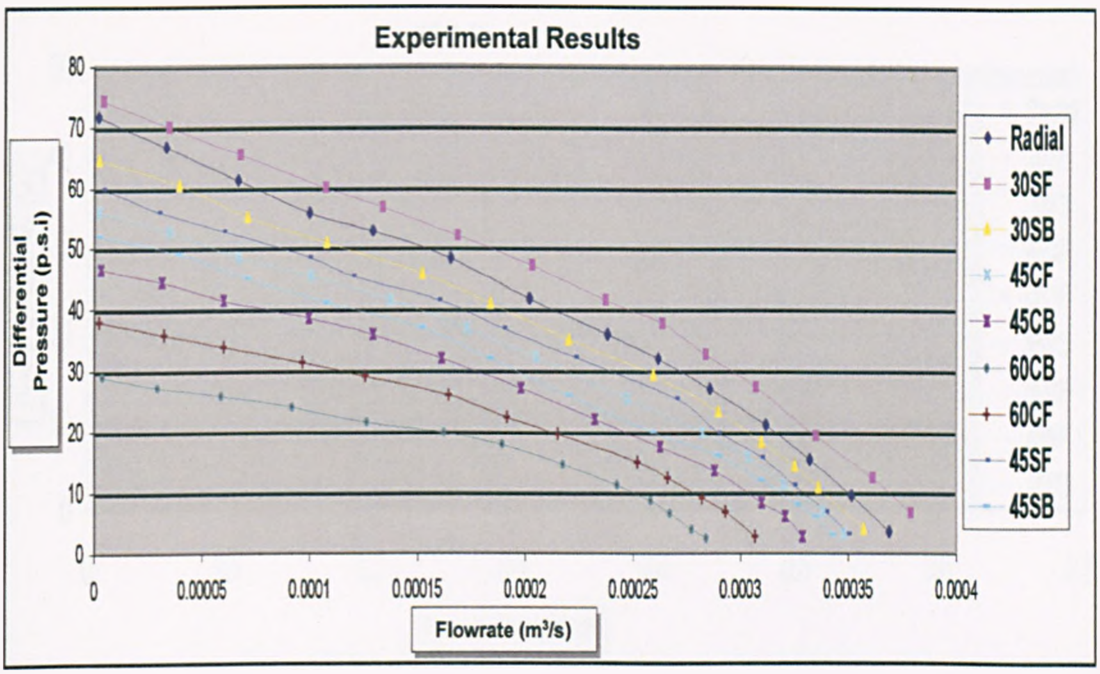

fig. 79 Differential pressure versus flowrate for experimental results

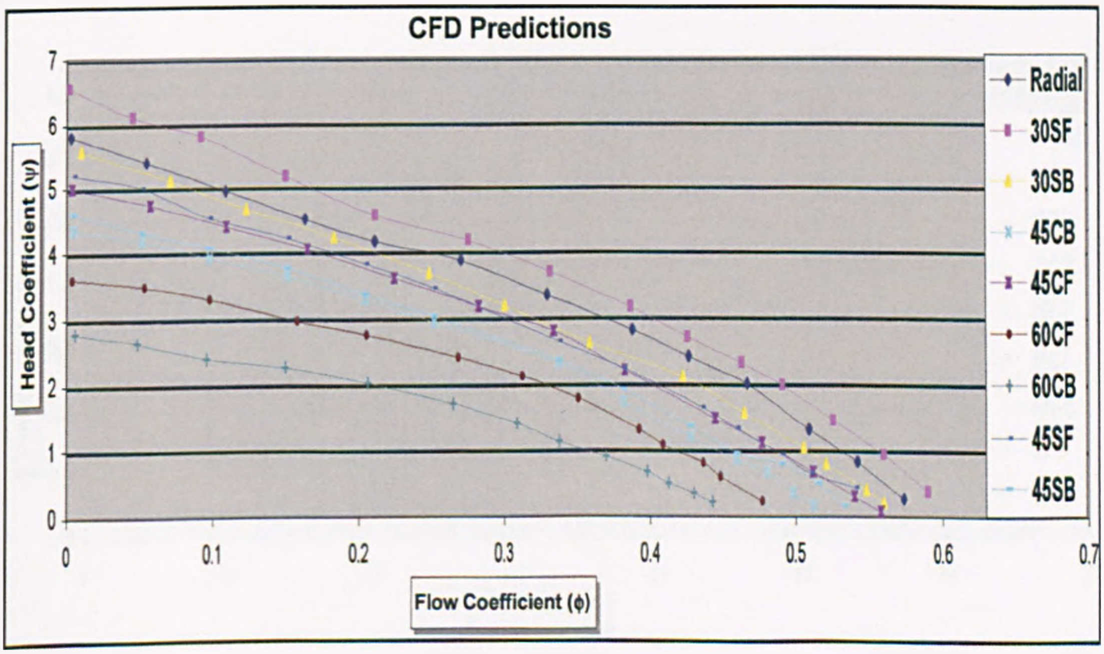

fig. 80 Head coefficient versus flow coefficient for CFD results

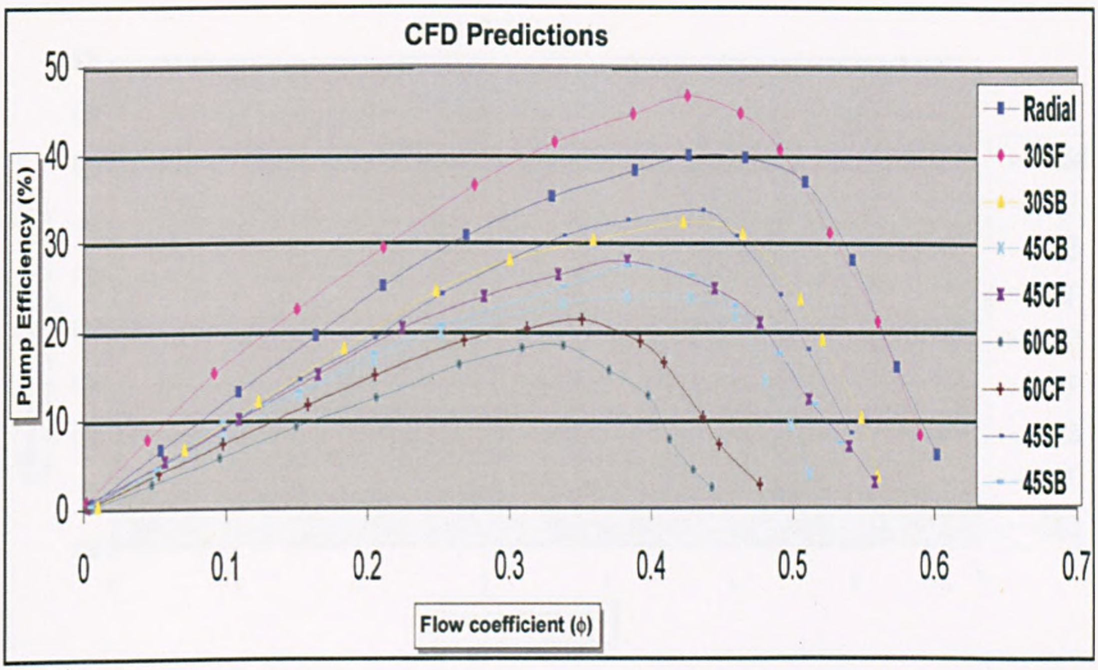

fig 81 Pump efficiency versus flow coefficient for CFD results

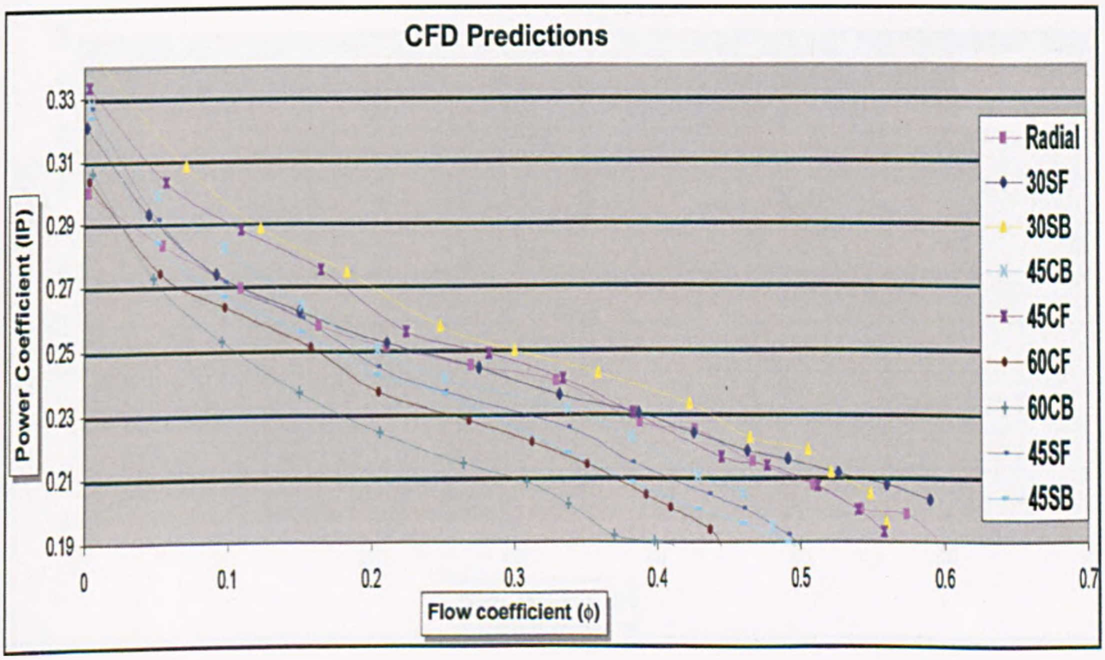

fig 82 Power coefficient versus flow coefficient for CFD results

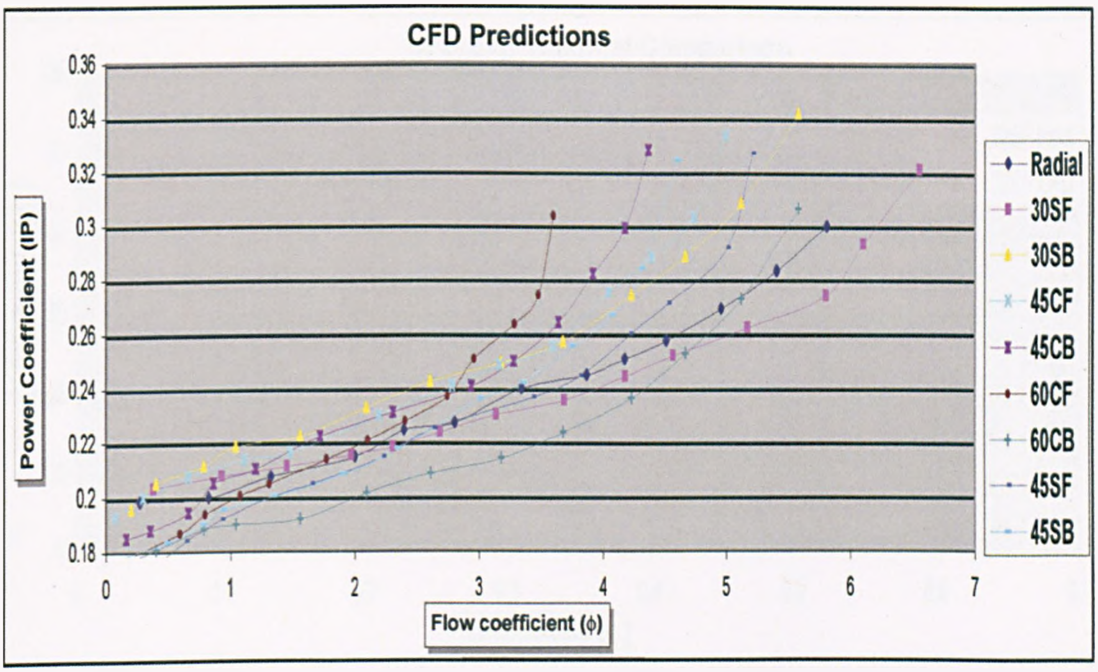

**fig. 83** Power coefficient versus head coefficient for CFD results

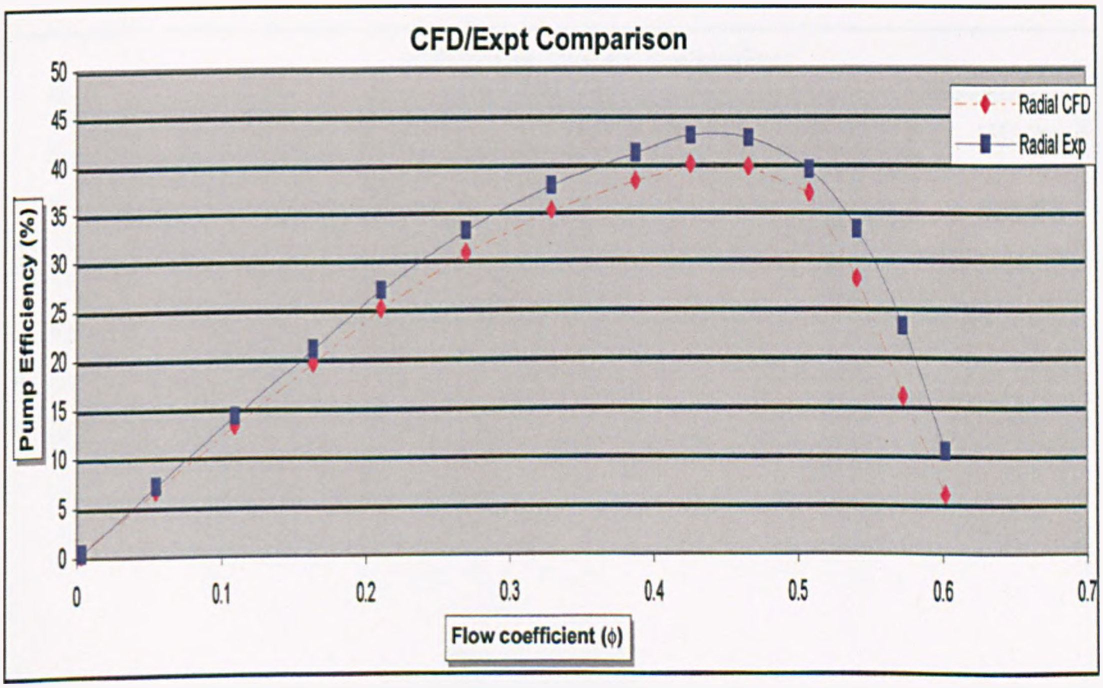

**fig. 84** Pump efficiency versus flow coefficient CFD/Expt. Comparison - Radial Blade

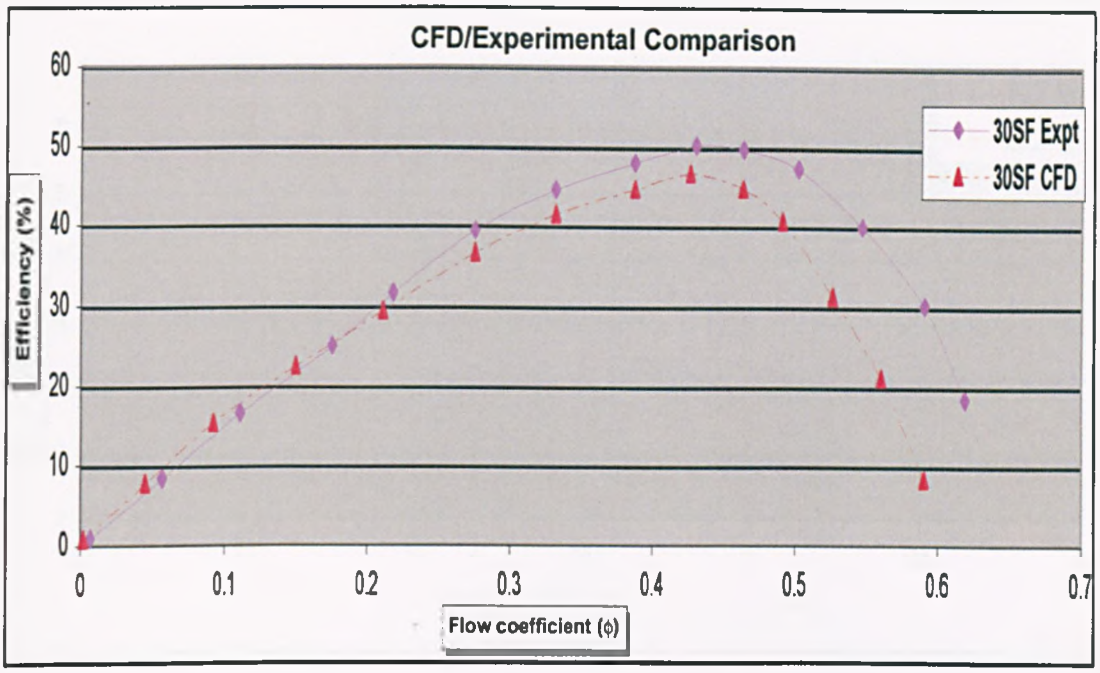

fig. 85 Pump efficiency versus flow coefficient CFD/Expt. Comparison- 30 deg swept forward

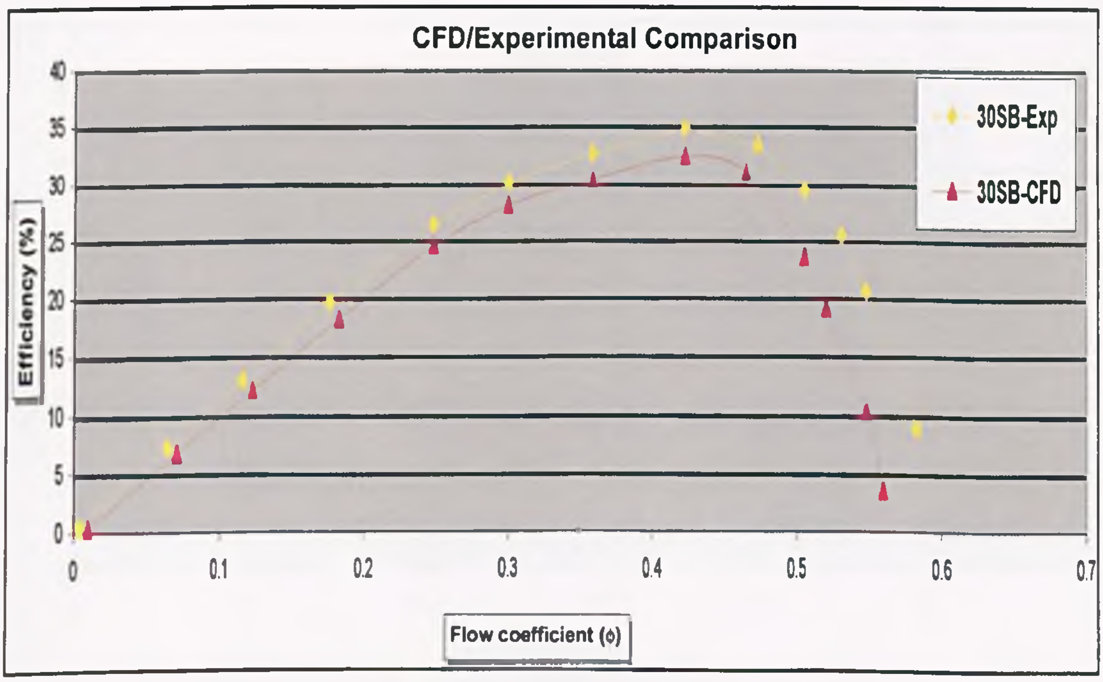

fig. 86 Pump efficiency versus flow coefficient CFD/Expt. Comparison- 30 deg swept backward

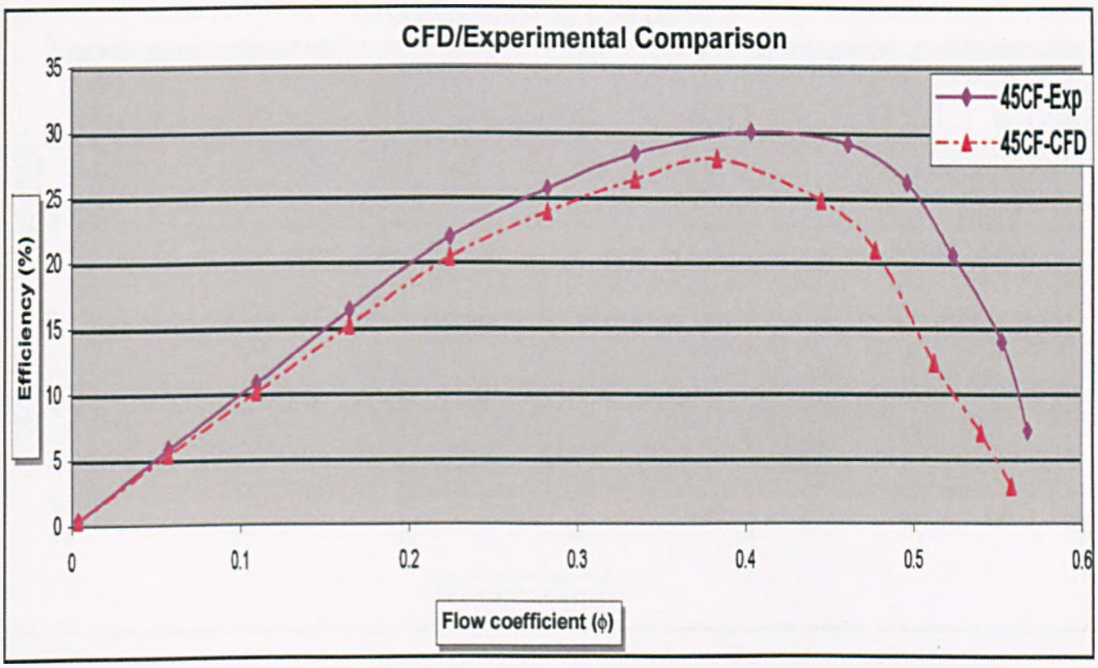

**fig. 87** Pump efficiency versus flow coefficient CFD/Expt. Comparison-45 deg chevron forward

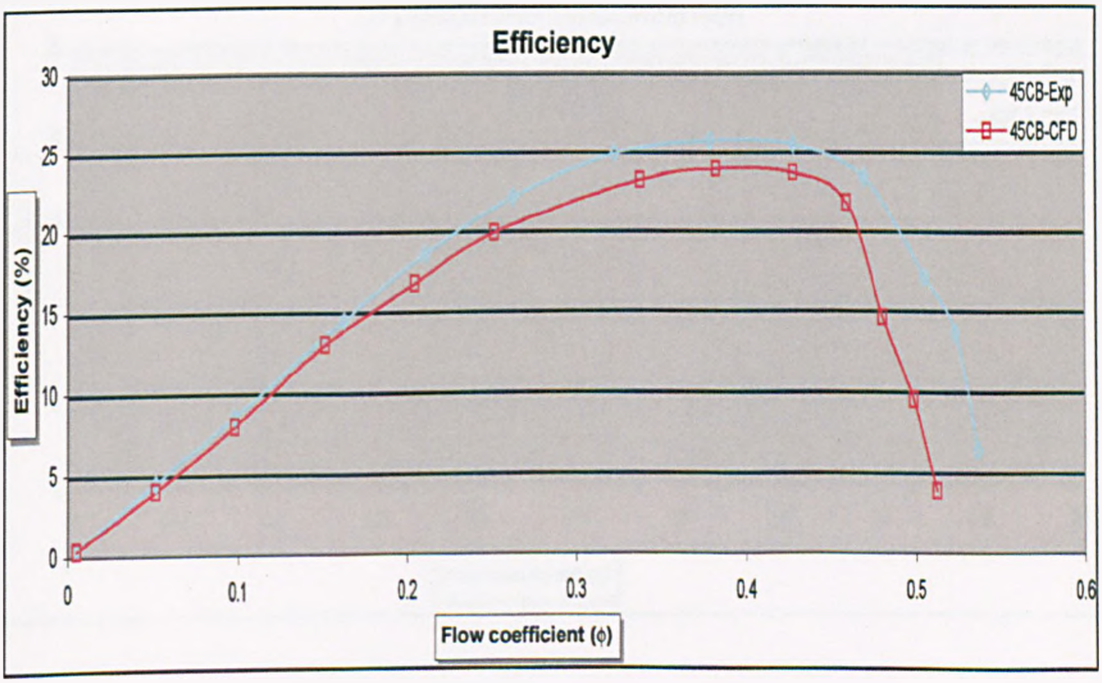

**fig. 88** Pump efficiency versus flow coefficient CFD/Expt. Comparison-45 deg chevron backward

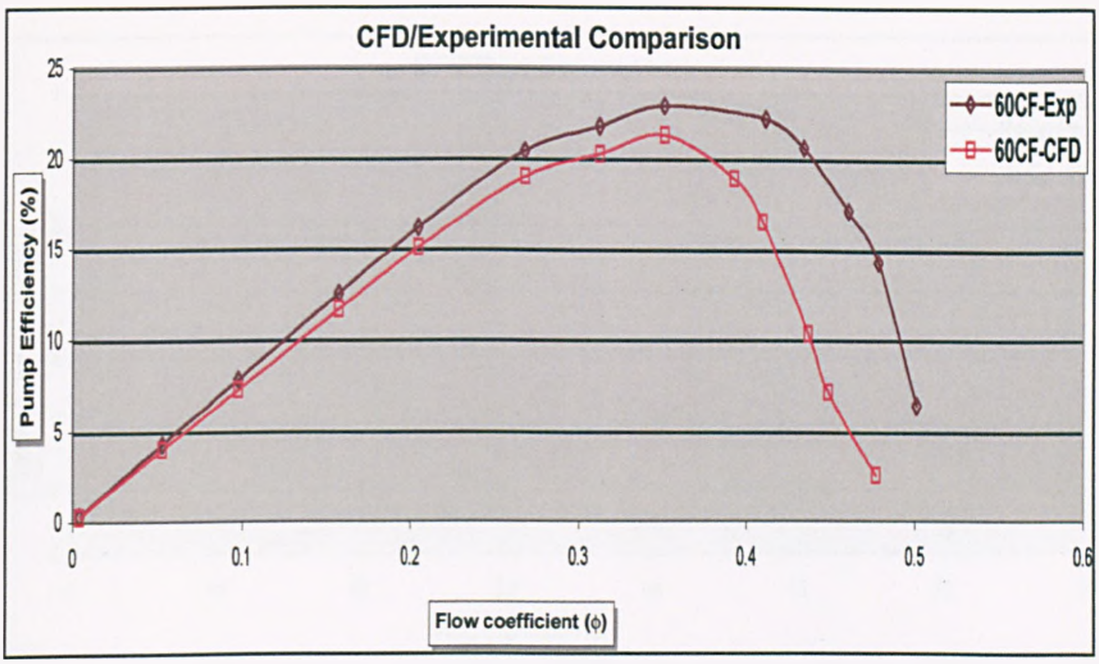

**fig. 89** Pump efficiency versus flow coefficient CFD/Expt. Comparison-60 deg chevron forward

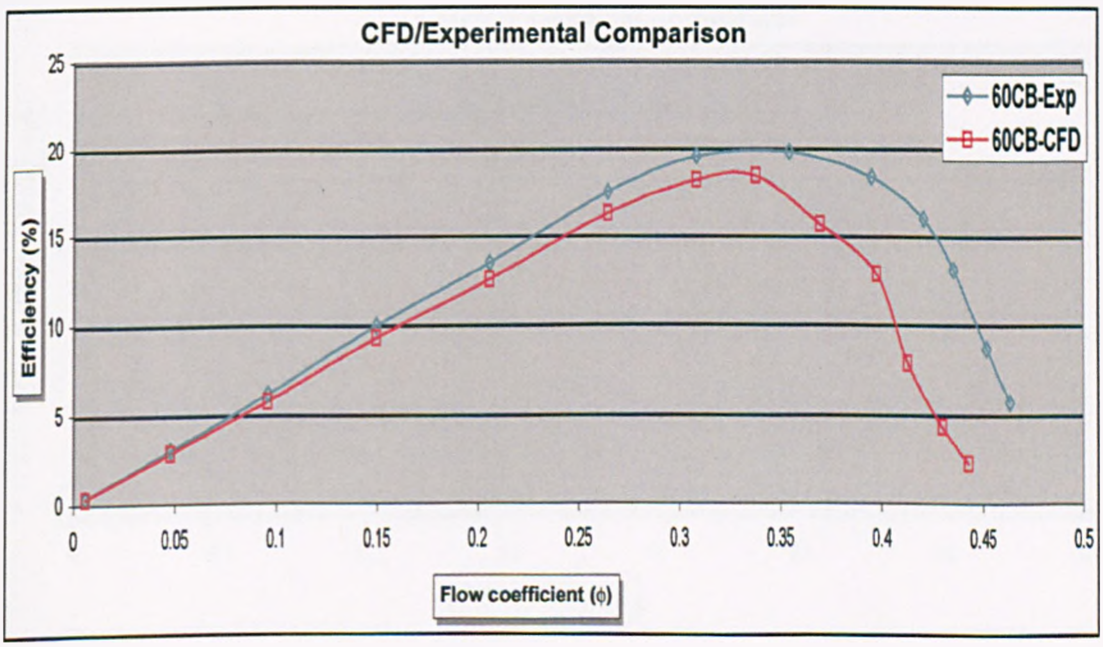

**fig. 90** Pump efficiency versus flow coefficient CFD /Expt. Comparison-60 deg chevron backward

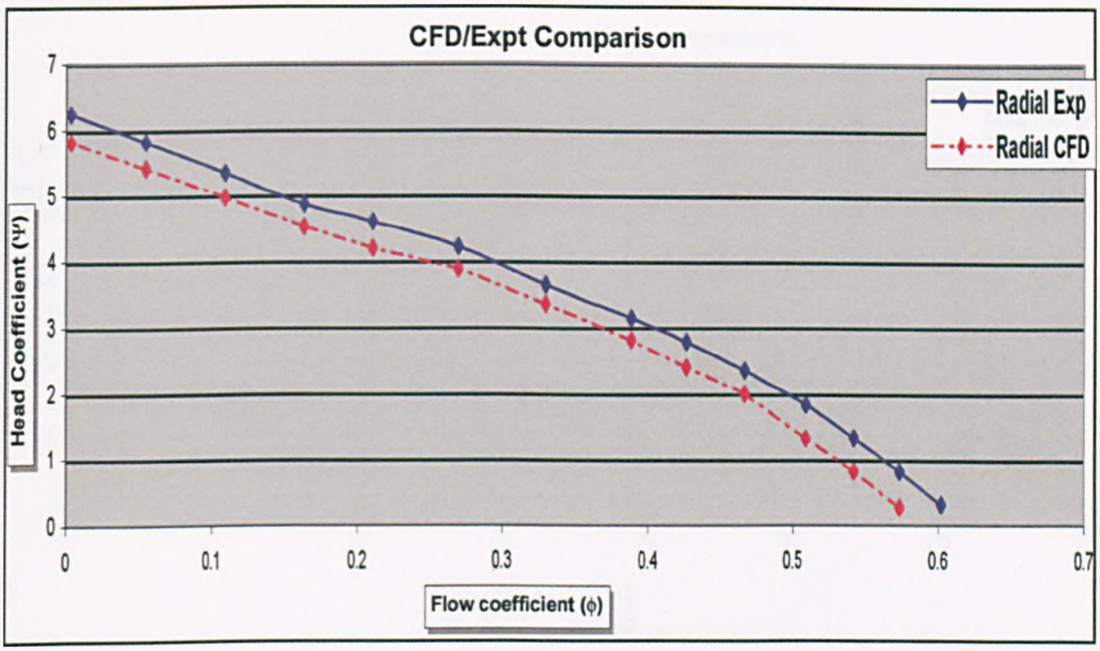

fig. 91 Head coefficient versus flow coefficient CFD/Expt - Comparison- radial

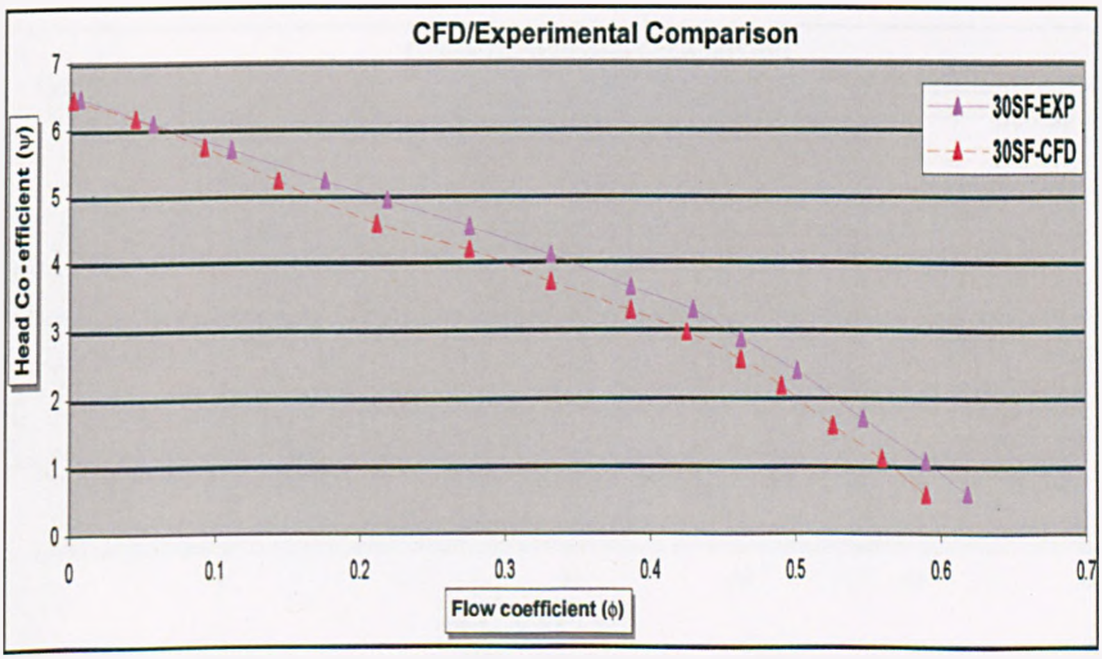

fig. 92 Head coefficient versus flow coefficient CFD/Expt - 30 deg swept forward

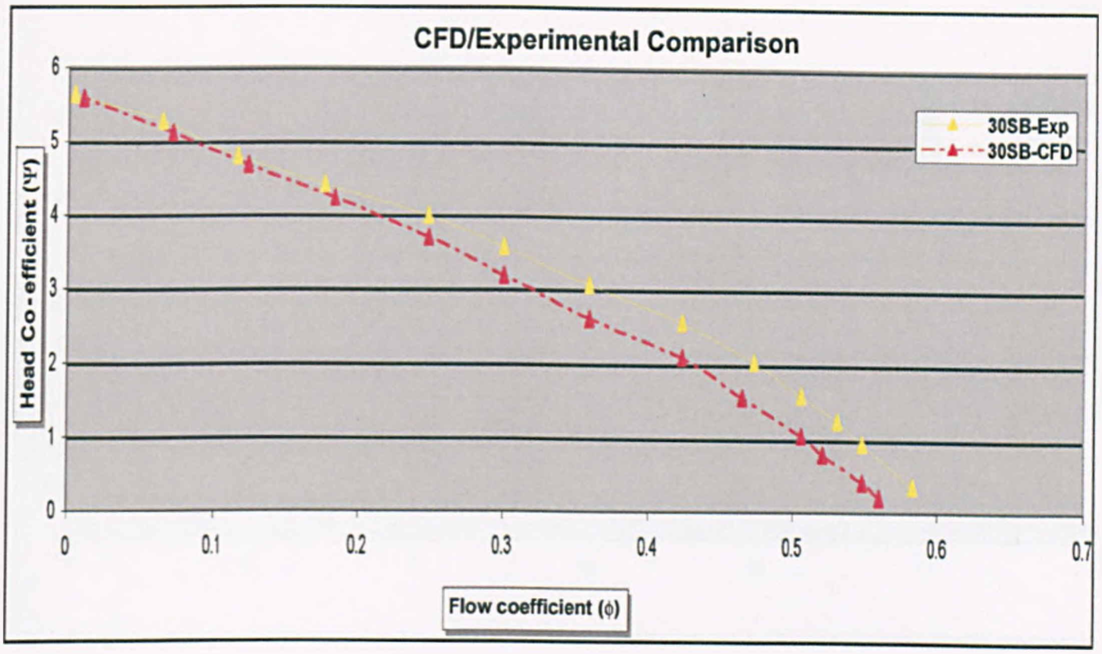

fig. 93 Head coefficient versus flow coefficient CFD/Expt - 30 deg swept backward

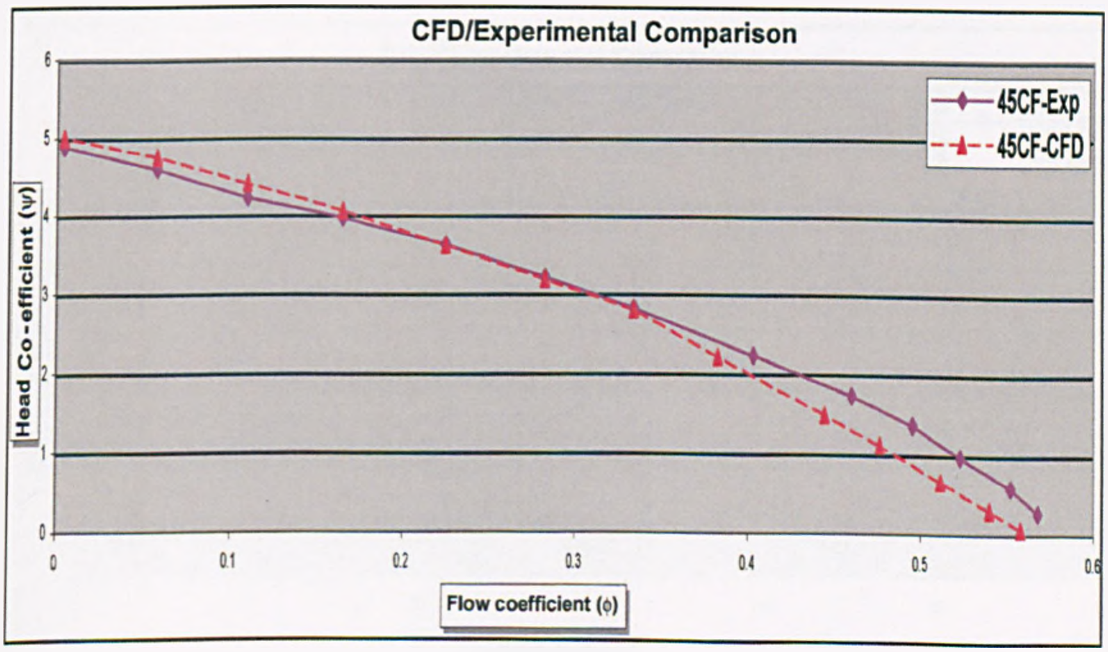

fig. 94 Head coefficient versus flow coefficient CFD/Expt - 45 deg chevron forward

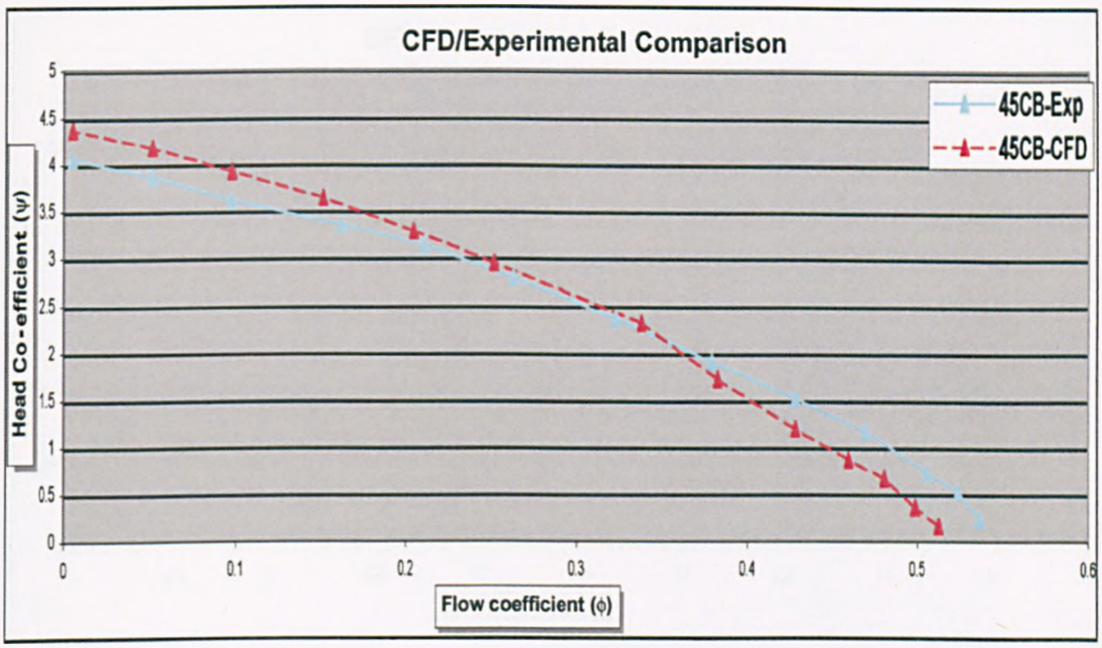

fig. 95 Head coefficient versus flow coefficient CFD/Expt - 45 deg chevron backward

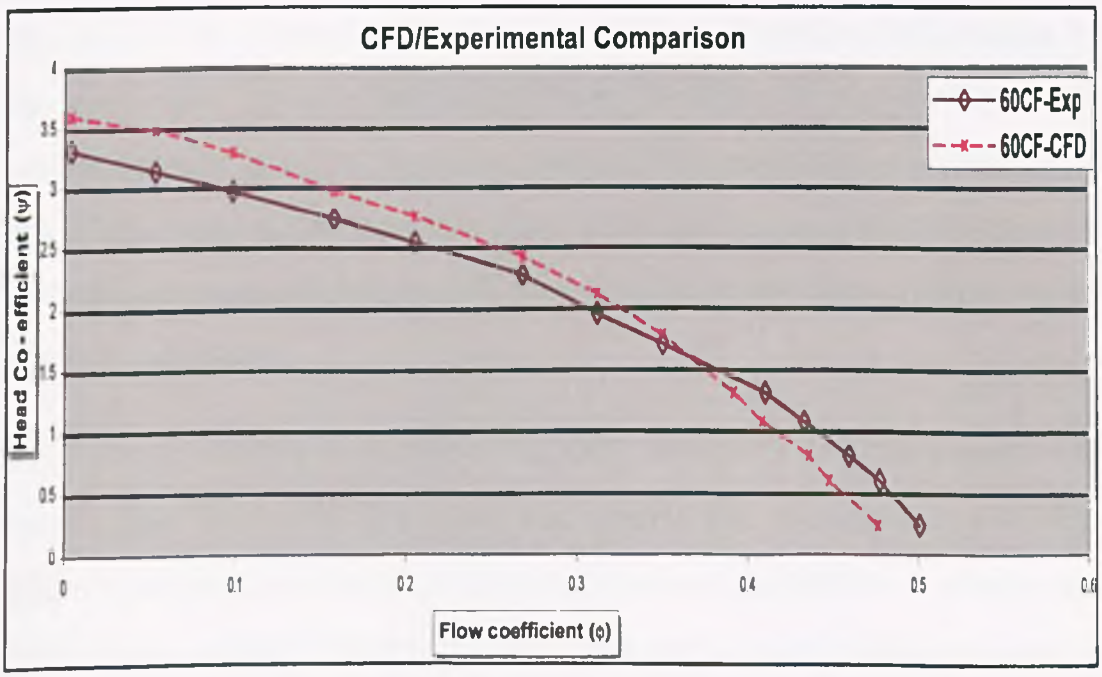

fig. 96 Head coefficient versus flow coefficient CFD/Expt - 60 deg chevron forward

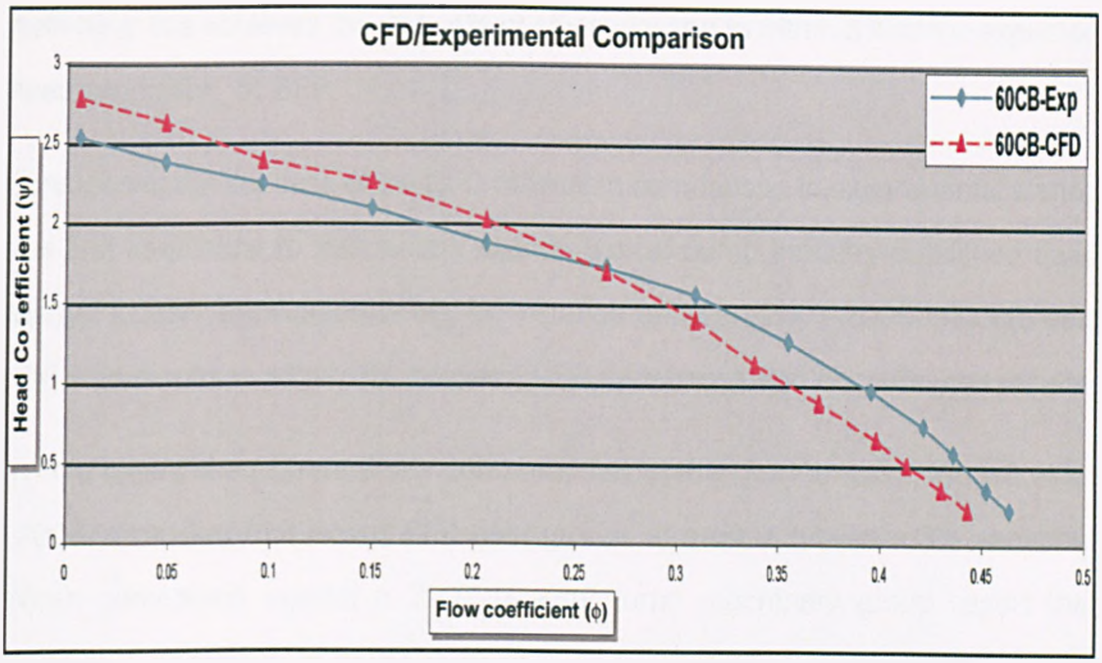

**fig. 97** Head coefficient versus flow coefficient CFD/Expt - 60 deg chevron backward

The characteristic curves for the obtained experimental data are illustrated in figs. 73-79. The obtained results follow expected performance characteristics for the regenerative pump, as detailed in Chap. 2.9. The plots represent the blade profiles coded in Table 20. The corresponding CFD model results are presented in figs. 80-83. Furthermore there are a series of selected comparative plots indicating the matched results between the CFD model results and the obtained experimental results in figs. 84-97.

When considering the matching of the CFD predictions and the experimental results, (figs. 84 to 97), it is clear that, despite the challenges in numerical modelling and experimental testing previously outlined, overall there is a reasonable concurrence between the two methods. Typically in pump simulation work of comparable size, FLUENT application briefs Ex 143 (2001), Ex 164 (2001) and Ex 232 (2005), using steady state MRF modelling approaches, the expectation is to have matching to within 7%. As indicated in figures 84-97 in the current study, matching was achieved to within 4% of efficiency and to within 3% of the expected head prediction, at BEP.

Considering the success of the CFD models in comparison to experimental testing it is first interesting to benchmark against typical pump industry published data. Many FLUENT application briefs for instance between 2001-2005 indicate best matched results to within 7% between CFD predictions and experimental results.

In this regard the current study compares favourably. Furthermore, Wollatt et al. (2005) indicated that expert CFD user groups at most achieved a 3% variation. When considered against a 2007 IMechE turbo machinery group report that suggest 3% variation in pump build to build uncertainty it is interesting that this level of comparison is of the same order.

*In the current study instrumentation variation of 6.6% was estimated* which is of the order expected in typical pump testing. Lindsay (1994) reported flowmeter uncertainty of the order of 5-10% and Martyr (2007) indicated 5% variation in dynamometer measurements. These terms seem to have the biggest effect in the variation of the efficiency terms. To a lesser degree Wulff (2006) and Doebelin (1990) reported uncertainty in head and speed measurement in pumps of the order of 0.6% and 0.06% respectively. Consequently when considering the calculated and predicted performance it is only seen beyond the BEP at high flowrates that the variation extends beyond 3 - 4%. Lindsay (1994) reported high flowmeter variation and in chapter 6 the significant effect of the shock loss terms at high flowrates adds to this trend. The current study focuses on the BEP region, as is typical in the pump industry. Better flow measurement techniques, chapter 8, will be considered to facilitate lower uncertainty at highest flows, which are regions of significantly higher performance variations, fig 85-90. Indeed at maximum flowrates the performance variation can be as high as 30%. However, it is worth mentioning that this region represents an area where regenerative pumps are typically not operated. This region produces the lowest head generation potential and most rapid drop in pump efficiency.

Clearly, overall, the results indicate that the highest head and power consumption occurs at the lowest flow rates (figure 73 and 75). As the flow rate increases through the regenerative pump, the efficiency increases, until there is a rapid drop off in efficiency at the higher flowrates (figure 74, 81). As with other kinetic pumps, the regenerative pump generates pressure from both tangential and circumferential velocity imparted to the fluid by the impeller. As the flowrate is reduced, for a fixed rotational speed (3000 rpm), there is more circulation through the blades which increase the circulatory power (fig 76 and fig 77). The head increases as more kinetic energy is imparted to the fluid and more power is consumed (fig 80 and fig 82). As the flowrate (through-flow) is increased there are less circulations in the pump. Less kinetic energy is imparted to the fluid by the impeller and consequently, the head and corresponding power decrease. This results in an increasing efficiency as the power consumption reduces. However, at highest flowrates, the corresponding shock losses increase until this dominates the flow, and there is a rapid drop in efficiency. The corresponding efficiency drop as the flowrate reduces is, in part, due to the increase power consumption. As the number of circulations rapidly increases however the slip losses soon dominate the flow and rapidly reduces efficiency. This is discussed further in Chapter 6.

Most authors, until now, have indicated that the mathematical models have limitations, and that precise CFD modelling is required to understand the flow mechanism, Meakhail et. al. (2005), and to predict unit performance. One of the objectives of this research was to not only match the performance but also to correlate this to the flow visualisation work of the 1940's and the 1950's. In the next series of figures, the CFD models are used to generate a series of representations of the flow within the pump. In so doing if a similar reasonable match to the expected flow patterns could be established, (as it was to performance), it would add further credance to the modelling approaches and asumptions adopted in this study.

Until now, the best interpretation of the flowfield came from experimental flow visualisation work carried out by Engels (1940), Bartels (1947), Lazo et al. (1953), Lutz (1953) and Wilson et al. (1955). Their work indicated a helical flowfield observed within the pump which can't be be accounted for in the work from Senoo (1948), Pfleiderer (1961), Iverson 1955), Crewdson (1956).

The modelling approach presented in this study replicates the expected flow, and is presented in the following series of plots figs. (98-105).

As illustrated in a pathlines plot (fig 98), spiral or corkscrew flow patterns occur in the pump's working section.

In fluid mechanics, helicity is the extent to which corkscrew-like motion occurs. If a body of fluid is moving, undergoing solid body motion rotating about an axis parallel to the direction of motion, it will have helicity. In the case of the regenerative pump this mechanism is created by the tangential (through flow) which is lower than the circulatory (impeller flow) uniting in the open channel. The resulting force in effect, induces and maintains the helical motion through the pump's working section. Tight clearances across the "stripper" region, in effect, strip the fluid of the circulatory component that induces the helix, and the leakage flow is typically that which is entrained in the impeller passages until the process continues once again at pump inlet.

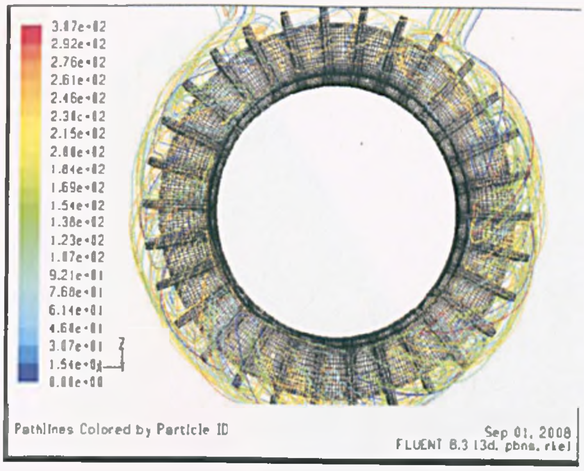

**fig. 98** CFD pathlines plot through regenerative pump working section

Furthermore, it is possible to plot an iso-surface through a section of the impeller and casing to represent the helical flow or the helicity contour profile (fig. 99).

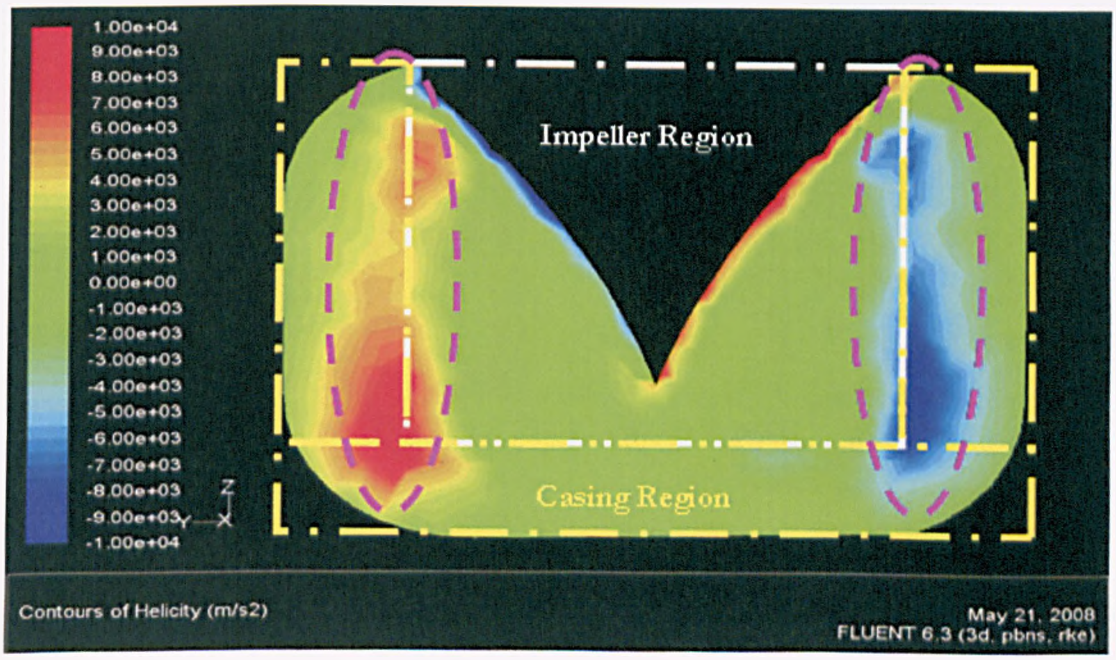

**fig. 99** CFD helicity contour plot through radial impeller blade standard

The following series of plots, fig's 100-105 indicate the varying helicity contour plots for the various blade profile standards (Table 21):

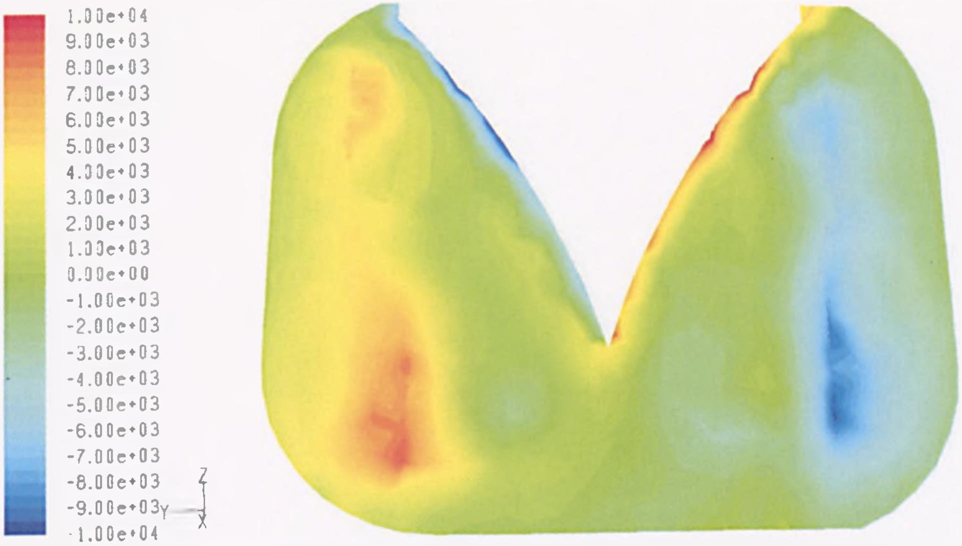

**fig. 100** CFD helicity contour plot through 30 deg swept fwd impeller blade standard

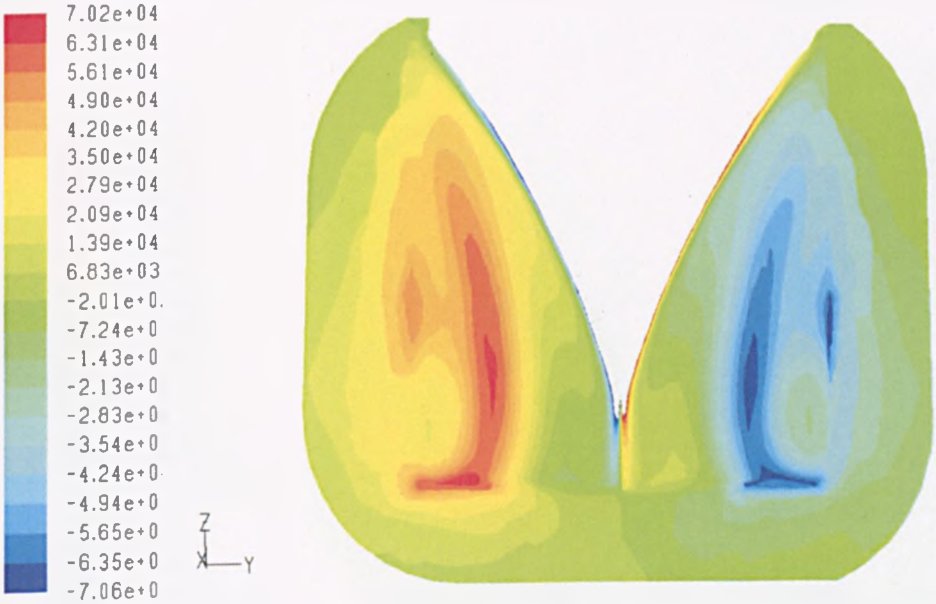

**fig. 101** CFD helicity contour plot through 30 deg swept bkw impeller blade standard

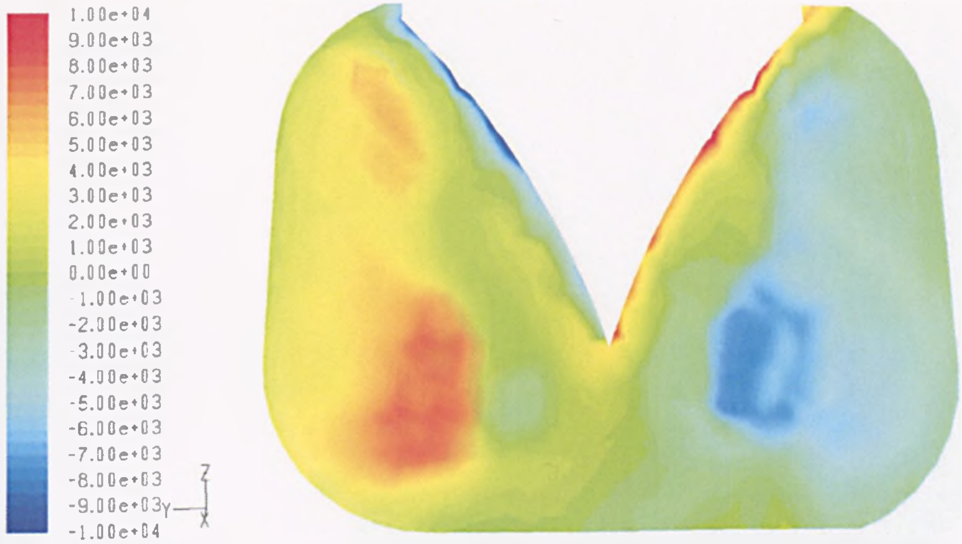

**fig. 102** CFD helicity contour plot through 45 deg swept fwd impeller blade standard

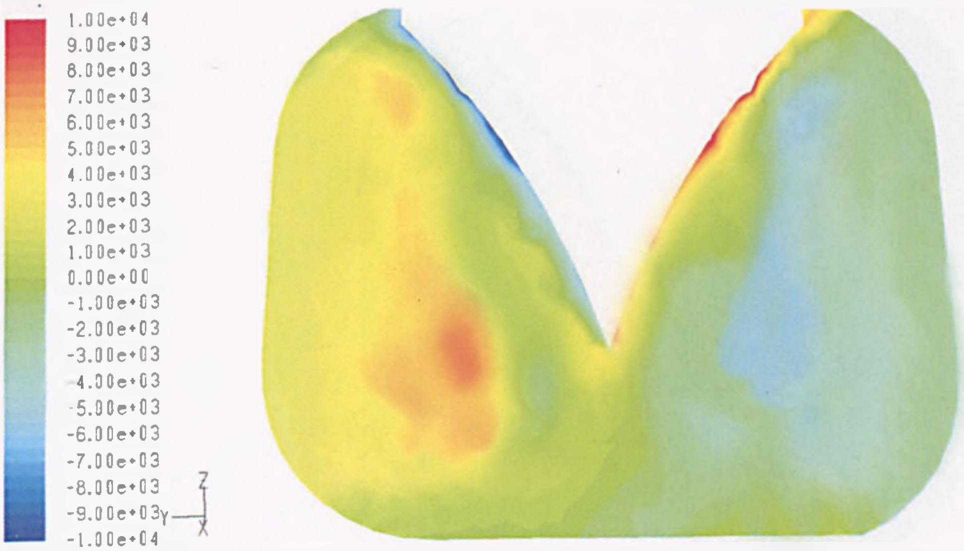

**fig. 103** CFD helicity contour plot through 45 deg swept bkw impeller blade standard

**fig. 104** CFD helicity contour plot through 45 deg chevron fwd. impeller blade standard

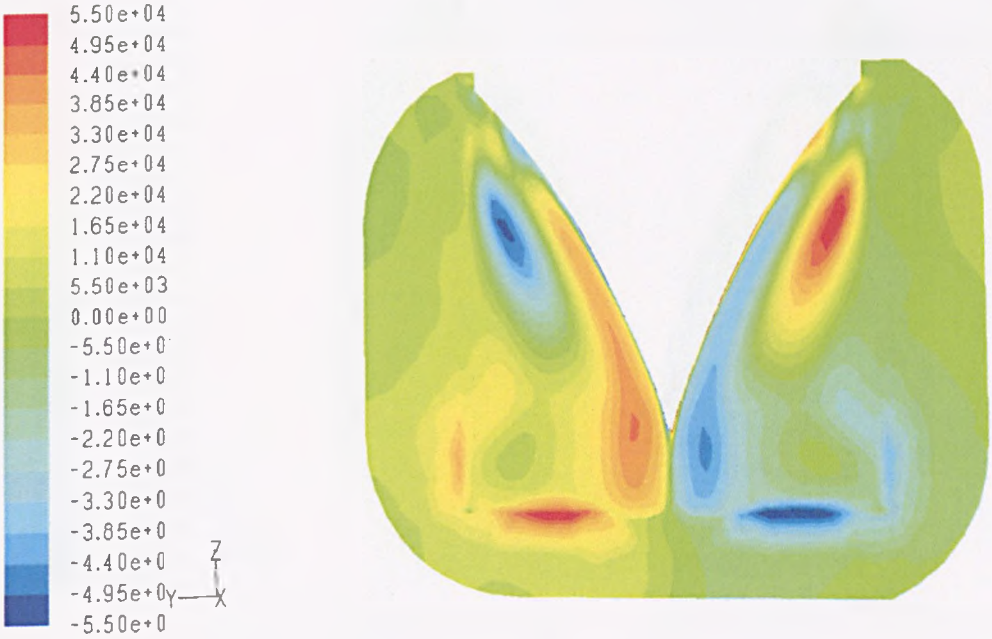

**fig. 105** CFD helicity contour plot through 45 deg chevron bkw impeller blade standard

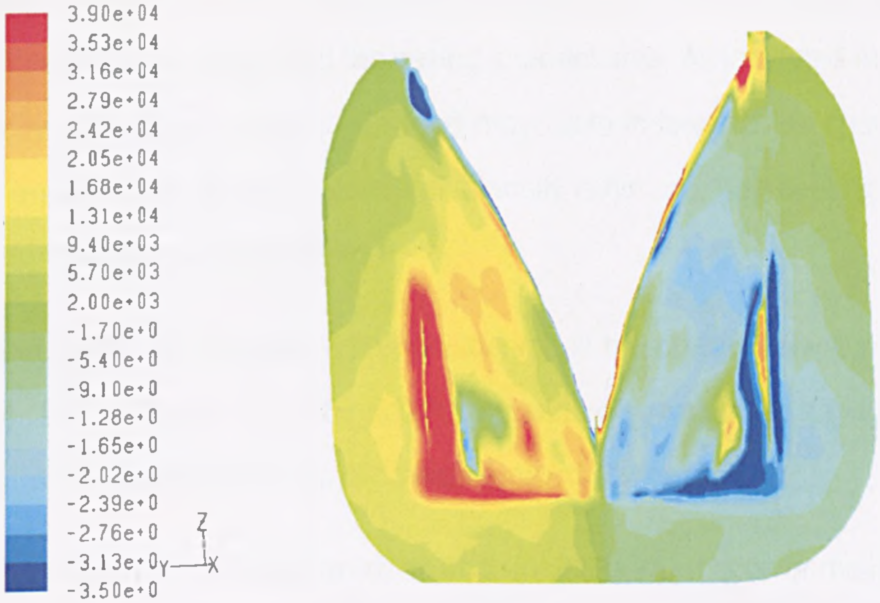

**fig. 106** CFD helicity contour plot through 60 deg chevron fwd. impeller blade standard

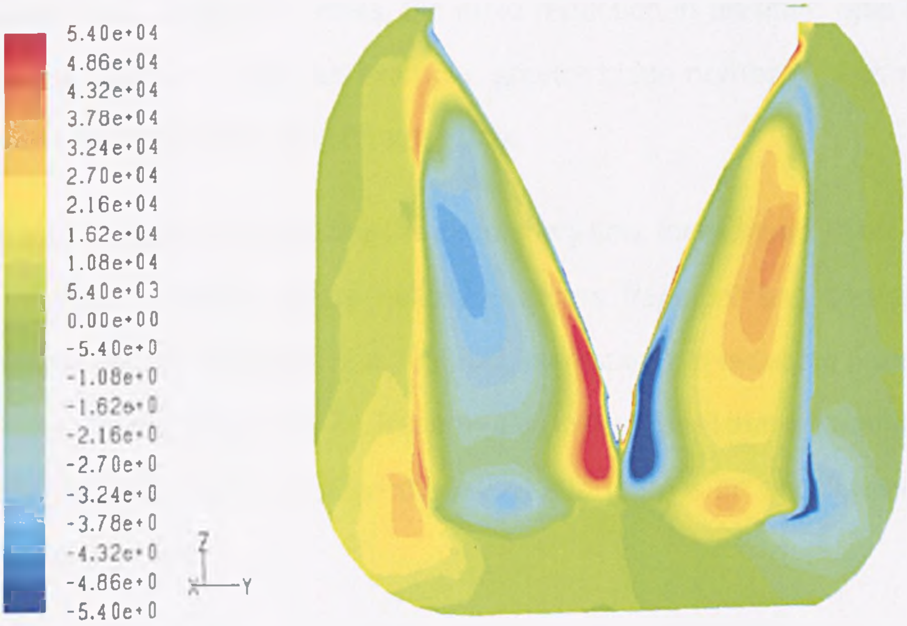

**fig. 107** CFD helicity contour plot through 60 deg chevron bkw impeller blade standard

When considering the helicity contour plots, some general observations can be made in relation to the different blade profile results.

In figures 99 and 100 the helicity intensity is clearly centred at the interface between the impeller region and the casing channel area. As indicated in fig. 101 the helicity intensity is starting to split and move both in towards the channel wall and the impeller hub. It would seem that intensity is not only fragmenting but also setting up multiple contour profiles.

This effect seems to increase when considering all the chevron blade profiles of fig's 104, 105, 106 and 107. The optimum standard seems to be a blade profile ranging from a purely radial to a 30° swept forward standard.

It would appear that the blades which seem to inhibit the formation or maintenance of the circulatory flows i.e. particularly the chevron blade profiles (fig. 104 - 107), have the most serious impact in overall performance.Wilson et al. (1955) considered that, at large flowrates, the rapid reduction in pressure ratio was due to large clearances or with, for example, greater blade numbers, thus reducing circulation flow and increasing through flow.

The effect of inhibiting or reducing the circulatiory flow, for example, in the chevron blade profiles is evident where helicity contours fragment and seperate. The fragmenting helicity contours, e.g. fig. 106, correspond to reducing performance as indicated for example in fig. 74. It seems also to be evident that at lower flowrates, the large circulations induce large slip losses and there is an equally detrimental effect on performance.

Experiments conducted by Lazo et al. (1953) and Lutz (1953)), used small thread probes at different points in the annular flow passage of the pump to determine the direction of the flow velocity. They were able to corroborate the helical streamlines when plotting the results. Engels (1940) demonstrated that, with decreasing flowrate, pump circulation is considerably increased, reaching a maximum as the flow from the pump is reduced.

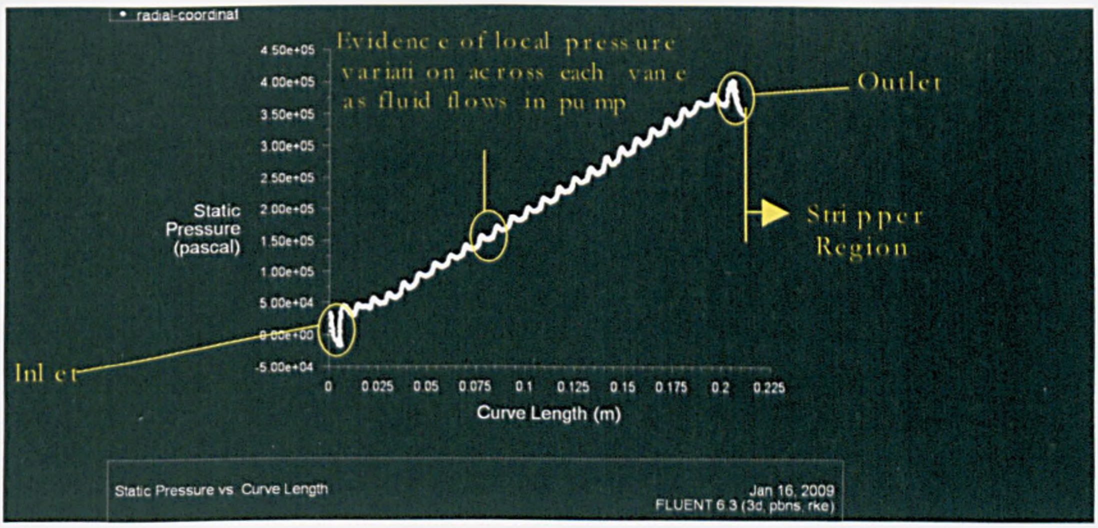

**fig. 108** Static pressure rise through regenerative pump working section

In the current study, fig. 108 not only indicates the pressure rise through the pump from inlet to outlet, but also how the pressure reduces and increases through each blade stage is indicated (fig. 109). Previous work, Pfleiderer (1961), do not describe the helical flow nature, instead conclude a constant circulation rate with reducing flowrate. These theories, instead, express that the circulation is only dependant on the resistance of the flow in the side channel and the impeller, and is independent of the pressure in the working channel. The current study can discount this, as demonstrated in figs. 108, 109.

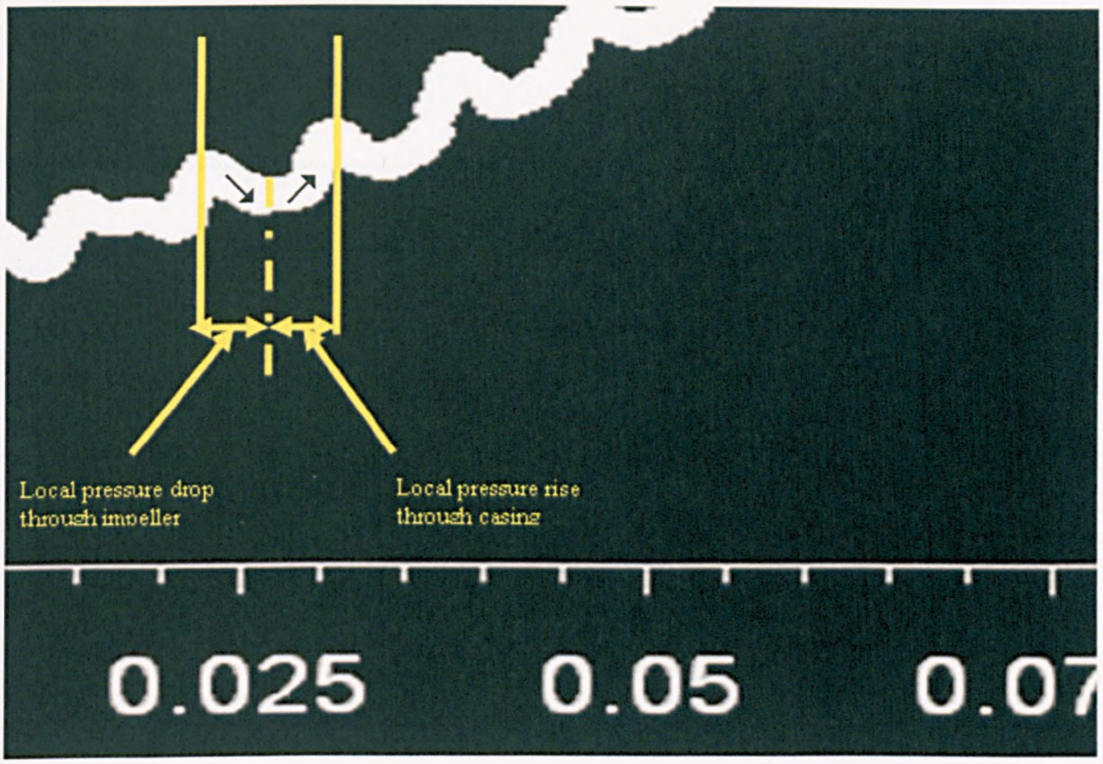

**fig. 109** Static pressure detail in impeller/casing section

Local pressure variations across each stage rise of the pump are indicated on a static pressure plot of fig. 109. Indeed all previous published mathematical assumptions of the tangential pressure gradient being independent of radius and also being constant, Chap. 2.5.5 (vi) and (vii), are not accurate, and as such add more uncertainty to the mathematical models published to date.

Until now, a typical straight linear representation (fig. 110), of pressure distribution has been presented, e.g. Wilson et al. (1955), Badami (1997), Song et al. (2003), Engeda (2003) and Raheel et al. (2005). The veracity of the current matching approach presented in this thesis captures not only the overall pump performance but also in doing so relates local pressure variations in the flowfield in a more precise manner to the observed helical contours (fig. 111).

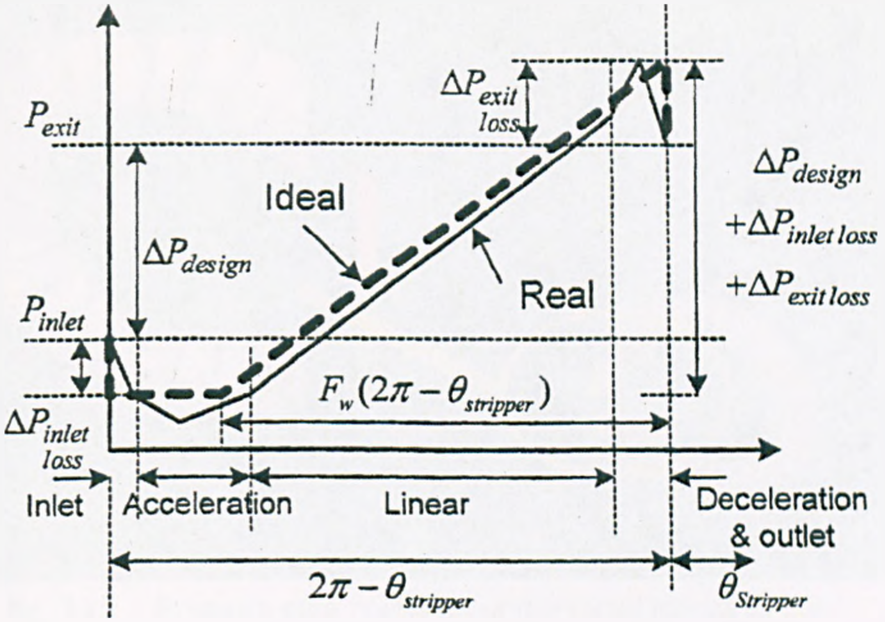

**fig. 110** Published static pressure rise through regenerative pump working section (Engeda et.al (2003))

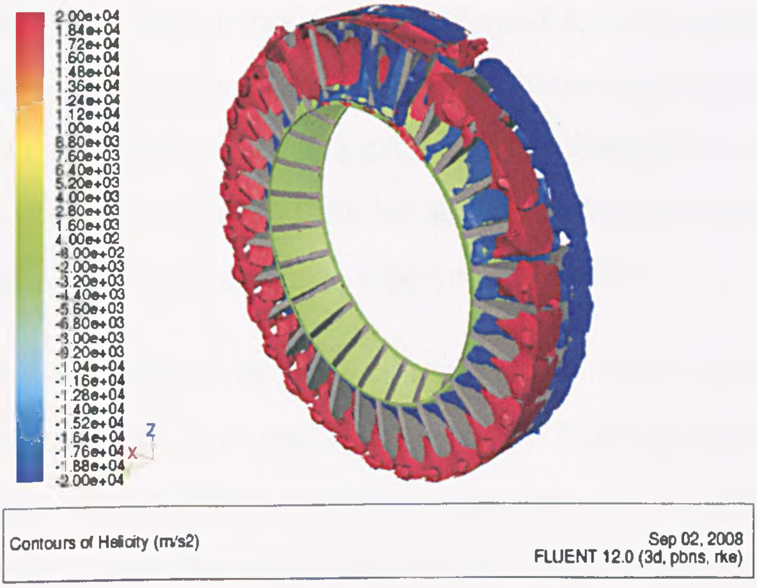

**fig. 111** Helicity contours across regenerative pump impeller

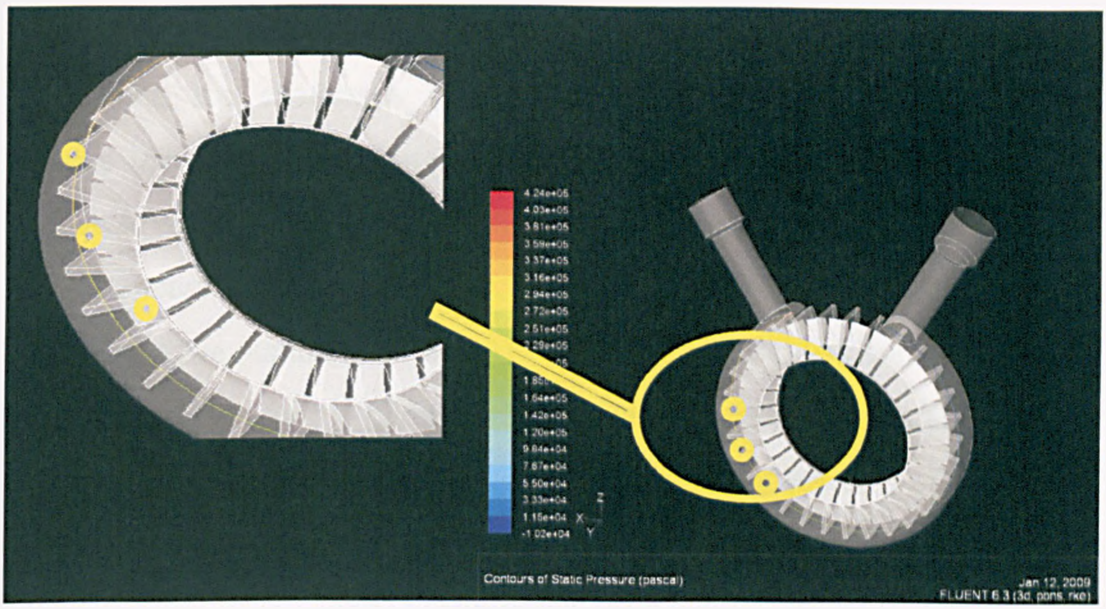

**fig. 112** Pressure rake points around a radial iso-surface in regenerative pump impeller

Clearly the reliance of the previously published data on empirically derived loss coefficients (chap. 2.7) limits their ability to assist in the design improvement process. Being essentially one dimensional, tools that take no account of spanwise variation, prevents adequate loss representation and, as a result until now, the design of regenerative pumps has largely depended on large and expensive amounts of testing. With the availability of fully 3 dimensional modelling that captures not only the observed flowfield (figs. 98-105), but also the performance (figs. 73-97), CFD is now becoming integrated into the experimental process.

For instance, the need to heavily instrument a test rig is diminished and data (e.g. the experiments conducted by Lazo et al. (1953) and Lutz (1953),) using small thread probes at different points in the annular flow, can be obtained using CFD (fig. 112). Indeed the intrusion effects from instrumentation discussed can be replaced with a well validated model. The following chapters will discuss the significance of these results and the likely future approach for regenerative pump design.

## 5.7 Summary

Considering the challenges of conducting a numerical and experimental analysis with respect to accuracy, repeatability and with the inherent strengths and weaknesses of both the results of the study are encouraging. An optimised blade standard has been tested and equaled the highest reported efficiency for the regenerative pump in this study. Furthermore not only has the expected flow visulisation results for the pump been captured in the CFD results to match the best published visulisation experimental results but that the CFD approach has enabled further information to be published namely the local pressure variation across impeller blades which until now has been considered linear.

# Chapter 6

## Discussion, of results

Previous published mathematical models have proved of limited use in the regenerative pump to resolve the complex flow regime within the pump. They have been inconclusive in being able to explain the energy dissipation mechanisms that reduce pump performance and what changes in design could be introduced to improve hydraulic efficiency. These mechanisms are discussed later in Chapter 6 with the introduction of a turbulance intensity factor and corresponding plots.

As indicated in Chapter 5, two fundamental assumptions for the tangential pressure gradient in these previous models have been shown to be inappropriate for the regenerative pump, with respect to gradient and radius.

However it is not only possible to demonstrate that the tangential pressure gradient varies through the pump as the kinetic energy increases in the impeller region and reduces in the channel region, as detailed in Chapter 5, it is also possible to capture inlet and outlet loss effects.

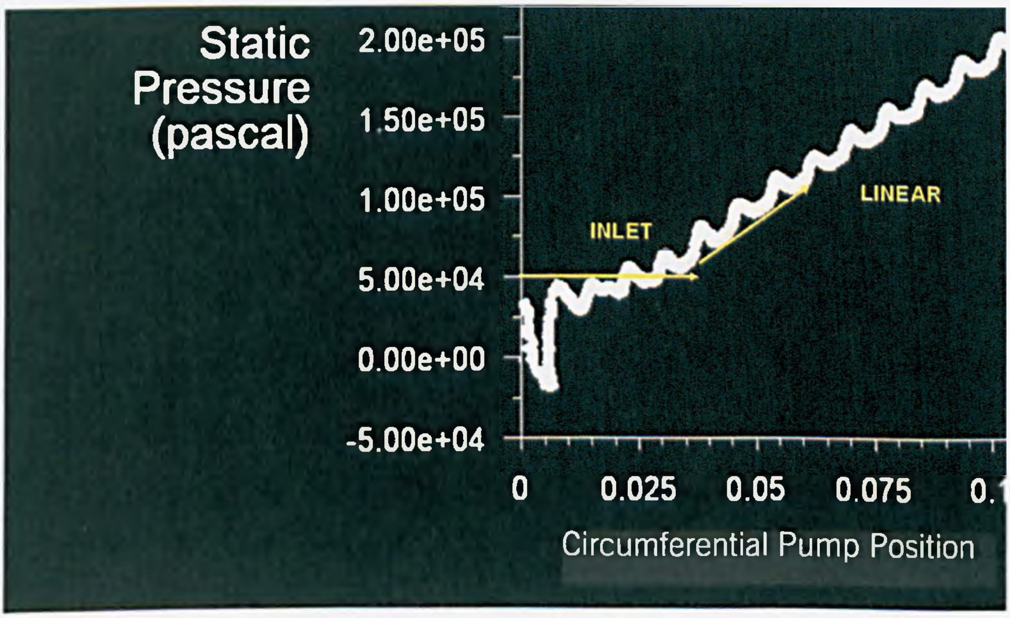

**fig. 113** Flat inlet pressure gradient for regenerative pump.

Clearly in the tangential pressure plot there is a relativley flat gradient over the first four impeller blade stages where there is virtually no net pressure increase, fig 113. This effect has been reported by Engeda (2003) and others in experiments concerned with the developing region. It is not until the linear section that the helical flow becomes fully developed and there is a steady pressure gradient rise established.

Senoo (1952), and others have conducted work in this so called developing region and indicated that there is potential to not only improve the performance of the pump but also improve the NPSH for the pump.

In the current work, modification of these features was not considered within the scope but this will be assessed in the future work where both inlet and channel area will be altered to quantify the performance effect.

To a lesser extent it is also possible to see the associated loss with the outlet or deceleration region. Here a flattened performance rise in pressure is evident over the last two blade stages approaching the outlet region.

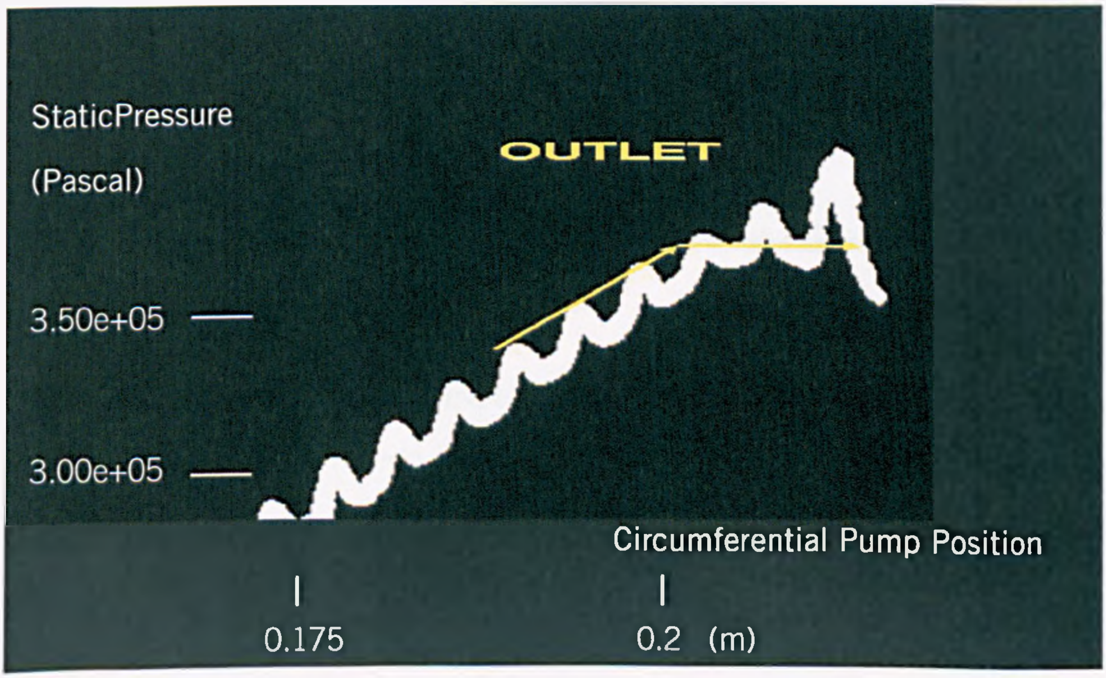

**fig. 114** Flat outlet pressure gradient for regenerative pump.

Consequently some 20% of the blades within the pump working section, (inlet to outlet), are not operating at optimal performance. As indicated in the future work, geometry modifications will be assessed to understand the potential for performance improvement in this regard.

Furthermore the main energy dissipation factors, in addition to the inlet and outlet losses, can be accounted for in terms of the slip and shock loss terms, chap 2.6, 2.7. These energy dissipation effects can be accounted for and compared to the blade geometry modifications of the current study and appear to have the biggest effect on the pump overall performance.

Pressure gradient between any two adjacent blades in an impeller leads to a tendency for fluid to deviate from the path prescribed by the blade in a rearwards direction, and instead slip backwards to the rotational direction. The tangential velocity at exit to the blade is thus less than that expected. Regenerative pumps as indicated above are primarily designed to develop tangential pressure gradient. Slip is basically a non-friction effect, and has a direct effect on the energy transfer.

In the regenerative pump the energy dissipation mechanisms that reduce the efficiency of the pump can be considered in terms of turbulent dissipation at the blade tips and at the blade entry.

In the turbomachinery industry the entry losses are termed shock losses $\alpha$ and the exit losses are termed slip losses $\sigma$.

Using the CFD results it is possible to illustrate these effects by plotting values of turbulent kinetic energy ($m^2/s^2$). For the purposes of the current study an additional non-dimensional expression is defined which captures this turbulent dissipation (irreversibility). Turbulence intensity can be expressed using an area weighted average turbulent kinetic energy term (net) for the impeller and channel regions of the pump and is expressed as:

Turbulence Intensity $T_i$:

$$T_i = \frac{k}{\omega^2 R^2} \qquad (31)$$

k = Turbulent kinetic energy term ($m^2/s^2$)

R = Impeller Radius ($m^2$)

ω = Impeller angular velocity ($rad/s^2$)

The turbulent intensity can be plotted against flow coefficient to indicate the characteristic for the regenerative pump and in particular how it compares across the range of considered blade geometries, fig 115.

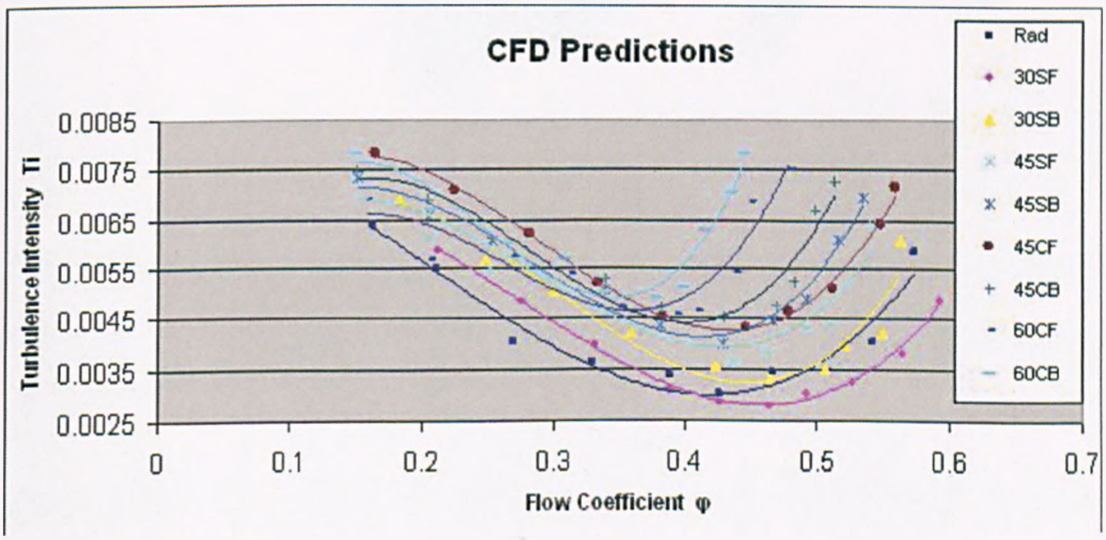

**fig 115** Turbulence intensity vs. flow coefficient CFD predictions

It can be seen that there is a strong region of turbulence intensity at both low flowrates and high flowrate regions of the pump characteristic. The profiles which seem to generate least turbulence intensity are the radial and least swept profiles. As the profiles become more swept and into the chevron profiles the intensity significantly increases. The turbulence generation will be discussed in terms of the slip and shock effects however at this point it is evident that the chevron and maximum swept blades increase the intensity, and the radial and the swept blade profiles reduce the intensity. It is possible to plot the turbulent kinetic energy for most of the blades profiles in the study. However the ability to create an iso-surface plot plane across a single chevron profile would not be possible as it would cross two blade planes, fig 116.

**fig 116** Iso-surface plot plane through swept blade profile

For the radial and swept blade profiles it is possible to plot the variation of turbulence intensity with flow coefficient as an indication of the energy dissipation in the pump.

As indicated in fig 117 there is for the 30° swept forward blade profile a distinct concentration of turbulent kinetic energy dissipation extending from entry of the blade. However there is little indication of turbulence at the blade tip, which suggests a more favorable design with respect to minimising blade slip effects.

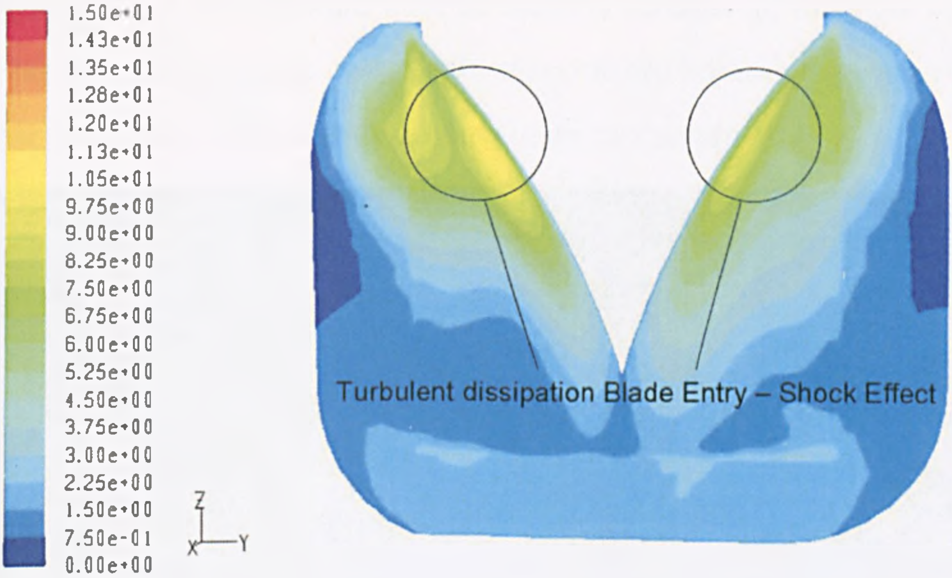

**fig 117** 30° swept forward blade turbulent kinetic energy distribution

As the blade takes a more typical straight radial profile there is a indication that the turbulent kinetic energy is increased in intensity not only at the blade entry but there is a small region of blade tip turbulent dissipation suggesting a less favorable design with respect to slip, fig 118.

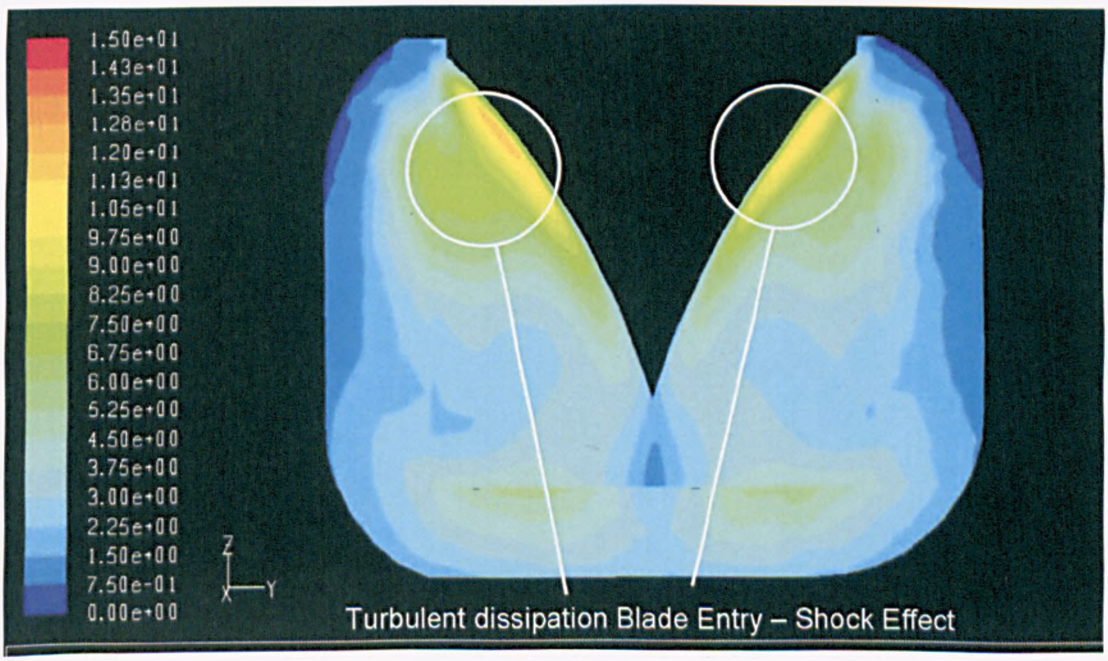

**fig 118** radial blade turbulent kinetic energy distribution

Again when a more forward inclined blade is considered, as in the 45° profile, there is a more favorable design with respect to slip however there is an indication that the shock effects at entry become more concentrated.

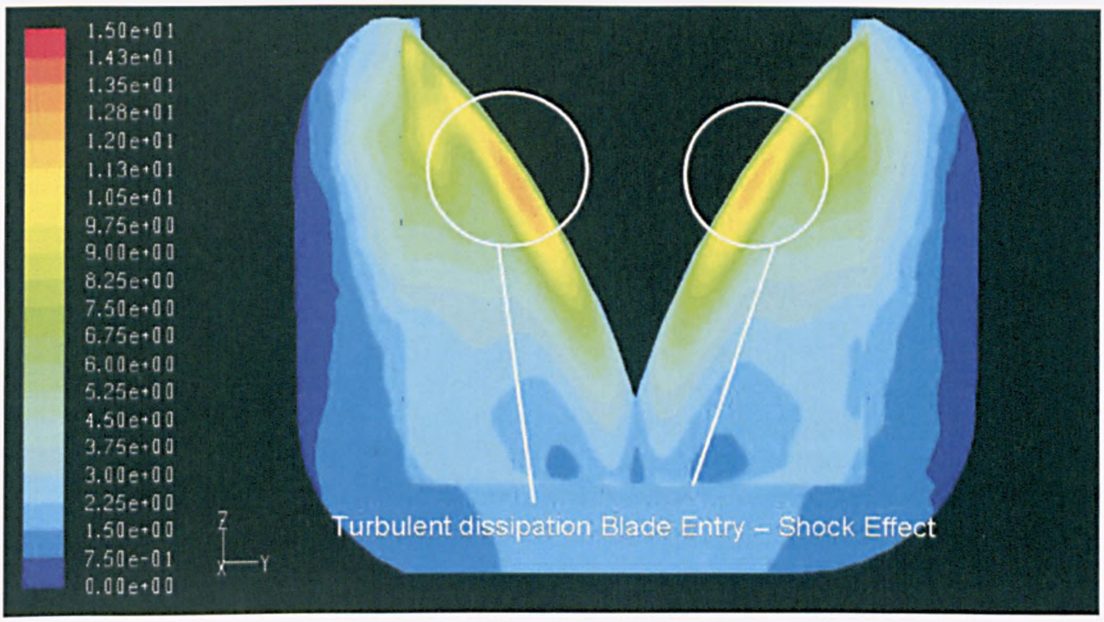

**fig 119** 45° swept forward blade turbulent kinetic energy distribution

In contrast as the blade profile takes a more swept rearward profile, 30° swept rearward, the slip effects at the blade tip regions increase. This is seen with the local concentration in turbulent kinetic energy, fig 120. There is a reduced level of shock losses from entry to the blade.

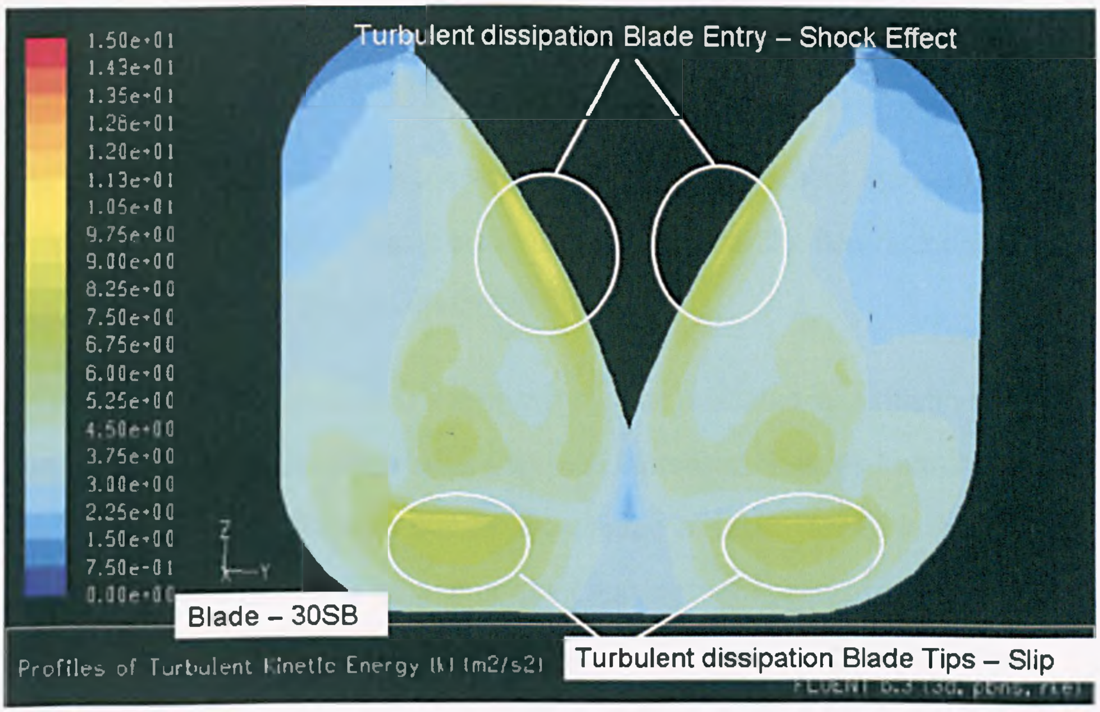

**fig 120** 30° swept backward blade turbulent kinetic energy distribution

Finally there is increased concentration in both entry and exit (shock & slip) losses for the 45° swept rearward profile as indicated in fig 121.

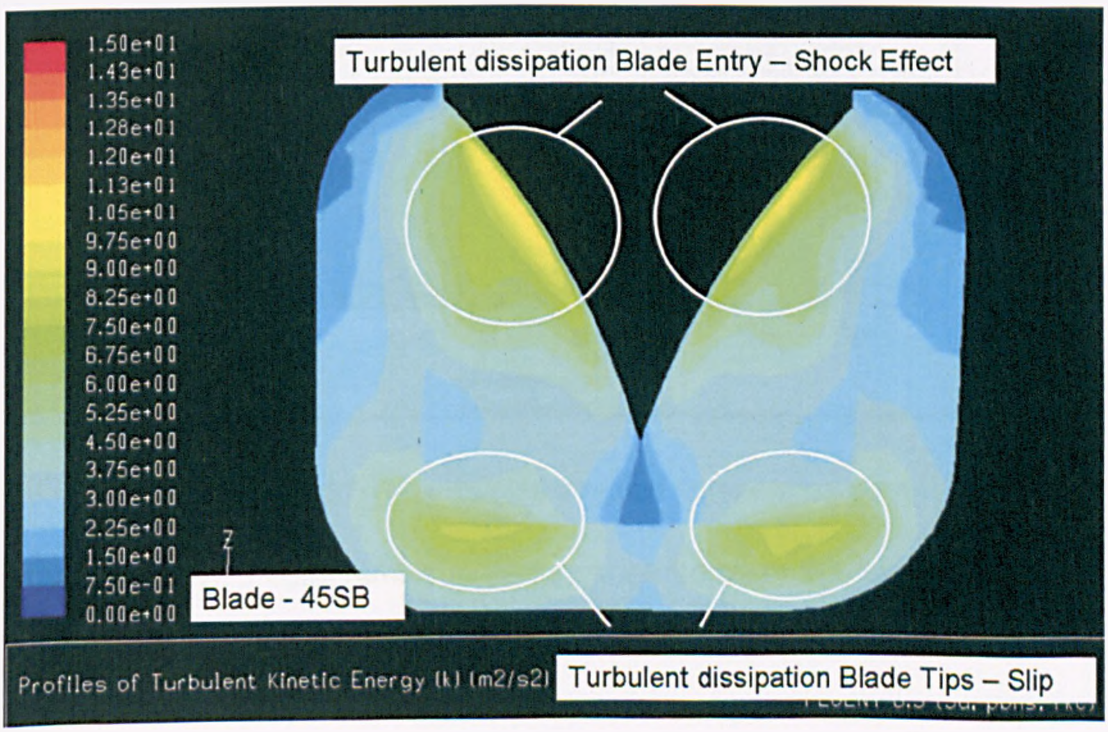

**fig 121** 45° swept backward blade turbulent kinetic energy distribution

The effects of the slip and shock effects will now be considered in relation to the overall performance of the regenerative pump.

Slip significantly increases as the tangential pressure gradient increases. This is indicated in the dramatic drop in efficiency, fig 122, over the flow region where the most significant head rise occurs in the pump.

Hollenberg (1978) conducted experiments that indicated a reduction in head and efficiency as the impeller clearance was increased. Results from the current study support these findings that as the degree of blade sweep increases, e.g. 30° → 60° blades, the effect is the same as increasing the impeller tip clearance which reduces the performance of these blades as the tip to casing gap increases.

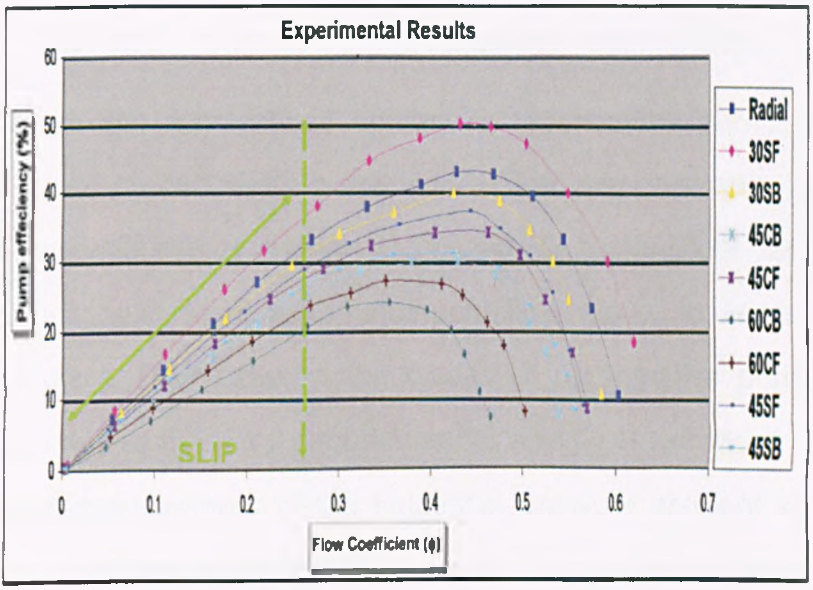

**fig 122** Slip loss dominant region regenerative pump

There is always a compromise in performance between the head rise and the efficiency in this type of kinetic pump; however the objective is to design a pump which extends and maximises the optimal working region e.g. Radial and 30SF in fig 123. The blades that minimise impeller tip clearance, (ie. 30 swept and radial blades), have a larger optimal working section, fig 123. Blades which over extend, ie increase tip clearance in effect reduce the optimal working section, (45° and 60°), fig 123.

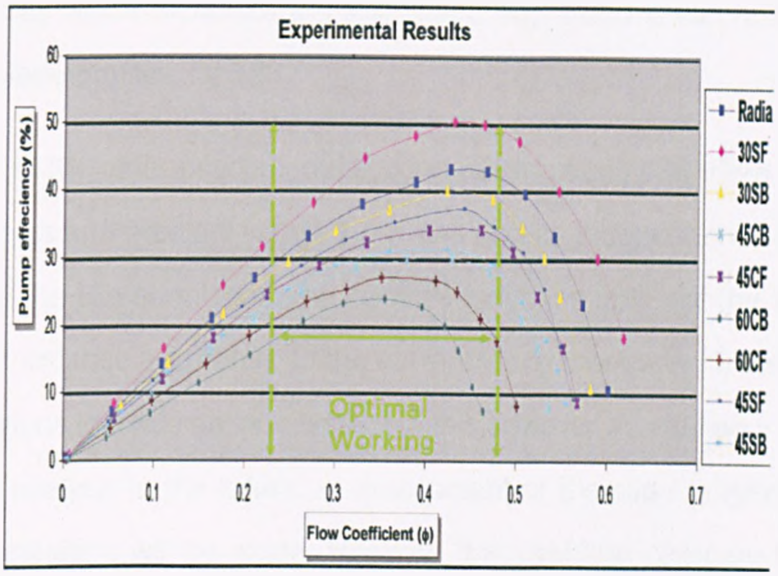

**fig. 123** Optimal working region regenerative pump

To date all the slip formulations applied to regenerative pump publications have been based on centrifugal pump work. These slip correlations do not take account of tangential energy gradient and thus these formulations cannot apply to regenerative machines which were fundamentally designed to develop tangential pressure gradient. Flow between the blades of regenerative pumps differ to centrifugal pumps as there is a circumferential velocity at exit which is not wholly radial. Careful measurement of the tangential pressure gradient at exit would provide the needed experimental assessment of slip in regenerative machines. This is within the scope of the future work to be conducted on the pump. However it is clear that currently the tangential pressure gradient increases the relative axial component of vorticity. The vorticity or tendency for fluids to spin is related to the amount of circulation, which has clearly been shown in Chapter 5, to reduce the efficiency of the pump at low flowrates.

As the flowrate reduces in the pump the fluid circulations increase as the fluid is subject to more impeller impacts for a constant rotational speed, the tangential pressure rises which increases the slip effect. This trend is eident across all the assessed blade profiles, fig 123.

In addition to the other previous publication assumptions that there is a constant tangential pressure gradient within the pump and its independence with radius it is clear that the slip correlation also severely limits the ability of the 1D models to predict performance accurately. In the current study there was no instrumentation in these regions to make an assessment of this however in addition to the need for a transient analysis in the future an assessment of the slip / tangential pressure gradient correlation will be made. However it is useful to compare the dramatic increase in tangential pressure gradient across the pump at lower flowrates to the drastic drop in pump efficiency as the slip factor dominates the energy transfer.

At the other end of the pump operating range, at higher flows, there is equally interesting results in terms of the performance. At the highest flowrates there is a equally dramatic drop in pump efficiency which can be accounted for in terms of a shock loss effect.

Shock losses occur when there is a difference between the blade angle and the flow angle at entry to the impeller. Only at one point does the fluid enter the blade relative to the blade line. At all other points the fluid must change direction sharply leading to large separation and turbulence and thus increasing the energy dissipation.

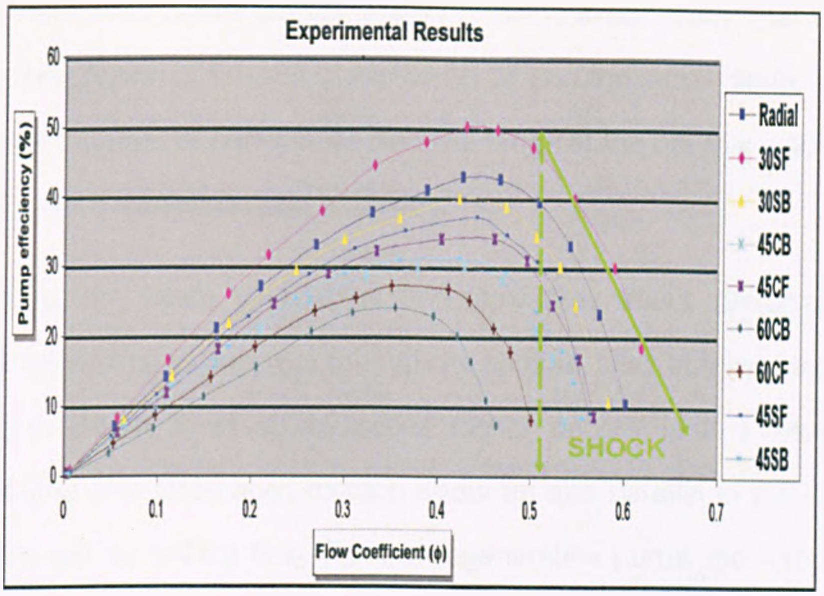

**fig. 124** Shock loss dominant region regenerative pump.

When the maximum through flows occur it is seen to have a rapid drop in efficiency. The larger the flow the greater the net effect of this incidence or shock loss is. As the tangential velocity component of flow increases this correspondingly alters the relative component and in doing so causes greater deviation to the ideal blade line. Consequently even though there is a significant reduction in the circulatory power consumption, as the flowrate increases which increases the efficiency the effect of the increased shock or incidence term soon dominates the flow and can be seen in the rapid drop in efficiency in fig 124. Spannhacke (1943) and others have shown the shock loss assosciated with increasing through flow to greatly increase as demonstrated in the current study, fig 124. Raheel (2003) also demonstrated the reduction in shock loss term with reducing flow which he indicated tends towards zero at high pressure ratios.

The effects of slip and shock losses are equally significant on all blade geometries at both low and high flows respectively indicating that they are the dominant factors in the performance trending. The blade geometries themselves can shift the trend lines according to factors discussed in the next section but the net effect of both determines how the pump performs away from the BEP region.

The most successful blade profiles tested in the current study that extend the optimal working region of the pump are the 30 SF and the radial blade. The blades which reduce the level of performace and the range of the optimal working region of the pump are the chevron profile blades.

In considering the blade geometries and how they affect performance it is particularly interesting to consider the helicity contour plots obtained in the study. The helicity or extent, to which corkscrew motion occurs, is as a result that if a fluid moves and also undergoes rotation about an axis parallel to the direction of motion there will be helical flow. For the regenerative pump the helicity comes from the circulation flow that produces the vorticity in the blade passages and the tangential flow which in effect stretches the vortices creating and impeding the circulation (vortex stretching). The vorticity or tendency for fluids to spin is related to the amount of circulation.

The worst performing blades are those which impede this circulation flow as indicated above. The chevron blades (45CF, 45CB, 60CF and 60CB) fig 122 present a bluff face across the blade circulation zone as they project rearwards or to a lesser extent forwards thus disrupting the helicity. This is demonstrated in the efficiency and head plots where the blades which impede the most i.e. project across the circulation flow path the most (fig 122) have the poorest performance results, (45 and 60 chevron blades). As the circulation or vorticity is impeded, the establishment of the helicity is effected. In chapter 5 it's clearly shown that all blade profiles indicate a degree of helicity at the interface region between the impeller and the channel. There is, however a clear demonstration in chapter 5 that blades which disrupt the circulation flow in the pump (chevron profiles) display helicity contours which fragment and indeed in some case change direction. Positive helicity (red colour range) occurs when the rotation is clockwise when viewed ahead of the fluid body. If the helicity is counterclockwise it will be negative (blue colour range) fig 125.

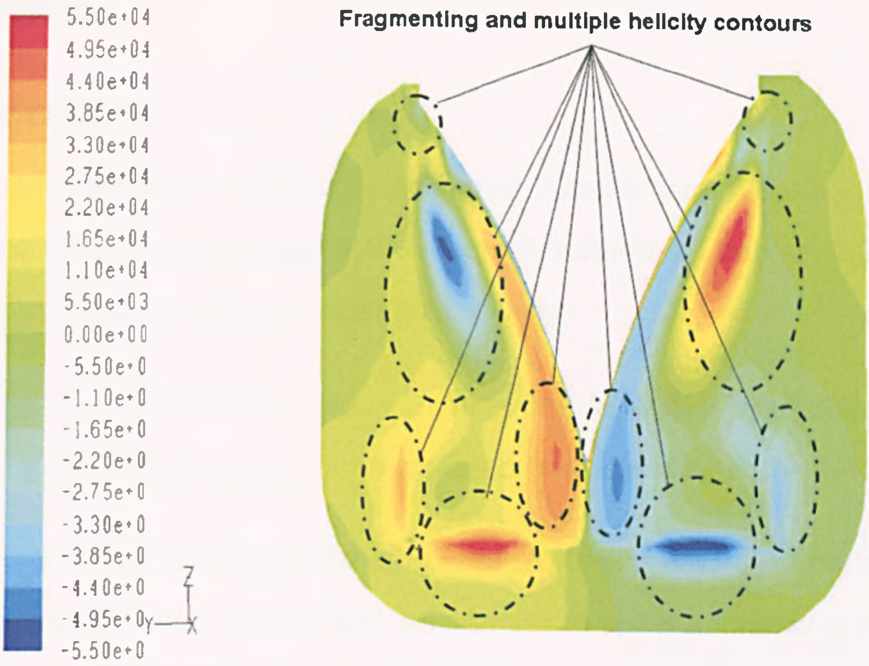

**fig. 125** Fragmenting helicity profile chevron blade geometry

The more the flow exhibits multiple circulations the more turbulence, and hence turbulent energy dissipation occurs which reduces the performance of the pump as the irreversibility's increase. As indicated in fig. 117, as the blade profile moves from a 30° swept or radial profile with little circulation impedance the more marked the drop in pump performance.

In the final analysis it would appear that the preferred blade profile would be one which is swept in a more forward inclination to assist the slip loss term, e.g. 30° swept fwd to radial blade. As the swept angle increases however this has to be balanced with not creating too large a tip to casing clearance which starts to reduce the efficiency e.g 45° swept profile. As the sweep is inclined in a rearwards attitude the performance once again reduces as the slip loss effects increase, (30° and 45° swept rearwards, blades), blades which impede the circulation flow, (chevron profiles), reduce the efficiency even when they present a forward swept profile.

# Chapter 7

## Conclusions

When considering the conclusions and main outputs from the study it is worth reviewing the initial objectives for the research outlined in Chapters 1.2 and 1.3. These can be summarised into four main criteria;

Resolving the complex flowfield, matching the best flow visulisation results, improving the pump efficiency and increased understanding of the fluid flow.

Until this point the existing published numerical models have been dependant on experimental correction factors and were limited in ability to predict performance through a range of points. As detailed in chapter 6 it is not only possible to match the performance of the regenerative pump to experimental data but to do so in a manner that does not depend on correction factors and does so for a range of performance points.

The CFD modelling carried out in the study has successfully replicated the very best flow visualisation results that were conducted in the 1940's and 1950's. Demonstration that the fluid flow within the regenerative pump is helical in nature vindicates the 3D approach to the numerical analysis. This has been done without the large expense associated with such testing.

Considering the regenerative pump and its limited deployment in comparison to other kinetic rotodynamic machines there is significant potential, as many authors have indicated, to increase the hydraulic efficiency of this pump type. The other potential benefits with the pump indicate that it would indeed offer a very viable alternative in many applications. The current study has not only equaled the highest ever reported efficiency of this pump type but has done so despite the limitations in the experimental and geometric arrangement of the studied pump. This will be addressed in the future research work.

Finally the new knowledge associated with the pump flowfield; in particular the nature of variation of the tangential pressure gradient within the pump has not only vindicated the 3D numerical analysis approach but is defining the scope of the future research in terms of the factors which this affects for instance in the need for an appropriate slip correlation. This is until now been an area of limitation in the previously published models.

There are a number of conclusions which may be drawn with respect to the design improvement process in the current study. Unless testing is fully integrated into the design process, there is a significant risk that it becomes an expensive activity of marginal benefit. Specifically, in the current work, cost considerations with relation to layout, instrumentation and measurement had a significant impact on the accuracy of the data particularly in flow and torque measurement. The future experimental work will not only include more accurate instrumentation but will extend the experimental testing to consider for example unsteady effects and slip correlation.

As the capabilities of CFD continue to develop, it is to be expected that the uncertainties associated with it should also reduce. At the very least it is to be expected that there will be a continuing growth in processing power for the foreseeable future, which will reduce, and perhaps remove, the geometric simplifications which currently have to be made.

This, as detailed in chapter 6, has also been significant in the way that, for the first time, performance data can also explain for example how spanwise variation is significant in the flowfield that is difficult to achieve using 1D modelling approximations.

The use of CFD can now be a confident starting point to consider features for an optimisation process with respect to blade and casing modifications in the future.

CFD can also be used to simulate experimental procedures and assess, for example, the intrusiveness of instrumentation before the costly set-up is incurred.

This is a very powerful tool to consider the arrangement needed to conduct transient and slip correlation work in the future.

The approach for performance improvement will be assessed on the basis of the results in the models to match that experimental performance. In 2006 the Fluid machinery group of the institution of Mechanical Engineers reported that upfront CFD has reduced the amount of research and development cost by some 65% in the European pump industry. The significant cost of expensive trial and error tests are particularly prohibitive for the regenerative pump were insufficient design guiding criteria currently exists.

The results of the numerical approach not only assist such future optimisation work, it does so on a greater understanding of the pump flow physics. There is new knowledge with respect to the tangential pressure gradient within the pump as well as more detail in the energy loss mechanics that reduce pump performance.

A novel rapid manufacturing technique has been developed in the current study that is not only accurate and robust enough to facilitate the experimental techniques applied, but will ensure that the component based analysis work can be extended in the future.

The outcomes for the current study have been the subject of an number of internationally peer reviewed publications. These include :

Quail, F.J., Scanlon, T.J., Stickland, M.T. 'Study of a regenerative pump using numerical and experimental techniques'. Proceedings of *8th European Turbomachinery Conference*, Graz, Austria, 23-27 March 2009.

Quail, F.J., Stickland, M.T., Scanlon, T.J. 'Rapid manufacturing technique used in the development of a regenerative pump impeller'. Proceedings of *World Congress on Engineering,* London , 1-3 July 2009.

Quail, F.J., Stickland, M.T., Scanlon, T.J. "Development of a Regenerative Pump Impeller Using Rapid Prototyping Techniques". International Journal of Rapid Prototyping (2009)

Quail, F.J., Stickland, M.T., Scanlon, T.J. "Design Optimisation of a Regenerative Pump using Numerical and Experimental Techniques". International Journal of Numerical Methods for Heat and Fluid Flow. (2009)

Additionally to put into context in energy efficiency terms, the work is mentioned in the proceedings of a Professional Institution as part of a submission requested by the Institution to the Scottish government on Energy Efficiency.

QUAIL, F.J.: *"Efficient use of energy".* Proceedings of the Institution of Engineers and Shipbuilders in Scotland. (2009)

With EU Directive-32-(2005), the indicators are that 10% of the poorer performing pumps could be removed for sale in the EU IMechE (2007). As detailed by for example Muller (2004), regenerative pumps can offer an efficient alternative to centrifugal devices.

# Chapter 8

## Future work

Whilst the results demonstrate that it is possible to resolve the flowfield for a regenerative pump, and that there is a reasonable concurrence between the CFD predictions and the experimental data, a number of key areas need to be addressed.

The quality of the experimental data was dependent on a number of constraints, and the physical hardware was one of the factors contributing to provide more understanding with respect to, for example, two phase flow and transient conditions. Adaptation of the models and the experiments will be performed in this respect.

In terms of trying to address a number of crucial design areas for the pump, the CFD modelling can be used to change critical design features to investigate the possible effect on pump performance in advance of prototype testing. This will be looked at in two areas: casing modifications and further impeller modification.

In order to ensure that the full range of major design variables are captured, and to ensure that the number of development units are minimised, the limitations of traditional methods can be overcome by using designed experiments. This enables a reduction in the number of design iterations, and focuses lab tests on pre-validated designs, ultimately reducing time-to-market and overall design costs.

The design of experiments (DOE) technique will be be used in the future for integration of the CFD and experimental process.

The use of other techniques, e.g. PIV, will be considered to advance the success in the flow representation achieved to this point.

# Bibliography

**ANDREW, D.N.:** *"The calculation of flow in regenerative turbomachines by a streamline curvature method"* Proceedings of IMechE Part A **(1990)**

**BADAMI, M.:** *"Theoretical and experimental analysis of traditional and new periphery pumps"* SAE Technical Papers Series, No 971074. pp 45-55 **(1997)**

**BAJBAKOV, O.W.:** *"Regenerative pumps"* Gidromasinostroenie Sb. Stat MVTU in Baumenn, Moskau pg 63-65. **(1960)**

**BARTELS, J.,** *"Performance of peripheral pump"*-Associate Professor Polytechnic Institute of Brooklyn- Discussion in ASME Trans ASME Vol 77 pp 19-28. **(1947)**

**BRENNEN, C.E.:** *"Hydrodynamics of Pumps"* - Concepts NREC. **(1994)**

**BURTON, D.W.:** *"Review of regenerative compressor theory"* Rotating machinery for gas cooled reactor applications. TID-7631. pp 19-28 **(1962)**

**BUSE, F.:** *"The effects of dimensional variations on centrifugal pumps"*– Chemical Engineering, New York. **(1977)**

**BUSEMANN, A.** The delivery head of radial centrifugal impellers with logarithmic spiral vanes. Z. angew. Math. u. Mech., 8, pg 372. **(1928)**

**CASADA, D.** *"Field Measurements in Pumping Systems - Practicalities and Pitfalls"*, Energy Matters. **(1999)**

**CREWDSON, E.** *"Water-ring self-priming pumps."* -Proceedings of the Institution of Mechanical Engineers Vol. 170 No. 13, pp. 407-425. **(1956)**

**DOEBELIN, E. O.:** *"Measurement Systems: Application and Design"*, 4th ed., McGraw–Hill, New York. **(1990)**

**ENGEDA, A.:** *"Flow analysis and design suggestions for regenerative flow pumps"* Proceedings of ASME FEDSM2003-45681 pp 1847-1857 **(2003)**

**ENGELS, H.:** *"Investigations of ring pumps (Regenerative Pumps)"* Tech Hoch Hannover **(1940)**

**ETSU, AEAT plc** *"Study on improving the energy efficiency of pumps'"* – Report produced for the European Commission. **(2001)**

**EUROPEAN PARLIAMENT.** *"Establishing a framework for the setting of ecodesign requirements for energy-using products"*, DIRECTIVE 2005/32/EC. **(2005)**

**FERGUSON, T.B.** *"The centrifugal compressor stage"*. Butterworth, London. **(1963)**

**FLUENT version 6.3.26.:** "User's Guide" © ANSYS Inc. All Rights Reserved **(2006)**

**FLUENT-** *"Best Practices For Rotating Machinery"*- © ANSYS Inc. All Rights Reserved - **(2006)**

**FLUENT-***"Backward inclined Centrifugal Fan"*- Ex143 Application briefs from FLUENT – **(2001)**

**FLUENT.** *"Automotive Water Pump"* - Ex164 Application briefs from FLUENT – Courtesy of TESMA Engine Technologies. **(2001)**

**FLUENT.** *"Mixed Flow Pump"* - Ex232 Application briefs from FLUENT – **(2005)**

**GRABOW, G** *"Comparison of several theories of the mechanisms of flow in regenerative pumps."* Proceedings 2nd Conference on flow machines **(1966)**

**GRIMM, T** *"User guide to rapid prototyping"* - society of manufacturing engineers **(2005)**

**HALSTEAD, D.E., WISLER, D.C., OKIISHI, T.H., WALKER, G.J., HODSON, H.P. and SHIN, H.W.:** *"Boundary Layer Developments in Axial Flow Compressors and Turbines"*: Transactions of ASME Journal of Turbomachinery, 119, pp. 114-127. **(1997)**

**HOLLENBERG, J.W,. POTTER, J, H.,** *"An Investigation of Regenerative Blowers and Pumps"* Trans ASME Vol 101pp 147-152 **(1979)**

**HYDRAULIC INSTITUTE,** *"Classification of pumps"* Parsippany NJ www.pumps.org **(2003)**

**I MECH E** – *"Energy saving in pumps and Pumping"* Fluid Machinery Group Symposium **(2007)**

**IVERSON, H. W.:** *"Performance of the Periphery Pump"* –Trans ASME Vol 77 pp 19-28 **(1955)**

**JAMESON, A.:** *'Re-Engineering the Design Process through Computation'*, AIAA Journal of Aircraft, 36, No. 1. **(1999)**

**KIRKUP, L.,** *"An introduction to the analysis of presentation of data"* – Experimental Methods – John Wiley and sons. **(1994)**

**KUPRJASIN, K.:** *"The present state of the theory and methods for the calculation of vortex pumps."* Vest, Mastro. Vol. 37. **(1957)**

**LAUNDER, B. E., SPALDING, D. B.:** *"The Numerical Computation of Turbulent Flows"*. Computer Methods in Applied Mechanics and Engineering, 3:269 289. **(1974)**

**LAZO, L., HOPTKINS, T,.** *"Theoretical and experimental analysis of a regenerative turbine pump"*. – Massachusetts Institute of Technology. **(1953)**

**LINDSAY, J.D., YE X.L.** *"Evaluation of Portable Ultrasonic Flowmeters in Pulp Suspension Flows",* IPST Technical Paper Series Number 525, Institute of Paper Science and Technology, Atlanta. **(1994)**

**LUO, X., ZANG, Y., PENG, J., XU, H., YU, W.:** *"Impeller inlet geometry effect on perfomance improvement for centrifugal pumps".* – Journal of Mechanical science and Technology. pp 1972-1976 **(2008)**

**LUTZ, G. F,.** *"Experimental Investigation of the pressure distribution in a regenerative turbine pump"..* – Massachusetts Institute of Technology. **(1953)**

**MARTYR, A., PLINT, M.A.:** *"Engine Testing: Theory and Practice"* B Edition: 3, illustrated, revised Published by Butterworth-Heinemann. **(2007)**

**MEAKHAIL, T., PARK, S.O,.:** *"An Improved theory for regenerative pump performance."* Proceedings of IMECHE Vol 219 Part A. **(2005)**

**MULLER, S.:** *"Consider regenerative pumps for low flow/low NPSH applications."* -Hydrocarbon Processing pg 55-57. **(2004)**

**PFAFF, M,** *"Comparative investigations of regenerative pumps with and without diffusor"* Tech Hoch-Hannover. **(1959)**

**PFLEIDERER, G.:** *"Centrifugal pumps for liquids and gases"* Springer-Verlag, 5th Edition. **(1961)**

**QUAIL, F.J.:** *"Efficient use of energy".* Proceedings of the Institution of Engineers and Shipbuilders in Scotland. **(2009:1)**

**QUAIL, F.J., SCANLON, T., STICKLAND, M.:** *"Study of a Regenerative Pump Using Numerical and Experimental Techniques".* Proceedings of 8th European Turbomachinery Conference **(2009:2)**

**QUAIL, F.J., SCANLON, T., STICKLAND, M.:** *"Rapid manufacturing techniques in the development of a regenerative pump impeller".* Proceedings of World Congress on Engineering **(2009:3)**

**QUAIL, F.J., SCANLON, T., STICKLAND, M.:** *"Design Optimisation of a Regenerative Pump using Numerical and Experimental Techniques".* International Journal of heat and fluid flow. **(2009:4)** In press

**QUAIL, F.J., SCANLON, T., STICKLAND, M.:** "Development of a Regenerative Pump Impeller Using Rapid Prototyping Techniques". International journal of Rapid Prototyping **(2009:5)** In press

**RAHEEL, M., ENGEDA, A.,:** *"Systematic design approach for radial blade regenerative turbomachines"* Journal for Propulsion and Power Vol. 21. pp 884-892 **(2005)**

**RAMMATI, S., AKBARIJ, J., BARATI, E.,:** *"Dimmensional accuracy analysis of wax patterns created by RTV"* Rapid prototyping journal **(2007)**

**SALISBURY, A.G.,** *"Current concepts in centrifugal pump hydraulic design."*- Proceedings IMECHE 177/82. **(1982)**

**SCHWEIGER, F.:** *"The shift in best efficiency point on changing the geometry of pumps"* – Fluid mechanics and fluid machinery – Academia Kaido. **(1969)**

**SENOO, Y.:** *"Theoretical research on Friction Pump"* Institute of Fluid Engineering Vol 5 No1 pp 23-38. **(1948)**

**SENOO, Y.:** *"Research on peripheral pumps"* Report. Res. Inst for Applied Mech., Vol III pp 53-113 **(1954)**

**SENOO, Y.:** *"Comparison of regenerative theories supported by new performance data"* Trans. ASME Vol 78. pp 1091-1102 **(1956)**

**SHIH, T.H., LIOU, W.W., SHIBBIR, A., YANG, Z., ZHU, J.,** *"A New k-ε Eddy-Viscosity Models for High Reynolds Number Turbulent Flows-Model Development and Validation"*, Computers Fluids, 24 (3), pp. 227-238. **(1995)**

**SIXSMITH, H, ALTMANN, H.,** *"A Regenerative Compressor"* Trans ASME Vol 99pp 637-647. **(1977)**

**SONG, J. W., ENGEDA, A., CHUNG, M.K,:** *"Modified theory for the flow mechanism in a regenerative flow pump"* Proceedings IMECHE, Power and Energy Vol 217 pp 311-321 **(2003)**

**SPALART, P., ALLMARAS, S.,** *"A One-Equation Turbulence Model for Aerodynamic Flows"*, AIAA-92-0439, Technical Report **(1992)**

**SPANNHACKE, W.,** *"Centrifugal pumps, turbines adn propellers"*, P.140 Technology press cambridge **(1943)**

**STANITZ, J.D.** *"Some theoretical aerodynamic investigations of impellers in radial- and mixed- flow centrifugal compressors"*. Trans. ASME, 74, 473--497. **(1952).**

**STRATASYS Inc.:** www.stratasys.com - Eden Prairie, Minnesota, **(2001)**

**VOLK, M.:** *"Pump characteristics & application"* -2nd edition – published by Taylor & Francis CRC Press **(2005)**

**WEBSTER, J.G.:** *"The Measurement, Instrumentation and Sensors Handbook"* – Published by CRC Press, **(1999)**

**WEINIG, P.S.:** *"Analysis of Traction Pumps"*, Hydraulic Division. ASME No. 55-SA-35 **(1955)**

**WIESNER, F.J.:** *"A review of slip factors for centrifugal impellers."* ASME J. Eng. for Power, 89, pp 558--572. **(1967).**

**WILSON, W.A., SANTALO, M.A., OELRICH, J.A.:** *"A Theory of the fluid dynamic mechanism of regenerative pumps"* Trans. ASME Vol 77 PP 1303-1316 **(1955)**

**WISLER, D.C.,** *"Loss Reduction in Axial-Flow Compressors through Low-Speed Model Testing"*, Transactions of ASME Journal of Turbomachinery, 107, pp. 354-363. **(1985)**

**WISLICENUS, G.F.:** *"Fluid mechanics of turbomachinery"*. McGraw-Hill, New York. **(1947)**

**WOOLLATT G., LIPPETT, D., IVEY, P.C., TIMMIS, P., CHARNLEY, B.A,** *"The Design, Development and Evaluation of 3d Aerofoils for High Speed Axial Compressors, Part 2: Simulation and Comparison with Experiment"*, ASME TURBOEXPO, Paper GT-2005-Nevada. **(2005)**

**WULFF, D.L.:** *"Unsteady pressure and velocity measurements in pumps"*Design and analysis of high speed pumps - Von Karman Institute Lecture series (AVT - 143). **(2006)**

**YAKHOT, V., ORSAG, S.A.:** *"Renormalization Group Analysis of Turbulence: I. Basic Theory"*. Journal of Scientific Computing, 1(1):151, **(1986)**

**YOO, I.S., PARK, M.R., CHUNG, M.K.:** *"Hydraulic design of a regenerative flow pump for an artificial heart pump"* Proceedings IMECH Vol. 220 Part A **(2006)**

# Appendices

Appendix A: Calculations

Appendix B: Experimental Arrangement

Appendix C: Drawings

Appendix D: Tabulated Results

# Appendix A

## List Of Calculations

## A.1 Specific speed/ specific diameter

At the beginning of any pump design process, neither the size nor the shape of the pump is known. In fluid mechanics a non-dimensional parameter (or parameters) is sought which distinguishes the pump. In this case, non-dimensional parametric groups are appropriate, known as the "specific speed", and "specific diameter".

$$N_s = \frac{N\sqrt{Q}}{(gH)^{\frac{3}{4}}} \qquad (32)$$

$$D_s = \frac{D(gH)^{\frac{1}{4}}}{\sqrt{Q}} \qquad (33)$$

Where N = 3000 rpm

D = 0.0745m

Q = 2.38 $X10^{-4}$ m³/sec (Flowrate)

ΔP = 248.211 kN/m²

$$H = \frac{\Delta P}{\rho g} \qquad (34)$$

= 248211/ (998.2X9.81) = 25.35m (Head)

$$\therefore N_s = \frac{3000\sqrt{2.38\ x10^{-4}}}{\left[9.81(25.347)\right]^{\frac{3}{4}}} = 0.739 \text{ (Specific speed)}$$

$$\therefore D_s = \frac{0.0745(9.81x25.347)^{\frac{1}{4}}}{\sqrt{2.38\ X10^{-4}}} = 19.176 \text{ (Specific diameter)}$$

In Dimensional terms;

$$N_s = \frac{N\sqrt{Q}}{(H)^{\frac{3}{4}}} \qquad (35)$$

$$\therefore N_s = \frac{3000\sqrt{2.38 \times 10^{-4}}}{\left[(25.347)\right]^{\frac{3}{4}}} = 4.097\ rpm, m^3/s, m$$

$$D_s = \frac{D(H)^{\frac{1}{4}}}{\sqrt{Q}} \qquad (36)$$

$$\therefore D_s = \frac{0.0745(25.347)^{\frac{1}{4}}}{\sqrt{2.38\ X10^{-4}}} = 10.836\ m$$

Though originally developed to allow evaluation of the shaft speed needed to produce a particular head and flow, the name "specific speed" is slightly misleading, because N is just as much a function of flow rate and head rise as it is of shaft speed. Note that the specific speed is a size-independent parameter, since the size of the machine is not known at the beginning of the design process.

The above definition of the specific speed has employed a consistent set of units, so that N is truly dimensionless. With these consistent units, the values of N for most common pumps lie in the range between 0.1 and 4.0.

## A2 Loadcell calibration / power estimation

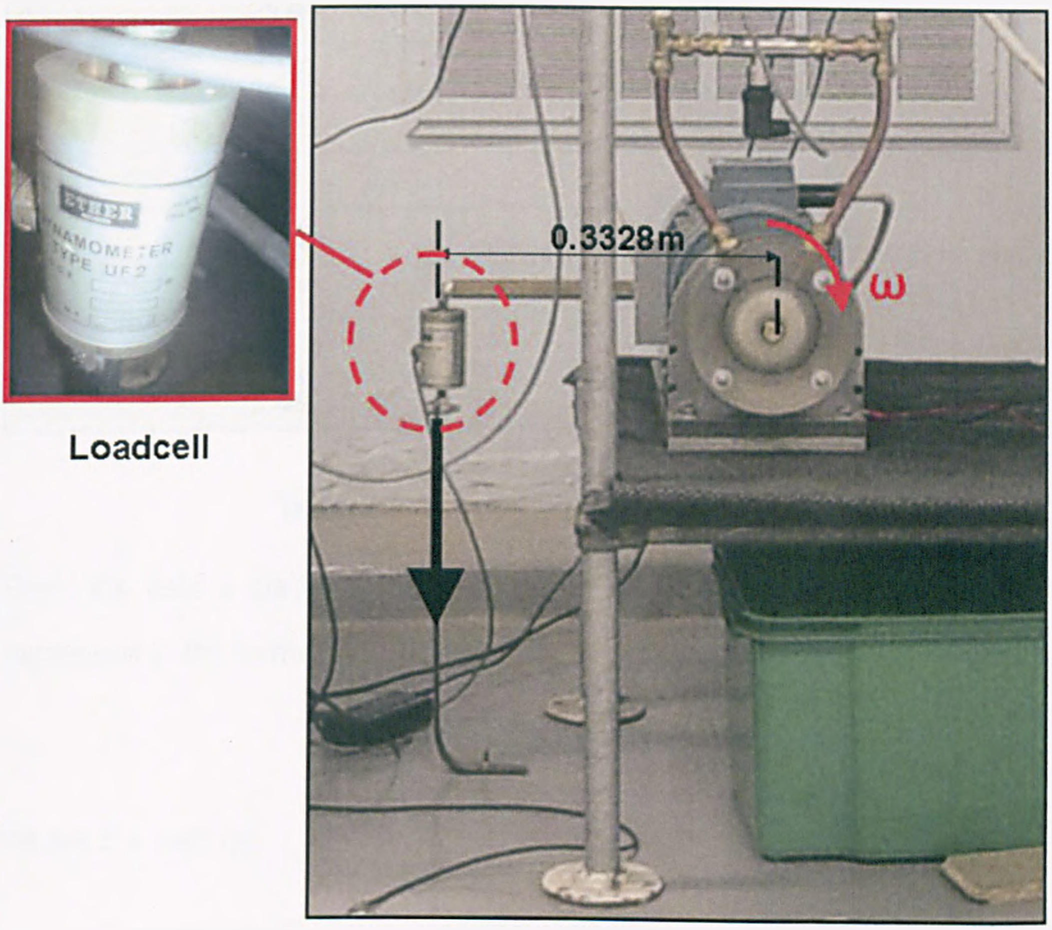

**fig 126** Dynamometer arrangement

The motor housing was coupled to a dynamometer containing a loadcell to measure strain (reaction) through a running characteristic. This strain value could be converted to an equivalent reaction load and force. Knowing the torque arm from the centre line of the loadcell to the centre of the impeller the force can be expressed as a reaction torque and hence impeller input power.

Prior to this it was necessary to calibrate the loadcell strain measurement. A range of loads were applied to the loadcell to assess the equivalent strain. The “dead weight” measurements were recorded from 0g to 400g and the corresponding strain value recorded:

| Strain (mV) | Load (g) |
|---|---|
| 0.7 | 0 |
| 0.8 | 50 |
| 0.86 | 100 |
| 0.95 | 150 |
| 1.1 | 200 |
| 1.2 | 250 |
| 1.25 | 300 |
| 1.4 | 350 |
| 1.45 | 400 |

**Table 22** Strain load calibration results

From the data a gradient and intercept of the best straight line (BSL) can be expressed in the form:

$$Y = 510X - 351 \qquad (37)$$

Where **Y** = load (g)

**X** = Strain (mV)

Considering a measured value for the radial impeller standard:

**Strain** = 1.2462mV measured using the dynamometer.

Applying this into (37) a corresponding Load was determined as 285.4g

This can be expressed as a force using (38).

$$Force = \frac{Load}{1000} x9.81 \qquad (38)$$

**Force** = 2.799N

$$Torque = Force x distance \tag{39}$$

**Length** = 0.3328m as detailed in fig. 113 and using (39)

**Torque** = 0.932Nm

$$Power\ (kW) = \frac{Torque}{9549}\ x\ 300 \tag{40}$$

**Power** = 0.2928kW

**Power** = 292.8W

All hydraulic machines suffer from losses in energy. The efficiency of a machine is defined as the ratio of power output of the machine to the power input to it. There are two main losses assosciated within a pump impeller. As the fluid moves over solid surfaces gives rise to boundary layer development and hence frictional losses. As the fluid changes direction rapidly often resulting in separation (Shock) losses. The mechanical losses in energy such as in the bearings and seals need to be accounted for.

In order to do this the pump was run dry to measure the power consumed by the pump due to these frictional effects and was evaluated as follows:

**Strain** = 0.972mV measured via the dynamometer, for this case.

Applying this into (37) a corresponding Load was determined as 145.448g

This can be expressed as a force by using (38)

**Force** = 1.4268N

using (39) & from fig. 113

**Torque** = 0.4749Nm

using (40)

**Power** = 0.1492kW

**Power** = 149.22W

For the purposes of the current study when considering the Shaft input power

$$P_{Shaft\ power\ input} = P_{mechanical\ loss} + P_{Hydraulic\ loss} + P_{Useful\ fluid\ power} \quad (41)$$

$$\eta_{overall} = \frac{P_{Shaft\ power\ input}}{P_{Useful\ fluid\ power}} \quad (42)$$

The efficiency are determined for a sample case in appendix A.4.

## A3 Net Positive Suction Head (NPSH)

In Rotodynamic pumps, cavitation occurs at inlet when the pressure falls to a value equal to or lower than the vapour pressure of the fluid at the given conditions. Net positive suction head is a measure of how much absolute head is available at pump inlet above the vapour pressure (cavitation inception).

$$NPSH = \frac{p_i - p_v}{\rho g} \qquad (43)$$

Where $p_i$ = pump inlet pressure (kPa)

$p_v$ = vapour pressure of the fluid (kN/m$^2$)

$\rho$ = fluid density (998.2 kg/m$^2$)

$g$ = gravitation constant (9.81m/s$^2$)

At 30°C the vapour pressure of water is 2.59kN/m$^2$

The lowest pressure measured occurred at a maximum flowrate for the regenerative pump and was determined from the Bourdon gauge to be 5kN/m$^2$.

Substituting in (43)

$$NPSH = \frac{5000-2590}{998.2x9.81}$$

= 0.246m

**Note:** This corresponds to a similar result published by Muller (2004) of 0.3 m for a regenerative pump where an equivalent centrifugal pump was assessed to need at least 6-8 times this value to prevent the onset of cavitation.

The most general and useful cavitation parameter is known as the cavitation coefficient or Thoma number $\sigma_{Th}$ .

$$\sigma_{Th} = \frac{p_i - p_v}{\frac{1}{2}\rho \overline{V_1}^2} \tag{44}$$

$p_i$ = pump inlet pressure (kN/m$^2$)

$p_v$ = vapour pressure of the fluid (kN/m$^2$)

$\rho$ = fluid density (998.2 kg/m$^2$)

$\overline{V_1}^2$ = mean upstream fluid velocity, previously determined as 3.59(m/s)

$$\sigma_{Th} = \frac{5000-2590}{\frac{1}{2}x998.2x3.59^2} = 0.3747 \tag{45}$$

Which falls in the Safe Region of the cavitation coefficient chart fig. 127

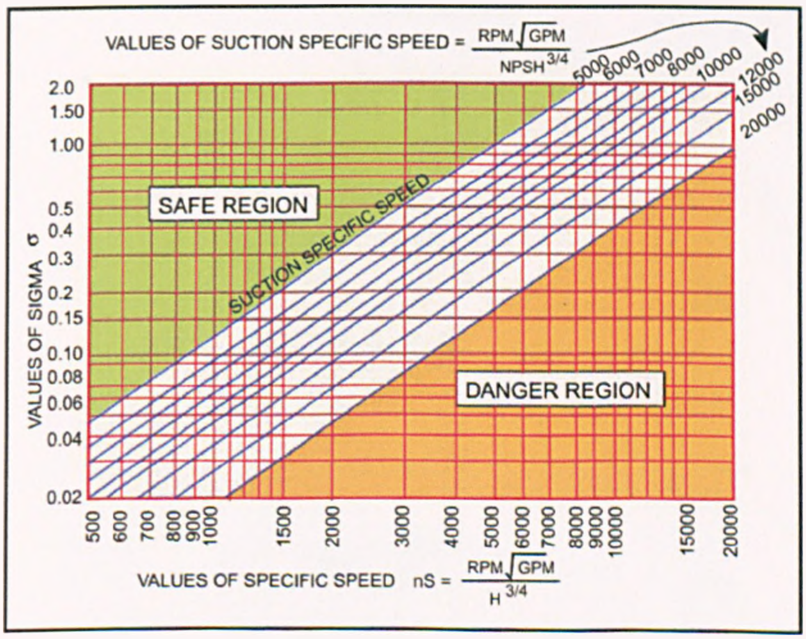

fig. 127 cavitation coefficient chart

**note:** $n_s = \frac{3000\sqrt{3.77}}{(83.17)^{0.75}} = 211.5$ - us units

## A4 Sample Calculation

Flowrate Q = 2.38x10-4m³/s

Input Power $P_i$ = 292.79W

Differential Pressure Δp = 248.211 kN/m²

$$\eta_{ov} = \frac{Q\Delta P}{P_i} \qquad (46)$$

$$\text{Overall Efficiency } \eta_{ov} = \frac{2.38x10^{-4}x248.211x10^{+3}}{292.8} = 20.17\%$$

$$P_{Shaft\ power\ input} = P_{mechanical\ loss} + P_{Hydraulic\ loss} + P_{Useful\ fluid\ power} \qquad (47)$$

$$\eta_{overall} = \frac{P_{Shaft\ power\ input}}{P_{Useful\ fluid\ power}} \qquad (48)$$

$$= 20.17\%$$

$$\eta_{mech} = \frac{P_i - P_{mech}}{P_i} \qquad (49)$$

$$= \frac{292.799 - 149.22}{292.799} = 49\%$$

$$\eta_{hyd} = \frac{\eta_{ov}}{\eta_{mech}} \qquad (50)$$

$$= \frac{20.17}{49} = 41.16\%$$

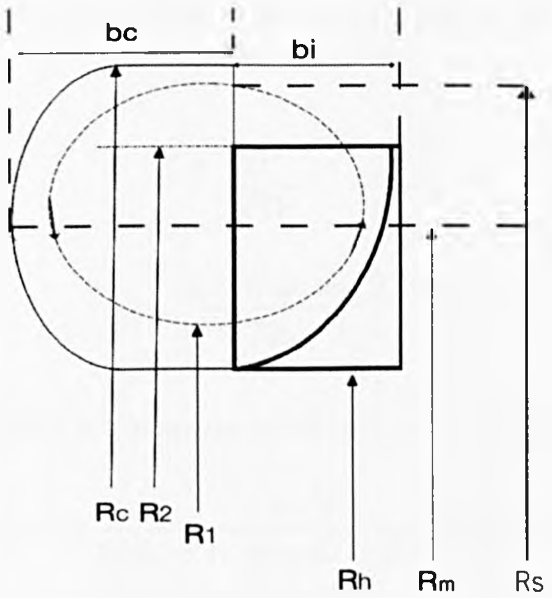

**fig. 128** Impeller and channel schematic

$$R_m = \sqrt{[0.5(R_2^2 + R_h^2)]} \tag{51}$$

$$R_1 = 0.5(R_m + R_h) \tag{52}$$

$$R_s = 0.5(R_c + R_m) \tag{53}$$

$$A_1 = \pi\left(\frac{R_m^2 - R_h^2}{Z}\right) \tag{54}$$

$$A_2 = \frac{2\pi R_2 b_i}{Z} \tag{55}$$

$$A_c = (R_c - R_h)b_c + (R_c - R_2)b_i \tag{56}$$

As detailed in Meakhail et al. (2005) the dimensionless coefficient for flow, for the regenerative pump can be expressed:

$$\phi = \frac{Q}{\omega D^3} = \frac{Q}{A_c R_m \omega} \tag{57}$$

$$= \frac{2.38 \times 10^{-4}}{6.15 \times 10^{-5} \times 0.03172 \times 314} = 0.3883$$

Hollenberg et al. (1979) showed that for the regenerative pump head coefficient is given in the form:

$$\psi = \frac{gH}{\omega^2 D^2} = \frac{gH}{u^2} \qquad (58)$$

$$= \frac{248.66}{8.905^2} = 3.1355$$

Luo et al. (2008) showed that the power coefficient can be expressed as:

$$IP = \frac{P}{\rho w^3 D^5} = \frac{P}{\rho A_i u^3} = \frac{143.58}{998.2 \text{ x } 8.333\text{x}10^{-4} \text{ x } 8.9053^3} = 0.24445$$

Where $u = \omega R_1 = 8.905$ m/s

$R_1 = 0.5 (R_m + R_h) = 0.02836$m

$\rho = 998.2$ Kg/m$^2$

Ac = area of side channel = $6.15 \times 10^{-5}$ m$^2$

Pi = 292.8W - 149.22W = 143.58W

$g = 9.81$ m/s$^2$

$b_i = 0.006$ m

$Rm = \sqrt{0.5 (R_2^2 + R_h^2)} = 0.03172$m

Arc = $3.3 \times 10^{-5}$m

Ai = $0.5 \times 0.006 (8.89 \times 10^{-3}) \times 30 = 8.001 \times 10^{-4}$

Arc = 2.1mm$^2$ = $2.1 \times 10^{-6}$m$^2$ $\times 30 = 6.3 \times 10^{-5} \times 50\% = 3.3 \times 10^{-3}$m$^2$

Ai + Arc = $8.001 \times 10^{-4} + 3.3 \times 10^{-3} = 8.33 \times 10^{-4}$m$^2$

$\omega = (2\pi N)/60$ Rad/s = 314 rad/s

N = 3000 rpm

$R_2 = 0.03725$m

The number of circulations in the casing for the given flowrate of:

@ sample pt

$Q = 2.38\text{x}10^{-4}\text{m}^3/\text{s}$

$$Q = \frac{Volume}{Time} \tag{59}$$

Volume of fluid in pump and casing = $4.81226x10^{-5}$ m³ (see A5)

Time inside the casing $= \frac{Volume}{Flowrate}$

$$= \frac{4.81226x10^{-5}}{2.38\text{x}10^{-4}} = 0.202 \text{ s} \tag{60}$$

Angular velocity of pump = $\omega = (2\pi N)/60$ Rad/s = 314 rad/s

$V = \omega r$ Linear velocity V = 314x (0.02836) = 8.9053 m/s

Circumferential length of the 1st circulation = CL

$$CL = (\frac{320}{360})x2\pi r$$

$$= 0.20804\text{m} \tag{61}$$

Circumferential length of any additional circulations = $2\pi r$

$= 0.234\text{m}$

$$\text{Length=speed x time} \tag{62}$$

Fluid travels a total distance of 8.9053x0.202 = 1.8006m

For additional circulations fluid travels 1.8006-0.20804 = 1.59257m

No. of additional circs = Distance travelled/circumferential length = $\frac{1.59257}{0.234}$

= 6.8045

## A5 Impeller / casing volume

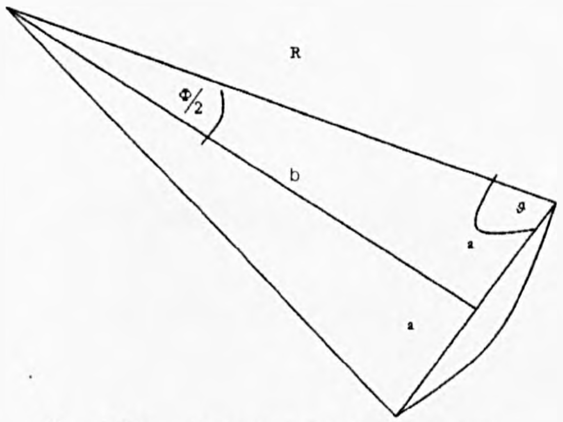

**fig. 129** Impeller blade arc area

2a= 9.5mm

a = 4.75mm

Cosθ = 0.1858

R = 25.4mm

θ= 79.29°

Φ/2 = 90°-79.29°  Φ=21.42°

$$A_1 = \tfrac{1}{2}R^2\Phi = \frac{1}{2}(25.4)^2 x 21.42\frac{\pi}{180} = 120.6mm^2 \quad (65)$$

$$b = \sqrt{25.4^2 - 4.75^2} = 24.95mm \quad (66)$$

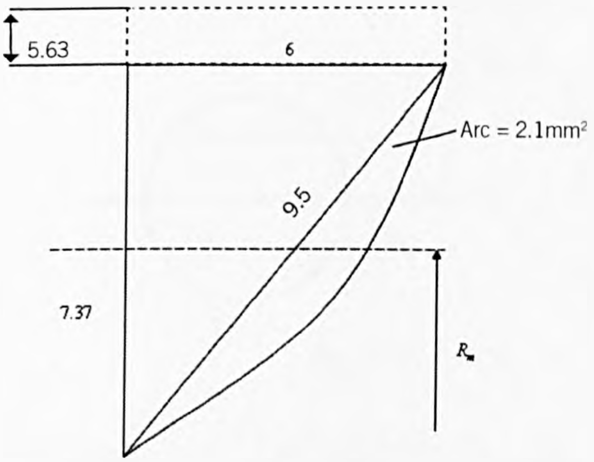

$$A_2 = \frac{1}{2} x a x b \therefore 2A_2 = 118.52mm^2 \quad (67)$$

Hence the arc Area = 120.6-118.52 = 2.1mm²

$$\therefore A = \frac{1}{2} x6x7.37 + 2.1 = 24.21mm^2$$

$$R = 25 + \frac{7.37}{2} = 28.69mm$$

Thus the plane cylindrical area = 5.36x6 = 32.16mm²

$$\therefore Total\ Area = 56.37mm^2$$

Bladeless Volume = 2πx28.69x56.37 = 10161.5mm³

1L=1000cc=10³cc=10³x10³mm³

∴ Bladeless Volume = 10.162cm³

Blade volume= 30xtx56.37=1691.1tmm³

Hence for the impeller t=1.25mm

Water volume = 8.048cm³

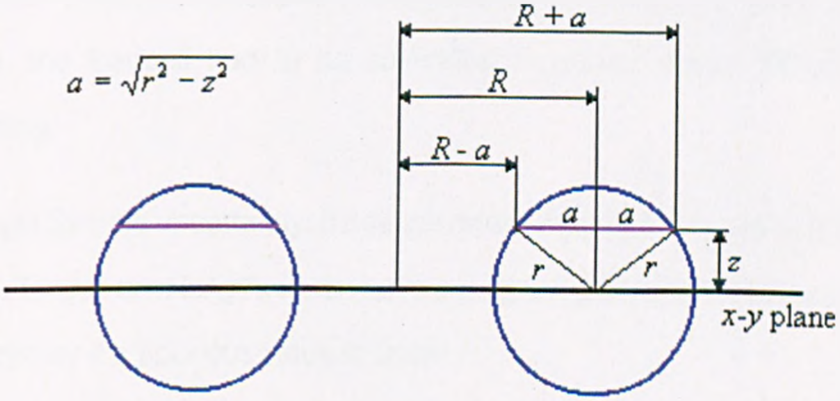

**fig. 130** Volume Torus

$$\text{Volume of torus} = (\pi r^2)(2\pi R) = 2\pi^2 R r^2 \quad (68)$$

Volume of fluid in pump and casing = impeller fixed volume + volume of the torus

$= 8.048x10^{-6}$ m³ + $4.0074x10^{-5}$ m³ = $4.81226x10^{-5}$ m³

## A6 Uncertainty Analysis.

Uncertainty analysis is a systematic mathematical process of estimating the uncertainty from a known set of equations in a result for a desired probability level. The input data to these equations are individual uncertainties of each parameter, which is either known previously or calculated accordingly. Before proceeding further, some definitions are discussed, which forms the base for the method of estimating uncertainty.

- Resolution uncertainty: The resolution limit of an instrument represents the smallest uncertainty that can be quoted in a single measurement of a quantity, e.g. in measuring the torque arm 332.8mm ±0.5mm.
- Reading uncertainty: While making a measurement if the quantity is changing significantly e.g. the flowmeter reading fluctuates (resonance).
- Calibration uncertainty, manufacturer's calibration are only valid often for limited periods of time and are dependent on the quality of the instrument. e.g. the loadcell had to be calibrated to assess conformity prior to the testing.
- Single Sample uncertainty: If a single measurement of a quantity is to be made e.g. Torque arm length, it can have a large effect on the overall experimental accuracy if a spurious value is taken.

## Systematic and Random uncertainties

There are two types of systematic uncertainty, offset uncertainty and gain uncertainty.

Offset tends to be a fixed error across reading irrespective of the magnitude of the reading. A gain error tends to increase as the magnitude of the quantity increases.

Random uncertainties can be less ordered and produce scatter over a range of measurements and can be introduced e.g noise or vibration in rotating machinery, effecting loadcell readings.

The propagation of all kinds of uncertainties, which includes uncertainty in measurement, parameter estimation, etc. are addressed by the root-sum of squares method. The mean of a set of data obtained by repeated experiments is regarded as the best estimate of the true value of the quantity being measured.

What is most often taken as a measure of the variability of the data is the mean of the sum of the squares of the deviations. This is referred to as the variance of the data and is defined as follows:

$$\mu = \sum_{i=0}^{n-1} \frac{x_i}{n} \qquad (69)$$

where is **mean**

**X** is the input sequence.

μ is the mean, or average, of the values in the input sequence **X**.

**standard deviation** is the standard deviation calculated from the values in the input sequence **X**.

**variance** is the calculated variance of the values in the input sequence **X**.

where μ is **mean** and *n* is the number of elements in **X**.

$$\sigma^2 = \sum_{i=0}^{n-1} \frac{(x_i - \mu)}{w} \qquad (70)$$

Where $\sigma^2$ =variance

where w is **weighting. Weighting** determines whether to calculate the population or the sample standard deviation and variance. For the study this was calculated for flowrate, strain and pressure for 10 repeat tests at the sample case point as follows:

| | | | | | | | | | | |
|---|---|---|---|---|---|---|---|---|---|---|
| Flowrate ($m^3/s$)x$10^{-4}$ | 2.28 | 2.43 | 2.01 | 1.74 | 2.56 | 2.37 | 2.93 | 2.39 | 2.51 | 2.60 |
| Strain (mV) | 1.20 | 1.54 | 1.35 | 1.01 | 1.21 | 1.05 | 1.25 | 1.15 | 1.23 | 1.47 |
| Pressure (p.s.i.) | 36.13 | 36.65 | 36.61 | 36.38 | 34.90 | 35.28 | 35.15 | 36.28 | 36.97 | 35.71 |

**Table 23:** 10 repeat measurements of the flow rate, strain and differential pressure for the sample case

Using equation (70) the mean values are :

2.38 x$10^{-4}$$m^3/s$

1.2462 mV

36psi

$$\text{Range} = \text{largest value} - \text{smallest value} \qquad (71)$$

$$\text{Uncertainty in mean} = \frac{\text{range}}{n} \qquad (72)$$

$$\%\ \text{uncertainty} = \frac{\text{range}}{n} \times 100 \qquad (73)$$

Using (71- 73):

$(2.382 \pm 0.119) \times 10^{-4} m^3/s$ ~ 5% uncertainty

$(1.246 \pm 0.053)$ mV ~ 4.3% uncertainty

$(36.008 \pm 0.207)$ psi ~ 0.6% uncertainty

## Data Monitoring

Pressure, strain, flow rate, and speed were monitored by using a laptop with National Instruments software. Data was sampled at a frequency of 1k (Hz.) The sample data was averaged and stored to the laptop hard disk at one second intervals. The signals from all the sensors were monitored simultaneously and the recorded data was kept in a spreadsheet format for further analysis.

Time averaging and variance filtering was applied to the software (fig. 118) to apply equations 69 and 70 in a manner to condition the signal.

The electric output signal from the instrument (e.g. flowmeter) would generally fluctuate with time. This maybe as a result of unsteady or transient effects in the flow, but another part will be due to the "noise" or influences on the device. This for example can be the resonant frequency of the motor at particular speeds which results in oscillation/noise generation. To mitigate such effects discretisation of the analogue signal or analogue filtering was applied.

**Averaging Configuration Weighting mode**—Specifies a linear or exponential weighting mode for the time averaging operation. The default is Exponential. **Averaging mode**—Sets the averaging mode. **Running avg.**—Specifies to calculate a running average of all input signals for the duration of the operation. **Data ready**—Indicates when the averaging process is done and the averaged data are ready

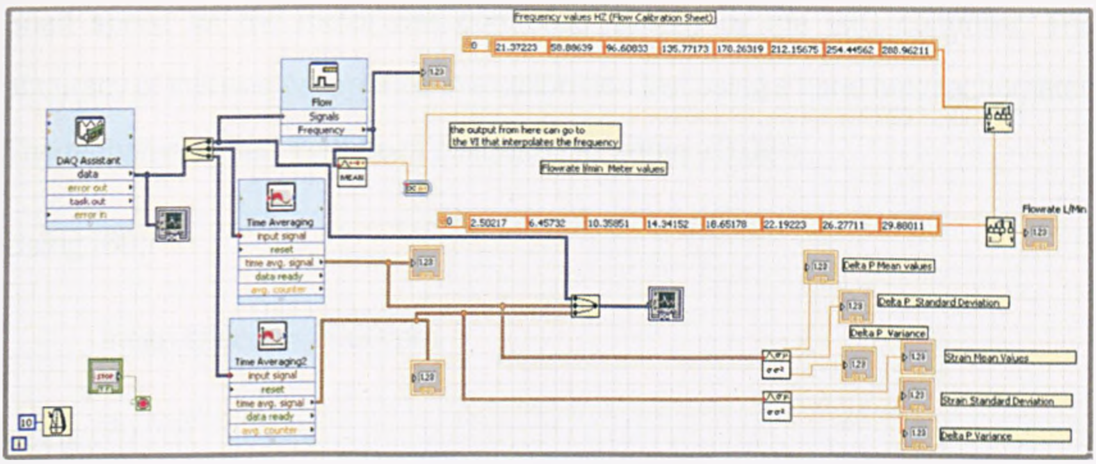

the output from here can go to the VI that interpolates the frequency

Fig 131 Filtering and Variance correction

The uncertainty results of the analysis are dependent upon the accuracy of the instrumentation that is used to make the efficiency measurement.

In this study the pressure and flow sensor manufacturer calibrations are assumed. A calibration test was conducted for the loadcell during the current study to verify the load/strain relationship as part of the operation for the dynanometer.

The ETHER UF2 loadcell calibrated by the direct application of weights (dead weight calibration), Appendix A.2

Casada (1999) pointed out that flowrate is usually the most difficult parameter to measure when assessing pump operation. Flow meters are usually capable of measuring volumetric flow rates with an accuracy range of ±5% of full-scale readings. Lindsay, et al. (1994). A calibration test was conducted on the flowmetre and the accuracy of the RS VI0981 flowmeter estimated to be 5% Appendix A6.

Having conducted a loadcell calibration of the Ether UF2 loadcell, it was estimated the uncertainty in the device was in the order of 4.3%. Dynamometers are typically within ±5% of full-scale readings; (as detailed by), Martyr et.al (2007)

Shaft speed for the motor was controlled directly by the IMO controller. The accuracy of this was determined in a calibration test using a hand held tachometer. The tachometer had itself been calibrated to within ±0.06%.

Using (69):

mean speed = 3000rpm

Using (70-72)

(3000 ± 2) rpm ~ 0.06%

According to Doebelin et al. (1999), typical shaft speed accuracy can be of the order of ± 0.06% of full-scale readings which is essentially a negligible error. In this study, we will follow Doebelin's reported accuracy and consider the error negligable.

For a standard radial blade case of the regenerative pump, a 5% error was determined for the flowrate, a 0.6% error for the head and 4.3% error in the power calculation.

$$\xi_R = \pm\sqrt{\Sigma(\delta_i \xi_{x_i})^2} \tag{74}$$

$$\delta_i = \frac{\delta R}{\delta X_i} \tag{75}$$

$$\xi_\eta = \pm \rho g \left[ \left( \xi_Q \frac{H}{P} \right)^2 + \left( \xi_H \frac{Q}{P} \right)^2 + \left( \xi_P \frac{QH}{P^2} \right)^2 \right]^{½} \tag{76}$$

Applying equation (76) this equates to a pump efficiency error of 6.6%. Whilst the random scatter was evaluated from repeatability tests and sensitivity analyses, the systematic inaccuracy due to aggregate systematic errors in transducers and changes in performance due to build-to-build differences are difficult to evaluate, Woollatt et al. (2005).

# A7 FLOW ALIGNMENT

In order to consider an analytical approach to selecting impeller blade angles that may offer some reduced shock losses the following approach was taken. Using a CFD model run for a design point run for the radial standard impeller blade the surface integral reports can be assessed to obtain the area weighted average velocity magnitude.

| Surface Integrals Area-Weighted Average Velocity Magnitude | | |
|---|---|---|
| | POSITION | POSITION |
| | Inlet Interior | Outlet Interior |
| Vr - Relative Velocity Magnitude (m/s) | 12.329174 | 10.078969 |
| Vf - Radial Velocity (m/s) | 3.4114122 | 3.0815425 |
| Vw - Relative Tangential Velocity (m/s) | 11.832516 | 9.5654602 |

**Table 24** Surface Integrals

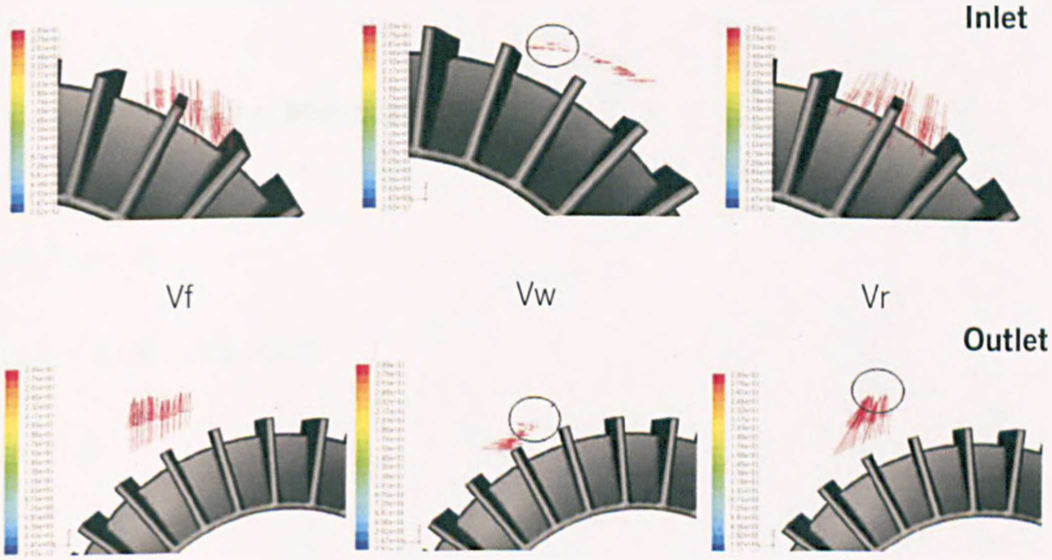

**fig. 132** Blade Velocity Vectors

Considering a basic velocity triangle at the inlet to the pump:

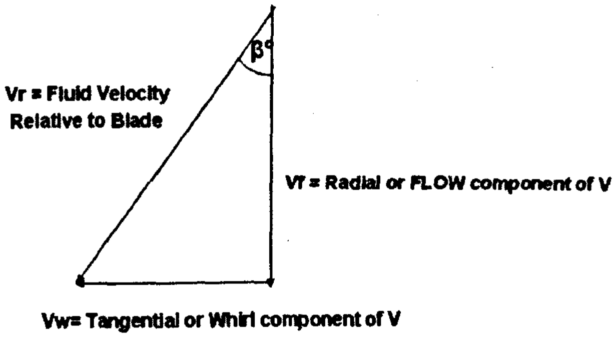

Approach Angle β°

$\tan\beta = 11.832/3.411$

$\beta = 73.9°$

Considering a basic velocity triangle at the outlet to the pump:

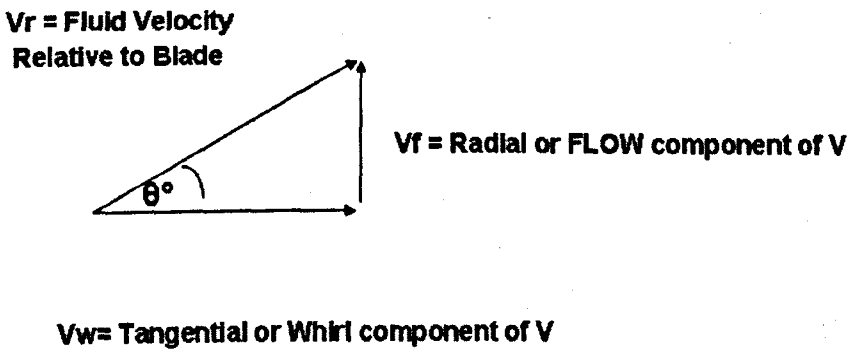

Exit Angle θ°

$\tan\theta = 3.08154/9.5654$

$\theta = 17.9°$

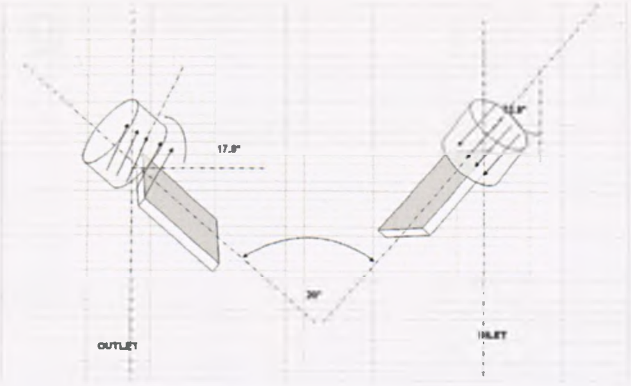

**fig. 133** Inlet/outler angles

Inlet = 74-15 ~ 60° Outlet = 17+15 ~ 30°

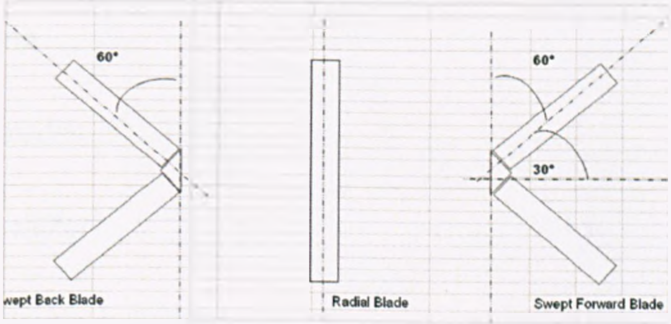

**fig. 134** Blade angles

In order to reduce the number of manufactured parts and models that would have to be built, it was considered to use the blades in a forward facing then rearward facing application. Thus it was decided that 9 blade profiles could be considered in the analysis and testing on the basis of this analysis of approach and exit angle. 5 blades would be manufactured and modeled then reversed to consider the effects:

Radial Blade
30° Swept Forward
30° Swept Backward
45° Swept Forward
45° Swept Backward
60° Chevron Forward
60° Chevron Backward
45° Chevron Forward
45° Chevron Backward

# Appendix B

## List Of Figures

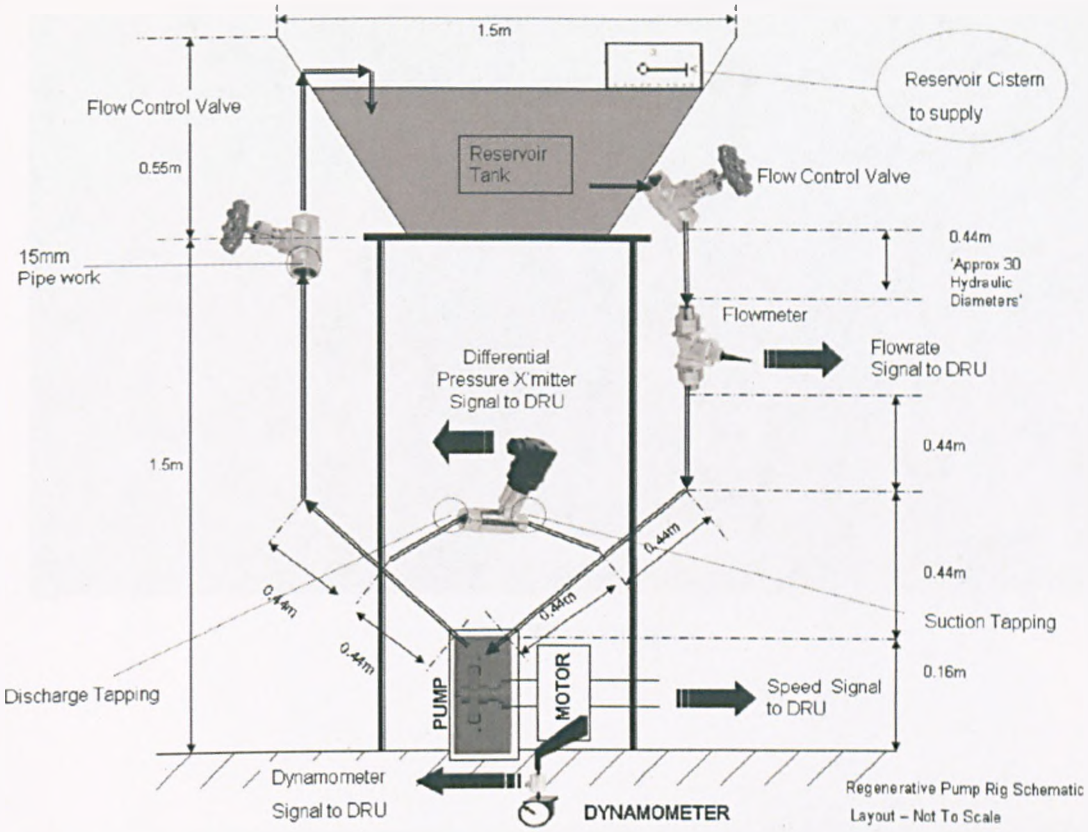

**B1** Rig Schematic

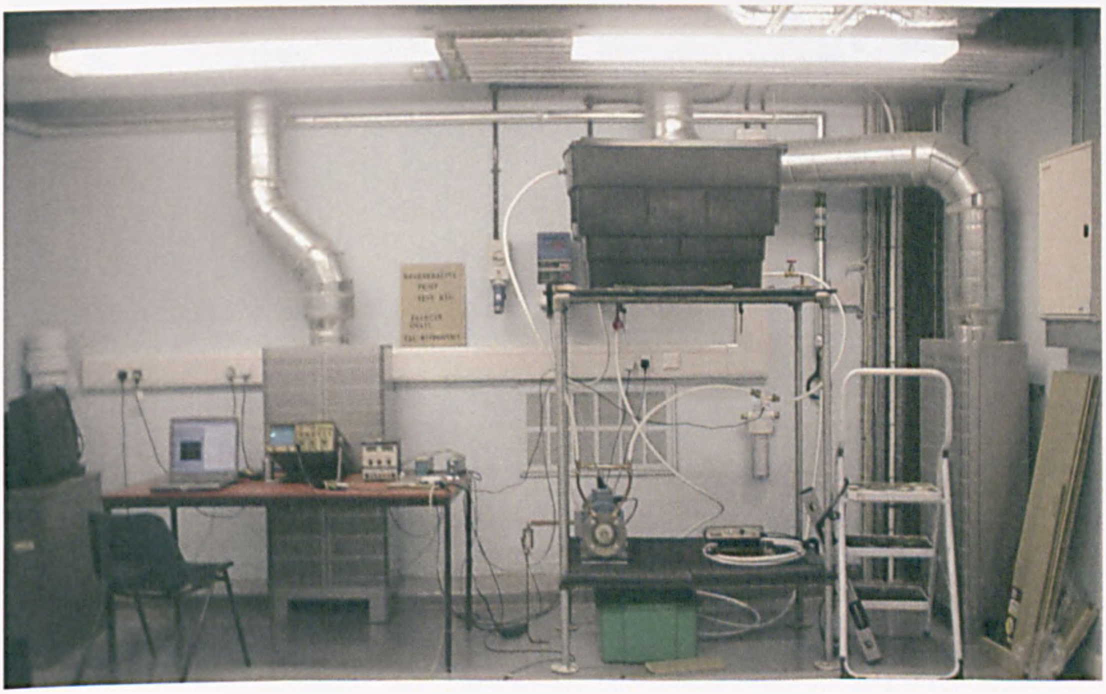

**B2** Rig arrangement

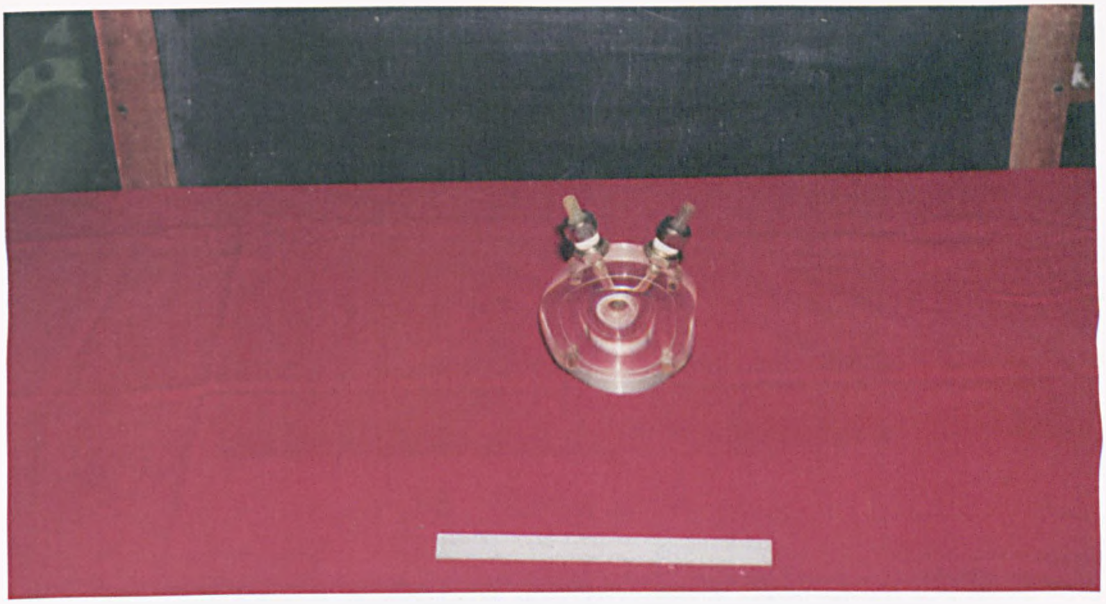

**B3** Front casing

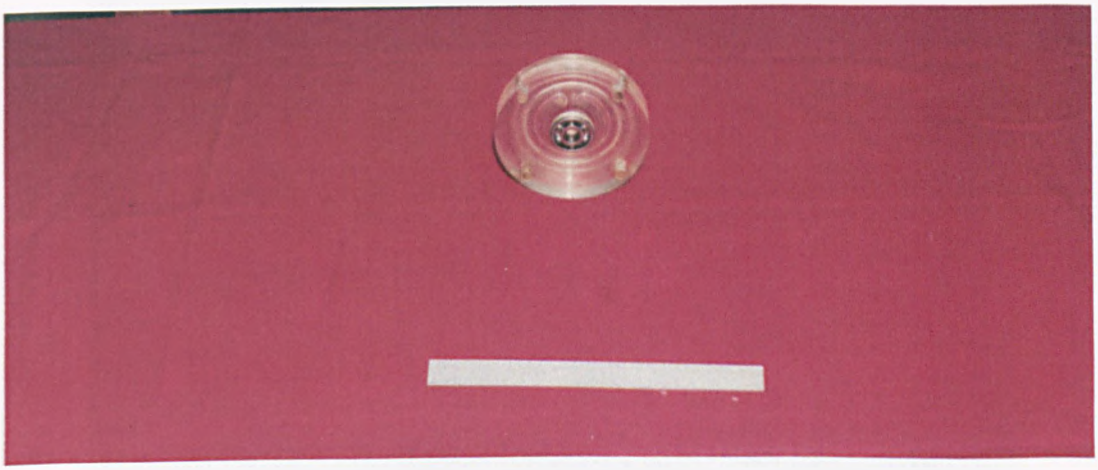

**B4** rear casing

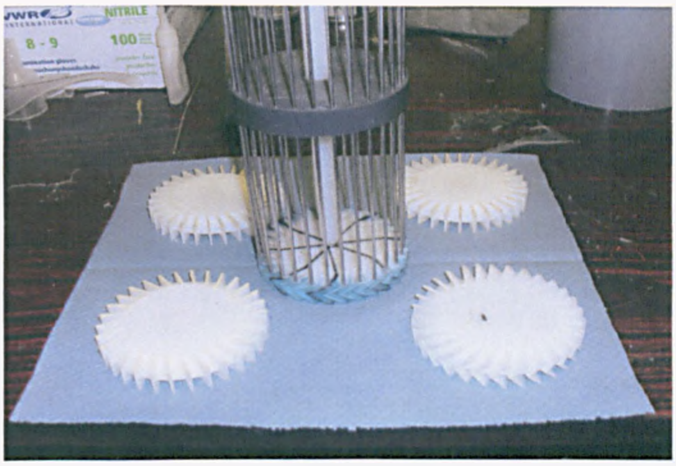

**B5** Impeller blades

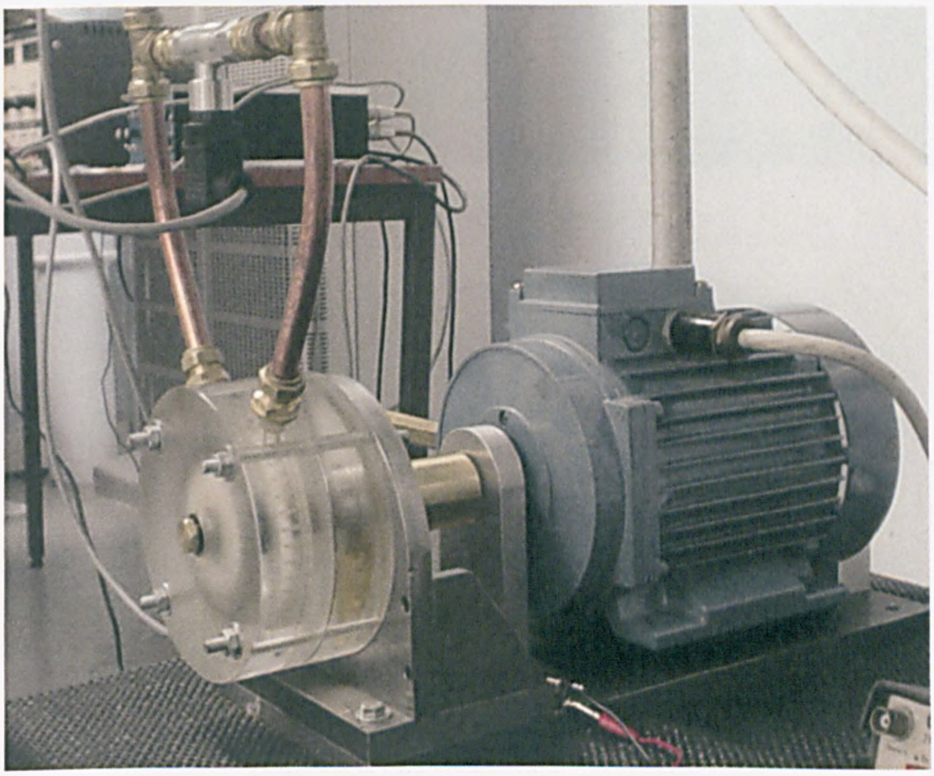

**B6** Motor

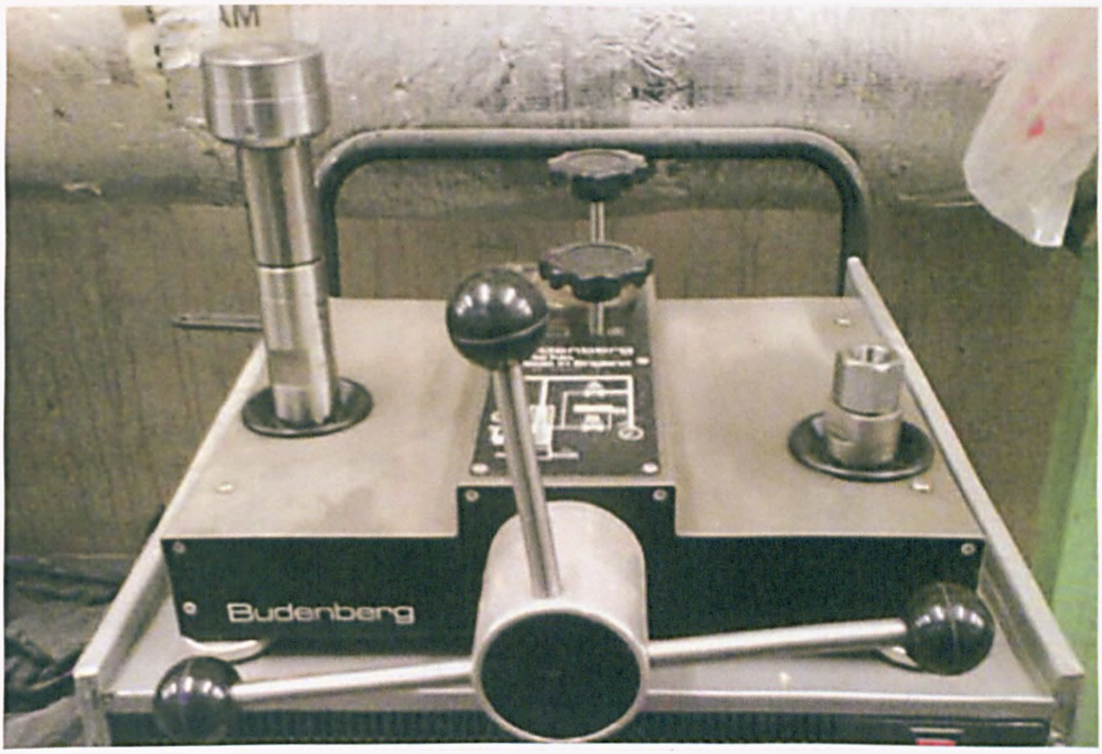

**B7** Pressure gauge calibration rig

**B8** Motor frequency controller

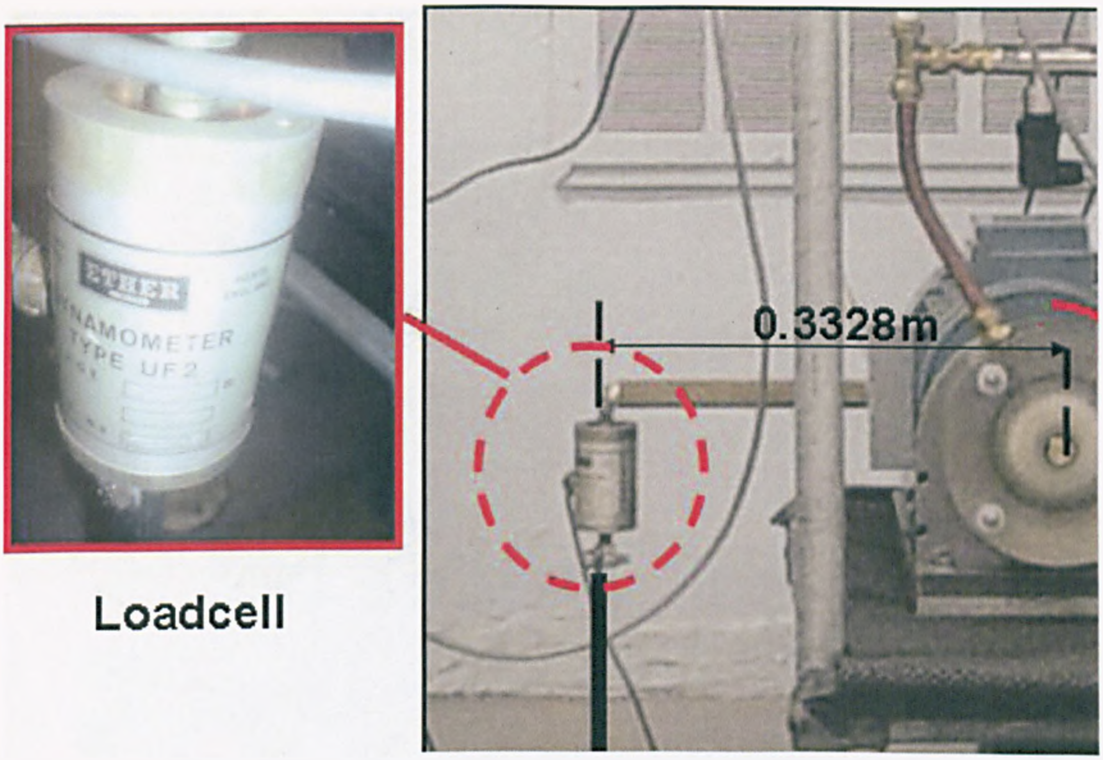

**B9** Dynomometer arrangement

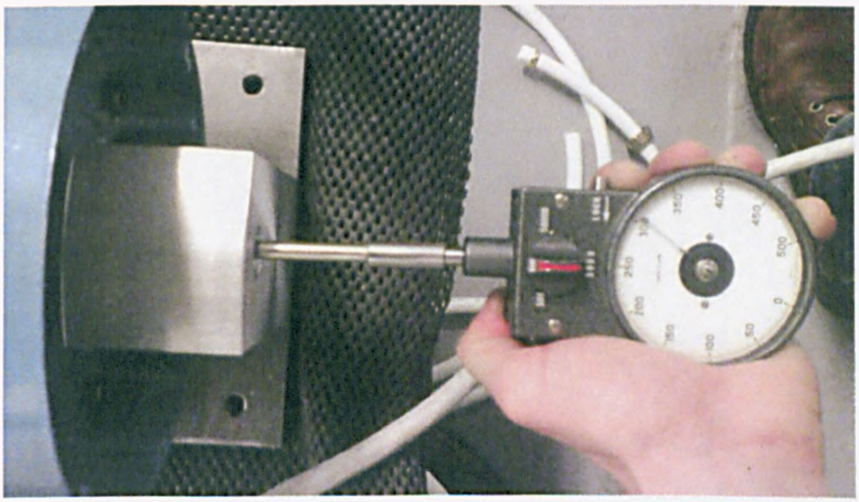

**B10** Tachometer calibration

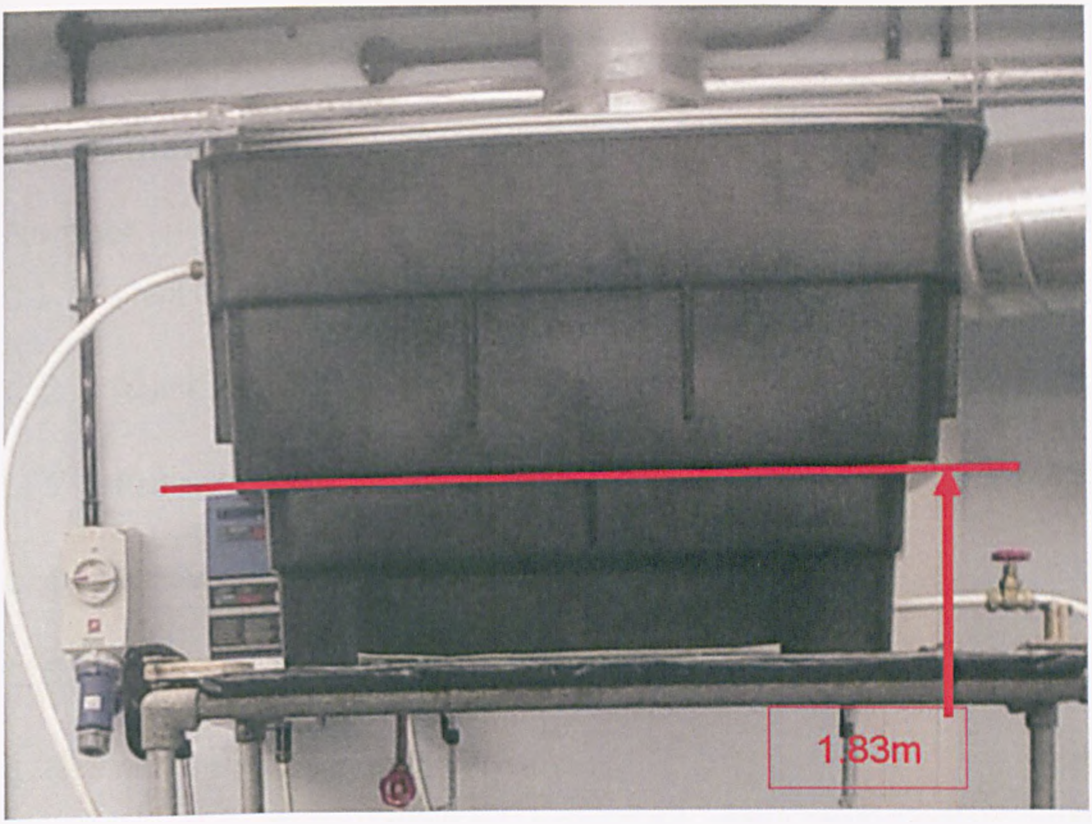

**B11** Reservoir tank fill line

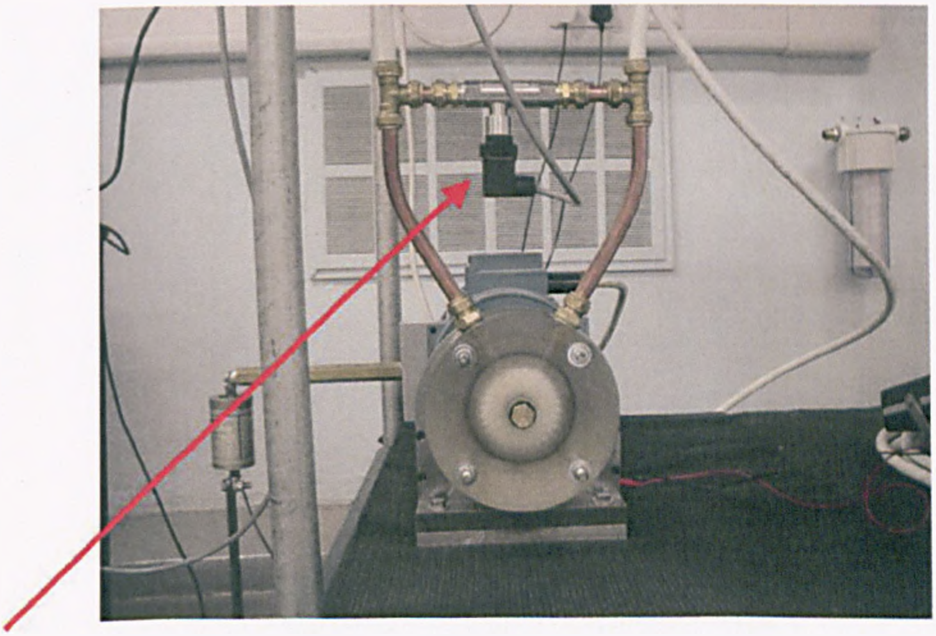

**B12** Differential pressure transducer

# Appendix C

## List Of Drawings

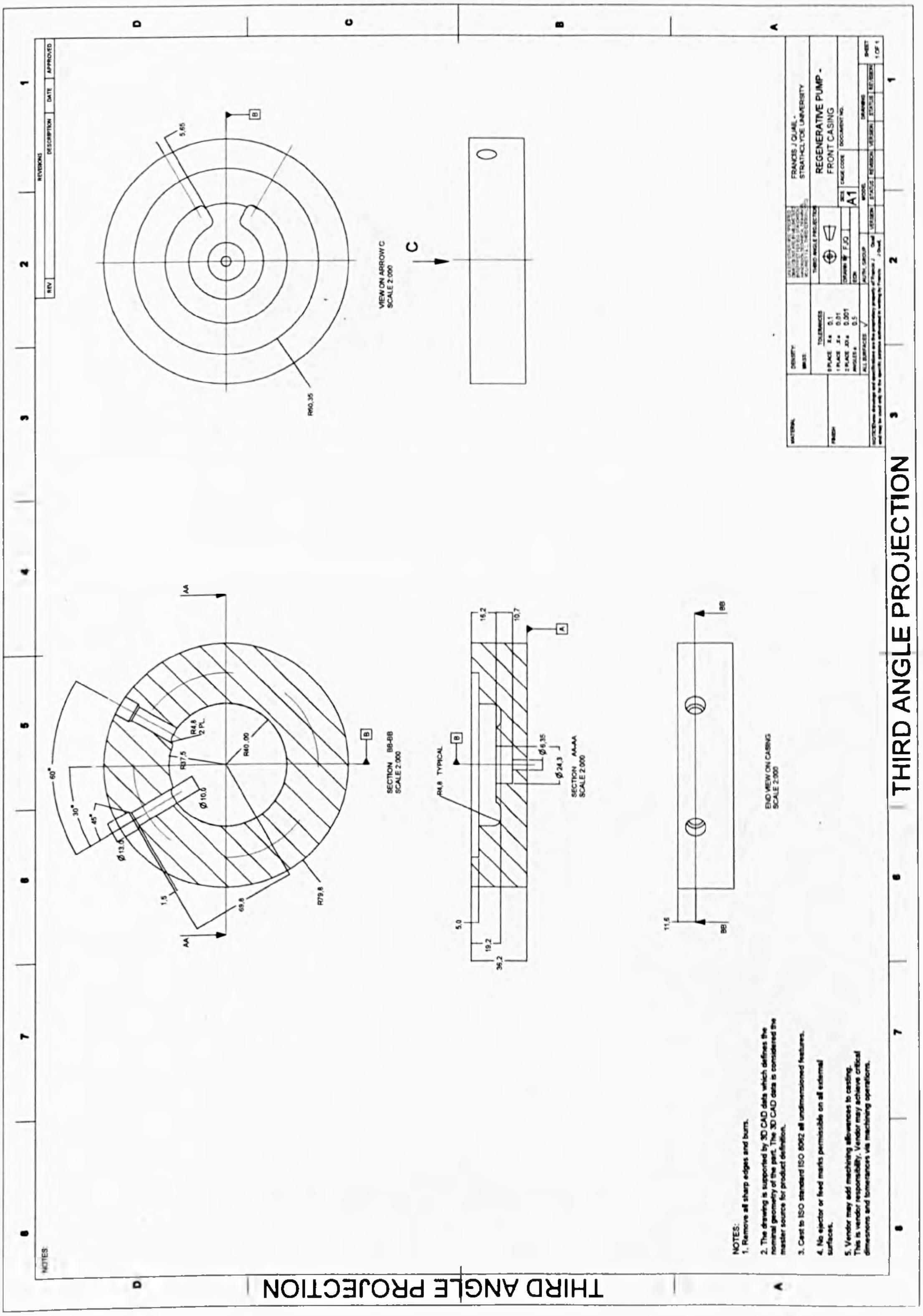

**C1** Front casing

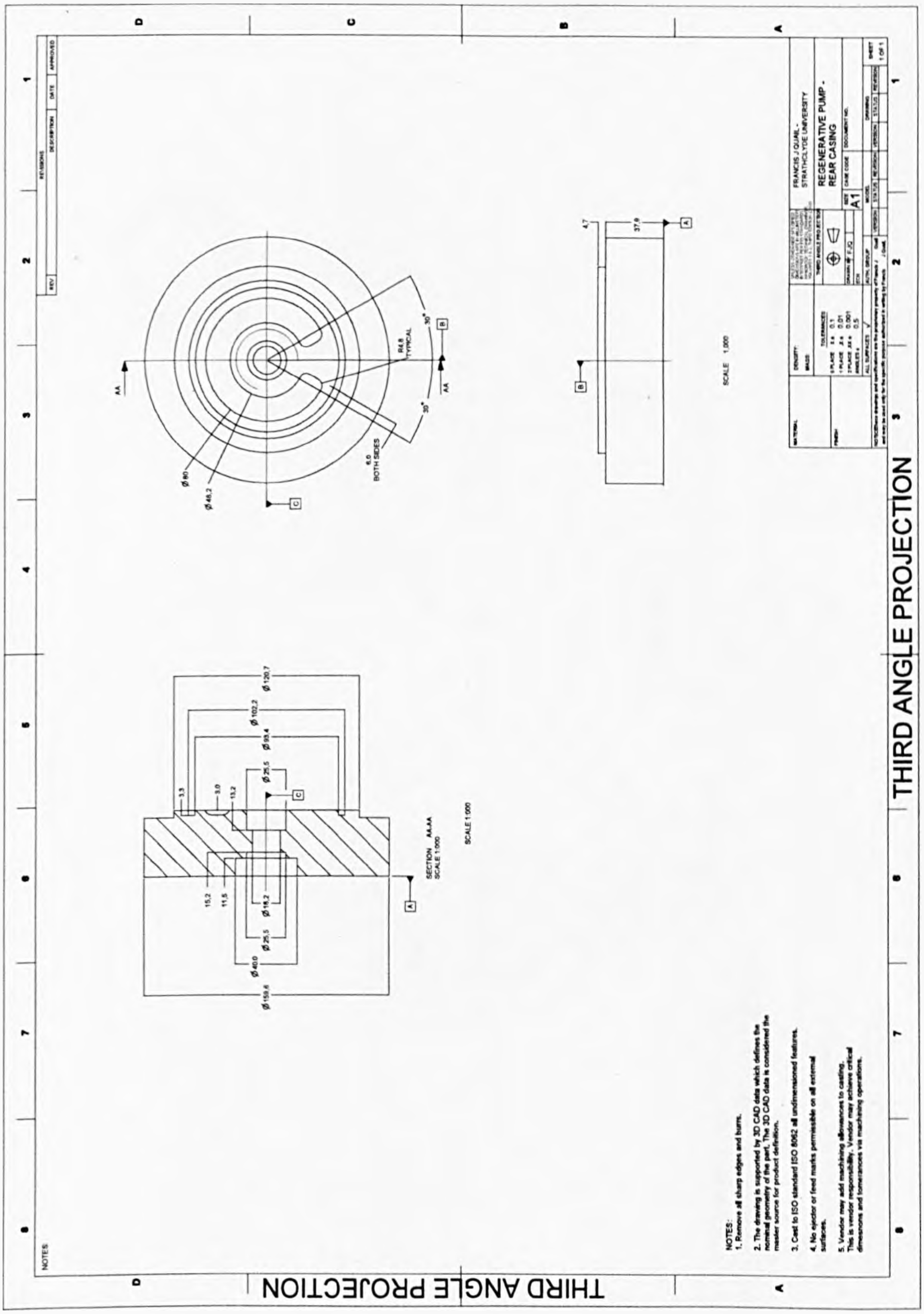

**C2** Rear Casing

## C3 Radial Impeller

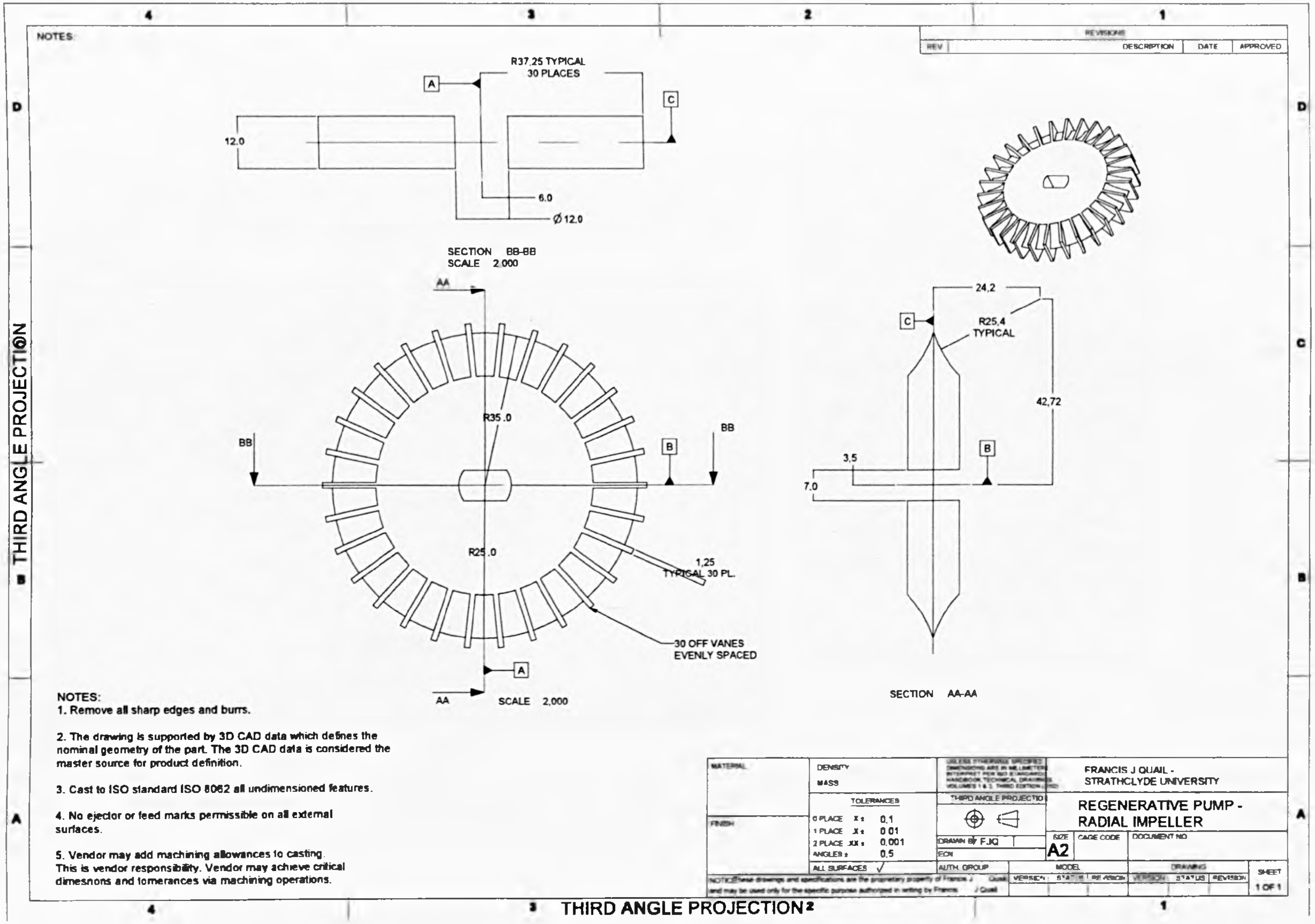

NOTES:

1. Remove all sharp edges and burrs.

2. The drawing is supported by 3D CAD data which defines the nominal geometry of the part. The 3D CAD data is considered the master source for product definition.

3. Cast to ISO standard ISO 8062 all undimensioned features.

4. No ejector or feed marks permissible on all external surfaces.

5. Vendor may add machining allowances to casting. This is vendor responsibility. Vendor may achieve critical dimesnons and tomerances via machining operations.

### C4 30° swept impeller

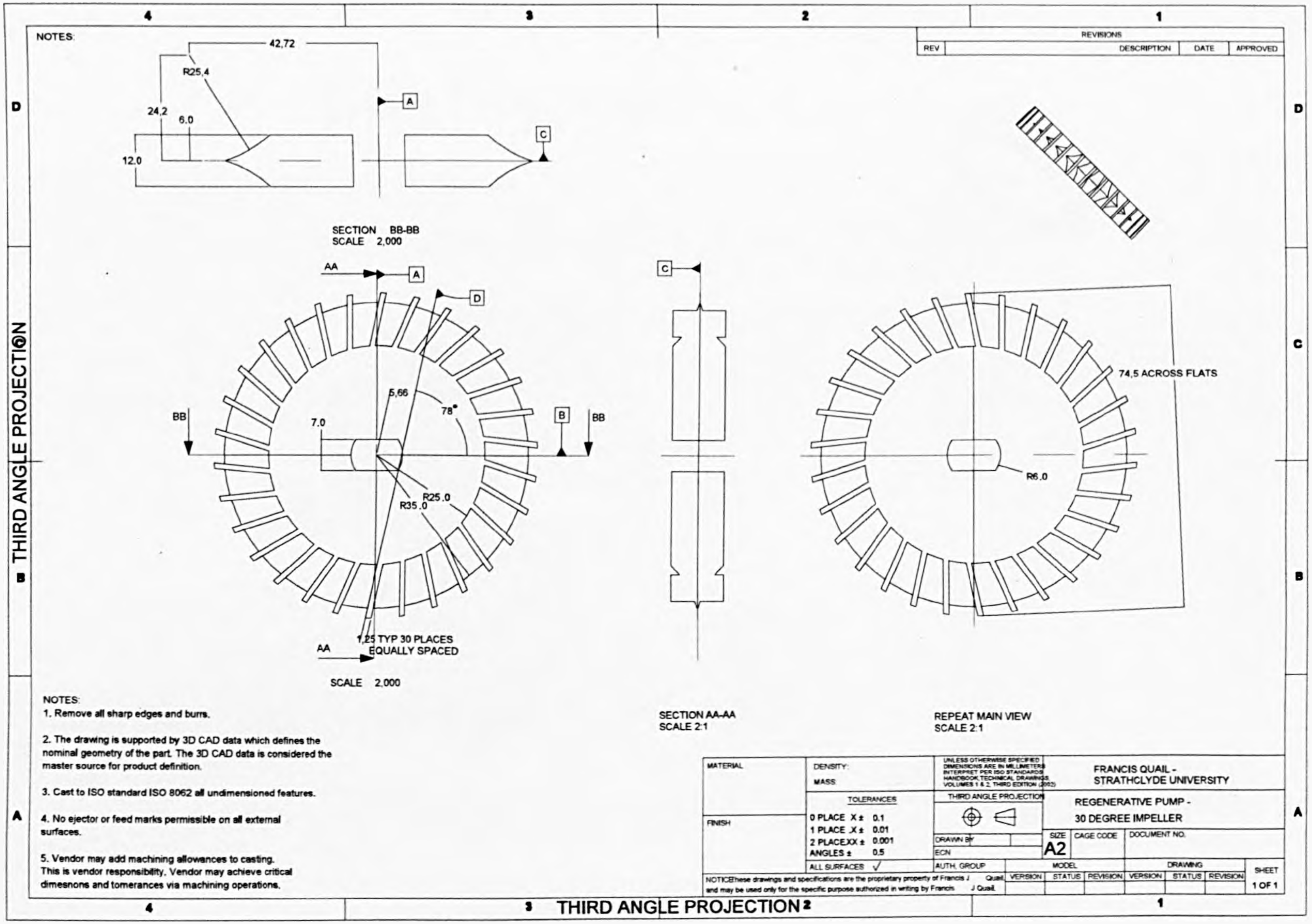

NOTES:

1. Remove all sharp edges and burrs.

2. The drawing is supported by 3D CAD data which defines the nominal geometry of the part. The 3D CAD data is considered the master source for product definition.

3. Cast to ISO standard ISO 8062 all undimensioned features.

4. No ejector or feed marks permissible on all external surfaces.

5. Vendor may add machining allowances to casting. This is vendor responsibility. Vendor may achieve critical dimesnons and tomerances via machining operations.

## C5 45° swept impeller

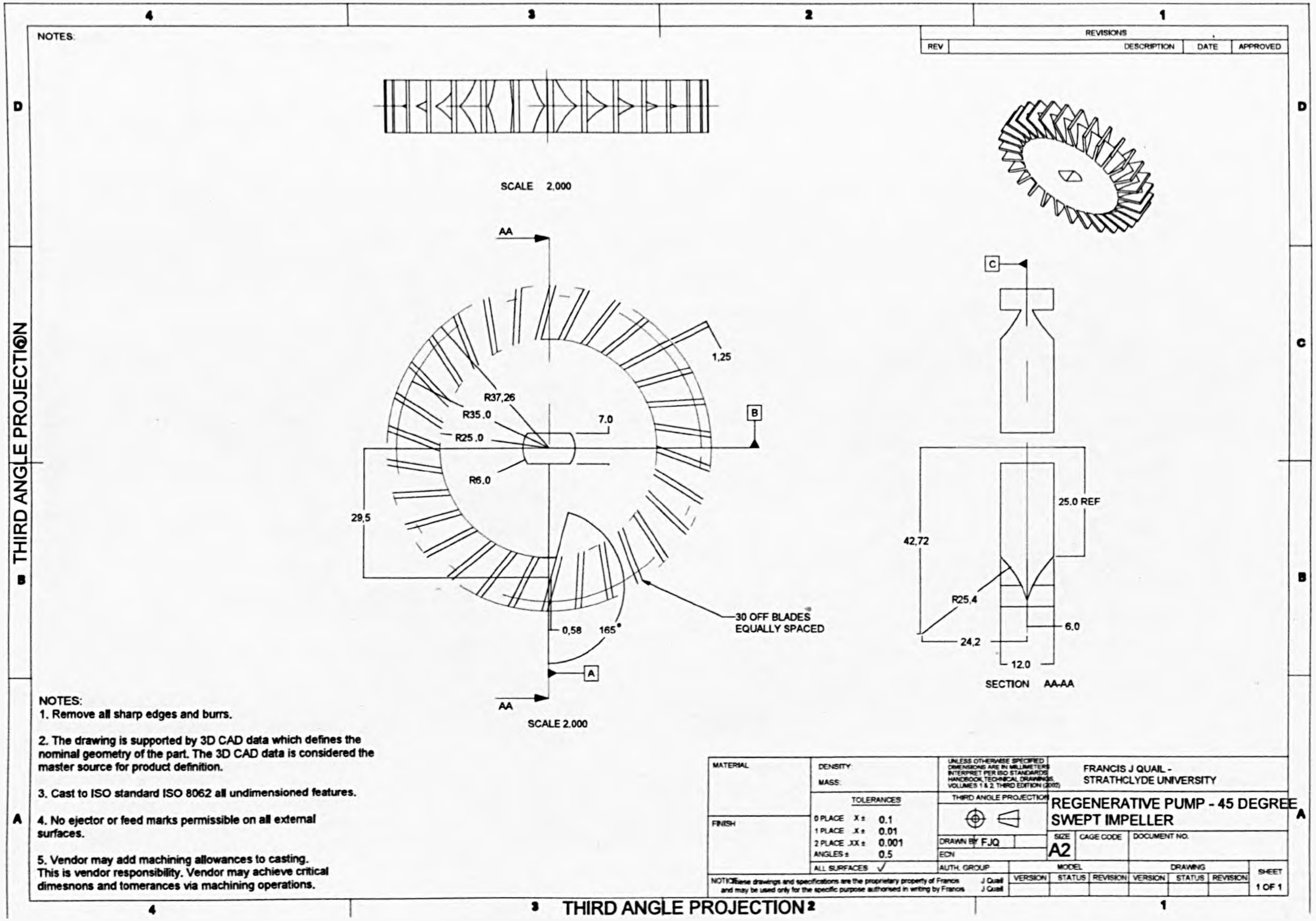

NOTES:

1. Remove all sharp edges and burrs.

2. The drawing is supported by 3D CAD data which defines the nominal geometry of the part. The 3D CAD data is considered the master source for product definition.

3. Cast to ISO standard ISO 8062 all undimensioned features.

4. No ejector or feed marks permissible on all external surfaces.

5. Vendor may add machining allowances to casting. This is vendor responsibility. Vendor may achieve critical dimesnons and tomerances via machining operations.

MATERIAL

FINISH

DENSITY:

MASS:

TOLERANCES

0 PLACE X ± 0.1
1 PLACE .X ± 0.01
2 PLACE .XX ± 0.001
ANGLES ± 0.5

ALL SURFACES ✓

UNLESS OTHERWISE SPECIFIED
DIMENSIONS ARE IN MILLIMETERS
INTERPRET PER ISO STANDARDS
HANDBOOK TECHNICAL DRAWINGS,
VOLUMES 1 & 2, THIRD EDITION (2002)

THIRD ANGLE PROJECTION

DRAWN BY FJQ

ECN

AUTH. GROUP

FRANCIS J QUAIL -
STRATHCLYDE UNIVERSITY

REGENERATIVE PUMP - 45 DEGREE
SWEPT IMPELLER

SIZE A2

CAGE CODE

DOCUMENT NO.

| MODEL | | | DRAWING | | | SHEET |
|---|---|---|---|---|---|---|
| VERSION | STATUS | REVISION | VERSION | STATUS | REVISION | 1 OF 1 |

NOTICE These drawings and specifications are the proprietary property of Francis J Quail and may be used only for the specific purpose authorised in writing by Francis J Quail

## C6 45° Chevron impeller

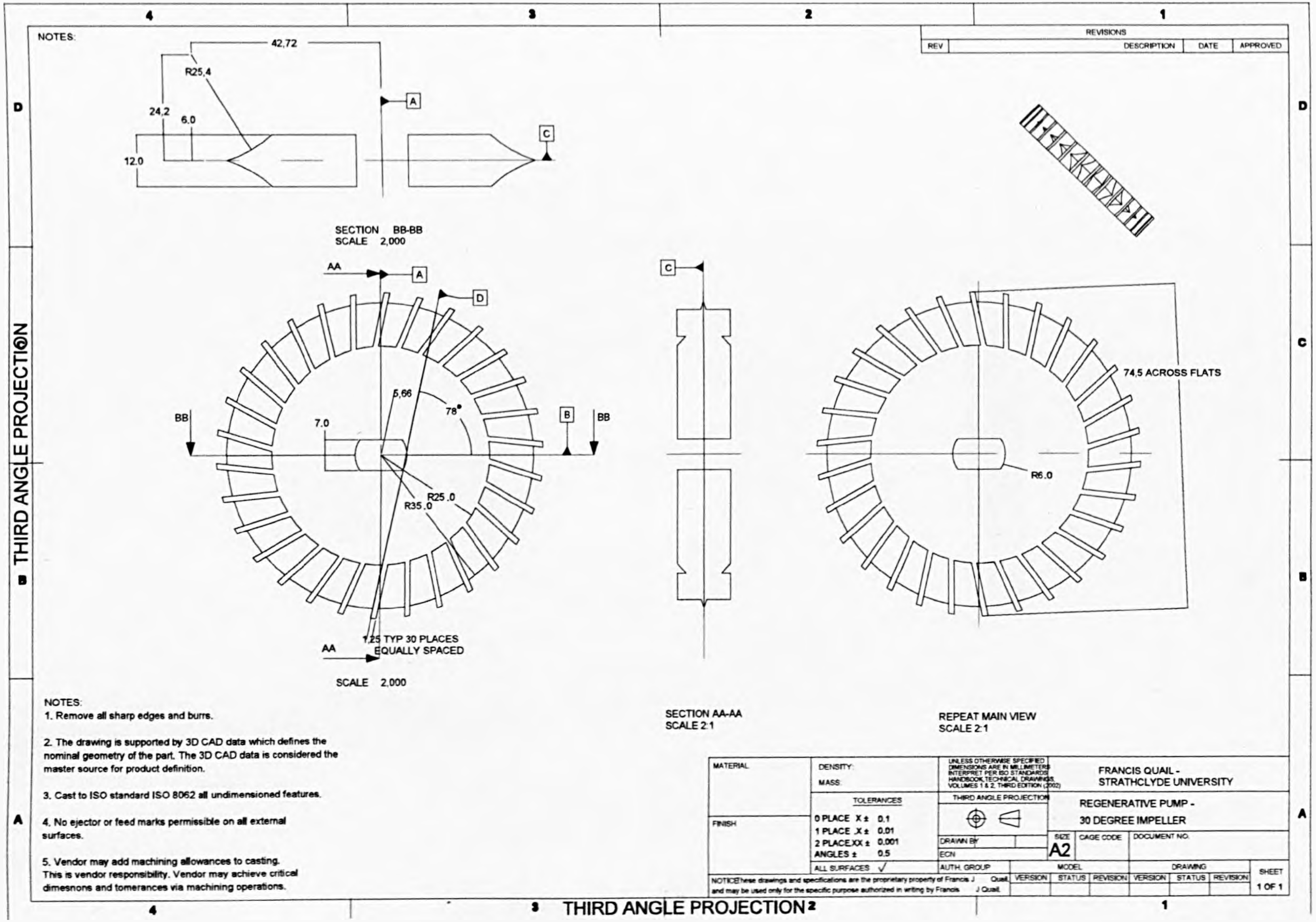

NOTES:

1. Remove all sharp edges and burrs.

2. The drawing is supported by 3D CAD data which defines the nominal geometry of the part. The 3D CAD data is considered the master source for product definition.

3. Cast to ISO standard ISO 8062 all undimensioned features.

4. No ejector or feed marks permissible on all external surfaces.

5. Vendor may add machining allowances to casting. This is vendor responsibility. Vendor may achieve critical dimesnons and tomerances via machining operations.

## C7 60° Chevron impeller

THIRD ANGLE PROJECTION

NOTES:

REVISIONS

| REV | DESCRIPTION | DATE | APPROVED |
|---|---|---|---|

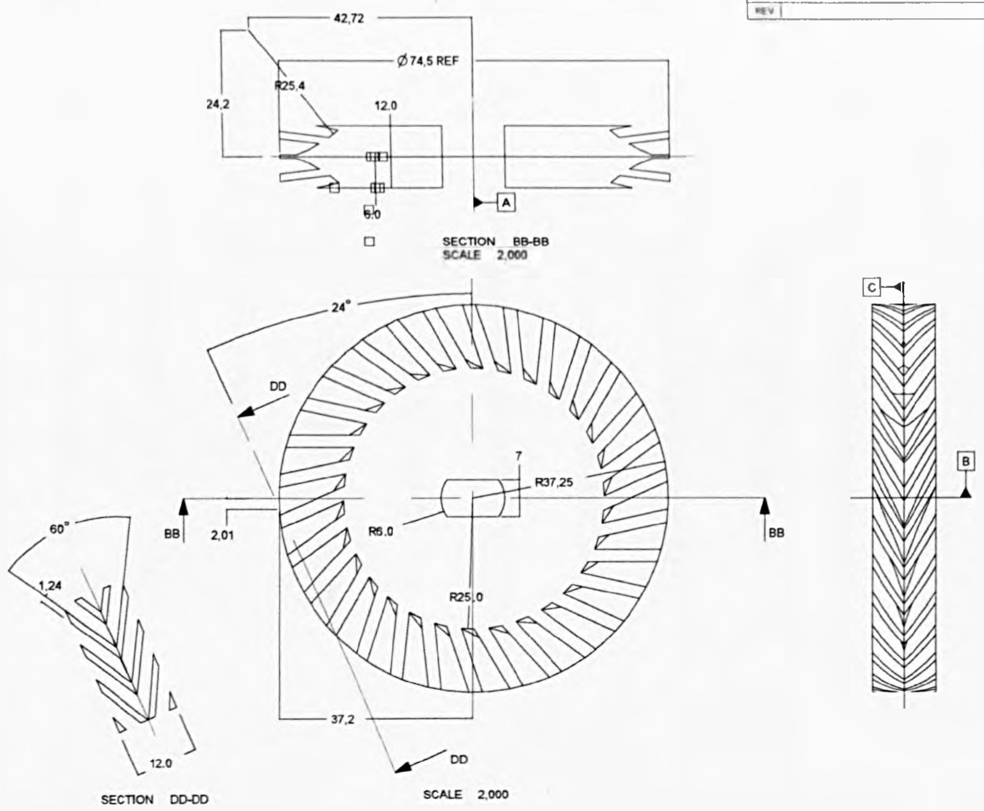

SECTION BB-BB
SCALE 2,000

SECTION DD-DD

SCALE 2,000

NOTES:
1. Remove all sharp edges and burrs.

2. The drawing is supported by 3D CAD data which defines the nominal geometry of the part. The 3D CAD data is considered the master source for product definition.

3. Cast to ISO standard ISO 8062 all undimensioned features.

4. No ejector or feed marks permissible on all external surfaces.

5. Vendor may add machining allowances to casting. This is vendor responsibility. Vendor may achieve critical dimesnons and tomerances via machining operations.

MATERIAL

FINISH

DENSITY:
MASS:

TOLERANCES
0 PLACE X ± 0.1
1 PLACE .X ± 0.01
2 PLACE .XX ± 0.001
ANGLES ± 0.5
ALL SURFACES ✓

UNLESS OTHERWISE SPECIFIED DIMENSIONS ARE IN MILLIMETERS INTERPRET PER ISO STANDARDS HANDBOOK TECHNICAL DRAWINGS. VOLUMES 1 & 2. THIRD EDITION (2002)

THIRD ANGLE PROJECTION

DRAWN BY
ECN
AUTH. GROUP

FRANCIS J QUAIL -
STRATHCLYDE UNIVERSITY

REGENERATIVE PUMP -
60-DEGREE CHEVRON IMPELLER

SIZE A2
CAGE CODE
DOCUMENT NO.

| MODEL | | | DRAWING | | | SHEET |
|---|---|---|---|---|---|---|
| VERSION | STATUS | REVISION | VERSION | STATUS | REVISION | 1 OF 1 |

NOTICEThese drawings and specifications are the proprietary property of Francis J Quail and may be used only for the specific purpose authorized in writing by FRancis J Quail.

THIRD ANGLE PROJECTION

# Appendix D

## List Of tabulated results

| Flowrate ($m^3/s$) | Differential Pressure ($kN/m^2$) | Power (W) | Flow Coefficient ($\Phi$) | Head coefficient ($\Psi$) | Power coefficient (¶) | Number of circulations | Hydraulic Efficiency (%) |
|---|---|---|---|---|---|---|---|
| 0.000369 | 24.82112625 | 237.1862409 | 0.602062652 | 0.313550003 | 0.198022618 | 4.073208694 | 10.41199641 |
| 0.0003515 | 64.81071855 | 247.6596064 | 0.573509545 | 0.818713897 | 0.206766646 | 4.320254804 | 23.14217948 |
| 0.0003322 | 105.4897866 | 254.9909623 | 0.542019548 | 1.332587512 | 0.212887466 | 4.622893194 | 33.13182896 |
| 0.000312 | 145.4793789 | 264.4169912 | 0.509061104 | 1.837751406 | 0.220757092 | 4.979745752 | 39.40184618 |
| 0.000286 | 186.1584469 | 273.8430201 | 0.466639346 | 2.351625022 | 0.228626718 | 5.513257992 | 42.72204732 |
| 0.0002615 | 220.6322334 | 283.4261495 | 0.426664996 | 2.787111137 | 0.236627504 | 6.113076725 | 42.99022082 |
| 0.000238 | 248.2112625 | 292.7998116 | 0.388322253 | 3.135500029 | 0.244453409 | 6.804447279 | 41.14398997 |
| 0.000202 | 287.5113791 | 302.697142 | 0.329584433 | 3.631954201 | 0.252716516 | 8.175536893 | 37.8411182 |
| 0.0001654 | 333.0167773 | 315.736482 | 0.26986765 | 4.206795873 | 0.263602831 | 10.18132881 | 33.07848043 |
| 0.0001291 | 363.3537093 | 323.1725715 | 0.210640348 | 4.590023654 | 0.269811092 | 13.29402364 | 26.96659399 |
| 0.0001 | 384.0379812 | 331.9701985 | 0.16316061 | 4.851315323 | 0.277156076 | 17.42125119 | 21.01441848 |
| 0.0000667 | 421.9591463 | 346.8947443 | 0.108828127 | 5.33035005 | 0.289616316 | 26.56259549 | 14.23790298 |
| 3.33333E-05 | 459.8803114 | 364.4376315 | 0.05438687 | 5.809384777 | 0.304262564 | 54.04153135 | 7.122732118 |
| 2E-06 | 494.3540979 | 403.4509179 | 0.003263212 | 6.244870892 | 0.33683407 | 914.6181151 | 0.388902314 |

**D1** Radial impeller experimental test

| Flowrate ($m^3/s$) | Differential Pressure ($kN/m^2$) | Power (W) | Flow Coefficient (Φ) | Head coefficient (Ψ) | Power coefficient (¶) | Number of circulations | Hydraulic Efficiency (%) |
|---|---|---|---|---|---|---|---|
| 0.0003792 | 45.50539813 | 243.4178934 | 0.618705034 | 0.574841672 | 0.203225315 | 3.93973455 | 18.31859263 |
| 0.0003616 | 84.8055147 | 251.2729175 | 0.589988767 | 1.071295843 | 0.209783336 | 4.174756045 | 30.04892792 |
| 0.0003351 | 133.0688158 | 260.9084138 | 0.546751205 | 1.680976405 | 0.217827842 | 4.575193498 | 39.92494481 |
| 0.0003076 | 188.2268741 | 271.6436134 | 0.501882037 | 2.377754189 | 0.226790472 | 5.063692412 | 47.29381449 |
| 0.000284 | 225.4585635 | 278.0323663 | 0.463376133 | 2.848079193 | 0.232124329 | 5.558343534 | 49.70831196 |
| 0.0002637 | 259.2428742 | 285.3637221 | 0.430254529 | 3.274855586 | 0.238245149 | 6.05466063 | 50.2135302 |
| 0.0002373 | 285.4429519 | 290.3385707 | 0.387180128 | 3.605825034 | 0.242398562 | 6.827141486 | 47.99922887 |
| 0.0002033 | 324.7430685 | 297.250992 | 0.331705521 | 4.102279205 | 0.248169621 | 8.117574505 | 44.59908233 |
| 0.0001687 | 358.5273792 | 308.1432921 | 0.27525195 | 4.529055598 | 0.257263411 | 9.964780394 | 38.05844769 |
| 0.0001337 | 390.2432628 | 314.532045 | 0.218145736 | 4.929702824 | 0.262597268 | 12.80605508 | 31.56192549 |
| 0.0001076 | 413.6854376 | 320.4494965 | 0.175560817 | 5.225833382 | 0.267537644 | 16.12796992 | 25.99591163 |
| 0.0000679 | 450.917127 | 334.6932735 | 0.110786054 | 5.696158387 | 0.279429523 | 26.07744407 | 16.50768635 |
| 0.0000348 | 482.6330105 | 350.6127891 | 0.056779892 | 6.096805613 | 0.292720446 | 51.72645617 | 8.33975531 |
| 0.0000042 | 512.9699426 | 388.6311058 | 0.006852746 | 6.480033394 | 0.32446127 | 435.0668273 | 0.899907191 |

**D2** 30° swept forward impeller experimental tests

| Flowrate ($m^3/s$) | Differential Pressure ($kN/m^2$) | Power (W) | Flow Coefficient ($\Phi$) | Head coefficient ($\Psi$) | Power coefficient (¶) | Number of circulations | Hydraulic Efficiency (%) |
|---|---|---|---|---|---|---|---|
| 0.0003574 | 27.57902917 | 260.7513133 | 0.583136021 | 0.348388892 | 0.217696682 | 4.234261665 | 8.83768334 |
| 0.0003362 | 73.77390304 | 270.0726085 | 0.548545972 | 0.931940287 | 0.225478867 | 4.557315775 | 20.52324537 |
| 0.0003255 | 98.59502929 | 275.4140249 | 0.531087787 | 1.245490289 | 0.229938322 | 4.736346159 | 25.43131106 |
| 0.00031 | 125.4845827 | 281.3838433 | 0.505797892 | 1.585169459 | 0.234922418 | 5.017607911 | 29.43342934 |
| 0.00029 | 161.3373207 | 289.5530683 | 0.47316577 | 2.038075019 | 0.24174276 | 5.424952518 | 33.34065996 |
| 0.0002593 | 202.7058644 | 300.2359011 | 0.423075463 | 2.560658357 | 0.250661669 | 6.172484069 | 34.80546412 |
| 0.00022 | 242.005981 | 312.5944724 | 0.358953343 | 3.057112529 | 0.260979623 | 7.433902057 | 32.58860447 |
| 0.000184 | 281.9955733 | 321.4444662 | 0.300215523 | 3.562276422 | 0.268368327 | 9.062274198 | 30.12772836 |
| 0.0001521 | 315.779884 | 331.4465302 | 0.248167288 | 3.989052815 | 0.276718874 | 11.14933602 | 26.35743401 |
| 0.000108 | 349.5641948 | 342.2340967 | 0.176213459 | 4.415829208 | 0.285725224 | 16.06494452 | 19.55972159 |
| 0.000071 | 379.9011268 | 356.0589391 | 0.115844033 | 4.799056989 | 0.297267341 | 24.9000408 | 13.04059964 |
| 0.0000393 | 417.1328162 | 377.0056701 | 0.06412212 | 5.269381994 | 0.314755398 | 45.70179834 | 7.19683185 |
| 0.0000024 | 446.0907969 | 413.9242834 | 0.003915855 | 5.635190331 | 0.345578099 | 762.0336144 | 0.404458778 |

**D3** 30° swept backward impeller experimental tests

| Flowrate (m$^3$/s) | Differential Pressure (kN/m$^2$) | Power (W) | Flow Coefficient (Φ) | Head coefficient (Ψ) | Power coefficient (¶) | Number of circulations | Hydraulic Efficiency (%) |
|---|---|---|---|---|---|---|---|
| 0.000348 | 22.06322334 | 256.9809017 | 0.567798924 | 0.278711114 | 0.214548832 | 4.372645617 | 7.125064153 |
| 0.0003385 | 46.88434959 | 263.3696546 | 0.552298666 | 0.592261117 | 0.219882689 | 4.520310544 | 13.90316437 |
| 0.0003206 | 77.22128168 | 269.9155081 | 0.523092917 | 0.975488898 | 0.225347707 | 4.822321367 | 20.51214203 |
| 0.0003038 | 108.2476895 | 274.9950903 | 0.495681934 | 1.367426402 | 0.229588561 | 5.138148662 | 26.1464843 |
| 0.0002824 | 136.5161944 | 281.6980442 | 0.460765564 | 1.724525016 | 0.235184739 | 5.594871763 | 29.10089956 |
| 0.0002473 | 175.816311 | 296.3607559 | 0.403496189 | 2.220979187 | 0.247426379 | 6.515130553 | 29.54960013 |
| 0.0002049 | 222.7006606 | 310.2379652 | 0.334316091 | 2.813240304 | 0.259012217 | 8.04724585 | 28.33937891 |
| 0.0001731 | 253.7270684 | 320.3971297 | 0.282431017 | 3.205177808 | 0.267493924 | 9.688892786 | 25.65779063 |
| 0.0001376 | 286.1324277 | 329.404224 | 0.224509 | 3.614534756 | 0.275013789 | 12.41789896 | 21.85092472 |
| 0.000101 | 313.0219811 | 343.1243328 | 0.164792216 | 3.954213926 | 0.286468466 | 17.23996268 | 16.30458282 |
| 0.000067 | 333.706253 | 355.6400045 | 0.109317609 | 4.215505595 | 0.29691758 | 26.43967839 | 10.83149239 |
| 0.000035 | 363.3537093 | 370.5645503 | 0.057106214 | 4.590023654 | 0.309377821 | 51.42579705 | 5.745524494 |
| 0.0000024 | 386.1064084 | 403.6080184 | 0.003915855 | 4.87744449 | 0.336965231 | 762.0336144 | 0.364269121 |

**D4** 45° swept forward impeller experimental tests

| Flowrate ($m^3/s$) | Differential Pressure ($kN/m^2$) | Power (W) | Flow Coefficient ($\Phi$) | Head coefficient ($\Psi$) | Power coefficient (¶) | Number of circulations | Hydraulic Efficiency (%) |
|---|---|---|---|---|---|---|---|
| 0.000329 | 18.61584469 | 246.3504357 | 0.536798408 | 0.235162502 | 0.205673643 | 4.676503233 | 6.305583695 |
| 0.000321 | 41.36854376 | 247.3454055 | 0.523745559 | 0.522583338 | 0.206504325 | 4.815204594 | 13.53305254 |
| 0.00031 | 57.22648553 | 253.3152238 | 0.505797892 | 0.722906951 | 0.211488422 | 5.017607911 | 17.04236332 |
| 0.000288 | 93.07922346 | 264.1551571 | 0.469902558 | 1.175812511 | 0.220538491 | 5.468798639 | 23.32351621 |
| 0.0002626 | 120.6582526 | 273.8430201 | 0.428459763 | 1.524201403 | 0.228626718 | 6.083746328 | 25.42465274 |
| 0.0002323 | 151.6846604 | 286.5157923 | 0.379022098 | 1.916138907 | 0.239206992 | 6.993220487 | 25.66463258 |
| 0.000198 | 186.8479226 | 297.9317607 | 0.323058008 | 2.360334744 | 0.248737983 | 8.358656606 | 24.8776553 |
| 0.0001612 | 220.6322334 | 310.4997993 | 0.263014904 | 2.787111137 | 0.259230817 | 10.4697588 | 22.05236747 |
| 0.0001292 | 247.5217868 | 322.0205013 | 0.210803509 | 3.126790307 | 0.268849249 | 13.28304616 | 18.5068312 |
| 0.0000996 | 265.4481558 | 333.0175351 | 0.162507968 | 3.353243087 | 0.278030478 | 17.49478589 | 14.38468705 |
| 0.00006 | 286.1324277 | 351.8695929 | 0.097896366 | 3.614534756 | 0.29376973 | 29.62801124 | 8.471758098 |
| 0.0000315 | 306.1272238 | 365.484968 | 0.051395592 | 3.867116703 | 0.305136967 | 57.23853994 | 4.458894775 |
| 0.0000031 | 321.2956899 | 396.9050645 | 0.005057979 | 4.058730594 | 0.331369052 | 589.7607911 | 0.402130999 |

**D5** 45° swept backward impeller experimental tests

| Flowrate ($m^3/s$) | Differential Pressure ($kN/m^2$) | Power (W) | Flow Coefficient (Φ) | Head coefficient (Ψ) | Power coefficient (¶) | Number of circulations | Hydraulic Efficiency (%) |
|---|---|---|---|---|---|---|---|
| 0.000348 | 22.06322334 | 256.9809017 | 0.567798924 | 0.278711114 | 0.214548832 | 4.372645617 | 7.125064153 |
| 0.0003385 | 46.88434959 | 263.3696546 | 0.552298666 | 0.592261117 | 0.219882689 | 4.520310544 | 13.90316437 |
| 0.0003206 | 77.22128168 | 269.9155081 | 0.523092917 | 0.975488898 | 0.225347707 | 4.822321367 | 20.51214203 |
| 0.0003038 | 108.2476895 | 274.9950903 | 0.495681934 | 1.367426402 | 0.229588561 | 5.138148662 | 26.1464843 |
| 0.0002824 | 136.5161944 | 281.6980442 | 0.460765564 | 1.724525016 | 0.235184739 | 5.594871763 | 29.10089956 |
| 0.0002473 | 175.816311 | 296.3607559 | 0.403496189 | 2.220979187 | 0.247426379 | 6.515130553 | 29.54960013 |
| 0.0002049 | 222.7006606 | 310.2379652 | 0.334316091 | 2.813240304 | 0.259012217 | 8.04724585 | 28.33937891 |
| 0.0001731 | 253.7270684 | 320.3971297 | 0.282431017 | 3.205177808 | 0.267493924 | 9.688892786 | 25.65779063 |
| 0.0001376 | 286.1324277 | 329.404224 | 0.224509 | 3.614534756 | 0.275013789 | 12.41789896 | 21.85092472 |
| 0.000101 | 313.0219811 | 343.1243328 | 0.164792216 | 3.954213926 | 0.286468466 | 17.23996268 | 16.30458282 |
| 0.000067 | 333.706253 | 355.6400045 | 0.109317609 | 4.215505595 | 0.29691758 | 26.43967839 | 10.83149239 |
| 0.000035 | 363.3537093 | 370.5645503 | 0.057106214 | 4.590023654 | 0.309377821 | 51.42579705 | 5.745524494 |
| 0.0000024 | 386.1064084 | 403.6080184 | 0.003915855 | 4.87744449 | 0.336965231 | 762.0336144 | 0.364269121 |

**D6** 45° chevron forward impeller experimental tests

| Flowrate ($m^3/s$) | Differential Pressure ($kN/m^2$) | Power (W) | Flow Coefficient (Φ) | Head coefficient (Ψ) | Power coefficient (¶) | Number of circulations | Hydraulic Efficiency (%) |
|---|---|---|---|---|---|---|---|
| 0.000329 | 18.61584469 | 246.3504357 | 0.536798408 | 0.235162502 | 0.205673643 | 4.676503233 | 6.305583695 |
| 0.000321 | 41.36854376 | 247.3454055 | 0.523745559 | 0.522583338 | 0.206504325 | 4.815204594 | 13.53305254 |
| 0.00031 | 57.22648553 | 253.3152238 | 0.505797892 | 0.722906951 | 0.211488422 | 5.017607911 | 17.04236332 |
| 0.000288 | 93.07922346 | 264.1551571 | 0.469902558 | 1.175812511 | 0.220538491 | 5.468798639 | 23.32351621 |
| 0.0002626 | 120.6582526 | 273.8430201 | 0.428459763 | 1.524201403 | 0.228626718 | 6.083746328 | 25.42465274 |
| 0.0002323 | 151.6846604 | 286.5157923 | 0.379022098 | 1.916138907 | 0.239206992 | 6.993220487 | 25.66463258 |
| 0.000198 | 186.8479226 | 297.9317607 | 0.323058008 | 2.360334744 | 0.248737983 | 8.358656606 | 24.8776553 |
| 0.0001612 | 220.6322334 | 310.4997993 | 0.263014904 | 2.787111137 | 0.259230817 | 10.4697588 | 22.05236747 |
| 0.0001292 | 247.5217868 | 322.0205013 | 0.210803509 | 3.126790307 | 0.268849249 | 13.28304616 | 18.5068312 |
| 0.0000996 | 265.4481558 | 333.0175351 | 0.162507968 | 3.353243087 | 0.278030478 | 17.49478589 | 14.38468705 |
| 0.00006 | 286.1324277 | 351.8695929 | 0.097896366 | 3.614534756 | 0.29376973 | 29.62801124 | 8.471758098 |
| 0.0000315 | 306.1272238 | 365.484968 | 0.051395592 | 3.867116703 | 0.305136967 | 57.23853994 | 4.458894775 |
| 0.0000031 | 321.2956899 | 396.9050645 | 0.005057979 | 4.058730594 | 0.331369052 | 589.7607911 | 0.402130999 |

**D7** 45° chevron backward impeller experimental tests

| Flowrate (m$^3$/s) | Differential Pressure (kN/m$^2$) | Power (W) | Flow Coefficient (Φ) | Head coefficient (Ψ) | Power coefficient (¶) | Number of circulations | Hydraulic Efficiency (%) |
|---|---|---|---|---|---|---|---|
| 0.000307 | 18.61584469 | 238.7572458 | 0.500903074 | 0.235162502 | 0.199334222 | 5.075326121 | 6.382922136 |
| 0.000293 | 46.88434959 | 245.669667 | 0.478060588 | 0.592261117 | 0.205105281 | 5.360305678 | 14.24284618 |
| 0.000282 | 62.74229137 | 252.3726209 | 0.460112921 | 0.79258473 | 0.210701459 | 5.604068586 | 17.15264452 |
| 0.000266 | 84.8055147 | 258.5519065 | 0.434007224 | 1.071295843 | 0.215860436 | 5.994622419 | 20.63291431 |
| 0.0002519 | 103.4213594 | 266.5116643 | 0.411001577 | 1.306458346 | 0.222505898 | 6.379924164 | 22.21124517 |
| 0.0002151 | 134.4477672 | 275.5187586 | 0.350958473 | 1.698395849 | 0.230025762 | 7.623496086 | 22.89794198 |
| 0.0001915 | 153.7530876 | 284.5258529 | 0.312452569 | 1.942268074 | 0.237545627 | 8.672541962 | 21.76093076 |
| 0.0001644 | 179.2636896 | 293.5329472 | 0.268236043 | 2.264527799 | 0.245065491 | 10.2486659 | 20.42161973 |
| 0.0001257 | 200.6374372 | 305.2631166 | 0.205092887 | 2.53452919 | 0.254858803 | 13.67765055 | 16.1623263 |
| 0.0000966 | 216.495379 | 316.3125171 | 0.15761315 | 2.734852803 | 0.264083753 | 18.06570747 | 12.51612555 |
| 0.00006 | 234.421748 | 328.8805557 | 0.097896366 | 2.961305583 | 0.274576587 | 29.62801124 | 7.828841232 |
| 0.0000324 | 247.5217868 | 338.6731524 | 0.052864038 | 3.126790307 | 0.282752254 | 55.62388914 | 4.233091188 |
| 0.0000024 | 262.0007771 | 371.1405854 | 0.003915855 | 3.309694475 | 0.309858742 | 762.0336144 | 0.28334601 |

**D8** 60° chevron forward impeller experimental tests

| Flowrate (m³/s) | Differential Pressure (kN/m²) | Power (W) | Flow Coefficient (Φ) | Head coefficient ( ) | Power coefficient (¶) | Number of circulations | Hydraulic Efficiency (%) |
|---|---|---|---|---|---|---|---|
| 0.000284 | 17.23689323 | 235.5105025 | 0.463376133 | 0.217743058 | 0.196623573 | 5.558343534 | 5.673049459 |
| 0.000277 | 27.57902917 | 237.9717434 | 0.451954891 | 0.348388892 | 0.19867842 | 5.721269985 | 8.607638606 |
| 0.000267 | 45.50539813 | 242.4229237 | 0.43563883 | 0.574841672 | 0.202394632 | 5.968841478 | 13.03607091 |
| 0.000258 | 59.29491272 | 244.8841646 | 0.420954375 | 0.749036118 | 0.204449479 | 6.208064631 | 15.99152473 |
| 0.0002423 | 76.53180595 | 250.0161137 | 0.395338159 | 0.966779176 | 0.208734053 | 6.667916757 | 18.3972751 |
| 0.0002173 | 100.6634565 | 259.7039767 | 0.354548006 | 1.271619456 | 0.216822279 | 7.537314553 | 19.79857868 |
| 0.0001892 | 123.4161555 | 268.6063374 | 0.308699875 | 1.559040292 | 0.224254703 | 8.788775001 | 19.55870667 |
| 0.0001622 | 136.5161944 | 275.9376932 | 0.26464651 | 1.724525016 | 0.230375523 | 10.39973015 | 17.47427988 |
| 0.0001262 | 148.2372818 | 288.5057318 | 0.20590869 | 1.872590295 | 0.240868357 | 13.61993843 | 13.43109908 |
| 0.0000917 | 165.474175 | 301.5974386 | 0.14961828 | 2.090333353 | 0.251798393 | 19.07854849 | 9.95818425 |
| 0.0000587 | 177.8847382 | 318.8784917 | 0.095775278 | 2.247108354 | 0.26622604 | 30.30385401 | 6.154635334 |
| 0.0000294 | 188.2268741 | 333.331736 | 0.047969219 | 2.377754189 | 0.278292799 | 61.39049914 | 3.005720098 |
| 0.0000037 | 200.6374372 | 370.7216508 | 0.006036943 | 2.53452919 | 0.309508981 | 493.9797619 | 0.335148747 |

**D9** 60° chevron backward impeller experimental tests

| Flowrate (m³/s) | Differential Pressure (kN/m²) | Power (W) | Flow Coefficient (Φ) | Head coefficient (Ψ) | Power coefficient (¶) | Number of circulations | Hydraulic Efficiency (%) |
|---|---|---|---|---|---|---|---|
| 0.0003515 | 64.81071855 | 247.6596064 | 0.573509545 | 0.2723165 | 0.19849598 | 4.320254804 | 16.1254342 |
| 0.0003322 | 105.4897866 | 254.9909623 | 0.542019548 | 0.8246372 | 0.200114218 | 4.622893194 | 28.2345621 |
| 0.000312 | 145.4793789 | 264.4169912 | 0.509061104 | 1.3284567 | 0.207511666 | 4.979745752 | 37.2345622 |
| 0.000286 | 186.1584469 | 273.8430201 | 0.466639346 | 2.0238912 | 0.214909114 | 5.513257992 | 39.73153746 |
| 0.0002615 | 220.6322334 | 283.4261495 | 0.426664996 | 2.4102993 | 0.224796128 | 6.113076725 | 39.98090536 |
| 0.000238 | 248.2112625 | 292.7998116 | 0.388322253 | 2.8132345 | 0.22734167 | 6.804447279 | 38.26391067 |
| 0.000202 | 287.5113791 | 302.697142 | 0.329584433 | 3.341397865 | 0.24008069 | 8.175536893 | 35.19223992 |
| 0.0001654 | 333.0167773 | 315.736482 | 0.26986765 | 3.870252203 | 0.245150633 | 10.18132881 | 30.7629868 |
| 0.0001291 | 363.3537093 | 323.1725715 | 0.210640348 | 4.176921525 | 0.250924315 | 13.29402364 | 25.07893241 |
| 0.0001 | 384.0379812 | 331.9701985 | 0.16316061 | 4.511723251 | 0.25775515 | 17.42125119 | 19.54340919 |
| 0.0000667 | 421.9591463 | 346.8947443 | 0.108828127 | 4.957225546 | 0.269343174 | 26.56259549 | 13.24124977 |
| 3.33333E-05 | 459.8803114 | 364.4376315 | 0.05438687 | 5.402727842 | 0.282964184 | 54.04153135 | 6.624140869 |
| 2E-06 | 494.3540979 | 403.4509179 | 0.003263212 | 5.807729929 | 0.30123451 | 914.6181151 | 0.361679152 |

**D10** radial impeller CFD results

| Flowrate ($m^3/s$) | Differential Pressure ($kN/m^2$) | Power (W) | Flow Coefficient ($\Phi$) | Head coefficient ($\Psi$) | Power coefficient (¶) | Number of circulations | Hydraulic Efficiency (%) |
|---|---|---|---|---|---|---|---|
| 0.0003792 | 45.50539813 | 243.4178934 | 0.5923456 | 0.3819274 | 0.203225315 | 3.93973455 | 8.243366685 |
| 0.0003616 | 84.8055147 | 251.2729175 | 0.5634562 | 0.9329464 | 0.207685503 | 4.174756045 | 21.03424954 |
| 0.0003351 | 133.0688158 | 260.9084138 | 0.5261234 | 1.4502387 | 0.211293007 | 4.575193498 | 31.14145695 |
| 0.0003076 | 188.2268741 | 271.6436134 | 0.4919475 | 1.9701284 | 0.215450948 | 5.063692412 | 40.67268046 |
| 0.000284 | 225.4585635 | 278.0323663 | 0.4632367 | 2.3153927 | 0.218196869 | 5.558343534 | 44.73748076 |
| 0.0002637 | 259.2428742 | 285.3637221 | 0.4261367 | 2.6930284 | 0.22395044 | 6.05466063 | 46.69858308 |
| 0.0002373 | 285.4429519 | 290.3385707 | 0.3872184 | 3.1428532 | 0.230278634 | 6.827141486 | 44.63928285 |
| 0.0002033 | 324.7430685 | 297.250992 | 0.3317276 | 3.6910385 | 0.23576114 | 8.117574505 | 41.47714657 |
| 0.0001687 | 358.5273792 | 308.1432921 | 0.2752182 | 4.1858293 | 0.24440024 | 9.964780394 | 36.5491231 |
| 0.0001337 | 390.2432628 | 314.532045 | 0.2111298 | 4.5710247 | 0.252093377 | 12.80605508 | 29.3525907 |
| 0.0001076 | 413.6854376 | 320.4494965 | 0.1501284 | 5.1712874 | 0.262186891 | 16.12796992 | 22.5183942 |
| 0.0000679 | 450.917127 | 334.6932735 | 0.0921038 | 5.8583628 | 0.273840933 | 26.07744407 | 15.35214831 |
| 0.0000348 | 482.6330105 | 350.6127891 | 0.0452847 | 6.1193747 | 0.293013167 | 51.72645617 | 7.755972438 |
| 0.0000042 | 512.9699426 | 388.6311058 | 0.0021037 | 6.5510385 | 0.321216657 | 435.0668273 | 0.836913688 |

**D11** 30° swept forward impeller CFD results

| Flowrate ($m^3/s$) | Differential Pressure ($kN/m^2$) | Power (W) | Flow Coefficient (Φ) | Head coefficient (Ψ) | Power coefficient (¶) | Number of circulations | Hydraulic Efficiency (%) |
|---|---|---|---|---|---|---|---|
| 0.0003574 | 27.57902917 | 260.7513133 | 0.56194625 | 0.217382 | 0.195927014 | 4.234261665 | 3.535073336 |
| 0.0003362 | 73.77390304 | 270.0726085 | 0.548545457 | 0.447385 | 0.205185769 | 4.557315775 | 10.26162268 |
| 0.0003255 | 98.59502929 | 275.4140249 | 0.5216235 | 0.789375 | 0.211543256 | 4.736346159 | 19.0734833 |
| 0.00031 | 125.4845827 | 281.3838433 | 0.505797892 | 1.049455 | 0.218477849 | 5.017607911 | 23.54674347 |
| 0.00029 | 161.3373207 | 289.5530683 | 0.4652845 | 1.56917463 | 0.222403339 | 5.424952518 | 31.00681376 |
| 0.0002593 | 202.7058644 | 300.2359011 | 0.423075463 | 2.1037585 | 0.233115352 | 6.172484069 | 32.36908163 |
| 0.00022 | 242.005981 | 312.5944724 | 0.358953343 | 2.61585838 | 0.242712031 | 7.433902057 | 30.30740216 |
| 0.000184 | 281.9955733 | 321.4444662 | 0.300215523 | 3.18294753 | 0.249582544 | 9.062274198 | 28.01878737 |
| 0.0001521 | 315.779884 | 331.4465302 | 0.248167288 | 3.68192874 | 0.257348553 | 11.14933602 | 24.51241363 |
| 0.000108 | 349.5641948 | 342.2340967 | 0.1831285 | 4.23018375 | 0.274296215 | 16.06494452 | 18.19054108 |
| 0.000071 | 379.9011268 | 356.0589391 | 0.1237392 | 4.6713751 | 0.288349321 | 24.9000408 | 12.12775766 |
| 0.0000393 | 417.1328162 | 377.0056701 | 0.0710274 | 5.12847583 | 0.30846029 | 45.70179834 | 6.693053621 |
| 0.0000024 | 446.0907969 | 413.9242834 | 0.0101284 | 5.58028475 | 0.342122318 | 762.0336144 | 0.376146663 |

**D12** 30° swept backward impeller CFD results

| Flowrate ($m^3/s$) | Differential Pressure ($kN/m^2$) | Power (W) | Flow Coefficient ($\Phi$) | Head coefficient ($\Psi$) | Power coefficient (¶) | Number of circulations | Hydraulic Efficiency (%) |
|---|---|---|---|---|---|---|---|
| 0.000348 | 22.06322334 | 256.9809017 | 0.54104827 | 0.43947562 | 0.17625295 | 4.372645617 | 8.582462 |
| 0.0003385 | 46.88434959 | 263.3696546 | 0.510623951 | 0.645837586 | 0.184179115 | 4.520310544 | 18.3837234 |
| 0.0003206 | 77.22128168 | 269.9155081 | 0.4912956 | 0.933947837 | 0.192096 | 4.822321367 | 24.837364 |
| 0.0003038 | 108.2476895 | 274.9950903 | 0.4619284 | 1.339846592 | 0.200424928 | 5.138148662 | 30.7.847262 |
| 0.0002824 | 136.5161944 | 281.6980442 | 0.4363857 | 1.650237408 | 0.204792 | 5.594871763 | 33.1928274 |
| 0.0002473 | 175.816311 | 296.3607559 | 0.382618375 | 2.235673298 | 0.214655834 | 6.515130553 | 31.4929274 |
| 0.0002049 | 222.7006606 | 310.2379652 | 0.338284756 | 2.64738374 | 0.225430663 | 8.04724585 | 29.4948272 |
| 0.0001731 | 253.7270684 | 320.3971297 | 0.251812847 | 3.448472634 | 0.237245 | 9.688892786 | 23.4848737 |
| 0.0001376 | 286.1324277 | 329.404224 | 0.20460284 | 3.82485737 | 0.2449865 | 12.41789896 | 19.3938272 |
| 0.000101 | 313.0219811 | 343.1243328 | 0.151528476 | 4.22948372 | 0.26018374 | 17.23996268 | 14.6939375 |
| 0.000067 | 333.706253 | 355.6400045 | 0.097896366 | 4.53857372 | 0.271329349 | 26.43967839 | 9.2828372 |
| 0.000035 | 363.3537093 | 370.5645503 | 0.051395592 | 5.0188372 | 0.291692875 | 51.42579705 | 4.6928374 |
| 0.0000024 | 386.1064084 | 403.6080184 | 0.005057979 | 5.218372722 | 0.327283476 | 762.0336144 | 1.982734 |

**D13** 45° swept forward impeller CFD results

| Flowrate ($m^3/s$) | Differential Pressure ($kN/m^2$) | Power (W) | Flow Coefficient ($\Phi$) | Head coefficient ($\Psi$) | Power coefficient (¶) | Number of circulations | Hydraulic Efficiency (%) |
|---|---|---|---|---|---|---|---|
| 0.000329 | 18.61584469 | 246.3504357 | 0.53474726 | 0.169484737 | 0.17874 | 4.449344371 | 7.397423 |
| 0.000321 | 41.36854376 | 247.3454055 | 0.516102934 | 0.5948373 | 0.183456 | 4.576824568 | 11.798742 |
| 0.00031 | 57.22648553 | 253.3152238 | 0.491983476 | 0.78949383 | 0.18998 | 4.710542328 | 17.5897634 |
| 0.000288 | 93.07922346 | 264.1551571 | 0.46562983 | 0.9594383 | 0.195579 | 5.017607911 | 22.89764 |
| 0.0002626 | 120.6582526 | 273.8430201 | 0.428459763 | 1.3594873 | 0.200280947 | 5.424952518 | 26.2727263 |
| 0.0002323 | 151.6846604 | 286.5157923 | 0.382609837 | 1.919393827 | 0.208413 | 6.172484069 | 27.39383738 |
| 0.000198 | 186.8479226 | 297.9317607 | 0.338987235 | 2.35939387 | 0.21762 | 7.433902057 | 25.828474 |
| 0.0001612 | 220.6322334 | 310.4997993 | 0.251885737 | 3.02949482 | 0.2363 | 9.062274198 | 20.6848272 |
| 0.0001292 | 247.5217868 | 322.0205013 | 0.204693839 | 3.36949828 | 0.2423 | 11.14933602 | 17.58383726 |
| 0.0000996 | 265.4481558 | 333.0175351 | 0.151584374 | 3.76943837 | 0.2558 | 16.06494452 | 13.28483727 |
| 0.00006 | 286.1324277 | 351.8695929 | 0.097896366 | 4.089494829 | 0.267 | 24.9000408 | 9.8837373 |
| 0.0000315 | 306.1272238 | 365.484968 | 0.051395592 | 4.329494838 | 0.283906 | 45.70179834 | 4.583733 |
| 0.0000031 | 321.2956899 | 396.9050645 | 0.005057979 | 4.61949384 | 0.324225 | 589.7607911 | 0.337350397 |

**D14** 45° swept backward impeller CFD results

| Flowrate ($m^3/s$) | Differential Pressure ($kN/m^2$) | Power (W) | Flow Coefficient ($\Phi$) | Head coefficient ($\Psi$) | Power coefficient (¶) | Number of circulations | Hydraulic Efficiency (%) |
|---|---|---|---|---|---|---|---|
| 0.000348 | 22.06322334 | 256.9809017 | 0.5581283 | 0.0727364 | 0.193093948 | 4.372645617 | 2.850025661 |
| 0.0003385 | 46.88434959 | 263.3696546 | 0.54823736 | 0.387634 | 0.200093247 | 4.520310544 | 6.951582184 |
| 0.0003206 | 77.22128168 | 269.9155081 | 0.51227346 | 0.669763 | 0.20731989 | 4.822321367 | 12.30728522 |
| 0.0003038 | 108.2476895 | 274.9950903 | 0.47717273 | 1.119187634 | 0.213517361 | 5.138148662 | 20.91718744 |
| 0.0002824 | 136.5161944 | 281.6980442 | 0.445837343 | 1.481245 | 0.21636996 | 5.594871763 | 24.73576463 |
| 0.0002473 | 175.816311 | 296.3607559 | 0.3838274 | 2.225677274 | 0.230106532 | 6.515130553 | 27.48112812 |
| 0.0002049 | 222.7006606 | 310.2379652 | 0.334316091 | 2.79938475 | 0.240881361 | 8.04724585 | 26.35562239 |
| 0.0001731 | 253.7270684 | 320.3971297 | 0.282431017 | 3.1792834 | 0.248769349 | 9.688892786 | 23.86174529 |
| 0.0001376 | 286.1324277 | 329.404224 | 0.224509 | 3.6384473 | 0.255762823 | 12.41789896 | 20.32135999 |
| 0.000101 | 313.0219811 | 343.1243328 | 0.164792216 | 4.05924787 | 0.275009727 | 17.23996268 | 15.16326203 |
| 0.000067 | 333.706253 | 355.6400045 | 0.109317609 | 4.429847297 | 0.288010053 | 26.43967839 | 10.07328792 |
| 0.000035 | 363.3537093 | 370.5645503 | 0.057106214 | 4.749287346 | 0.303190264 | 51.42579705 | 5.34333778 |
| 0.0000024 | 386.1064084 | 403.6080184 | 0.003915855 | 5.9238476 | 0.333595578 | 762.0336144 | 0.338770283 |

**D15** 45° chevron forward impeller CFD results

| Flowrate ($m^3/s$) | Differential Pressure ($kN/m^2$) | Power (W) | Flow Coefficient ($\Phi$) | Head coefficient ($\Psi$) | Power coefficient (¶) | Number of circulations | Hydraulic Efficiency (%) |
|---|---|---|---|---|---|---|---|
| 0.000329 | 18.61584469 | 246.3504357 | 0.512584746 | 0.1624567 | 0.185106278 | 4.676503233 | 3.783350217 |
| 0.000321 | 41.36854376 | 247.3454055 | 0.498742536 | 0.357144515 | 0.187918936 | 4.815204594 | 9.473136777 |
| 0.00031 | 57.22648553 | 253.3152238 | 0.48197857 | 0.661128384 | 0.194569348 | 5.017607911 | 14.48600882 |
| 0.000288 | 93.07922346 | 264.1551571 | 0.468473957 | 0.86737484 | 0.205100797 | 5.468798639 | 21.69087007 |
| 0.0002626 | 120.6582526 | 273.8430201 | 0.428459763 | 1.2948475 | 0.21033658 | 6.083746328 | 23.64492705 |
| 0.0002323 | 151.6846604 | 286.5157923 | 0.382673746 | 1.72928485 | 0.222462503 | 6.993220487 | 23.8681083 |
| 0.000198 | 186.8479226 | 297.9317607 | 0.338737283 | 2.31656372 | 0.231326324 | 8.358656606 | 23.13621943 |
| 0.0001612 | 220.6322334 | 310.4997993 | 0.251884837 | 2.94938474 | 0.24108466 | 10.4697588 | 19.84713073 |
| 0.0001292 | 247.5217868 | 322.0205013 | 0.204693848 | 3.282934876 | 0.250029801 | 13.28304616 | 16.65614808 |
| 0.0000996 | 265.4481558 | 333.0175351 | 0.151594847 | 3.6419847 | 0.264128955 | 17.49478589 | 12.94621835 |
| 0.00006 | 286.1324277 | 351.8695929 | 0.097896366 | 3.929387465 | 0.282018941 | 29.62801124 | 7.878735032 |
| 0.0000315 | 306.1272238 | 365.484968 | 0.051395592 | 4.1875637 | 0.299034227 | 57.23853994 | 3.96841635 |
| 0.0000031 | 321.2956899 | 396.9050645 | 0.005057979 | 4.379234876 | 0.328055362 | 589.7607911 | 0.34181135 |

**D16** 45° chevron backward impeller CFD results

| Flowrate ($m^3/s$) | Differential Pressure ($kN/m^2$) | Power (W) | Flow Coefficient (Φ) | Head coefficient (Ψ) | Power coefficient (¶) | Number of circulations | Hydraulic Efficiency (%) |
|---|---|---|---|---|---|---|---|
| 0.000307 | 18.61584469 | 238.7572458 | 0.47773635 | 0.235162502 | 0.1794008 | 5.075326121 | 2.553168854 |
| 0.000293 | 46.88434959 | 245.669667 | 0.448537475 | 0.592261117 | 0.186645806 | 5.360305678 | 7.121423091 |
| 0.000282 | 62.74229137 | 252.3726209 | 0.436717634 | 0.79258473 | 0.193845342 | 5.604068586 | 10.29158671 |
| 0.000266 | 84.8055147 | 258.5519065 | 0.409237463 | 1.071295843 | 0.200750205 | 5.994622419 | 16.50633145 |
| 0.0002519 | 103.4213594 | 266.5116643 | 0.392572646 | 1.306458346 | 0.204705426 | 6.379924164 | 18.87955839 |
| 0.0002151 | 134.4477672 | 275.5187586 | 0.350958473 | 1.7721245 | 0.213923959 | 7.623496086 | 21.29508604 |
| 0.0001915 | 153.7530876 | 284.5258529 | 0.312452569 | 2.116542 | 0.220917433 | 8.672541962 | 20.23766561 |
| 0.0001644 | 179.2636896 | 293.5329472 | 0.268236043 | 2.41374656 | 0.227910907 | 10.2486659 | 18.99210635 |
| 0.0001257 | 200.6374372 | 305.2631166 | 0.205092887 | 2.75747362 | 0.237018687 | 13.67765055 | 15.03096346 |
| 0.0000966 | 216.495379 | 316.3125171 | 0.15761315 | 2.9598436 | 0.250879565 | 18.06570747 | 11.63999676 |
| 0.00006 | 234.421748 | 328.8805557 | 0.097896366 | 3.285847362 | 0.263593524 | 29.62801124 | 7.280822345 |
| 0.0000324 | 247.5217868 | 338.6731524 | 0.052864038 | 3.4826365 | 0.274269686 | 55.62388914 | 3.936774805 |
| 0.0000024 | 262.0007771 | 371.1405854 | 0.003915855 | 3.684746 | 0.303661567 | 762.0336144 | 0.263511789 |

**D17** 60° chevron forward impeller CFD results

| Flowrate (m$^3$/s) | Differential Pressure (kN/m$^2$) | Power (W) | Flow Coefficient ($\Phi$) | Head coefficient ($\Psi$) | Power coefficient (¶) | Number of circulations | Hydraulic Efficiency (%) |
|---|---|---|---|---|---|---|---|
| 0.000284 | 17.23689323 | 235.5105025 | 0.44338474 | 0.217743058 | 0.176961216 | 5.558343534 | 2.269219784 |
| 0.000277 | 27.57902917 | 237.9717434 | 0.4347362 | 0.348388892 | 0.180797362 | 5.721269985 | 4.303819303 |
| 0.000267 | 45.50539813 | 242.4229237 | 0.41383764 | 0.547464 | 0.188227008 | 5.968841478 | 7.821642546 |
| 0.000258 | 59.29491272 | 244.8841646 | 0.39863525 | 0.66245 | 0.190138015 | 6.208064631 | 12.79321978 |
| 0.0002423 | 76.53180595 | 250.0161137 | 0.3774635 | 0.891245 | 0.192035328 | 6.667916757 | 15.63768384 |
| 0.0002173 | 100.6634565 | 259.7039767 | 0.3388326 | 1.13546253 | 0.20164472 | 7.537314553 | 18.41267817 |
| 0.0001892 | 123.4161555 | 268.6063374 | 0.308699875 | 1.4737262 | 0.208556874 | 8.788775001 | 18.1895972 |
| 0.0001622 | 136.5161944 | 275.9376932 | 0.26464651 | 1.77373645 | 0.214249237 | 10.39973015 | 16.25108029 |
| 0.0001262 | 148.2372818 | 288.5057318 | 0.20590869 | 2.027563535 | 0.224007572 | 13.61993843 | 12.49092214 |
| 0.0000917 | 165.474175 | 301.5974386 | 0.14961828 | 2.26236545 | 0.236690489 | 19.07854849 | 9.261111353 |
| 0.0000587 | 177.8847382 | 318.8784917 | 0.095775278 | 2.392747575 | 0.252914738 | 30.30385401 | 5.723810861 |
| 0.0000294 | 188.2268741 | 333.331736 | 0.047969219 | 2.63374564 | 0.272726943 | 61.39049914 | 2.795319691 |
| 0.0000037 | 200.6374372 | 370.7216508 | 0.006036943 | 2.7823746 | 0.306413891 | 493.9797619 | 0.311688335 |

**D18** 60° chevron backward impeller CFD results